

Guide to the K600 magnetic spectrometer

R. Neveling, F.D. Smit, H. Fujita, P. Adsley, K.C.W. Li,
J.W. Brümmer, D.J. Marín-Lambárrí and R.T. Newman

February 9, 2017

Contents

1 A brief description of the K600	5
1.1 Focal-plane detectors	11
1.1.1 The original focal-plane detector package	11
1.1.2 The new focal-plane detector package	15
1.1.3 VDC spatial resolution	17
1.1.4 Position resolution simulation	20
1.1.5 VDC efficiency	21
1.2 Spectrometer transmission	24
2 Electronics and DAQ: VME and MIDAS	27
2.1 Hardware notes	28
2.2 For beginners: Analysis notes (2014 version)	30
2.2.1 Getting started	30
2.2.2 Comments regarding the analyzer code (2014 version)	36
2.3 The ODB (2014 version)	36
2.4 Cable length offsets	38
2.4.1 JJ's script	39
2.5 LUT	39
2.5.1 Creating a proper LUT	40
2.5.2 Verification of proper LUT	43
2.6 Typical outline of analysis procedure (2014 version)	43
2.7 Outline of analysis of PR236 (Jan 2017 version)	52
2.8 Analysis of coincidence experiments (Jan 2016 notes)	62
2.8.1 CAKE PID	64
2.9 Analysis of PR259 (Daniel's notes)	67
2.9.1 Correction using TOF	67
2.9.2 Correction using TOF (θ_{scat})	68
2.9.3 Peak Identification	70
2.9.4 Calibration using Magnetic Rigidity	72
2.9.5 Calibration of the Excitation Energy of ${}^9\text{B}$ using the ${}^{26}\text{Al}$ Calibration	76
2.9.6 Silicon Energy V.S. Excitation Energy	77
3 The K600 magnetic fields	80
3.1 Setting the spectrometer fields	80
3.1.1 Theory	80
3.1.2 The SET FIELD procedure	81

3.2	SPEXCIT	83
3.3	Measuring D1 and D2 fields	87
3.4	Superknob	87
3.5	Adjusting the K and H-coils	87
3.6	TRACK calculations for the K600	88
3.7	Adjusting the entrance hexapole/sextupole magnet	89
4	The K600 collimator carousel	90
5	K600 angle change and beamstop configuration	100
5.1	External beamstop for $\theta_{K600} > 21^\circ$	100
5.2	Internal beamstop for $5^\circ < \theta_{K600} < 21^\circ$	100
5.3	Internal beamstop for angles $2^\circ < \theta_{K600} < 5^\circ$	100
5.4	$\theta_{K600} = 0^\circ$ beamstop for (p, p')	101
5.5	$\theta_{K600} = 0^\circ$ beamstop for (p, t)	102
5.6	To move the spectrometer	103
5.7	Small manual K600 angle adjustments	107
5.8	Scattering chambers	107
5.8.1	The scattering chamber rotating table	107
5.8.2	Sliding seals	109
6	Miscellaneous hardware	112
6.1	Hall probes	112
6.2	Target ladder and frames	112
6.3	BeamLossMonitors: the halo detectors	113
6.4	Beamviewers	115
6.5	The focal plane beamblocker	115
6.6	Al E-degrader plates for paddles	117
6.7	Slits at 9X	118
7	Gasflow to the driftchambers	119
7.1	Gas pipe connections	119
7.2	Turning the gas on	119
7.3	Turning the gas off	120
7.4	Replacing a gas bottle	121
7.5	Specs of a good gas	121
7.6	The hydrosorb and oxysorb	122
8	Vacuum	123
8.1	K600 vacuum	123
8.2	Scattering chamber vacuum	124
9	Dispersion matching	125
9.1	Theoretical background	125
9.2	Comment on Beam-line elements	128
9.3	Comments on practical matching for $\theta_{K600} \neq 0$	129
9.4	The faint beam method for $K \neq 0$ experiments	132
9.5	Kinematic factor: some numbers	134

9.6	Good resolution records	135
9.7	SSC transmission: historical numbers	137
9.7.1	66 MeV protons	139
9.8	α beam	140
10	The 0° and 4° modes	142
10.1	Notes on zero degree beam-tuning	144
10.1.1	The RCNP experience	144
10.1.2	iThemba LABS: PR137 (p,t) at 100 MeV	145
10.1.3	iThemba LABS: the PR138 (p,p') experience	147
10.1.4	iThemba LABS: the PR183/184 (p,p') experience	150
10.1.5	iThemba LABS: summary of what we know so far and what you should do: 151	151
10.1.6	iThemba LABS: experience from other runs	152
10.2	K and H coil settings for measurements	154
10.3	The faint beam method for K=0 experiments	155
10.3.1	Beam attenuation meshes	155
10.3.2	Faintbeam: original DAQ and VDCs	155
10.3.3	Faintbeam: PR137	156
10.3.4	The myth of the K-coil during faintbeam tuning	156
10.4	Scattering angle calibration and resolution	158
10.4.1	Over and under focus mode	158
10.4.2	Vertical scattering angle resolution	160
10.4.3	Horizontal scattering angle resolution	160
10.4.4	Calibration	161
10.5	Miscellaneous for Zero Degrees	165
10.5.1	Zero degree beamline to beamdump	165
10.5.2	0° interlock	165
10.5.3	Small K600 angle adjustments	167
10.5.4	Maximum angle of K600 with detectors in high dispersion focal plane	167
10.5.5	Historical numbers	168
10.6	Historical high dispersion focalplane magnet settings	168
A	Software notes	170
A.1	SPANC	170
A.2	SPEXCIT	171
B	Old Electronics and DAQ: CAMAC and XSYS	173
B.1	The autotrim procedure	173
B.2	Autotrim problems	176
B.3	General electronics notes	177
B.4	Focal-plane detector trips	180
B.5	Data acquisition hardware	182
B.6	Data acquisition software	182
B.7	Setting up the lookup table	183
C	Hiro: beamline comparison between iTL and RCNP	186

D Single-turn extraction from the injector cyclotron 2 (SPC2) and the separated-sector cyclotron (SSC).	190
E List of proposals since November 2004	194
F Zero degree experiment run checklist	197
G Setting up CAKE	198
G.1 Mounting the Detectors	198
G.2 Putting CAKE in the chamber	205
G.3 Electronic Gubbins	206
G.3.1 Using CAKE in experiments	210

Chapter 1

A brief description of the K600

This guide will introduce the new user to the K600 magnetic spectrometer, and remind the seasoned user of necessary and important procedures.



Figure 1.1: The K600 magnetic spectrometer in 2016.

The iThemba LABS K=600¹ ² QDD magnetic spectrometer is a copy of the original K=600 magnetic spectrometer designed and built at IUCF (Indiana, USA) [?]. It was first commissioned at iThemba LABS (then NAC) in October 1991 [AnRep91]. The Indiana K600 was decommissioned in 1999 and now forms part of the WS beamline at RCNP, Osaka, Japan. As an indication of its size, the average flight path for a particle from target to detector is approximately 8m.

The K600 consists of five active elements namely a quadrupole, two dipoles and two trim coils (K and H) as shown in Fig. 1.2. The two dipole magnets, D1 and D2, allow the momentum dispersion to be varied by varying the ratio of the two dipole magnets, while vertical focussing is achieved with the the quadrupole. The two trim coils, located inside the dipoles, are used to achieve the final focusing at the focal-plane. The so-called K-coil, a pole face current winding which introduces both a dipole and quadropole component, is used to adjust for first-order kinematic variations of momentum with angle ($x | \theta$) (notation as used in [Eng81]). The H-coil, a pole face current winding which introduces both a dipole and sextupole (sometimes also referred to as a hexapole) component, is used to correct for ($x | \theta^2$) abberations. In addition an entrance hexapole is located just after the collimator carousel (indicated as HE on the figure). However, this magnetic element has never been used (at least not in the past 10 years).

In front of the quadrupole is a carousel which houses six collimators. A 524mm diameter scattering chamber is situated at the turning axis of the spectrometer. Inside the scattering chamber is a target ladder with six target positions and a turntable on which detectors or the internal beamstop can be mounted. Behind the second dipole is the focal plane position-sensitive detectors package. Most of the dedicated electronics for the spectrometer is in the electronics tower located on the spectrometer platform next to the low dispersion focal plane. Technical specifications of the K600 are listed in table 1.1.

The intrinsic momentum resolution of a spectrometer can be given as [Wak02]

$$\Delta p/p = 1/R = |(M_x/D)\Delta x_0| , \quad (1.3)$$

or from [Fuj02]:

$$\Delta p/p = 1/R = 1/2x_0 \times \left(\frac{s_{16}}{s_{11}b_{11}T - s_{16}b_{21}K} \right) . \quad (1.4)$$

Refer to chapter 9 for a description of these terms.

¹The energy constant K of a magnetic device is defined as $K = \frac{mE}{q^2}$.

²The Lorentz force exerted by a magnetic field \vec{B} on a particle with charge q , mass m and velocity \vec{v} is

$$\frac{d\vec{v}}{dt} = \frac{q}{\gamma m} x \vec{B}, \quad (1.1)$$

For the momentum of the particle $p = \gamma mv$ the magnetic rigidity can be written as

$$R = \frac{pc}{q}. \quad (1.2)$$

K600 SPECTROMETER

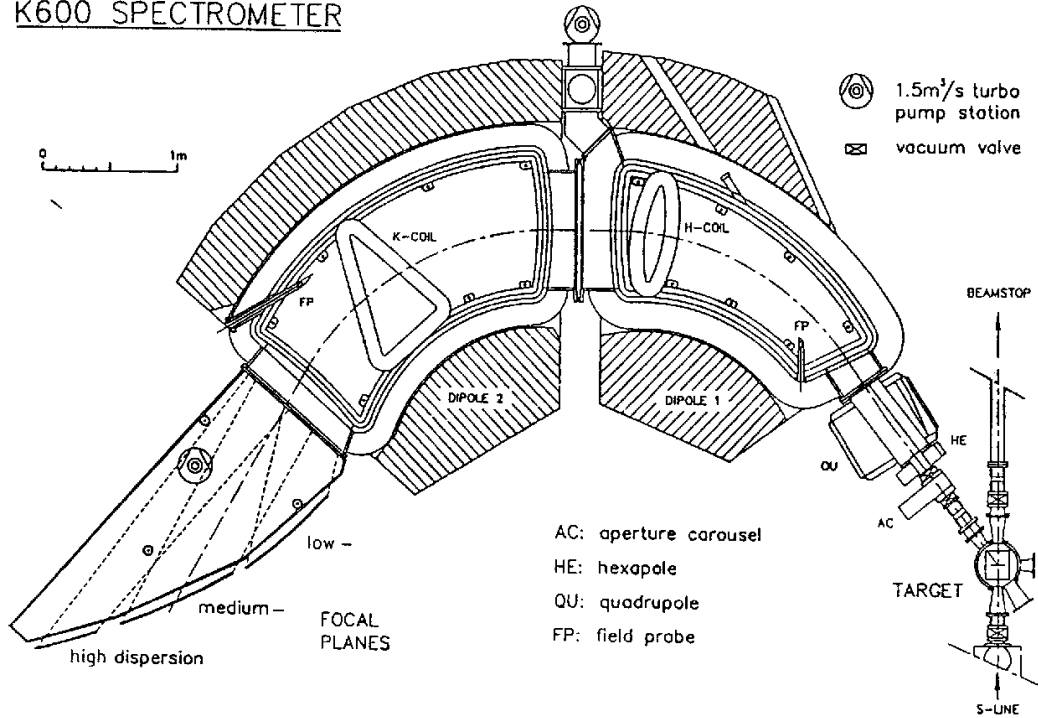


Figure 1.2: A schematic overview of the K600 magnetic spectrometer.

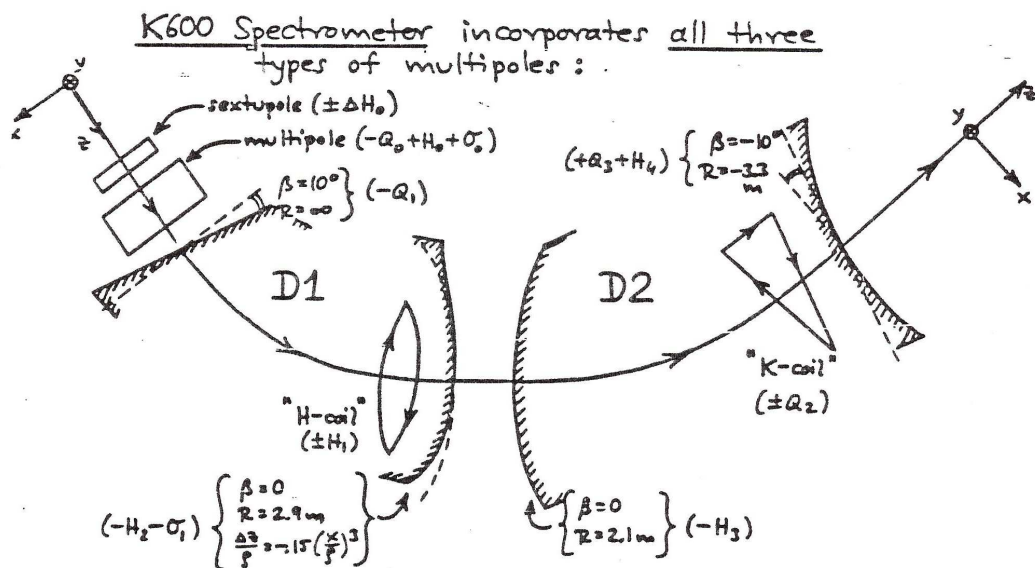


Figure 1.3: A schematic overview of the magnetic elements in K600 magnetic spectrometer (from a 1986 talk by P.Schwandt [Sch86]).

3. Dipole Pole-Face Current Windings

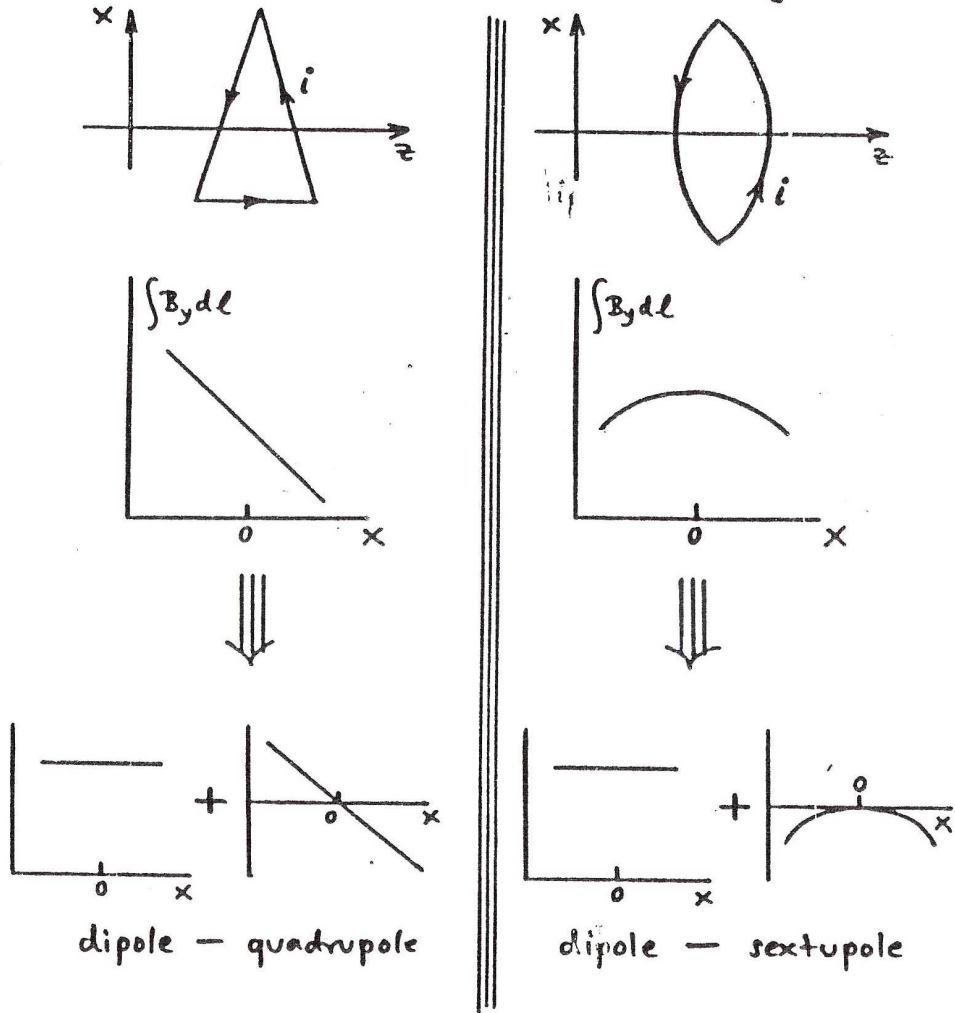


Figure 1.4: Dipole face windings: showing how the K coil has a quadrupole component (and the H-coil a sextupole component) as well as dipole components. (from a 1986 talk by P.Schwandt [Sch86]).

Nominal bend radius	2.1 m
Nominal bend angle	115°
Dipole Field ratio	1
Maximum dipole field	1.64 Tesla
Maximum magnetic rigidity	3.60 Tm
Momentum dispersion ($x \frac{\Delta p}{p} $)	8.4 cm/%
Energy dispersion for 200 MeV proton setting	42 keV/mm at 200 MeV
Momentum range, P_{max}/P_{min}	1.097
Resolving power, $P/\delta P$ (with 0.6mm object width)	28000
Horizontal magnification at P_{max}	-0.52
Vertical magnification at P_{max}	7.4
Tilting angle of focal plane w.r.t. central ray	35.75°
Distance: target to back of collimator	735.5 mm
Maximum diameter collimator	55 mm
Maximum solid angle $\Delta\theta\Delta\phi$	4.39msr
Maximum vertical acceptance: $\Delta\theta$	± 37.4 mrad , or $\pm 2.14^\circ$
Maximum vertical acceptance: $\Delta\phi$	± 37.4 mrad , or $\pm 2.14^\circ$
Floor angle indicator value for beam direction	15.1 ^{circ}

Table 1.1: Technical specifications for the medium dispersion mode of K600 Magnetic Spectrometer. Note that the maximum diameter collimator refers to the maximum diameter that was tested. According to the Schwandt lectures [Sch86] the maximum acceptance is $\pm 44\text{mr}$.

Property	Low	Normal	High
Maximum momentum per charge p/Q (MeV/c)	860	1080	1005
Maximum proton energy (MeV)	334	493	437
Maximum magnetic rigidity (T-m)	3.00	3.60	3.50
Maximum dipole fields, D1/D2 (T)	1.23/1.64	1.64/1.64	1.64/1.23
Nominal bend radius (m)	2.1	2.1	2.1
Nominal bend angle (degrees)	115	115	115
Maximum solid angle $\Delta\theta\Delta\phi$ (msr)	6.0	6.0	6.0
Maximum radial acceptance $\Delta\theta$ (mrad)	± 44	± 44	± 44
Maximum axial acceptance $\Delta\phi$ (mrad)	± 44	± 44	± 44
Momentum range p_{max}/p_{min}	1.131	1.097	1.063
$p/\delta p$: Resolving power	$\sim ?$	~ 28000	$\sim ?$
$(x \frac{\Delta p}{p})$: Momentum dispersion (cm/%)	6.2	8.4	9.8
Energy dispersion (keV/mm) (for 200MeV protons)	65	50	40
$(x x)$: Horizontal magnification at p_{max}	-0.42	-0.54	-0.68
$(y y)$: Vertical magnification at p_{max}	-4.0	-5.7	-11.8
$(\theta \theta)$:	$\sim 1/(x x)$	$-1.90 (\sim 1/(x x))$	$\sim 1/(x x)$
$(\phi \phi)$:	$\sim 1/(x x)$	$-0.17 (\sim 1/(y y))$	$\sim 1/(x x)$
Focal plane length, horizontal (cm)	81	78	62
Tilting angle of focal plane w.r.t. central ray	?	35.75°	32.2°
Beam dispersion (according to L.Conradie)	1/16000	1/16000	1/16000
Beam dispersion (according to L.Conradie)	16 cm/%	16 cm/%	16 cm/%

Table 1.2: Design parameters of the three dispersion modes of the K600 spectrometer from [Sch86]. Note that some of these values are different from those in table 1.1. (From Ricky's notes these values originate from 1983 IUCF proposal for fp detectors and electronics) These matrix elements can also be calculated with the MATRIX command of TRACK.

Matrix element/ characteristic	Medium dispersion $R = 1.00$	High dispersion $R = 1.49$
$(x x)$	-0.52	-0.74
$(\theta \theta)$	-1.89	-1.37
$(y y)$	-5.45	-7.05
$(\phi \phi)$	-0.20	-0.13
$(x \frac{\Delta p}{p})$	-8.4 cm/%	-10.9 cm/%
p_{max}/p_{min}	1.097	1.048

Table 1.3: TRACK calculated ion-optical properties near the central momentum of the medium and high-dispersion focal-planes of the $K = 600$ magnetic spectrometer in vertical focus mode. Note the High dispersion focal plane is used in a new mode where the ratio of magnets are different from the designed 1.33.

1.1 Focal-plane detectors

1.1.1 The original focal-plane detector package

The focal-plane detector package consist of three multi-wire drift chambers and a pair of plastic scintillation detectors. Technical details of the detectors are summarized in table 1.4. Two different geometric configurations of the drift chambers exist: the two vertical drift chambers (VDC's) are used to determine position information along the length of the focal-plane as well as the angle at which a charged particle crossed the focal plane. The Horizontal Drift Chamber (HDC) is used to measure particle position in the vertical of the focal-plane³. Electron drift velocities are of the order of 4-6m/ μ sec, thus for 8mm one expects drift times of 133-200ns.

These drift chambers, both developed and built at iThemba LABS (1989-1993), consist of two high-voltage cathode planes with a signal-wire anode plane midway between them. A cross-sectional view of the original VDC is shown in Fig. 1.5, while the a figure of the new drift chamber is given in Fig. 1.6. Two 25 μ m thick mylar planes are used to isolate the interior of the VDC from atmosphere. The volume between the two cathode planes is filled with gas mixture of 90% Ar and 10% CO_2 . The cathode planes are made of 27 μ m thick aluminum foil separated by a distance of 16 mm. A negative high voltage of \sim 3800 V was applied to these planes. The signal-wire plane of a VDC consists of 198 signal wires, 20 μ m in diameter, spaced 4 mm apart and made from gold-plated tungsten. These signal wires are kept at 0 V potential. Interspersed between these wires are 199 so-called guard wires (or field wires), which provide field shaping and define cells, associated with each signal wire, of about 4 mm. These wires are made of 50 μ m diameter gold-plated tungsten, also spaced 4 mm apart. A negative voltage of \sim 500 V is applied to the guard wires. The HDC is of a similar make-up, with 16 signal wires and 17 guard wires in horizontal planes opposed to the 198 and 199 vertical wires of the VDC. Typical HV on the HDC cathode planes are \sim -2000V, and for the HDC guard wires \sim -1200V. In the NAC Annual Report of 1995 page 22 it is mentioned that the HDC can also be used as a ΔE detector together with one scintillar for low-energy particles. The use of special preamp cards are mentioned.

The anode plane of the first VDC is placed such that it coincides with the focal-plane

³Note that the terms *VDC* and *HDC* do not relate to the physical orientation of the signal wires, but rather to the mode of operation of the drift chamber. In a VDC the main drift direction of electrons is perpendicular to the signal wire plane. In the HDC the electrons drift in the plane of the signal wires.

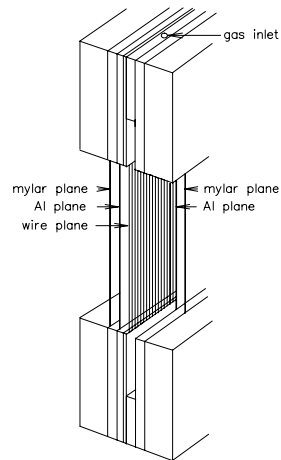


Figure 1.5: The main components of the original VDC.

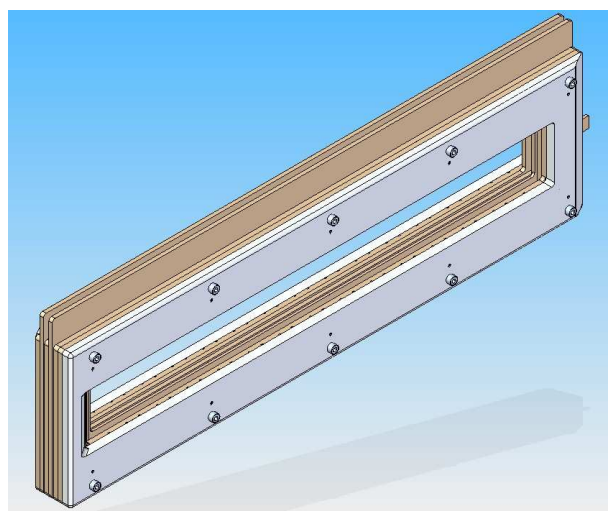


Figure 1.6: A design drawing of the new VDC.



Figure 1.7: An old paddle with the black paper stripped off

of the magnetic spectrometer (to first order, keeping in mind that the real focal-plane is not a flat surface). The position where a charged particle traversed the focal-plane can thus be established by interpolation to a high degree of accuracy, thus providing accurate momentum information of such a particle.

Two 122 cm × 10.2 cm plastic scintillator detectors (also referred to as *paddle* detectors because of their geometry) are positioned close to the focal-plane just downstream from the drift chambers. The main purpose of these detectors are to provide event trigger signals and also to aid in particle identification through $\Delta E - \Delta E$ particle identification spectra.

NEED PICTURES AND DRAWINGS

1.1.1.1 Comments on drift chamber operation by Ricky Smit

The vertical drift chamber consists of two 100 x 800 mm aluminium foils, 16 mm apart to which a negative high voltage of 3600 volts is applied (HV plane into the page in Fig. 1.8). In between these foils are, alternately, 20 μm and 50 μm thick wires that are all 100 mm long (into the page in Fig. 1.8). A negative voltage is applied to the foils. Positively charged particles ionize a track through the detector producing electrons that drift along the field lines down to the wire. Charge multiplication takes place very close the wire. The smaller the radius the more the multiplication (therefore the signal wires are 20 μm). In between are thicker wires that have a negative voltage applied to them to help shape the field. In the figure the proton crosses the path of five wires marked 1 to 5. One can see the variation in drift times within a field cell of a wire that go on to form a pulse and also how the drift times for cell 3 will be incorrect considering the short and varied paths they drift. In our case the drift times are all measure relative to the time a pulse is recorded from the scintillator which sits behind the vertical drift chamber. Furthermore the time zero from the scintillator is delayed, by a time a , after all the pulses from the wires have arrived. If perfect then the drift time Y_i on either side of the wire is given by

$$Y_i = a - t_i \quad \text{if} \quad t_{i+1} < t_i \quad (1.5)$$

Original Vertical Drift Chamber	
Wire configuration	vertical
Horizontal VDC acceptance	78 cm
Vertical VDC acceptance	10 cm
Signal wire	20 μ m gold plated tungsten
Guard wire	50 μ m gold plated tungsten
Cathode planes	27 μ m Al foil
Number of signal wires	198
Number of guard wires	199 (+4?)
Cathode-anode spacing	8 mm
Signal wire spacing	4 mm
Guard wire spacing	4 mm
Gas mixture	90% Ar 10% CO ₂
Entrance and exit windows	25 μ m mylar
Pre-amplifier	Lecroy 2735 (13 units)
Guard wire voltage	~ -500 V
Cathode plane voltage	~ -3800 V
Horizontal Drift Chamber	
Wire configuration	horizontal
Horizontal HDC acceptance	78 cm
Vertical HDC acceptance	10 cm
Signal wire	20 μ m gold plated tungsten
Guard wire	50 μ m gold plated tungsten
Cathode planes	27 μ m Al foil
Number of signal wires	16
Number of guard wires	17 (+4?)
Cathode-anode spacing	8 mm
Signal wire spacing	6 mm
Guard wire spacing	6 mm
Gas mixture	90% Ar 10% CO ₂
Entrance and exit windows	25 μ m mylar
Pre-amplifier	Lecroy 2735 (1 unit)
Guard wire voltage	~ -1200 V
Cathode plane voltage	~ -2000 V
Paddles	
Scintillating material	Bicron BC-408
Scintillator dimensions	48 × 4 × 0.5 (or 0.25 or 0.125) inch ³ = 1219.2 × 101.6 × 12.7 (or 6.4 or 3.2) mm ³
Lightguide	Bicron Fishtail
PMT	Hamamatsu R329-02 PMT tube with a Hamamatsu E934 base
Typical PMT voltage for 200 MeV protons	~ -1700V for 0.5 inch ~ -1900V for 0.25 inch
Max PMT voltage	2700V

Table 1.4: Technical specifications for the original focal plane detectors.

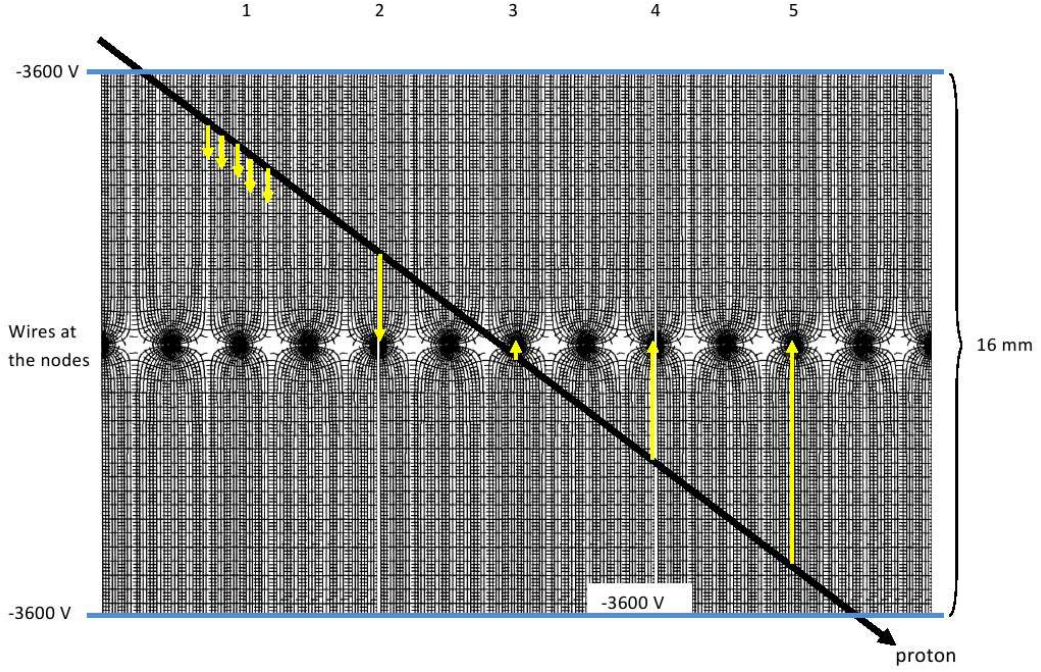


Figure 1.8: Garfield calculated VDC fieldlines.

$$Y_i = -(a - t_i) \quad \text{if} \quad t_{i+1} \leq t_i \quad (1.6)$$

where t_i is the raw drift time from the TDC. However there is some offset on each t_i . Each event has between four and seven wires firing so we know that the pairs (X_i, Y_i) , with X_i being the wire number, need to lie on a straight line. As the drift time over the part of the curved field lines close to each wire become a larger fraction of the total drift time, the drift times become increasingly non-linear. Because of this we normally discard the shortest drift time which then gives us a better chi squared on the fit of a straight line through the data. The aim is to determine where, along the plane formed by the wires, the particle crossed. The position along the wire plain is then correlated to energy. There are then also offsets to each drift time that is determined by the path length of the track to the preamp, the path in the preamp, the variations in cables from the preamp to the TDCs and also the path in the TDCs. These make up the offsets for each wire. As you mentioned, the non-linear drift times close to the wires also affect the offsets. If the proton only clips the top corner of a cell it can of course also upset the average drift times.

1.1.2 The new focal-plane detector package

Accurate determination of the scattering angle in 0° measurements requires the accurate determination of both the horizontal as well as vertical components of particle tracks in the focal plane. Two new VDCs, each with two wire-planes, were manufactured at iThemba LABS for this purpose (2006-2009) due to the very limited vertical position detection capabilities of the HDC. A UX configuration was selected for the signal-wires of the new drift chambers. The X

signal-wires are perpendicular to the scattering plane while the U signal-wires are angled at 50° with respect to the scattering plane.

As in the case of the original VDCs the new VDC X wire-plane consists of 198 gold-plated tungsten signal-wires, 20 μm in diameter, spaced 4 mm apart. Interspersed between these wires at equal distances are 199 field shaping wires made of 50 μm diameter gold-plated tungsten. Similarly the U wire-plane consists of 143 signal-wires and 144 field shaping wires, also spaced 4 mm apart. In addition there is 1 extra guard wire at both ends of both wireplanes. These are made from 125 μm diameter Ni-Cr wires (80%/20%), and are necessary to reduce the electric field at the ends of the drift chambers to suppress spontaneous discharge and reduce leakage currents. A negative voltage of 500 V was applied to the field shaping wires. The three cathode planes that sandwich the wire-planes are made of 20 μm thick aluminum foil and are separated by a distance of 16 mm, resulting in 8 mm spacing between the signal-wire and cathode planes. Typically a high voltage of -3700V (-3500V) was applied to these planes for 200 MeV proton (100 MeV triton) detection. Two 25 μm thick Mylar planes are used to isolate the interior of the MWDC from atmosphere. The volume between the two Mylar planes is filled with gas mixture of 90% Ar and 10% CO₂. The signal and guard wires of each wire-plane are soldered onto a single 417 mm × 936 mm printed circuit board.

Some misc technical info:

- Resistors for low-pass filter are 1.2 Mohm now. It was 1Mohm. Nieldane says it will not make much of a difference.
- Resistance of signal wire = 29.9 ohm. Resistance of wire and Cu track and edge connector: 30ohm.
- For the guard wire the resistance is 5.3 ohm, same for wire+track
- On 30 July 2008 we tested the HV remote control setting in dataroom HV1 in vault HV2 in vault -1kV 0.97 0.95 -2kV 1.95 1.90 -3kV 2.93 2.86 -3.5kV 3.41 3.34 -4kV 3.91 3.80

Two new paddles were built, with 90° twisted pair adiabatic lightguides (from Saint Gobain Crystals) to allow for the scintillator to be positioned closed to the beampipe as the PMT is placed vertically. This is illustrated in Fig. 1.9.



Figure 1.9: The new trigger scintillators/paddles

New X&U Vertical Drift Chamber	
Wire configuration	vertical and 50°
Horizontal VDC acceptance	78 cm
Vertical VDC acceptance	10 cm
Signal wire	20 μ m gold plated tungsten
Guard wire	50 μ m gold plated tungsten
Cathode planes	20 μ m Al foil
Number of signal wires	198 and 143
Number of guard wires	201 (=199+2) and 146 (=144+2)
Cathode-anode spacing	8 mm
Signal wire spacing	4 mm
Guard wire spacing	4 mm
Gas mixture	90% Ar 10% CO ₂
Entrance and exit windows	25 μ m mylar
Pre-amplifier	Lecroy 2735 (13 units)
Typical guard wire voltage	~ -500 V
Typical cathode plane voltage	~ -3800 V
Paddles	
Scintillating material	Bicron BC-408
Scintillator dimensions	48 × 4 × 0.5 (or 0.25) inch ³ = 1219.2 × 101.6 × 12.7 (or 6.4) mm ³
-	
Lightguide	Saint Gobain Crystals 90° adiabatic twisted pair
PMT	Hamamatsu R329-02 PMT tube with a Hamamatsu E934 base
Typical PMT voltage for 200 MeV protons	~ -1700V for 0.5 inch ~ -1900V for 0.25 inch
Max PMT voltage	2700V

Table 1.5: Technical specifications for the new focal plane detectors.

1.1.3 VDC spatial resolution

This section is taken from Richard Newman's PhD thesis on the study of the $^{55}\text{Mn}(\text{d}, ^3\text{He})^{54}\text{Cr}$ ($E_d = 46$ MeV) reaction, published in Phys. Rev. C54 (1996) 1773.

The position accuracy, σ_x , obtainable with a single drift cell is the usual figure-of-merit reported for a VDC [Ber77]. It is a factor which contributes to the overall position resolution achievable with the spectrometer and also determines the angle accuracy, σ_θ , which can be achieved with the VDC.

A schematic representation of a charged particle trajectory traversing a VDC, having a signal-wire spacing s is shown in Fig. 1.10. In the trajectory shown, six primary ionizations in the gas-filled VDC were caused, each associated with a separate drift cell. The drift time from the point of primary ionization to the point where avalanching occurs in each cell is measured experimentally. By using the time-to-position relationship provided by a lookup table it is possible to determine the position along the drift cell where the primary ionization occurred.

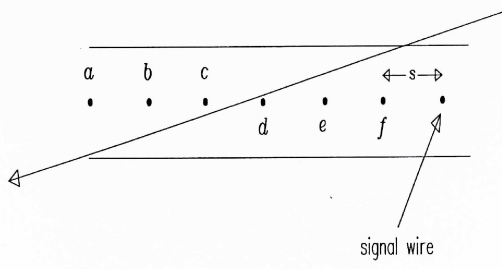


Figure 1.10: *Schematic representation of a trajectory associated with a charged particle intersecting the VDC resulting in a six-wire event.* (from RTN PhD)

It is therefore possible to reconstruct trajectories of particles across the VDC wire-plane. Since the trajectories of particles in the vicinity of the VDC are to a good approximation straight lines, the slope of each trajectory should be constant. This property of the trajectories was used to determine σ_x .

The slope of the trajectory shown in Fig. 1.10 can be calculated in a number of ways. One way in which this can be done is to use the drift distances associated with two adjacent wires, say wires a and b . In this case the trajectory slope, S , is given by:

$$S_{a,b} = \frac{d_b - d_a}{s}, \quad (1.7)$$

where d denotes drift distance. The slope could also be determined using the drift distances associated with for example wires e and f . Since the slope should be constant, the difference between the two slopes, denoted by D , given by

$$D = S_{a,b} - S_{e,f} \quad (1.8)$$

should ideally be zero. However because of statistical fluctuations a distribution centered around zero is obtained when one calculates the difference in slope for a number of events. Let us denote the standard deviation of this distribution by σ_D . By applying the general law of error propagation to equation 1.8, with covariances assumed to be zero, one obtains:

$$\Delta D^2 = \Delta d_a^2 + \Delta d_b^2 + \Delta d_e^2 + \Delta d_f^2. \quad (1.9)$$

If each Δ appearing in equation 1.9 is replaced by its mathematical expectation, namely a standard deviation, and it is assumed that

$$\Delta d_a = \Delta d_b = \Delta d_e = \Delta d_f = \sigma_c, \quad (1.10)$$

σ_D is then related to the intrinsic cell accuracy, σ_c , by [Ber77]

$$\sigma_D = 2\sigma_c. \quad (1.11)$$

With a least squares fit to n datapoints is used to determine where the particle track intersects the focal plane the relationship between intrinsic cell accuracy and the cell position accuracy is given by [Ber77]

$$\sigma_x = \frac{\sigma_c}{\sqrt{n}}. \quad (1.12)$$

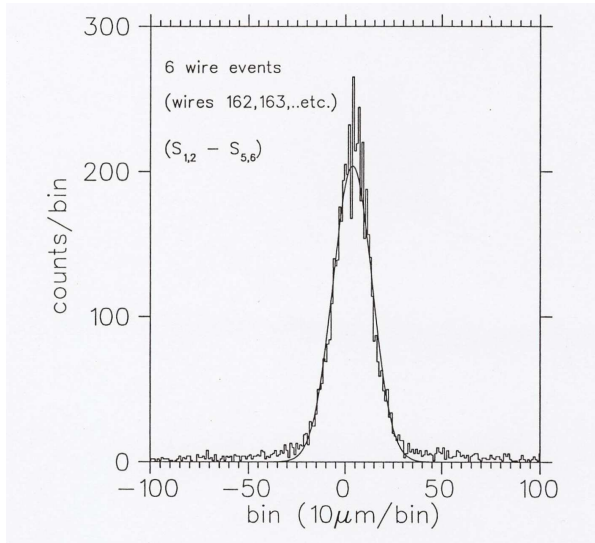


Figure 1.11: *Typical result obtained after fitting a Gaussian lineshape to a distribution of differences in slope D .* (from RTN PhD)

distribution no.	FWHM (μm)	type B uncertainty (%)
1	239.5	1.3
2	220.2	1.3
3	239.0	1.3

Table 1.6: *FWHM($= 2.35\sigma_D$) associated with the three distributions of D , obtained by fitting Gaussians lineshapes to the distributions as described in the text. The type B (non-statistical) uncertainty quoted was obtained using the MINOS subroutine in MINUIT [Jam75, Jam89].*

For the next example 6000 events associated with the $^{55}\text{Mn}(d,d)^{55}\text{Mn}(\text{g.s.})$ reaction at a beam energy of 46 MeV and $\theta = 16^\circ$ were used. These data were acquired with the VDC operated in the manner detailed in the PhD thesis of R.T. Newman. Each event selected was a six-wire event. Three distributions of D were obtained. The first was obtained using $S_{1,2}$ and $S_{5,6}$, the second using $S_{2,3}$ and $S_{4,5}$ and third using $S_{1,2}$ and $S_{4,5}$. Each distribution was fitted with a Gaussian lineshape in order to determine its associated standard deviation, σ_D . A typical fit to one of the distributions is shown in Fig. 1.11. The results obtained from the fitting procedure are summarized in table 1.6. Taking the average of these results one obtains, via equation 1.11, a mean intrinsic cell accuracy (σ_c) of $198.2 \pm 9.4 \pm 2.6 \mu\text{m}$, where the uncertainties are of types A (statistical) and B (non-statistical) respectively. From equation 1.12 it is seen that the position accuracy is dependent on the number of drift cells, n , used to reconstruct the trajectory. In this work (i.e. for the $^{55}\text{Mn}(d,d)^{55}\text{Mn}(\text{g.s.})$ study) n varied between 3 and 10. An average cell position accuracy (σ_x) achievable with the VDC was calculated by assuming that six drift cells were used to calculate the focal plane position. By using this assumption the mean position accuracy was found to be $\sim 80.9 \mu\text{m}$.

1.1.3.1 (p, p') results

The 1.6mm thick Al cover for the focal plane exit window of the K600 is typically a few mm thick. In the second weekend of PR153 (100 MeV protons) it was seen that this Al can result in $\sigma \sim 1.2\text{mm}$ for the position resolution when one forgets to take it out, compare to $\sigma \sim 0.45\text{mm}$ without the metal cover.

200 MeV protons: compare the following PR167: WE2 and WE3; Au tgt HV dependent resolution runs 15134-15136 run 15131 pos sigma = 0.469 run 13498 pos sigma = 0.36

Look at effect on resolution as well as efficiency

Also use PR153 data for protons to see what was pos res for 100 MeV protons

1.1.4 Position resolution simulation

In an effort to understand the resolution problems with the K600 during inelastic alpha particle scattering measurements, a simulation written by K.C.W. Li (<https://github.com/KevinCWLi/K600>) was utilised by P. Adsley to investigate how much the Kapton exit window from the spectrometer or the air gap before the first VDC contributes to an increase in position resolution. In the simulation a beam of 200-MeV protons or alpha particles was incident upon the focal plane from behind the Kapton vacuum exit window. In successive simulations the air gap and the Kapton window were removed to see the resulting effect on the resolution.

For protons (see Fig. 1.12), the black line shows the position resolution without the Kapton window but including the air gap, the blue without the air gap but with the Kapton window, and the green with both the Kapton window and the air gap. It is clear that the focal plane position degradation is primarily due to the Kapton exit window from the spectrometer and that the air gap has a relatively small effect. One is thus forced to conclude that using a helium bubble at the focal plane to mitigate the effects of scattering in the air gap is unlikely to have a large effect on the focal-plane position resolution.

For alpha particles (see Fig. 1.13), the green line shows the position resolution without the Kapton window but including the air gap, the red without the air gap but with the Kapton window and the blue with both the Kapton window and the air gap. Again, the effect of the Kapton exit window is clear. For completeness, a summary of position resolutions in each case is given in Table 1.7.

Stopping Material	Proton position resolution (σ in mm)	Alpha position resolution (σ in mm)
Both Kapton and Air	0.055	0.1005
No Kapton, Air	0.022	0.045
Kapton, No Air	0.051	0.091

Table 1.7: *Position resolution in the first X-wireplane of 200 MeV protons and alphas as per simulation.*

Finally, the effect of the Kapton window may be mitigated somewhat by moving the VDC closer to the spectrometer exit window. This, it should be noted, introduces problems with the VDCs being damaged if the exit window of the spectrometer fails. However, it is clear

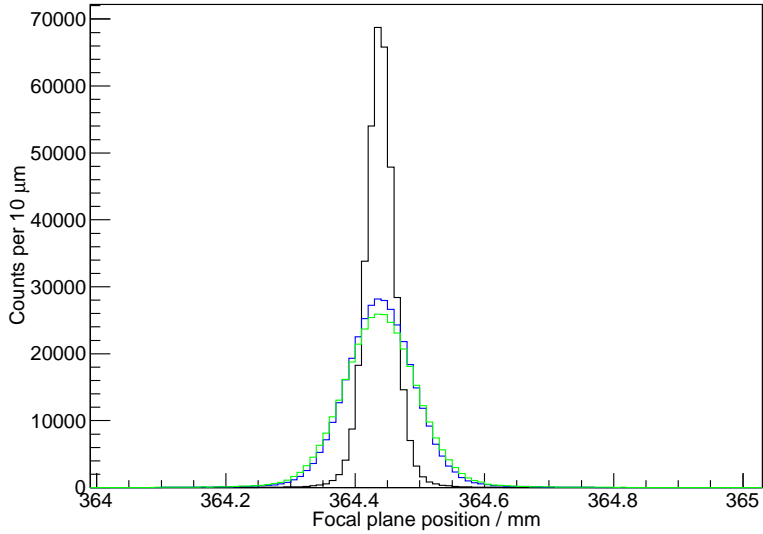


Figure 1.12: Simulation of 200 MeV protons incident on the first X-wireplane, illustrating the effect that different materials has on the position resolution. See text for details.

from Fig.1.14 that the focal plane position resolution is improved considerably by reducing the distance between the focal plane exit window and VDC1. Note also that there are mechanical limitations as to how close this VDC may be moved.

1.1.5 VDC efficiency

The efficiency, ε , of the VDC is an indication of its ability to detect charged particles in the focal-plane and is an excellent monitor for gas quality and functioning of the TDC-cards. It is given by the product of the geometric efficiency (ε_g) and the intrinsic efficiency (ε_i) parameters [Leo87]:

$$\varepsilon = \varepsilon_g \cdot \varepsilon_i . \quad (1.13)$$

/home/neveling/K600/PICS/DETECTORS/PADDLES/NEW/ For the K600 spectrometer at iThemba LABS it was determined with a horizontal drift chamber (HDC) that the particles of a selected rigidity were well-focused in the vertical direction in the focal plane position. In view of this, the geometric efficiency is assumed to be 100%. The intrinsic efficiency on the other hand is defined as

$$\varepsilon_i = \frac{N_{\text{accepted}}}{N_{\text{tot}}} , \quad (1.14)$$

where N_{tot} denotes the total number of events of a selected rigidity recorded in the focal-plane of the spectrometer. The quantity N_{accepted} denotes the number of *valid* events recorded. There are several definitions of N_{accepted} and N_{tot} .

1.1.5.1 Definition 1

Both N_{accepted} and N_{tot} are defined only in terms of events that are within a selected locus in the TOF and paddle PID spectra. In other words, we are only considering a specific charged

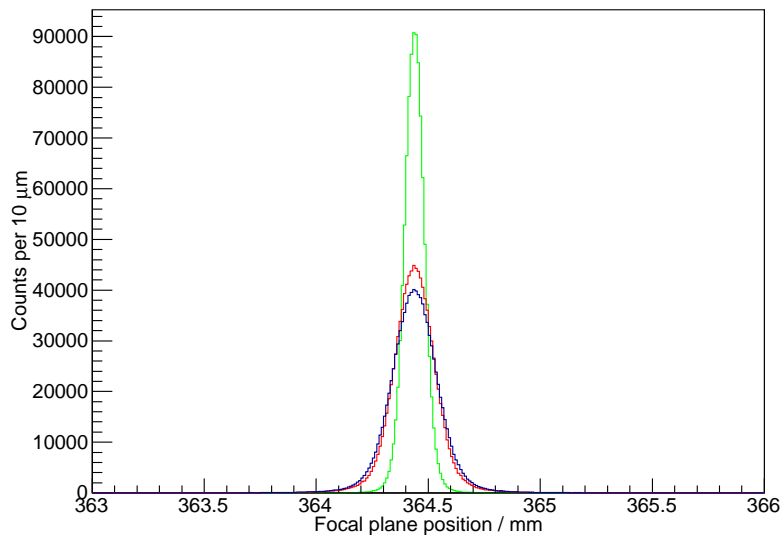


Figure 1.13: Simulation of 200 MeV alphas incident on the first X-wireplane, illustrating the effect that different materials has on the position resolution. See text for details.

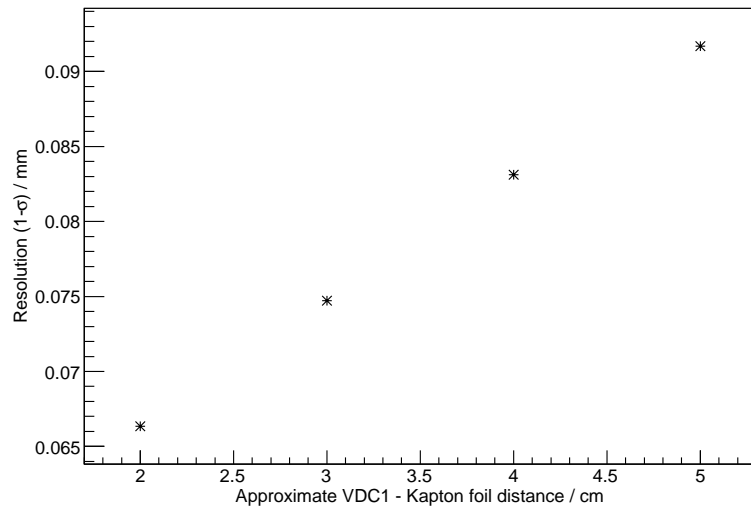


Figure 1.14: Simulation of 200 MeV alphas incident on the first X-wireplane, illustrating the effect of the detector position has on position resolution. See text for details.

particle. $N_{accepted}$ can then be defined as:

$$N_{accepted} = N_{tot} - (N_{\geq \text{max}} + N_{\leq \text{min}} + N_{idt} + N_{nogroup}) , \quad (1.15)$$

where

- $N_{\geq \text{max}}$ is the number of events for which more than 8 wires fired,
- $N_{\leq \text{min}}$ is the number of events for which less than 3 wires fired,
- N_{idt} is the number of events for which the drift-time is outside the valid drift-time range,
- $N_{nogroup}$ is the number of events where a valid three-wire group could not be found in an otherwise valid event.

The average intrinsic efficiency obtained per individual VDC typically varied between 93% and 95%. As an extra condition one can automatically ignore events that passed the PID gate but where no wire or only 1 wire hit are ignored.

1.1.5.2 Definition 2

In a memo by H. Fujita (25 June 2004) the efficiency for X1 was defined as follows:

$$\text{Eff} = \frac{\text{Number of good events in X1, X2 and Y chambers}}{\text{Number of good events in X2 and Y chambers}} \quad (1.16)$$

If a K600 event satisfies the following requirements it is assumed to be a good event for the X1 and X2 VDCs:

- TOF and Paddle signal are in good regions
- Number of hit wires is 3-6
- χ^2 (reduced) < 1.

For the HDC a good event is defined as

- TOF and Paddle signal are in good regions
- Number of hit wires is 1 or 2

Efficiencies of each chamber for Run 319 (example) are 92%, 92%, 96% for X1, X2 and Y chambers respectively. Therefore the total detector system has an efficiency of 81%.

1.1.5.3 Definition 3

In an RCNP annual report 1989 contribution by Noro *et al.* the detection efficiency of the i'th signal wire is defined as

$$\text{Eff}_i = \frac{N(\text{i}'\text{th and 2 adjacent signal wires hit})}{N(2 \text{ adjacent signal wires hit})} \quad (1.17)$$

This is the same manner in which the efficiency is calculated for the Jlab Hall A VDCs [Fis01].

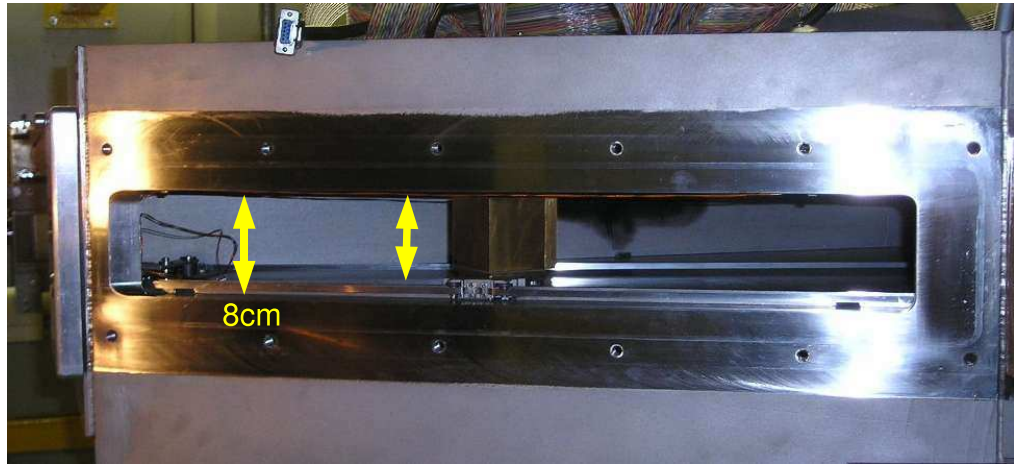


Figure 1.15: The high dispersion focal plane opening of the K600 vacuum chamber. The arrow on the right indicates the effective size of the vertical opening, which is 7cm and is also the case for the medium and low dispersion planes.

1.2 Spectrometer transmission

The nominal height of the opening of the K600 vacuum chamber at the focal planes is 8cm. However due to the drive mechanism for the focal plane beam blocker (refer to section 6.5) one centimeter on the bottom is blocked out.

The remainder of this section is from Richard Newman's PhD thesis on the study of the $^{55}\text{Mn}(\text{d},^3\text{He})^{54}\text{Cr}$ ($E_{\text{d}} = 46$ MeV) reaction, published in Phys. Rev. C54 (1996) 1773.

One of the concerns related to the horizontal transmission through the spectrometer was the possibility that, for a collimator having a specific width, particles which are supposed to move through the spectrometer hit instead the spacers separating the yokes of the spectrometers's magnets, thereby resulting in a loss of yield at the focal plane. A schematic two-dimensional representation of the trajectory associated with a particle moving from the target through the spectrometer magnets to the focal plane is shown in Fig. 1.16. With respect to the vertical transmission, concern surrounded the possibility that, for a collimator having a specific height, particles which are supposed to move through the spectrometer hit the top or the bottom of the dipole magnets and/or the H -coil, also resulting in a yield loss at the focal plane.

The horizontal and vertical transmission through the spectrometer was studied using a 51.0 mm thick brass collimator which comprised seven slots, each of which could be independently blanked or opened. The location and dimensions of these slots on the collimator are

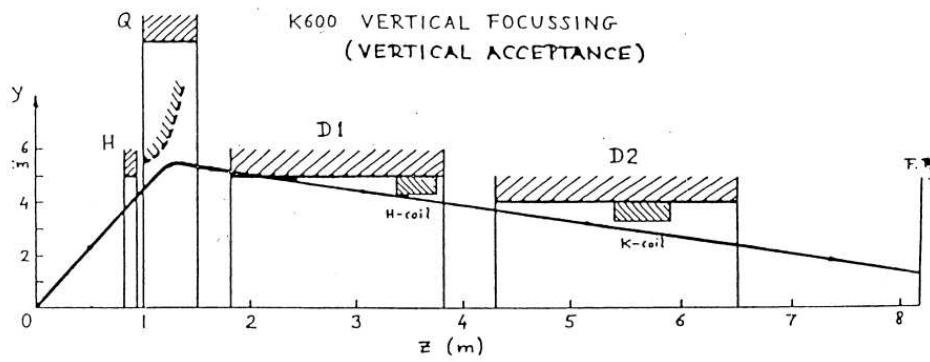


Figure 1.16: Schematic two-dimensional representation of the trajectory associated with a particle moving from the target to the K600 spectrometer focal plane (reproduced from Ref. [Sch86]).

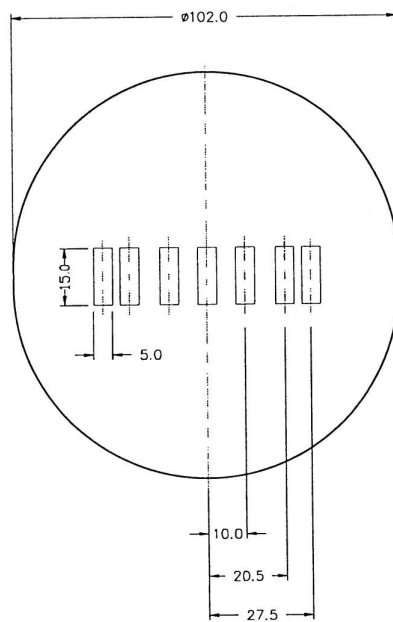


Figure 1.17: Drawing of the 51.0 mm thick variable-slot/multi-slot collimator used to study spectrometer transmission. All dimensions are in mm.

shown schematically in figure 1.17. In order to check the horizontal transmission the collimator was positioned inside the collimator carousel with its slots orientated horizontally (i.e. as shown in figure 1.17) and the spectrometer tuned for $H(p,p)$ ($E_p = 66$ MeV, $\theta = 20^\circ$) elastic reaction using a CH_2 target. Relative differential cross sections associated with this reaction were then measured with first the extreme left slot and then the extreme right slot open. The centre of each of these slots was 27.5 mm from the centre of the collimator. The collimator was then rotated through 90° resulting in the slots being orientated vertically. Measurements of the same cross section were then made with first the extreme top slot and then the extreme bottom slot open in order to check the vertical transmission (all other experimental parameters remained unchanged).

collimator orientation	open slot	differential cross section (arb. units)
horizontal	extreme right	327.6 ± 3.2
	extreme left	323.8 ± 3.4
vertical	extreme top	328.3 ± 3.3
	extreme bottom	331.0 ± 3.3

Table 1.8: *Results for the measurement of the relative differential cross sections associated with the $H(p,p)$ ($E_p = 66$ MeV, $\theta = 20^\circ$) elastic reaction using extreme slots and different orientations of the variable-slot collimator (see figure 1.17). Only type A (statistical) uncertainties associated with yields are quoted.*

The results of these measurements are shown in table 1.8. All four relative differential cross sections are consistent to within the quoted statistical uncertainties. Given this, and in particular the fact that the two cross sections measured using extreme left and right slots respectively were consistent, no loss of yield due to particles of interest hitting the spacers or the edges of the magnets was indicated. The horizontal transmission for a collimator having a width of ≤ 55.0 mm should therefore be 100%. Furthermore since the two cross sections measured using the extreme top and bottom slots respectively were consistent, no loss of transmission in the vertical direction due to particles of interest hitting the dipole magnets or the H -coil when using a collimator of height ≤ 55.0 mm was indicated.

Chapter 2

Electronics and DAQ: VME and MIDAS

The original CAMAC electronics and XSYS data acquisition system (see Appendix B) was replaced in the winter of 2009 with VME electronics and the MIDAS DAQ [Mid]. An overview of the K600 trigger electronics for the VME DAQ is given in Fig. 2.1.

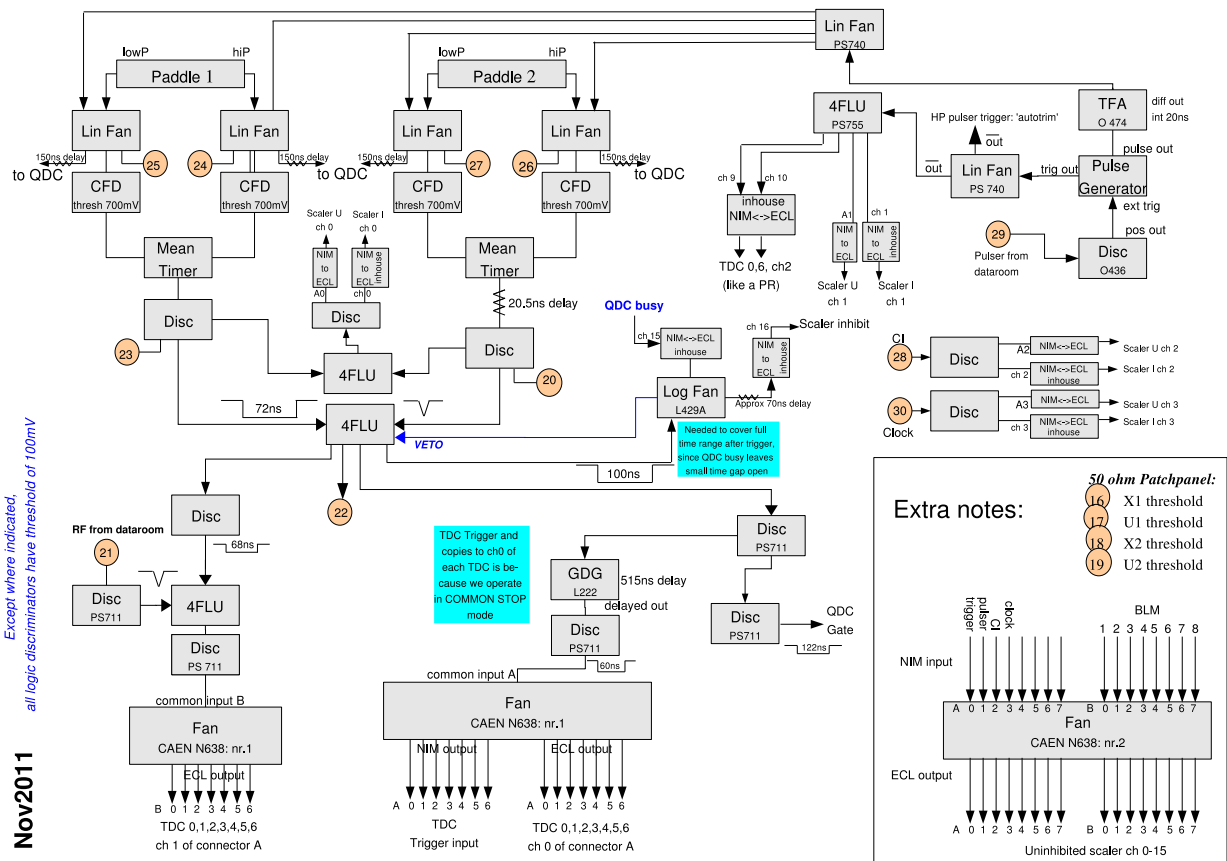


Figure 2.1: A typical layout of the K600 trigger electronics.

2.1 Hardware notes

- Data for the TDC and QDC (and ADC if it is used) is acquired event-by-event. The scaler data is acquired at 1Hz.
- The VME QDC (Caen V792) has a fullscale range of 400 pC.
- The VME ADC (Caen V785) is a 12 bit ADC.
- The VME TDC (Caen V1190) has 100 ps time resolution. It is possible to emulate a common stop mode as described in the user manual of the board through the use of the so-called *Trigger Matching Mode*. In this mode one can define a trigger window with programmable boundaries with respect to the trigger signal. Only the hits belonging to the trigger window will be recorded. If the window position is programmed in order to cover a specific interval before the trigger, you will have the common stop emulation. It is worth to notice that the trigger signal (lemo input) does not have a high time resolution, thus it cannot be used to define the common stop time reference. An accurate time reference must use one of the channels of the board (ECL/LVDS inputs). In other words, your Common Stop signal must be connected to one TDC input channel (for the time reference) *as well as* to the trigger input (for trigger matching).
- The preamp cards are P-TM 005 16 channel preamplifier/discriminator cards from the company Technoland Corporation Ltd. (13-12 Nishimatsubara Mizuho Tokyo, Japan). They are supposed to be copies of the Lecroy 2735-DC preamplifier/discriminator cards. Seventy (70) were purchased during 2006. They had to be sent back for modification immediately on arrival for a minor modification, as the delivered preamp cards were not 100% the same as the one we bought earlier as a test module. We do not have a manual, only the following from email correspondence between Hiro Fujita and the Technoland company as well as a basic electronic diagram:

Required electric power of the new preamp:

0.33A at +5V and 0.6A at -5V.

(0.27A at +5V and 0.56A at -5.2V for the old preamps)

In an email from Hiro on 13 Jan 2011:

The attached drawing was NOT originally prepared by Tecnoland, but by the different company, which made the LeCroy 2735DC compatible preamp card. For some reason, person who ordered this card also asked Technoland to make this card following the circuit drawing. Therefore, Technoland people does not understand whether it is exactly the same as the 2735DC or not and they do not have any documents.

- When connecting the ribbon cables to the preamplifier, make sure that the channel numbering conforms to the order in which it is used at the VME TDC input. For the V1190A the lower channel numbers are at the bottom of the input connector. For the preamplifier cards (both Lecroy and Technoland) the pins at the top of the 34-pin connector (i.e. at the side of the +5V edge connectors) are connected to channel 16. This means that if the purple wire of the ribbon cable is at the top of the VDC connector, then purple should also be at the top of the preamplifier. Figure 2.2 shows some detail from a 2007 logbook on this matter.

11
Saturday 11/8/07

X-chamber and y-chamber pre-amp ribbon cables were found to be connected the wrong way round. Reversed connectors, hand-around at pre-amps and re-soldered.

MUST CHECK RIBBON CABLES PRE-AMP TO TDC'S

Correct polarities, do auto-trim.
Auto-trim looking much better.
10V threshold. This is not good.

Preamplifier
Preamp Panel
Up 10

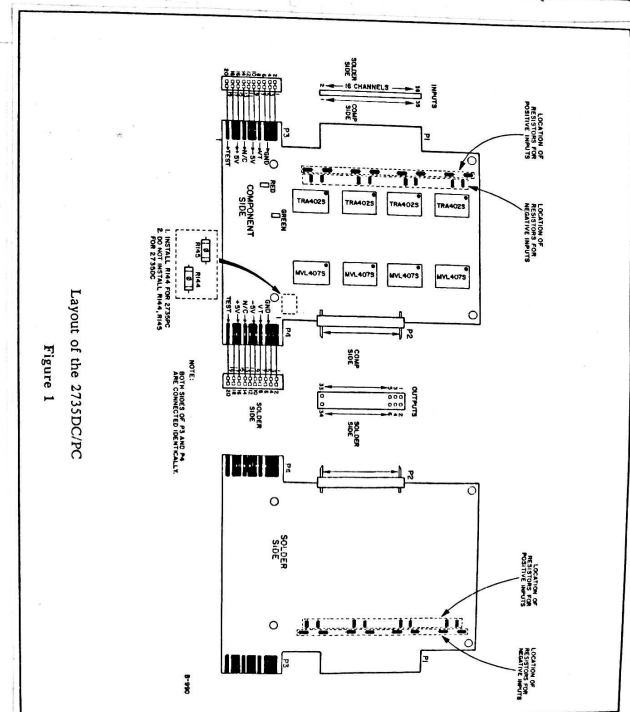


Figure 2.2: Extract from logbook of PR128, where the channel numbering of the preamplifier cards are indicated in.

- Please keep all 50 ohm patchpanel connectors in dataroom terminated. Otherwise there is some potential for signal reflections into K600 vault nim electronics.
- **Important note:** It is very easy to damage the VME QDC with the BNC pulser. Be sure that the signal you put into the QDC is very small. A signal of only 130 mV with a rising edge of roughly 46ns and trailing edge of 300 ns (which is very small signal for the BNC pulser) is already 25% of the full scale!
- The wire number to TDC conversion table depends on the type of detector being used (old or new VDCs) as well as the orientation of the new VDCs (whether X or U wireplane first sees the particles). As an example consider the conversion table for 2 new VDC's in the XU configuration as shown in Fig. 2.3. Table 2.1 lists the conversion table for a old X followed by a new XU detector setup.
- For some reason the Phillips 711 discriminator unit and the BNC BH-1 tail pulse generator does not want to be in the same NIM bin. For various types of NIM bins a \sim 60Hz noise of 20mV was seen on the output of the BNC when the PS711 is also plugged into the NIM bin (i.e. this is not a NIM bin fault). To solve the problem the pulser related electronics are housed in a separate NIM bin.
- The deadtime per event is approximately $6 \mu\text{s}$. This is due the conversion time of the QDC.

2.2 For beginners: Analysis notes (2014 version)

This section assumes that you have MIDAS and ROOT installed on your machine, that the analyzer was successfully compiled and that your **ODB**, **lookup table** files (if you use all 4 wireplanes: lut-x1.dat, lut-u1.dat, lut-x2.dat and lut-u2.dat) and **CableLength.dat** file are good and were set up for you by someone with experience. (For more on these refer to sections 2.3, 2.5 and 2.4.) This section also assumes a singles measurement, i.e. a K600 only experiment.

2.2.1 Getting started

Let us assume that you have already acquired some data and you are eager to take your first look at the results. For now, complete knowledge and understanding of the analysis software is not your number 1 priority¹. The following is therefore intended to get you familiarized with the analysis environment:

1. For each run data is stored in an event-by-event format in a midas file with the extension *.mid*. These files are normally gzipped for space considerations, so look out for files with the extension *.mid.gz*
2. A run is analyzed as follows:

```
./analyzer -i /dir/filename.mid.gz
```

¹It is, however, very important to realize that ultimately you must understand the software to be able to properly analyze the data.

Applicable to the new VDCs only, with X wireplanes seeing particle before the U-wireplane

	preamp	total preamp nr	start at 1 signal wire	start at 0 preamp channel	new VME TDC			start at 0 raw TDC channel ('channel' in f-plane)	start at 0 modified TDC channel ('channelnew' in f-plane)
					TDC nr	connector nr	connector name		
X1	1	1	16	1	0	15	A2	16	31
	2	2	32	17	16	31	B1	32	47
	3	3	48	33	32	47	B2	48	63
	4	4	64	49	48	63	C1	64	79
	5	5	80	65	64	79	C2	80	95
	6	6	96	81	80	95	D1	96	111
	7	7	112	97	96	111	D2	112	127
	8	8	128	113	112	127	A2	144	159
	9	9	144	129	128	143	B1	160	175
	10	10	160	145	144	159	B2	176	191
	11	11	176	161	160	175	C1	192	207
	12	12	192	177	176	191	C2	208	223
	13	13	198	193	192	197	D1	224	229
U1	1	14	1	16	0	15	D2	240	255
	2	15	17	32	16	31	A2	272	287
	3	16	33	48	32	47	B1	288	303
	4	17	49	64	48	63	B2	304	319
	5	18	65	80	64	79	C1	320	335
	6	19	81	96	80	95	C2	336	351
	7	20	97	112	96	111	D1	352	367
	8	21	113	128	112	127	D2	368	383
	9	22	129	143	128	142	A2	400	414
X2	1	23	16	1	0	15	B1	416	431
	2	24	32	17	16	31	B2	432	447
	3	25	48	33	32	47	C1	448	463
	4	26	64	49	48	63	C2	464	479
	5	27	80	65	64	79	D1	480	495
	6	28	96	81	80	95	D2	496	511
	7	29	112	97	96	111	A2	528	543
	8	30	128	113	112	127	B1	544	559
	9	31	144	129	128	143	B2	560	575
	10	32	160	145	144	159	C1	576	591
	11	33	176	161	160	175	C2	592	607
	12	34	192	177	176	191	D1	608	623
	13	35	198	193	192	197	D2	624	629
U2	1	36	1	16	0	15	A2	656	671
	2	37	17	32	16	31	B1	672	687
	3	38	33	48	32	47	B2	688	703
	4	39	49	64	48	63	C1	704	719
	5	40	65	80	64	79	C2	720	735
	6	41	81	96	80	95	D1	736	751
	7	42	97	112	96	111	D2	752	767
	8	43	113	128	112	127	A2	784	799
	9	44	129	143	128	142	B1	800	814

To understand the
TDC connectors are
mapped to TDC chan nr:

Connector name	Channel range	
A1	0	15
A2	16	31
B1	32	47
B2	48	63
C1	64	79
C2	80	95
D1	96	111
D2	112	127

Figure 2.3: Mapping of wire number to TDC channel for 2 new VDC's in an XUXU wireplane configuration.

Wireplane	Preamp	Signal wires	Preamplifier channels	TDC	TDC connector	TDC channels	DAQ channels
X1	1	1 - 8	9 - 16	1	A2	24 - 31	0 - 7
	2	9 - 24	17 - 32	1	B1	32 - 47	8 - 23
	3	25 - 40	33 - 48	1	B2	48 - 63	24 - 39
	4	41 - 56	49 - 64	1	C1	64 - 79	40 - 55
	5	57 - 72	65 - 80	1	C2	80 - 95	56 - 71
	6	73 - 88	81 - 96	1	D1	96 - 111	72 - 87
	7	89 - 104	97 - 112	1	D2	112 - 127	88 - 103
	8	105 - 120	113 - 128	2	A2	144 - 159	104 - 119
	9	121 - 136	129 - 144	2	B1	160 - 175	120 - 135
	10	137 - 152	145 - 160	2	B2	176 - 191	136 - 151
	11	153 - 168	161 - 176	2	C1	192 - 207	152 - 167
	12	169 - 184	177 - 192	2	C2	208 - 223	168 - 183
	13	185 - 198	193 - 206	2	D1	224 - 237	184 - 197
X2	1	16 - 1	1 - 16	4	B1	32 - 47	515 - 500
	2	32 - 17	17 - 32	4	B2	48 - 63	531 - 516
	3	48 - 33	33 - 48	4	C1	64 - 79	547 - 532
	4	64 - 49	49 - 64	4	C2	80 - 95	563 - 548
	5	80 - 65	65 - 80	4	D1	96 - 111	579 - 564
	6	96 - 81	81 - 96	4	D2	112 - 127	595 - 580
	7	112 - 97	97 - 112	5	A2	16 - 31	611 - 596
	8	128 - 113	113 - 128	5	B1	32 - 47	627 - 612
	9	144 - 129	129 - 144	5	B2	48 - 63	643 - 628
	10	60 - 145	145 - 160	5	C1	64 - 79	659 - 644
	11	176 - 161	161 - 176	5	C2	80 - 95	675 - 660
	12	192 - 177	177 - 192	5	D1	96 - 111	691 - 676
	13	198 - 193	193 - 198	5	D2	112 - 117	697 - 692
U2	1	1 - 16	1 - 16	6	A2	16 - 31	800 - 815
	2	17 - 32	17 - 32	6	B1	32 - 47	816 - 831
	3	33 - 48	33 - 48	6	B2	48 - 63	832 - 847
	4	49 - 64	49 - 64	6	C1	64 - 79	848 - 863
	5	65 - 80	65 - 80	6	C2	80 - 95	864 - 879
	6	81 - 96	81 - 96	6	D1	96 - 111	880 - 895
	7	97 - 112	97 - 112	6	D2	112 - 127	896 - 911
	8	113 - 128	113 - 128	7	A2	16 - 31	912 - 927
	9	129 - 143	129 - 143	7	B1	32 - 46	928 - 942

Table 2.1: Mapping of wire number to TDC channel for a old X followed by a new XU detector setup.

where `/dir/` represents the full directory path where the midas files are stored, and `filename.mid.gz` refer to the name of the gzipped midas datafile.

3. A root file is created by the analyzer. The generic name for the rootfile is test.root, and it is created in the directory from which you issue the analyzer command in bullet 1.

4. Open the root file:

```
root test.root
```

Now you are inside the root commandline.

5. You can open the TBrowser by typing:

```
TBrowser t
```

which allows you to browse through the content of the root file (under *ROOT Files*). You will notice that there are 2 data-types in the root file: histograms (one and two-dimensional) and variables (branches) in the TTree² called *DATA*. The histograms are filled as the analysis of the event-by-event data is performed by the analyzer. They are static data structures in the sense that for any particular event the correlation between different variables cannot be recovered. The only way to modify/refill these histograms is to re-run the analyzer with different ODB gates or with software changes to the analyzer. The variables in the TTree, however, still contain the event-by-event character, and can be described as a type of relational database. It is therefore possible to place conditions on any of the variables (branches) in *DATA*, allowing you to easily manipulate the data based on these conditions (also referred to as *gates*). For example, you can view the plot of energy loss in paddle 1 *versus* the energy loss in paddle 2 in the histogram *hPad1Pad2* by typing the following in the root commandline:

```
hPad1Pad2->Draw("col")
```

where the three letters *col* simply indicate that the histograms should be plotted using the standard ROOT color palette. Or you can plot it with the TTree variables

```
DATA->Draw("pad1:pad2>> h2D(999,1,3997,1000,0,4000)", "", "col")
```

where *pad1* and *pad2* are variables (branches) in the TTree named *DATA*, and

```
h2D(999,1,3997,1000,0,4000)
```

is a definition of a 2-dimensional histogram called *h2D*. This histogram is defined as having 999 bins in the horizontal axis, which has the range 1 to 3997, and 1000 bins in the vertical axis, which will range from 0 to 4000. So far *hPad1Pad2* and *h2D* looks the same. But you can start to place conditions on the way in which *h2D* is filled. See for example:

```
DATA->Draw("pad1:pad2>> h2D(999,1,3997,1000,0,4000)", "tof > 5070", "col")
```

where the paddle 1 *versus* paddles 2 histogram is plotted on condition that the *tof* parameter of each event is more than 5070.

6. In general one of the first steps in the data analysis procedure is particle identification (PID). The first step towards PID is plotting the pulse-height of paddle 1 against the TOF, e.g:

²Please refer to ROOT documentation if you require a more detailed discussion of these data types/objects.

```
DATA->Draw("pad1:tof>> h(100,0,4000,100,0,10000)", "", "col")
```

7. Note that some of us prefer to create a script file with pre-defined histograms, e.g.

```
TH2F *hpad1vstof = new TH2F("hpad1vstof", "Pad1 vs tof", 1500, 4000, 5500, 2000, 0, 4000)
```

instead of having to define a histogram in the Draw command. Such a definition can be placed in a script file e.g. histos.C. Then once you are inside ROOT you can execute this script file

```
.x histos.C
```

which then allows you to do away with the histogram definition in the *Draw* command, so that you only have to type:

```
DATA->Draw("pad1:tof>> hpad1vstof", "", "col")
```

8. Further PID can also be carried out by using the energy loss information in the second scintillator, either in combination with TOF:

```
DATA->Draw("pad2:tof>> hpad2vstof", "", "col")
```

or in combination with information from paddle 1:

```
DATA->Draw("pad1:pad2>> hpad1vspad2", "", "col")
```

9. In the previous bullets we discussed how to view data that can be used for PID. Now we discuss how to use that information to create gates. Two-dimensional gates can be created with scripts such as *create_gate_pad1t0f.C*, in the case where we construct a gate for the PID plot pad1 *versus* tof. The script looks something like this:

```
{
TCutG *cut=new TCutG();
CUTpad1t0f = (TCutG*) gPad -> WaitPrimitive("CUTG");
CUTpad1t0f -> SetName("CUTpad1t0f");
CUTpad1t0f -> SetVarX("t0f");
CUTpad1t0f -> SetVarY("pad1");
file20 = new TFile("CUTpad1t0f_run33116.root","NEW");
CUTpad1t0f -> Write();
file20 -> ls();
file20 -> Close();
}
```

You should first plot the variables you want to create the gate for. In this case that is tof on the horizontal axis, and pad1 on the vertical axis.

```
DATA->Draw("pad1:t0f>> hpad1vstof", "", "col")
```

Then you execute the script

```
.x create_gate_pad1tof.C
```

after which you go to the View menu (on the canvas that was created with your plot) to select *Toolbar*. Click on the little scissors on the far right of the toolbar. Now you can select the region you want to gate on by left-clicking at suitable points along the contour of interest. A double-click will indicate that the selection process is finished. A new gate file is now created, and it is called *CUTpad1tof_run33116.root*. This gate file can now be conveniently read back at any point.

Please note that once you executed this script the focus of ROOT will be on the newly created rootfile. If you want to continue your analysis you should change the focus back to your original rootfile by typing

```
_file0->cd()
```

Note however that this is not necessary when you work with chained runs.

10. The gates can be read back with scripts such as *rd_gate_pad1tof.C*:

```
{
TFile * file20 = new TFile("CUTpad1tof_run33116.root","OLD");
TCutG *cut    = (TCutG*) file20 -> Get( "CUTpad1tof" );
cut->SetVarX("tof");
cut->SetVarY("pad1");
}
```

If the C file exists you only have to execute the script in the ROOT commandline:

```
.x rd_gate_pad1tof.C
```

11. Different types of gates can be grouped together in *TCut* definitions such as:

```
TCut CUTbasic = "CUTpad1tof & CUTpad2tof && CUTpad1pad2 && CUTtofX1 && X1flag==0
&& U1flag==0 && U2flag==0";
TCut CUTlimits = "X1pos>-100 && ThSCAT>-2 && ThSCAT<2";
TCut CUTY = "Y1>-25 && Y1<0";
```

which allows for compact *Draw* commands such as:

```
DATA->Draw("X1pos>>hX1pos",CUTbasic && CUTlimits && CUTY,"")
```

Compare this with the following, which does the same thing:

```
DATA->Draw("X1pos>>hX1pos","CUTpad1tof & CUTpad2tof && CUTpad1pad2
&& CUTtofX1 && X1flag==0 && U1flag==0 && U2flag==0 && X1pos>-100 && ThSCAT>-2
&& ThSCAT<2 && Y1>-25 && Y1<0 ","")
```

2.2.2 Comments regarding the analyzer code (2014 version)

Now that you are able to access the data, let us take one step back and briefly discuss the analysis code. From the *Makefile* you will notice that the following files represent the main analysis modules of importance to the user:

```
f-plane.c  
adc.c  
qdc.c  
scaler.c
```

Note that for experiments that only employ the K600 the adc module is not relevant.

1. The file *scaler.c* is responsible for the creation of histograms related to the inhibited and uninhibited scalers, as well as providing an indication of elapsed time (during the data acquisition process), measured in seconds, to the rest of the analysis code through the parameter *runtime*.
2. The file *qdc.c* is mainly used to extract the qdc values for each event from the raw data and passing them on to *f-plane.c*.
3. The file *f-plane.c* contains the vast majority of code used to analyze the raw data from the K600 focal plane. It contains various variable definitions and subroutines, in particular the initialization routine (*focal_init*), begin-of-run (BOR) routine (*focal_bor*), and the event routine (*focal_event*).

Histograms and TTree branches are defined in *focal_init*. The CableLength.dat file is read in (and cable offset table created) and the lookup tables for the wireplanes are loaded into the code in *focal_bor*, and horizontal focal plane position offsets can be programmed into the analyzer at this stage.

2.3 The ODB (2014 version)

The Online Database (ODB) forms part of the MIDAS data acquisition system. From the PSI MIDAS website:

The Online Database contains information that system and user wants to share. Basically all transactions for experiment setup and monitoring go through the ODB. It also contains some specific system information related to the "Midas client" currently involved in an experiment (/system).

The ODB can be accessed from the linux commandline through the *odbedit* utility by typing

```
odbedit
```

If the environmental variable *MIDAS_DIR* is not set in your .bashrc file, or if you analyze a lot of different experiments and do not want a fixed definition of this variable, you must make sure that once you are in the analysis directory you set the environmental variable as follows:

```
export MIDAS_DIR=$PWD
```

One can navigate in the ODB with the `odbedit` commandline in similar fashion to the linux commandline i.e. using the `cd` command. The only sections of the ODB that concerns us in the offline analysis can be found in the directories

```
Analyser/Parameters/focalplane/
```

and

```
Analyser/Parameters/GLOBAL/
```

The parameters in these 2 directories are used in *f-plane.c*. As an example, the gate value *hitof* which can be found in *Analyser/Parameters/focalplane/* is used in *f-plane.c* referenced as *gates.hitof*. On the other hand, the parameter *misswires* in *Analyser/Parameters/GLOBAL/* is used in *f-plane.c* referenced as *globals.misswires*.

If you start a new analysis you have to ensure that you have a functional ODB database. You can load an existing one as follows: enter the ODB utility by typing

```
odbedit
```

Assuming you got a ODB file called `myexperiment.odb` you can load it by typing inside the odb editor

```
load myexperiment.odb
```

While the parameters in *Analyser/Parameters/focalplane/*, used in rudimentary PID selections, angle calculations, line shape correction etc., are routinely changed by the individual doing data analysis, those in *Analyser/Parameters/GLOBAL/* change less often. However, before you start your analysis please ensure that the following parameters in *Analyser/Parameters/GLOBAL/* are correctly set, namely the distances *z_x1x2* and *x_x1x2* (which represents the distance between the first wire of the 2 wireplanes) and the LUT offsets. The LUT offsets should all be at zero at the start of a data analysis campaign. Also, in the initial stages of the analysis, when the LUT files and *CableLength.dat* are created, it is important to have the PID gates in *Analyser/Parameters/focalplane/* correctly set before creating rootfiles that will be used for LUT of offset table creation. The PID gates in the ODB (*lowpad1*, *hipad1*, *lowpad2*, *hipad2*, *lowtof*, *hitof*) are changed as follows:

```
set hipad1 4200
```

If you fail to consider the ODB PID gates before embarking on LUT or *CableLength.dat* creation you may end up creating a LUT for the wrong particle, or smear out the information of the particle of interest by allowing data from background events. Eventually, when a final analysis is performed and you would prefer to make all PID selections by means of the TTree data structure, the ODB PID gates can be changed to include all events.

If you made changes to the current ODB and wish to save these you simply do that in the ODB commandline

```
save filename.odb
```

Reading back this ODB file at a later stage is then simply done as explained earlier on with the `load filename.odb` command in the ODB commandline.

2.4 Cable length offsets

Earlier in this chapter reference was made to the *CableLength.dat* file. In this section we will briefly discuss what this files does and how it is generated.

For each drift cell in the VDC the conversion of measured drift times to drift distances is achieved by a lookup table (LUT). There is only one lookup table per drift plane. Therefore one must ensure that the measured time range for the drifttimes of all the wires per wireplane are similar.

Several factors cause variations (a few ns) in the arrival time of the pulses at the TDC:

1. differences in track lenghts on the VDC PCB between the signal wire and preamplifier channel
2. different response characteristics of individual preamplifier channels
3. variations in length of the different twisted pairs in the ribbon cables that connect the preamplifier output to the TDC input.

These variations has to be corrected if the drift distance calculation, and hence the calculated focal plane position calculation, is to be accurate.

The histogram *hChanVsRefTime* illustrates how the TDC channels fail to align before the application of the correction. The offset-corrected results is shown in the histogram *hChanVsOffsetTime* as well as in the PID selected histogram *hChanVsOffsetTimePID*. Note that these histograms show the TDC channels for all 7 TDCs in numerical order, i.e. the first TDC is represented by channels 0-127, the 2nd by 128-255 etc. On the other hand the histograms *hWireVsOffsetTime* and *hWireVsOffsetTimePID* show the same information, but ordered into the different wireplanes:

- X1 wires 1-198 = channel nrs 0-197
- U1 wires 1-143 = channel nrs 300-443
- X2 wires 1-198 = channel nrs 500-697
- U2 wires 1-143 = channel nrs 800-943

The correction is achieved by adding a time offsets for each TDC channel. All 896 of these offsets, one for each of the 128 channels of the 7 TDCs, are given in the file *CableLength.dat*. The addition is achieved inside the loop through all the TDC dataword in *f_plane.c*, and looks something like this:

```
offset_time = ref_time - int(cableOffset[channel]);
```

Please note that the line number in the file *CableLength.dat* refers to the TDC channel number before conversion from the raw TDC channel numbers to the above channel ranges.

One can edit *CableLength.dat* by hand, or employ a script created by JJ van Zyl, which is explained below.

2.4.1 JJ's script

Use this script together with a statistically significant white tune dataset to get the correct offsets so that all the TDC channels can be aligned. This script determines the minimum gradient of the peak on the short drift time side of the drift time spectra for each individual channel, and calculates the necessary offset relative to a parameter $t0corr$ which is defined in the script.

It is important, but not critical, that you ensure only events for the relevant particle of interest are selected in order to create a good offset table, i.e. you should ensure proper PID selection by means of the ODB.

For the code *JJ_autotrim.C* to work one has to modify the part of the analysis code *f-plane.c* so that the 1D histograms referred to as *hTDC_REF* are filled. Un-comment the line `#define _JJAUTOTRIM` at the top of *f-plane.c*, or if you have an earlier version of the code, uncomment the sections in the code where these histogram are declared, defined and filled. Then make the appropriate changes to *JJ_autotrim.C* (runnumbers, pathnames etc.), analyze the white tune run or runs and execute JJ's script. This will automatically create a new *CableLengthtmp.dat* file.

Some basic notes applicable to the values in *CableLength.dat*:

- The script cannot be expected to provide a proper offset if a particular channel has insufficient statistics. Therefore it is very important that you look at *CableLength.dat* to ensure that the numbers look reasonable. Replace any ridiculously big numbers with a number close to that of its more sane-looking neighbours.
- To move to the locus in e.g. the histogram *hChanVsOffsetTime* to the right, change the value in *CableLength.dat* to a bigger negative number.
- A value of *1* in *CableLength.dat* denotes a change of 1 *in value (not bin)* in the histogram *hChanVsOffsetTime*.
- If your interest is in TDC channel nr *z*, then change the *z'th* line in *CableLength.dat*.

As with all software this script has limitations, and one should not blindly apply it and assume all is right. After you created the new offsets, re-analyze all the white tune runs (after making sure that you re-commented the line `#define _JJAUTOTRIM` and recompiled the *analyzer*). Verify in the histograms *hChanVsOffsetTimePID* and *hWireVsOffsetTimePID* that all the channels are nicely aligned.

2.5 LUT

Accurate information on the position of the particles passing through the focal plane can be obtained once the drift-time characteristics of the detector is established. Knowing the drift-time distribution $\frac{dN}{dt}$, the distance y from the signal wire to the position where the particle passed through a specific drift-cell in the VDC can in principle be obtained from

$$y(t) = \left(\frac{dN}{dy} \right)^{-1} \int_{t_0}^t \left(\frac{dN}{dt'} \right) dt' , \quad (2.1)$$

where t_0 is the arrival time of the particle in the drift-cell, and t is the time at which the pulse appears at the anode [Ber77]. The quantity $\frac{dN}{dy}$ is a measure of the spatial distributions of events in the drift-cell.

A characteristic drift-time distribution is obtained by uniformly illuminating the focal-plane with particles and measuring the average timing response of all the signal wires. A uniform distribution of events in the focal-plane, a situation experimentally obtained by setting the spectrometer magnets to observe particles in the continuum, ensures a constant value for $\frac{dN}{dy}$. For such a *white spectrum* the drift-time distribution $\frac{dN}{dt}$ is thus proportional to the drift velocity $\omega(t)$, and it follows that

$$y(t) = \int_{t_0}^t \omega(t') dt' \propto \int_{t_0}^t \left(\frac{dN}{dt'} \right) dt'. \quad (2.2)$$

With Eq. (2.2) and the drift-time distribution acquired through the above white spectrum a lookup-table is generated, where drift-distances are correlated with drift-times.

2.5.1 Creating a proper LUT

It is important to create a lookup table for each experiment (and each wireplane) as it may differ depending on the high voltage, the gas mixture, the energy and charge state of the particles that cause the ionization, and the physical condition of the chamber. It is furthermore very important to create a LUT for the specific particles that one is interested in. In other words, one has to be careful to use only the PID selected drifttimes, ignoring all the background particles or other particles with different rigidities.

Assuming a suitable white tune data-run exists from which the LUT can be generated, the following procedure can be followed to create a LUT for each wireplane in the focal plane:

- Ensure that the ODB gate settings for the drifttimes, tof and paddle pulseheights are such that you select good drifttimes for only the particle of interest. Also make sure that the lut offsets in the ODB are set to zero.
- Analyze the run you want to use to create the LUTs.
- Create a histogram into which you can copy the drifttime spectrum for the wireplane you are going to create a LUT for:

```
TH1F *h1 = new TH1F("h1","drifttime",14999,0.,14999.);
```

and put the histogram that you are interested in into this newly defined histogram. Assuming you do this process first for the X1 wireplane then:

```
h1=hX1_DriftTimeGood
```

- Now execute the script *DriftTimeInt.C*, which will do the integration and produce a LUT in the file *lutfile*.
- This LUT file should now be copied in the appropriate file used by the analyzer to extract drift distances, e.g. :

```
cp lutfile lut-x1.dat
```

- Do this process also for the other wireplanes.

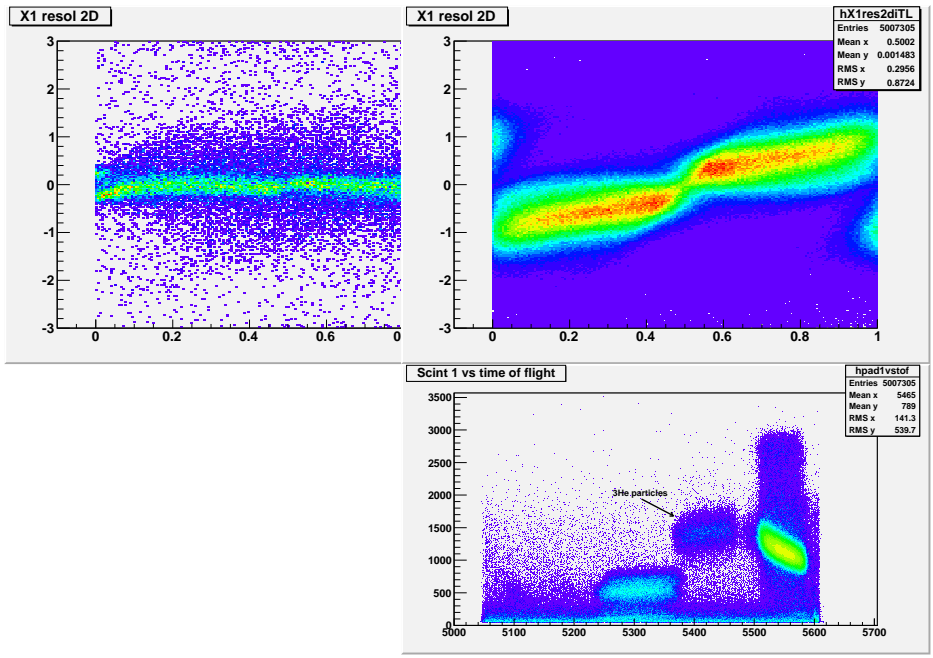


Figure 2.4: Top left: two dimensional resolution plot as optimized for ${}^3\text{He}$, compared to the two dimensional resolution plot for all events, shown in the top right. From the paddle1-versus-tof PID plot in the bottom right it is clear that the ${}^3\text{He}$ particles are not as abundant as the protons, which is represented by the strongest locus. Clearly an optimized LUT offset for one type of particle is not optimized for another type of particle. This is from experiment PR153, $E_{beam} = 80 \text{ MeV}$ and $\theta_{K600} = 30^\circ$.

- If you have a good LUT the driftlength spectrum should have a flat distribution between 0 and 8mm. The 2 dimensional resolution plots must also show straight lines as indicated in Fig. 2.6. A bad LUT results in driftlength and resolution spectra as shown in Figs. 2.7 and Figs. 2.8.
- To correct the LUT a small shift may be required. See Fig.2.5 for an example. This can be performed in the ODB, in the directory

`/Analyzer/Parameters/GLOBAL`

As an example. the offset for the X1 LUT can be changed to -10 with the command

```
set lut_x1_offset -10
```

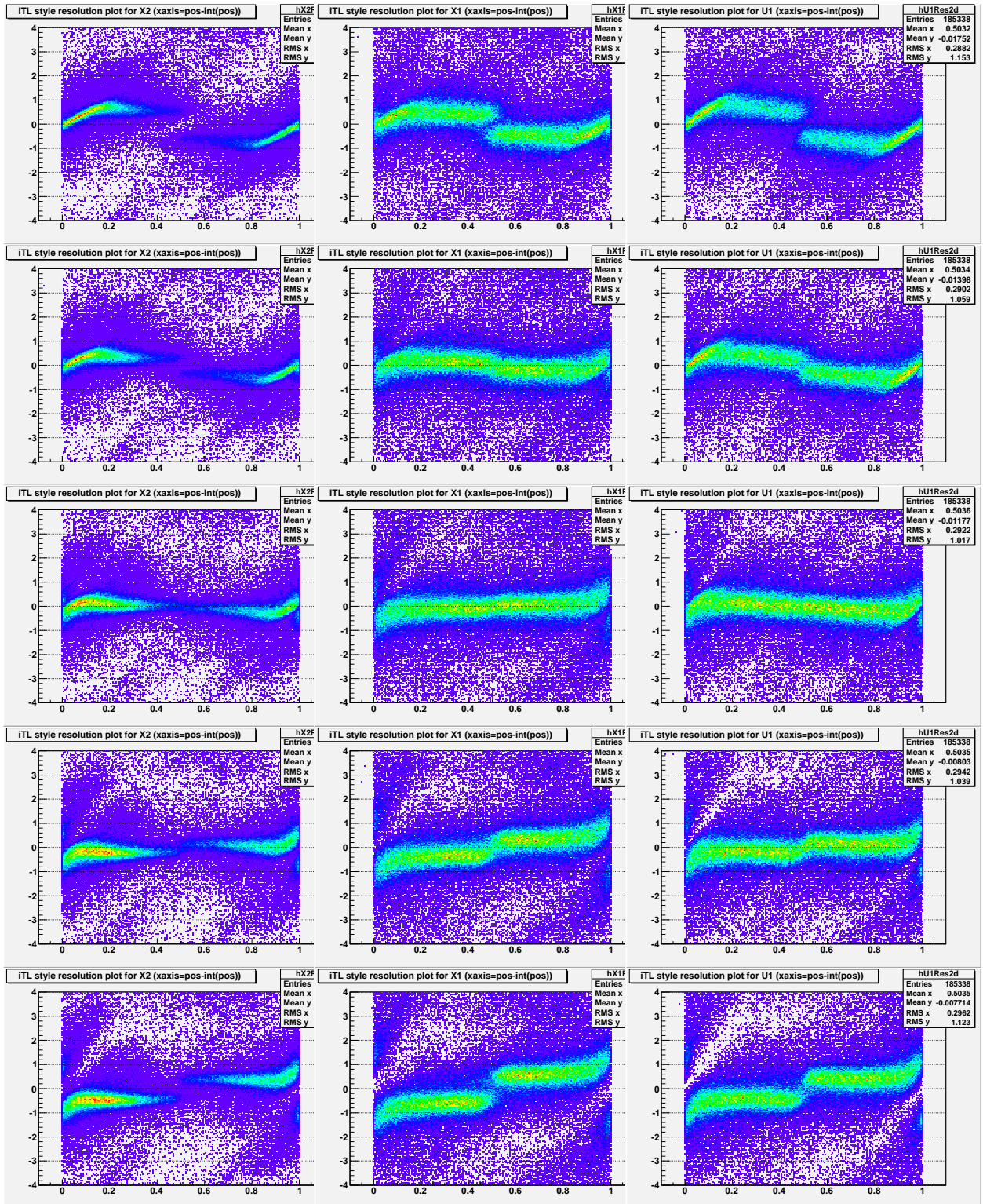


Figure 2.5: Left column: X2 Res2D for LUT offset (from top to bottom): 60,40,20,0,-20. Middle column: X1 Res2D for LUT offset (from top to bottom): 40,20,0,-20,-40. Right column: U2 Res2D for LUT offset (from top to bottom): 60,40,20,0,-20.

2.5.2 Verification of proper LUT

If the LUT is good and the LUT offsets are properly selected the resulting driftlength spectrum should be flat and the 2 two-dimensional plots of the TTree variables *res1 versus res0* and *res8 versus res5* should result in horizontal and vertical straight lines, respectively. This is shown in Fig. 2.6, contrasted with the results of bad LUT offsets shown in Figs. 2.7 and 2.7. Note that too many 0mm or 8mm events in the driftlength spectrum may be due to electronic noise issues, and does not necessarily indicate a problem.

2.6 Typical outline of analysis procedure (2014 version)

Now that you understand the basics, consider the following steps that are required to analyze a set of runs acquired over a specific weekend. This outline should not be considered a fixed template, since the analysis procedure may differ slightly from experiment to experiment. What is described here applies specifically to the zero degree (p, p') experiment PR210, analyzed with the analyzer as it was in 2014.

1. I choose a few runs that can be used in the cable length offset determination. In weekend-1 I select runs 232-234 (note that this procedure should only be performed once per experiment, and it is not necessary to do it for every weekend, provided that the VDC setup did not change). The conditions (DAQ and BEAM) were not very stable during this weekend. But at least it seemed to be somewhat stable during these runs. Prior to the analysis of these runs the *lowtof*, *hitof*, *lowpad1* and *hipad1* parameters in the ODB are changed so that only the particles of interest (protons for PR210) are selected in the pad1vstof spectrum. In order for the analysis code to output useful information (drifttime histograms of each TDC channel) you need to edit *f-plane.c* and uncomment the line

```
#define _JJAUTOTRIM
```

after which you should recompile (i.e. *make*) the analysis software. Now you can analyze runs 232-234. I prefer to rename the resulting rootfiles to something like *autotrim-run00xxx.root* (where xxx refers to the runnumber) so that it is clear for future reference that these runs are for autotrim purposes. The next step is to ensure that your script (*JJ_autotrim-straightline.C*) is pointing to the correct runnumbers and directory for the rootfiles (see lines 14 and 66). Once you are satisfied that this is the case you can start root and execute the script:

```
.x JJ_autotrim-straightline.C
```

The output file is called *CableLengthtmp.dat* and it needs some work before you can use it. For a start, some of the TDC channels which are not associated with drift wires have ridiculously big offset numbers in them, e.g. 2147475648. In fact anything bigger than 1000 should be changed to either 0 or a value similar to those in the immediate region.

Once all the corrections to the file *CableLengthtmp.dat* are made, it should be saved as the file *CableLength.dat* and the file *f-plane.c* should be updated by commenting out the line

```
#define _JJAUTOTRIM
```

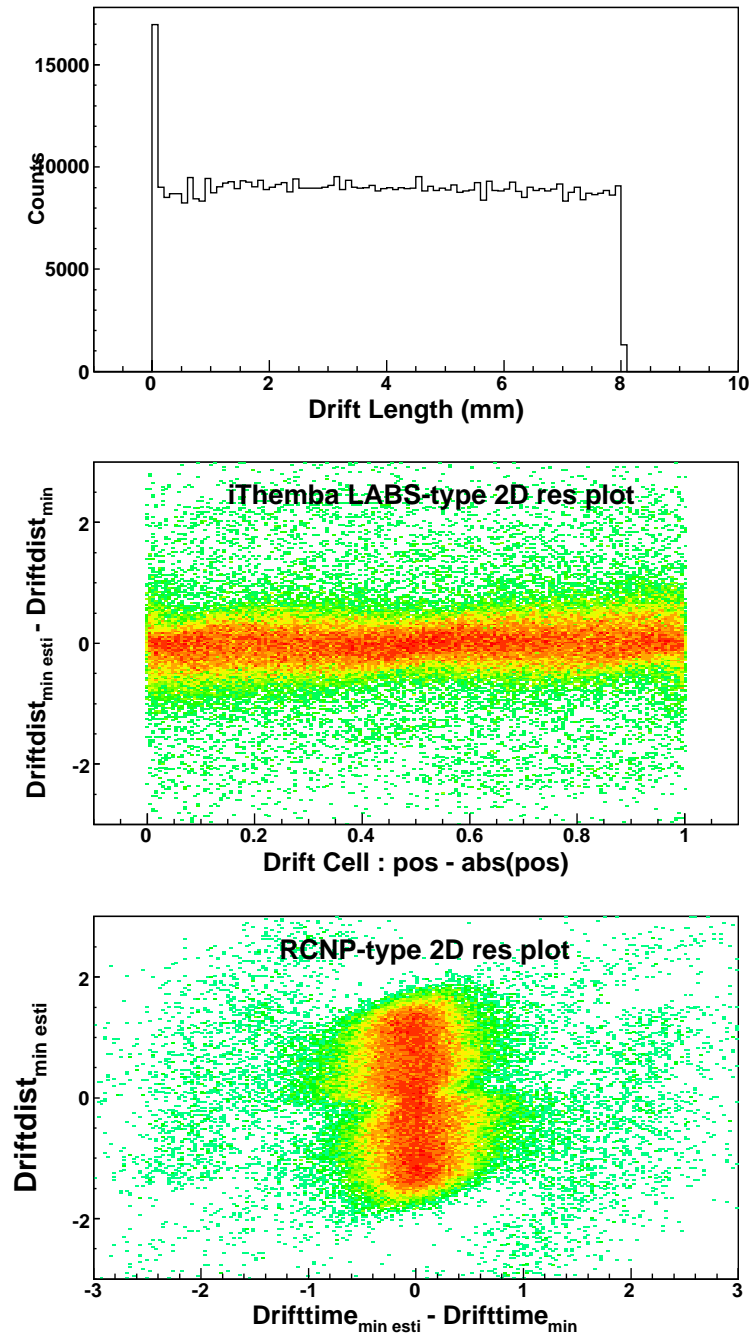


Figure 2.6: Driftlength and resolution plots for a good LUT.

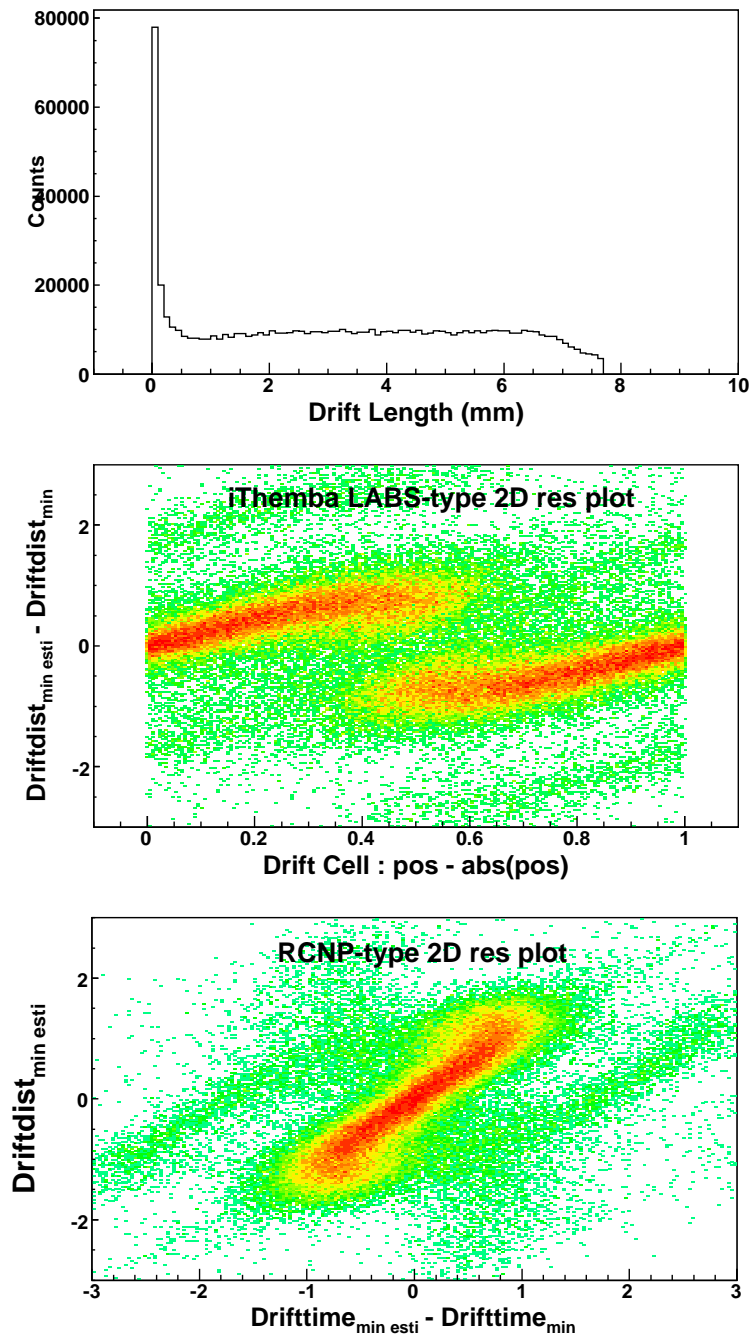


Figure 2.7: Driftlength and resolution plots for a good LUT but in need of a **negative** LUT offset correction.

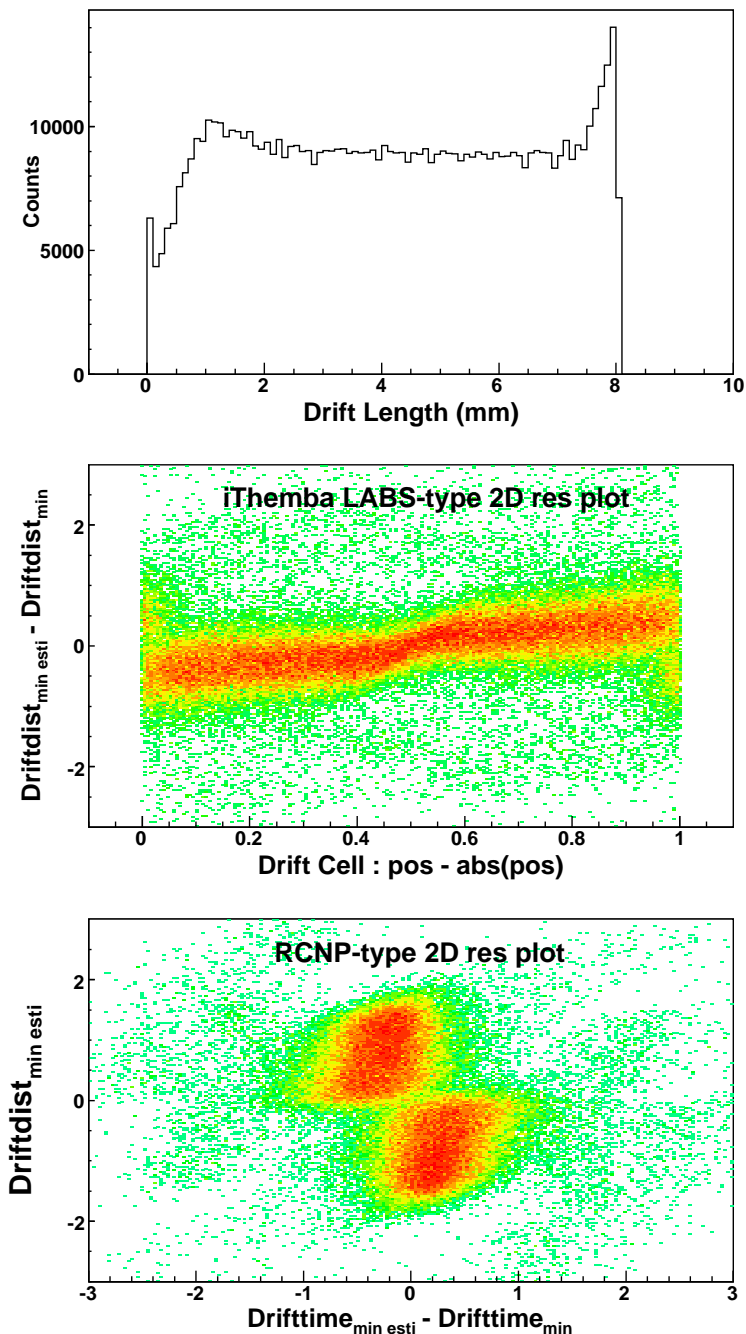


Figure 2.8: Driftlength and resolution plots for a good LUT but in need of a **positive** LUT offset correction.

and recompiling the analyzer. The runs used to create the cable offset file should not be re-analyzed, with the aim to see how well aligned the different TDC channels are. This can be seen clearly in the histograms

```
hWireVsOffsetTimePID->Draw("col")
hChanVsOffsetTimePID->Draw("col")
```

in any of the newly created rootfiles. Visual inspection will indicate which channels needs some offsets correction. The channel numbers in *hChanVsOffsetTimePID* are directly correlated with the row number in the file *CableLength.dat*.

2. Once satisfied that the cable offsets are properly corrected, the next step is the LUT creation procedure. This process is performed with the PID selecton implemented in the ODB. Follow the procedure discussed in section 2.5.1, by using run 234 (it has the most statistics of runs 232,233,234). Note that a LUT should be created for each wireplane. My final lut offset values in the ODB are as follows:

<code>lut_x1_offset</code>	0
<code>lut_u1_offset</code>	10
<code>lut_x2_offset</code>	-10
<code>lut_u2_offset</code>	-5

To verify that you have proper lookup tables refer to section 2.5.2.

3. Now that we have a good LUT and a good cable offset, go into the ODB and open up the PID gates (TOF gates should allow the full TOF range of the experiment, not just that of the particles of interest; similarly open the paddle gates to go from e.g. 1-4000), so that all PID selection in subsequent analysis is done only with software cuts.
4. The next step is to make a horizontal angle calibration from θ_{fp} as measurend in the focal plane by the drift chambers, to θ_{scat} relative to the central angle of the K600. Before you do anything else ensure that the detector separation as used in the software is correct. These are determined by parameters `z_x1x2` and `x_x1x2` in

`/Analyzer/Parameters/GLOBAL/`

in the ODB. For experiment PR210 the values were 285 mm and 515 mm respectively.

For experiment PR210 the runs 128, 132 and 133 represents data-runs with the pepperpot collimator. Data for the $^{44}\text{Ca}(\text{p},\text{p}')$ reaction at 6.9° were acquired for three different magnetic fields, moving the elastic peak from the horizontal position of 305 mm on the focal plane to 650 mm. For each of these runs the position of the the different pepperpot peaks in the ThFP spectrum should be determined. This can be obtained with the help of the primitive peakfitting script *fit-ThFP.C*. For each run the approximate position in X1pos of the elastic peak is to be obtained and entered in the *X[i]* array. The output of this script to the commandline can be save as a file, which will become an input to yet another primitive script *ThFPtoThSCAT-v2.C*.

The parameters

```
a0, a1, a2, b0, b1, b2
```

in the ODB directory

```
/Analyzer/Parameters/focalplane
```

should be set according to your calibration. These parameters are used to calculate Θ_{SCAT} as follows

$$\Theta_{SCAT} = (a0 + a1 \cdot X1pos)\Theta_{FP} + (b0 + b1 \cdot X1pos) . \quad (2.3)$$

The parameters I used are:

a0	-1.01703
a1	-6.25653e-05
a2	0
b0	33.6679
b1	-0.0025703
b2	0

When you have entered the new parameters into the ODB remember to save it with a command similar to:

```
save pr183-we1.odb
```

in the ODB commandline.

5. Analyze a data run (in this case ^{44}Ca runs) from the early, middle and late parts of the weekend. Establish whether the same software gate settings can be used for the whole dataset of this particular weekend. If that is the case, you can create two-dimensional PID gates with the following scripts (depending on the type of measurement you may or may not use all these gates)

```
create_gate_pad1pad2.C  
create_gate_pad1tof.C  
create_gate_pad2tof.C  
create_gate_tofX1.C
```

which can be read back with the scripts such as *rd_gate-pad1tof.C*. Refer to section 2.2 for more information on these scripts.

6. Analyze all the calibration runs of the weekend: in experiment PR210 this means the ^{24}Mg runs. Since there is structure in the position spectrum of these runs one can quickly see which periods of beamtime over a specific weekend may potentially be ignored due to bad data quality. For example, the Mg run00237 in the first weekend of PR210 yielded no meaningful peaks in the position spectrum, which means that the halo was excessive. This potentially means that one or 2 runs prior to and after run 237 may also be of bad quality. Each run should therefore be scrutinized to come up with a final list of useful runs.

7. The calibration runs with its well-defined peaks in the focal plane are used to determine potential drifts in the focal plane position spectrum over time, and is also used to determine the lineshape correction. First of all we will establish which lineshape correction parameters are needed in order to optimize the position resolution. Keep in mind that the lineshape can have both θ_{scat} and y dependence:

```
DATA->Draw("(X1pos+0.6*ThSCAT-0.04*Y1)>>hX1pos",CUTbasic && CUTlimits && CUTY,"")
```

Also note that there can be higher order dependence than the first order examples shown here. Put these lineshape correction factors into the ODB. You will see the parameters

```
a0xcorr, a1xcorr, a2xcorr, a3xcorr, b0xcorr, b1xcorr
```

in the ODB directory

```
/Analyzer/Parameters/focalplane
```

which are used by the subroutine *CalcCorrX* in *f-plane.c*:

```
void CalcCorrX(Double_t X, Double_t Y, Double_t ThetaSCAT, Double_t *Xcorr)
{
    *Xcorr= X - (gates.a0xcorr*ThetaSCAT + gates.a1xcorr*ThetaSCAT*ThetaSCAT
    + gates.a2xcorr*ThetaSCAT*ThetaSCAT*ThetaSCAT
    + gates.a3xcorr*ThetaSCAT*ThetaSCAT*ThetaSCAT*ThetaSCAT
    + gates.b0xcorr*Y + gates.b1xcorr*Y*Y);
}
```

At present the code only makes provision for first and second order terms for the Y dependence, but up to 4th order dependence on the scattering angle. These corrections are built into the TTree variable $X1posC$.

For experiment PR210 (first weekend of 2013 dataset) I used these values:

a0xcorr	-0.4
a1xcorr	-0.1
a2xcorr	-0.14
a3xcorr	0
b0xcorr	-0.02
b1xcorr	0
b2xcorr	0

Please Note! From time to time modifications to the source code are implemented to calculate $X1posC$ from $Y2$ instead of $Y1$, or using a different angle parameter. So please make sure what is the status in the version of the code you have, and ensure that it actually does what you think it does, i.e. PLEASE LOOK IN THE CODE AND VERIFY.

8. Re-analyze the calibration runs after you updated the ODB. Also remember to save your ODB.
9. Now we will determine the position and resolution of the prominent peak(s) in the calibration runs. The difference in peak positions relative to the first calibration run can be established with a script such as *get-peakpos-Mg-we1.C*. Please note that any run that exhibits markedly lower energy resolution should be investigated and possibly discarded in future analysis.
10. In the begin-of-run (BOR) routine in *f-plane.c* you will find a *switch* statement similar to the following:

```
switch(runinfo2.run_number){
    case 154: x1offset=0; printf("run %d: x1 offset= %f \n",runinfo2.run_number,x1offset);
    case 163: x1offset=0.507141; printf("run %d: x1 offset= %f \n",runinfo2.run_number,x1offset);
    case 171: x1offset=0.502258; printf("run %d: x1 offset= %f \n",runinfo2.run_number,x1offset);
    case 172: x1offset=0.53009; printf("run %d: x1 offset= %f \n",runinfo2.run_number,x1offset);
    case 173: x1offset=0.588928; printf("run %d: x1 offset= %f \n",runinfo2.run_number,x1offset);
    case 179: x1offset=0.331604; printf("run %d: x1 offset= %f \n",runinfo2.run_number,x1offset);
    case 238: x1offset=-3.05005; printf("run %d: x1 offset= %f \n",runinfo2.run_number,x1offset);
    case 244: x1offset=-3.08893; printf("run %d: x1 offset= %f \n",runinfo2.run_number,x1offset);
    case 248: x1offset=-2.63568; printf("run %d: x1 offset= %f \n",runinfo2.run_number,x1offset);
}
```

Here you can insert the position difference (in mm) between the prominent peak in the first calibration run relative to the other calibration runs, referred to as *x1offset* in the code. In this case run 154 was the first calibration run, hence the offset value of 0 mm (the *get-peakpos...C* script will create an output that you can paste into *f-plane.C*). Since the change that is made here is to the *C* code, you have to recompile the analyzer executable (using the *make* utility) before moving on to the next step.

11. Re-analyze all the calibration runs again. The energy resolution of the individual runs should now not differ significantly from the *chained* data set.
12. Multiple runs can be chained together with a script that looks typically as follows:

```
{
    TChain *DATAChain = new TChain("DATA","MEGA Tree");
    char name[128];
    Int_t nrofruns=9;
    Int_t run_no[128]={154,163,171,172,173,179,238,244,248};
    for(Int_t i=0;i<nrofruns;i++) {
        sprintf(name,"~/DATA/ROOT/PR210/run00%3d.root",run_no[i]);
        cout<< name<<endl;
        DATAChain->Add(name);
    }
    DATAChain->Draw("X1posC>>hX1pos",CUTbasic && CUTlimits && CUTY,"")
}
```

and is issued in the ROOT commandline as e.g.

```
.x chain-we1-24Mg.C
```

You can now plot any TTree variable for the chained set of runs, as long as you use *DATAChain* instead of *DATA* in the *Draw* commands.

13. Only once you can successfully illustrate that the chained calibration runs have good energy resolution (i.e. you successfully take the peakshifts into account) should you continue to do data analysis of the non-calibration targets. You should now decided which *x1offset* values you will assign to which of your data runs, based on proximity in time of these runs to the various calibration runs.
14. With the begin-of-run (BOR) routine in *f-plane.c* suitably modified to take care of *x1offset* for all the runs of interest, compile the analyzer and analyze all these runs.
15. Once all the data runs are analyzed they should be chained together and suitable cuts/gate conditions should be applied.
16. Some more information regarding the cuts/gate conditions: in section 2.2 it was shown how to define cuts using *TCut*:

```
TCut CUTbasic = "CUTpad1tof & CUTpad2tof && CUTpad1pad2 && CUTtotofX1 && X1flag==0
&& U1flag==0 && U2flag==0";
TCut CUTlimits = "X1pos>-100 && ThSCAT>-2 && ThSCAT<2";
TCut CUTY = "Y1>-25 && Y1<0";
```

In the above *CUTpad1tof*, *CUTpad2tof*, *CUTpad1pad2* and *CUTtotofX1* are all from pre-defined *TCutG* objects that were created with scripts e.g.

```
.x create_gate_pad1tof.C
```

and read back into memory with scripts such as

```
.x rd_gate_pad1tof.C
```

(refer to section 2.2). I prefer to read all the gates in through a single *read-gates.C* script such as the following;

```
{
Char_t name1[30];
sprintf(name1,".x rd_gate_tofX1-we1-run234.C");
gROOT->ProcessLine(name1);
sprintf(name1,".x rd_gate_pad1tof-we1.C");
gROOT->ProcessLine(name1);
sprintf(name1,".x rd_gate_pad2tof-we1.C");
gROOT->ProcessLine(name1);
sprintf(name1,".x rd_gate_pad1pad2-we1.C");
gROOT->ProcessLine(name1);
```

```

TCut CUTbasic = "CUTpad1tof & CUTpad2tof && CUTpad1pad2 && CUTtotoX1 && X1flag==0 &&
TCut CUTlimits = "X1pos>-100 && ThSCAT>-2.5 && ThSCAT<2.5 && Y1>-50 && Y1<50";
TCut CUTY = "Y1>-5 && Y1<20";
}

```

where all the necessary cuts/gates are grouped together in a few *TCut* objects. The *flag* variables ($X1flag, U1flag, X2flag, U2flag$) are used as a test for a valid event in a wireplane. You will find a description of the meaning of different values of the flag in the *raytrace* subroutine in *f-plane.c*. The value 0 is assigned to good events. **The test for a zero value of the wireplane flags is an important and necessary cut/gate condition.**

17. If all went well all that remains now is background subtraction (especially for a small angle or zero degree experiment) and energy calibration. An example of a zeroth order background subtraction procedure for zero degree experiments can be found in the K600 zero degree NIM paper (Nuclear Instruments and Methods in Physics Research A 654 (2011) 2939).

2.7 Outline of analysis of PR236 (Jan 2017 version)

Consider the following steps that are required to analyze a set of runs acquired over a specific weekend. What is described here applies specifically to the zero degree (α, α') experiment PR236, and the state of the analyser in January 2017.

1. We assume that the LUT files and the cable length file provided by iTL staff members are sufficient.
2. There are parameters in the ODB as well as the configuration file, config.cfg³, that must be correctly set. In the config file is listed which focal plane drift chambers are used. In this experiment it was both the new detectors. Also, the distances between these detectors should be defined in the config file. The relevant section of the config file looks as follows:

```

%-----
%  VDC related issues
%-----
VDC1 new
VDC2 new

VDCSeparationDistanceZ 285
VDCSeparationDistanceX 515

```

Later on we will get back to the config file (i.e. when we do scattering angle calibration, line shape correction, energy calibration etc) but for now this is all that is needed.

The lut offset values in the ODB are all set to zero, and the relevant directory in the ODB looks as follows

³If there are multiple .cfg files, how do you know which one is the relevant one? The answer is to see which one is referred to in Parameters.c, specifically in the ReadConfiguration() routine.

```
[local:Default:S]GLOBAL>pwd
/Analyzer/Parameters/GLOBAL
[local:Default:S]GLOBAL>ls
misswires                                2
max_tdc_channels                          1000
min_x_wires                               3
min_u_wires                               3
max_x_wires                               9
max_u_wires                               8
lut_x1_offset                            0
lut_u1_offset                            0
lut_x2_offset                            0
lut_u2_offset                            0
x1_1st_wire_chan                         0
x1_last_wire_chan                        200
x2_1st_wire_chan                         500
x2_last_wire_chan                        700
u1_1st_wire_chan                         300
u1_last_wire_chan                        443
u2_1st_wire_chan                         800
u2_last_wire_chan                        943
```

The other ODB directory that used to be important, where all the lineshape corrections terms used to be, now only has 14 entries and looks like this:

```
[local:Default:S]main>pwd
/Analyzer/Parameters/main
[local:Default:S]main>ls
x1_driftt_low                            6100
x1_driftt_hi                             8050
x2_driftt_low                            6100
u1_driftt_low                            6100
u2_driftt_low                            6100
x2_driftt_hi                             8050
u2_driftt_hi                             8050
u1_driftt_hi                            8050
lowtof                                    2000
hitof                                     7000
lowpad1                                   0
lowpad2                                   0
hipad1                                    4096
hipad2                                    4096
```

There should not be any need for you to change anything in the ODB.

3. Lets start by considering the ^{26}Mg runs of the 1st weekend, for the period after the power failure. The runs of interest are 1093, 1100, 1104, 1108, 1112, 1117, 1123, and 1128. It

is easier to start with a target that has clear structure in the position spectrum such as the magnesium calibration target, as it helps to get an idea of the resolution of the measurement.

Run 1104 is much longer than 1093 and 1100, so I start with that run.

4. First thing is to get a proper PID gate. The best is to make 2-dim gates in the TOF *versus* X1 as well as paddle 1 *versus* TOF plots. For the first I use a script (saved as create_gate_pad1tof.C) that looks like this

```
{
// you have to first plot the

TCutG *cut=new TCutG();
CUTtotoX1 = (TCutG*) gPad -> WaitPrimitive("CUTG");

CUTtotoX1 -> SetName("CUTtotoX1");
CUTtotoX1 -> SetVarX("X1pos");
CUTtotoX1 -> SetVarY("toto");

// uncomment next section only if you want to write the gate to somewhere

file20 = new TFile("CUTtotoX1_run01104.root","NEW");
CUTtotoX1 -> Write();
file20 -> ls();
file20 -> Close();

// in order to get back to the root file you were looking at
// you should cd back into that file:      file->cd()

}
```

and for the second I use a script (saved as create_gate_tofX1.C) that looks like this

```
{
// you have to first plot the

TCutG *cut=new TCutG();
CUTpad1tof = (TCutG*) gPad -> WaitPrimitive("CUTG");

CUTpad1tof -> SetName("CUTpad1tof");
CUTpad1tof -> SetVarX("toto");
CUTpad1tof -> SetVarY("pad1");

// uncomment next section only if you want to write the gate to somewhere

file20 = new TFile("CUTpad1tof_run01104.root","NEW");
CUTpad1tof -> Write();
```

```

file20 -> ls();
file20 -> Close();

// in order to get back to the root file you were looking at
// you should cd back into that file:      file->cd()

}

```

To actually create the gates, plot the TOF *versus* X1 and then execute in the ROOT command line the first script

```
.x create_gate_pad1tof.C
```

after which you go to the View menu (on the canvas that was created with your plot) to select *Toolbar*. Click on the little scissors on the far right of the toolbar. Now you can select the region you want to gate on by left-clicking at suitable points along the contour of interest. A double-click will indicate that the selection process is finished. A new gate file is now created, and it is called *CUTpad1tof_run01104.root*. This gate file can now be conveniently read back at any point.

Please note that once you executed this script the focus of ROOT will be on the newly created rootfile. If you want to continue your analysis you should change the focus back to your original rootfile by typing

```
_file0->cd()
```

Note however that this is not necessary when you work with chained runs.

Similarly plot paddle 1 *versus* TOF and execute the second script

```
.x create_gate_tofX1.C
```

and proceed to create the necessary gate.

5. The gates can be read back with scripts such as *rd_gate_pad1tof.C*:

```
{
TFile * file20 = new TFile("CUTpad1tof_run01104.root","OLD");
TCutG *cut    = (TCutG*) file20 -> Get( "CUTpad1tof" );
cut->SetVarX("tof");
cut->SetVarY("pad1");
}
```

If the C file exists you only have to execute the script in the ROOT commandline:

```
.x rd_gate_pad1tof.C
```

You can create a similar file and use the same method for reading the tof *versus* X1 gate.

- Once the gate files exists I find it efficient to have one single read-gate script such as this saved as *read-gates-we1.C*:

```
{
gStyle->SetPalette(1,0);

Char_t name1[30];

sprintf(name1,".x SCRIPTS/rd_gate_tofX1-run01104.C");
gROOT->ProcessLine(name1);
sprintf(name1,".x SCRIPTS/rd_gate_pad1tof-run01104.C");
gROOT->ProcessLine(name1);

//sprintf(name1,"_file0->cd()");
//gROOT->ProcessLine(name1);

sprintf(name1,".x SCRIPTS/histosPR236.C");
gROOT->ProcessLine(name1);

TCut CUTbasic = "CUTpad1tof && CUTtofX1 ";
TCut CUTlimits = "X1flag==0 && U1flag==0 && U2flag==0 && X1pos>-100 && thetaSCAT>-2
TCut CUTy = "Y1>-15 && Y1<25";
TCut CUTybckg = "Y1>-40 && Y1<-20";
TCut CUTtrigvsCI = "triggerI/CII<3";
}
```

which can be used to read all the necessary gates into the memory with the single command:

```
.x read-gates-we1.C
```

The *flag* variables (*X1flag*, *U1flag*, *X2flag*, *U2flag*) are used as a test for a valid event in a wireplane. You will find a description of the meaning of different values of the flag in the *raytrace* subroutine in *FocalPlane.c*. The value 0 is assigned to good events. **The test for a zero value of the wireplane flags is an important and necessary cut/gate condition.**

Please note that once you executed this script the focus of ROOT will be on the newly created rootfile. If you want to continue your analysis you should change the focus back to your original rootfile by typing

```
_file0->cd()
```

Note however that this is not necessary when you work with chained runs.

The two-dimensional PID gates are indicated by the black lines in the two PID plots in Fig. 2.9.

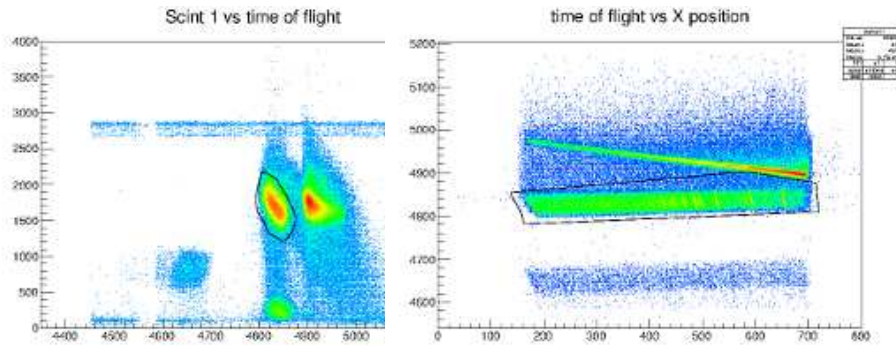


Figure 2.9: PID plots, showing the position of the gated regions (black solid line)

7. Another gate/CUT related topic that should be pointed out is the use of the CI and trigger rates that are available in the TTree during analysis. These parameters now allow us to, on an event-by event basis, decide if we want to discard the data if the ratio of trigger/CI is too big. In other words, we can now easily discard sections of a run where we had localised halo problems. Such a gate/CUT is defined in the file *read-gates-we1.C* in the TCut

```
TCut CUTtrigvsCI = "triggerI/CII<3";
```

The value of 3 used here is not necessarily right. You will have to check the different runs to see what is a sensible ratio limit to use.

8. To see if the PID gates were properly done, plot the position spectrum with and without the PID gates, which can be achieved by using the TCut *CUTbasic* as defined above as the condition in the Draw command:

```
DATA->Draw("X1pos>>hX1pos",CUTbasic,"col")
```

Note that the TCut does not have to be within parenthesis.

9. Analyze a few Mg runs from the early, middle and late parts of the weekend. Establish whether the same software gate settings can be used for the whole dataset of this particular weekend.
10. The next step is to calibrate the angles measured within the approximately ± 2 degrees acceptance of the spectrometer. This is done for the following reasons:
 - To ensure you have a horizontal scattering angle parameter centered around zero for all focal plane positions. This makes it easier to perform line shape corrections.
 - In experiments where one wants to divide the acceptance of the K600 into smaller angle ranges, you need to calibrate the scattering angle. For measurements at big angles it is sufficient to calibrate only the horizontal scattering angle. However, where possible for zero and 4 degree measurements, information about the vertical scattering angle is also required to get accurate scattering angle information. In these cases the K600 should have been operated in vertical off-focus mode.

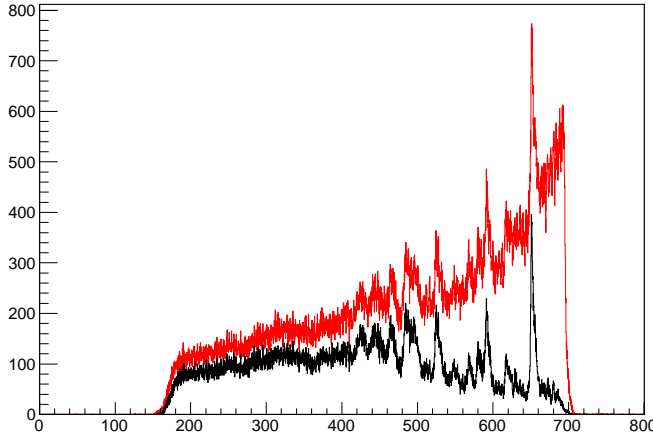


Figure 2.10: Focal plane position spectrum for the X1 wireplane for run 1104 of PR236, with (black line) and without (red line) PID cuts.

For experiment PR236 the spectrometer was operated in vertical focus mode. As the measurements were performed at zero and 4 degrees, this means that the only reason for doing an angle calibration is to make sure we have a scattering angle parameter centered around zero degrees. This is the only reason to make a horizontal angle calibration from thetaFP, the angle of particle tracks as measured in the focal plane by the drift chambers, to thetaSCAT, the scattering angle relative to the central angle of the K600.

The parameters used to get from thetaFP to thetaSCAT are no longer located in the ODB, nor are they hardcoded in *FocalPlane.c*. In the latest version of the analysis code these parameters are in the config file in the VDC related section, and looks as follows:

```

ThFPSCATOffsetTerms 3
0 1
1 35.0792
2 -0.0119133
EndThFPSCATOffsetTerms

ThFPSCATSlopeTerms 3
0 1
1 -1.05242
2 0.00022768
EndThFPSCATSlopeTerms

```

These parameters are used by the subroutine *CalcThetaScat* in *FocalPlane.c* as follows:

```

for(int i=0;i<NThFPSCATOffset;i++)
{
    if(i==0) result = 0;
    if(i>0) result += ThFPSCATOffset[i] * pow(X1,i-1);
}

```

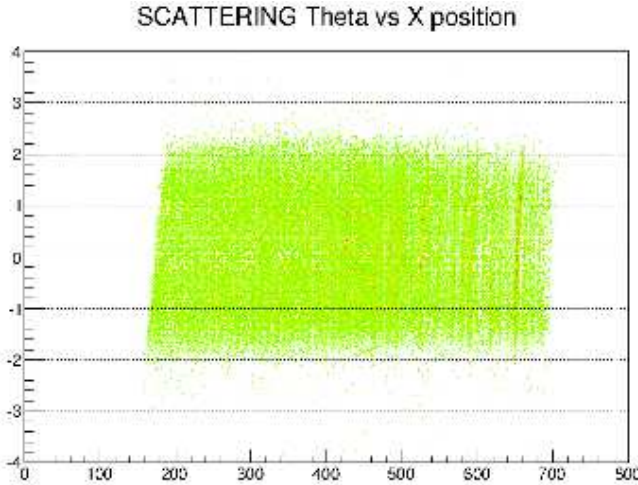


Figure 2.11: Plot of thetaSCAT *versus* the focal plane position spectrum for run 1104 of PR236. Some modifications to the conversion parameters are still required to ensure that the band of events form a rectangle in the $\pm 2^{\circ}$ angle range.

```

    }

    for(int i=0;i<NThFPSCATSlope;i++)
    {
        if(i==0) result = result;
        if(i>0) result += ThFP * ThFPSCATSlope[i] * pow(X1,i-1);
    }
    return result;
}

```

The focal-plane position-sensitive calibration of the horizontal scattering angle can be written in terms of the horizontal focal-plane angle as

$$\theta'_{scat} = \theta_{fp} \sum_{i=0}^2 a_i x_{fp}^i + \sum_{i=0}^2 b_i x_{fp}^i. \quad (2.4)$$

The important thing to check is whether the angle calibration parameters results in a plot of thetaSCAT versus position that looks like a horizontal rectangle, with the angle range approximately ± 2 degrees. The result in Fig.2.11 is already looking ok, but some improvements are still needed.

11. The calibration runs with its well-defined peaks in the focal plane are used to determine potential drifts in the focal plane position spectrum over time, and are also used to determine the lineshape correction.

First of all we will establish which lineshape correction parameters are needed in order to optimize the position resolution. Keep in mind that the lineshape can have both θ_{scat} and y dependence. A very simple correction can look like the following:

```
DATA->Draw("(X1pos+0.6*ThSCAT-0.04*Y1)>>hX1pos",CUTbasic && CUTlimits && CUTY,"")
```

Also note that there can be higher order terms as well, not just the first order terms shown in the example above.

The lineshape correction parameters are no longer located in the ODB. In the latest version of the analysis code these parameters are in the config file in the VDC related section, and looks as follows:

```
ThSCATCorrectionTerms 4
0 1
1 -2.7
2 -0.7
3 0.02
EndThSCATCorrectionTerms

Y1CorrectionTerms 3
0 1
1 -0.01
2 +0.0
EndY1CorrectionTerms
```

These parameters are used by the subroutine *CalcCorrX* in *FocalPlane.c* as follows:

```
for(int i=0;i<NXThetaCorr;i++)
{
    if(i==0)result = X;
    if(i>0)result += XThetaCorr[i] * pow(ThetaSCAT,i);
}
for(int i=0;i<NXY1Corr;i++)
{
    if(i==0)result = result;
    if(i>0)result += XY1Corr[i] * pow(Y,i);
}
*Xcorr = result;
```

As shown the routine first does the thetaSCAT correction

$$X_{corr} = X + X\Theta_{Corr}*\theta_{SCAT}^0 + X\Theta_{Corr}*\theta_{SCAT}^1 + X\Theta_{Corr}*\theta_{SCAT}^2 + X\Theta_{Corr}*\theta_{SCAT}^3 \quad (2.5)$$

and then the Y correction in similar fashion. The code can handle as many parameters as you put into the config file, provided you remember to change the number of parameters (given after e.g. *ThSCATCorrectionTerms* in the config file).

Please Note! From time to time modifications to the source code are implemented to calculate $X1posC$ from $Y2$ instead of $Y1$, or using a different angle parameter. So please make sure what is the status in the version of the code you have, and ensure that it actually does what you think it does, i.e. PLEASE LOOK IN THE CODE AND VERIFY.

12. Re-analyze the calibration runs after you updated the config file.
13. Now we will determine the position and resolution of the prominent peaks in the calibration runs. The difference in peak positions relative to the first calibration run can be established with a script such as *get-peakpos-Mg-we1.C*. Please note that any run that exhibits markedly lower energy resolution should be investigated and possibly discarded in future analysis.

In the begin-of-run (BOR) routine in routine *main_bor* in *main.c* you will find a *switch* statement similar to the following:

```
switch(runinfo2.run_number){
    case 1064: x1offset=0; printf("run %d: x1 offset= %f \n",runinfo2.run_number,x1offset);
    case 1093: x1offset=1.31073; printf("run %d: x1 offset= %f \n",runinfo2.run_number,x1offset);
    case 1100: x1offset=0.754578; printf("run %d: x1 offset= %f \n",runinfo2.run_number,x1offset);
    case 1104: x1offset=-0.309448; printf("run %d: x1 offset= %f \n",runinfo2.run_number,x1offset);
    case 1108: x1offset=-0.585632; printf("run %d: x1 offset= %f \n",runinfo2.run_number,x1offset);
    case 1128: x1offset=-0.0202026; printf("run %d: x1 offset= %f \n",runinfo2.run_number,x1offset);
}
```

Here you can insert the position difference (in mm) between the prominent peak in the first calibration run relative to the other calibration runs, referred to as *x1offset* in the code. In fact, the script *get-peakpos-Mg-we1.C* should print out these lines that you can then just paste into *main.c*. In this example above run 1064 was the first calibration run, hence the offset value of 0 mm. Since the change that is made here is to the C++ code, you have to recompile the analyzer executable (using the *make* utility) before moving on to the next step.

14. Re-analyze all the calibration runs again. The energy resolution of the individual runs should now not differ significantly from the *chained* data set. Test this.
15. Multiple runs can be chained together with a script that looks typically as follows:

```
{
    TChain *DATAChain = new TChain("DATA","MEGA Tree");
    char name[128];
    // WE1
    Int_t nrofruns=8;
    Int_t run_no[128]={1128,1123,1117,1112,1108,1104,1100,1093};
    for(Int_t i=0;i<nrofruns;i++) {
        sprintf(name,"~/DATA/ROOT/PR236/run0%3d.root",run_no[i]);
        cout<< name<<endl;
        DATAChain->Add(name);
    }
    DATAChain->Draw("X1posC>>hX1pos",CUTbasic && CUTlimits && CUTY,"")
}
```

and is issued in the ROOT commandline as e.g.

```
.x chain-we1-24Mg.C
```

You can now plot any TTree variable for the chained set of runs, as long as you use *DATAChain* instead of *DATA* in the *Draw* commands.

16. Only once you can successfully illustrate that the chained calibration runs have good energy resolution (i.e. you successfully take the peakshifts into account) should you continue to do data analysis of the non-calibration targets. You should now decide which *x1offset* values you will assign to which of your data runs, based on proximity in time of these runs to the various calibration runs. Or, if your data (i.e. other than calibration) has sufficiently strong and narrow peaks, the peakfit and offset determination procedure can be performed for those runs directly.
17. With the begin-of-run (BOR) routine in *main.c* suitably modified to take care of *x1offset* for all the runs of interest, compile the code and analyze all the runs.
18. Once all the data runs are analyzed they should be chained together and suitable cuts/gate conditions should be applied.
19. If all went well all that remains now is background subtraction (especially for a small angle or zero degree experiment) and energy calibration. An example of a zeroth order background subtraction procedure for zero degree experiments can be found in the K600 zero degree NIM paper (Nuclear Instruments and Methods in Physics Research A 654 (2011) 2939).

2.8 Analysis of coincidence experiments (Jan 2016 notes)

For the purposes of this CAKE analysis guide, we assume that you are using the official K600 analyser, as found on the Github repository github.com/padsley/k600analyser. You are strongly encouraged to join the list of collaborators on the Github repo.

The purpose of the SiliconData class and the related sort code (MMM.c in this case) is to sort the silicon data, placing conditions on the front-back energy etc. The silicon channels are set according to the config (.cfg) file. You can see how to use that code by looking within the prototype code. In summary, for CAKE (or anything else) you set the relevant ADC and TDC channels for that detector and give the location of the ADC and TDC calibration files.

The structure of the SiliconData class and the associated sort codes bears a brief mention. The SiliconData class is basically storage for information about the silicon detectors. The sort codes (e.g. MMM.c) populate the SiliconData class and then the SiliconData class is written out in the output ROOT file. SiliconData includes useful functionalities such as checking to see that all of the SiliconData class items have been properly populated and clearing the event when that event is done. I would suggest that you take a moment to read through the SiliconData.c/h and MMM.c/h codes to see how they operate before you try to use them.

The procedure for sorting silicon data is:

1. The code first runs multiTDC.c - this is a code which looks to see how many TDC hits per TDC channel there were in the event and checks to see that there aren't too many. It's currently (July 2016) is a slightly incomplete form and should rather throw error messages instead of fixing all of the TDC problems. If you see lots of error messages, this is likely why. You may have to fix multiTDC. Sorry. Contact me (Phil) if this comes up.

2. The code next loops over TDC events. It looks for a hit in a TDC channel corresponding to the front of a silicon detector.
 3. Now the code loops over TDC events again and looks for a hit in a back TDC channel and also checks that the two TDC channels correspond to the same detector. If you have not put both front and back TDC values into the DAQ, you're going to have to comment this out because there are no back TDC entries to match with.
 4. The code now works out which detector you've hit and saves that information.
 5. Now the code loops over the ADC values for the front and finds the ADC value for the same silicon strip that was found for the TDC front hit - N.B. this is silly because I should have just got that particular ADC value right from the start and not worried about looping over the detector.
 6. This procedure is repeated for the ADC values from the back.
 7. The code now computes the energy measured for the front and back strips. Then it compares these values and uses this as a test as to whether the event should be accepted. Currently this is done by saying $|E_{\text{front}} - E_{\text{back}}| < 3\sigma$ where σ is a resolution parameter set at the top of MMM.c (for the MMM sort code).
 8. If this conditions is met, then the event is stored with a variety of information (angles,
- The first step is to enable the relevant sections of the sort code - more detailed instructions can be found at <https://github.com/padsley/k600analyser/wiki> but briefly, you must uncomment the lines:

```
#define _SILICONDATA
#define _MMM
```

Having done this, you will now be sorting the data with the silicon detector sort enables in the output.

- Its often helpful to include the RawData class - which dumps ADC, calibrated ADC, TDC and QDC values into the output file - when running the code for the first few times as this helps with identifying possible problems in the data. To do this, uncomment:

```
#define _RAWDATA.
```

- Next, you need to define what detectors were used and what channels in the ADCs and TDCs they were plugged into. This is done in the .cfg configuration file. That file contains instructions for how you should include those mapping values - this configuration file is read in automatically when the code is run.
- Once you have set the .cfg file, you must set the correct path in Parameters.c. Search for the function ReadConfiguration(). The line

```
input.open("name_of_file.cfg");
```

should be changed to whatever is appropriate in your case (i.e. the path to your configuration file).

- Having done this, the next main task is to calibrate the silicon detectors. This is usually done using a 228Th or a 226Ra calibration source. An example of a code which can be used for this calibration can be found at: <https://github.com/padsley/AlphaCalibration> though it will probably require some minor modifications to be used on your system. More details can be found on the wiki on that repo.
- Once you have calibrated your ADCs, you should save that information in a text file and add the relevant path to that file after CalibrationFile in config.cfg. The format is: ADC_Channel_Number Offset Gain and the calibration is given by $E = c + mx$ where c is the offset, m the gain and x the ADC value recorded (from 0 to 4095 for the CAEN ADCs). This file **must** end with ‘eof’ to tell the code that it’s the end of the file.
- Having done that, you should now have a working silicon sorting algorithm. You should try resorting your alpha-particle calibration file with the calibration included to make sure that it produces the correct spectra.
- The next step is to calibrate the TDCs. I (PA) did this for PR244 data using beam data. In theory, it can be done using pulser data for experiments with lower statistics (such as (p, t)). I haven’t tried it, though. The calibration procedure was very simple and can be found at <https://github.com/padsley/TimeForCAKE>. It might not work for pulser data, though. You should bear this in mind if you use TimeForCAKE.
- You then need to resort using the calibrated TDCs in your analysis. This will change the branch in the data called SiliconTimeOffset
- The singles analysis proceeds in the same way as described elsewhere. However, for the coincidence spectra, in order to speed up analysis, I filter the ROOT trees using the focal plane conditions (PID, Y etc.) and the CAKE PID. This can be done by using the command:

```
DATA->CopyTree("CUTpad1vstof && !X1flag && !X2flag && !U1flag
&& !U2flag && Y1>-25 && Y1<15 && CUTSiliconPID_protons");
```

for example (in this case, this selects proton decays in CAKE). You can then save this as a new file which is gated on proton decays.

2.8.1 CAKE PID

In order to use the silicon time to determine the particle species, the silicon times must first be aligned in software to correct for channel-by-channel differences in the timing behaviour of the system. To do this, a channel-specific offset is subtracted so that the peak of the timing distribution for each channel sits around 0. Plotting these times versus the energy deposited in the silicon detectors (Figure 2.12(a)), reveals two indistinct loci corresponding to protons above and alpha particles below. This distortion in the separation of the time-of-flight is due to how the timing events are processed in the K600 data acquisition: the recorded time is the time difference between the focalplane trigger and the hit in the silicon detector. However, the timing

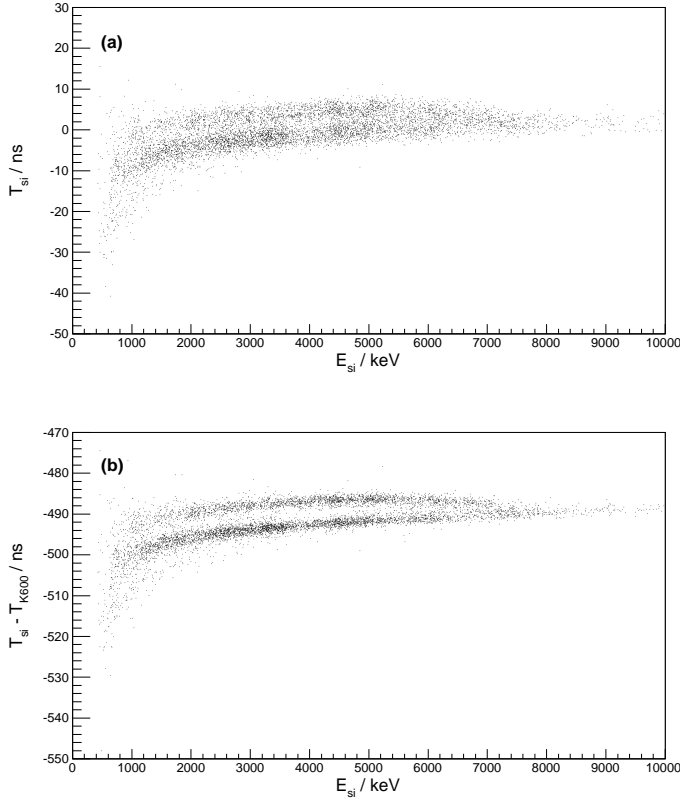


Figure 2.12: Relative time-of-flight to the CAKE vs silicon energy loci for (a) the case where no correction is made for shifts in the trigger time relative to the RF pulse and (b) with the correction in the shift of the trigger time included. The upper locus, terminating at around 7000 keV represents the observed protons and the lower locus is represents α particles.

quantity of physical interest is the time difference between the beam pulse hitting the target and the hit in the silicon detector. The trigger time (and thus the reference time) is not a fixed quantity: it has a variation relative to the RF signal from the accelerator (and thus the time that the beam-pulse hits the target) due to the different possible flight-paths through the K600 magnetic spectrometer. To correct for this effect, the silicon time used in particle-identification is the difference between the silicon time and the spectrometer time-of-flight. This results in a clearer separation of the PID loci for CAKE, as shown in Figure 2.12(b). A simplified diagram showing the relationship between the various timing quantities is shown in Figure 2.13: from this figure, it is clear that the silicon time-of-flight relative to the accelerator RF is given by $T_{si} - T_{K600}$.

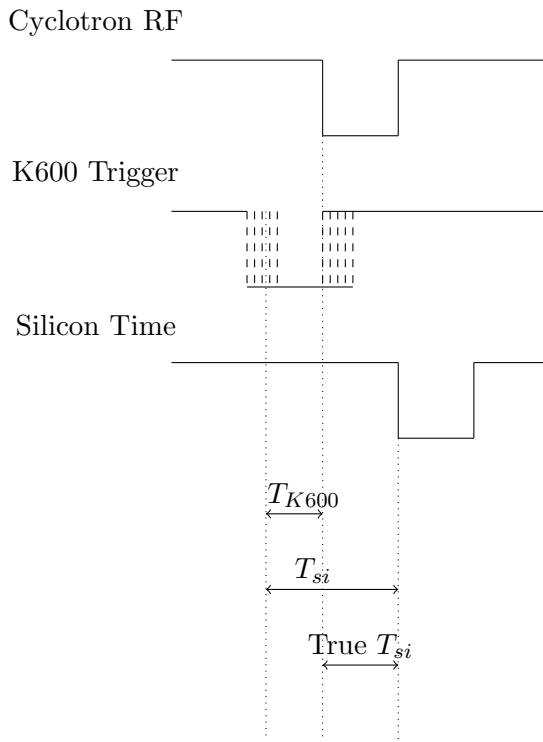


Figure 2.13: Simplified diagram to show the relative timing information for the RF reference from the cyclotron, the K600 trigger time and the time of the event recorded in the silicon detectors. Note that the K600 trigger time is drawn with a jitter (dotted lines) to account for the different flightpaths through the spectrometer. The spectrometer time-of-flight as previously defined is labelled ' T_{K600} '. The silicon time, as recorded by the data acquisition, is ' T_{si} '. The true silicon time-of-flight is labelled 'True T_{si} '.

2.9 Analysis of PR259 (Daniel's notes)

Experiment PR259 studied the ${}^9\text{Be}({}^3\text{He},t){}^9\text{B}$ reaction at a beam energy of 50 MeV in June 2016. The focal plane detectors consisted of an XU MWDC and a 1/2 inch paddle in the medium dispersion focal plane. Particle decay information was acquired by using the CAKE in coincidence with the K600.

2.9.1 Correction using TOF

2.9.1.1 How to plot pad1 v.s. tof

In order to select the particles of interest (in this case tritons), plotting "pad1 v.s. tof" is required. The command to do it is:

```
DATA-> Draw("pad1:tof","!X1Flag && !U1Flag")
```

And the plot obtained is shown in Fig. 2.14

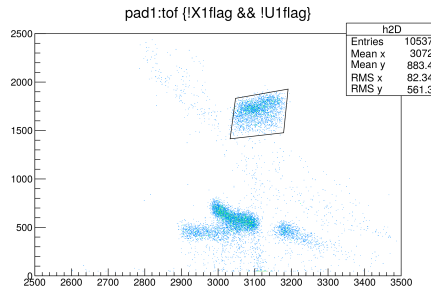


Figure 2.14: Paddle-one versus time-of-flight for the ${}^{26}\text{Mg}({}^3\text{He},t){}^{26}\text{Al}$ reaction, black-line box represents the selection of the particles of interest (tritons).

Once the gate is created, it has to be saved (**cutTritonsMg.C**) and edited. Where it says

```
TCutG *cutg = new TCutG("CUTG",10);
```

the term "**CUTG**" has to be changed for that of the cut:

```
TCutG *cutg = new TCutG("cutTritonsMg",10);
```

Then, on the command line, if the cut is required, first we type:

```
x cutTritons.C
```

It is important to mention that the gate in Fig. 2.14 correspond to those tritons of interest for a ${}^{26}\text{Mg}({}^3\text{He},t){}^{26}\text{Al}$. Just for clarification, the gate that will be used further ahead during the analysis of the ${}^9\text{Be}({}^3\text{He},t){}^9\text{B}$ reaction is shown in Fig. 2.15.

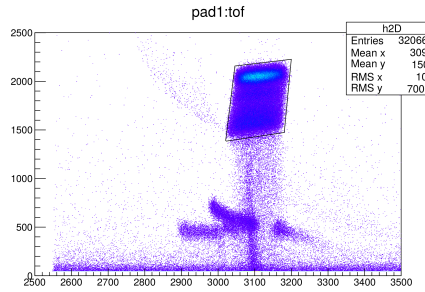


Figure 2.15: *Paddle-one versus time-of-flight for the ${}^9\text{Be}({}^3\text{He},t){}^9\text{B}$ reaction, black-line box represents the gate used for the selection of the particles of interest (tritons).*

2.9.2 Correction using TOF (θ_{scat})

Lineshape correction by means of the TOF is only done in experiments such as this where only one focal plane detector was in use. First the Focal Plane position is plotted without the "cutTritonsMg" cut as shown in Fig. 2.16 where it is possible to observe the contribution of the background, for which some "flags" and corrections have to be implemented and will be explained further ahead.

For plotting the focal plane position, in the terminal it is typed:

```
DATA-> Draw("X1pos>>h1(2000,0,700)", "cutTritonsMg && !X1Flag && !U1Flag", "col")
```

Notice that the selection of the tritons by the cut is included in "**cutTritonsMg**" as well as the two X1 and U1 flags.

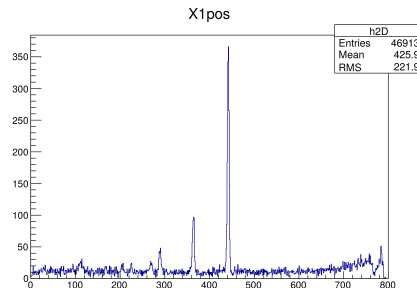


Figure 2.16: *Focal plane position (X1pos) without any cut.*

The next step will be the correction of the "tof v.s. X1pos" plot, for which the vertical loci shown in Fig. 2.17 should be straight vertical lines which are clearly not by looking the zoom-in shown in Fig. 2.18. This effect is due to the momentum distribution of the particles that reach the focal plane, and so, some bend more than others, therefore the TOF is different (**explain it better?**).

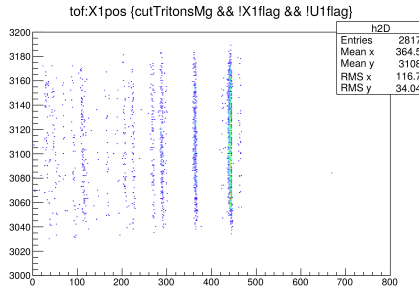


Figure 2.17: *TOF v.s. focal lane position (X1pos).*

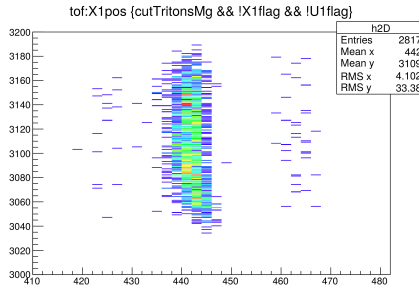


Figure 2.18: *Zoom-in of Fig. 2.17, TOF v.s. Focal Plane position (X1pos).*

2.9.2.1 Creating a graph to plot some selected points for the correction

For the correction, some points in Fig. 2.18 are selected and a polynomial of order two was used for the fitting as shown in Fig. 2.19. For the "y" coordinates, 3120 was subtracted to set the middle of the vertical line at zero.

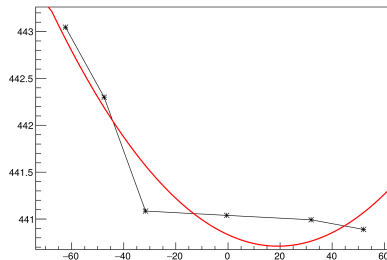


Figure 2.19: *Plot and fitting of the set of points selected in Fig. 2.17.*

Here the steps for the fitting and plotting of the selected points typed in the terminal, for which first a "TGraph" has to be created:

```
TGraph *g =new TGraph()
g->SetPoint(0,52.03,440.899)
g->SetPoint(1,31.91,440.992)
g->SetPoint(2,-5.17,441.039)
```

```

g->SetPoint(3,-31.65,441.085)
g->SetPoint(4,-47.54,442.300)
g->SetPoint(5,-62.37,443.047)
g->Draw("AL*")
g->Fit("pol2")

```

For the fitting, the coefficients obtained are the following, for which only the "p1" and "p2" values were included:

```

TGraph *g =new TGraph()
p0 = 440.833
p1 = 0.0127483
p2 = 0.000332362

```

The coefficients are included for the correction, and it is typed in the terminal for plotting the "tof v.s. X1pos" as follows:

```

DATA->Draw("X1pos+0.0127483*(tof-3120)-0.000332362*pow(tof-3120,2.)>>h1D(2000,0,700)"
,"cutTritons && !X1flag && !U1flag","col")

```

As a result, a straight vertical line is obtained, which in principle will have a better resolution. It is also possible to include the "!X1Flag" and "!U1flag" which will add an extra background reduction, in this case, bad events for which more than 5 to 7 wires are fired in one event are discarded or are fired less than certain number (<3). This correction is shown in Fig. 2.20 and the zoom-in of it in Fig. 2.21, which is easier to observe the correction.

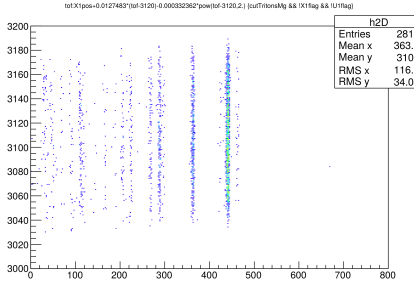


Figure 2.20: *Corrected TOF v.s. Focal Plane position X1pos.*

If "X1pos" is plotted again, including the cut, flags, and the coefficients, the result should be an improvement in the efficiency of the peaks. In Fig. 2.22 it is obvious the reduction of the background compared with that in Fig. 2.16. As well, by fitting the different peaks, before and after, different σ values are obtained ($\sigma_{blue}=1.91074$ and $\sigma_{red}=1.77037$).

2.9.3 Peak Identification

For this, a rough calibration was performed. First, two peaks of the red spectrum in Fig. 2.22 (right to left) were fitted and their centroid obtained. Assuming the first prominent peak is the 0.228 MeV (first excited state) in ^{26}Al and the second prominent one the 1.05773 MeV (third

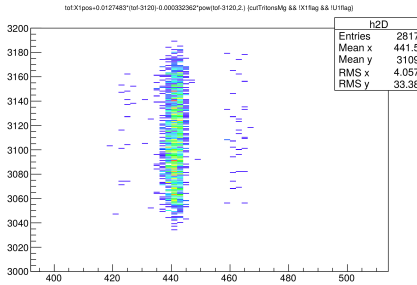


Figure 2.21: *Zoom of corrected TOF v.s. Focal Plane position.*

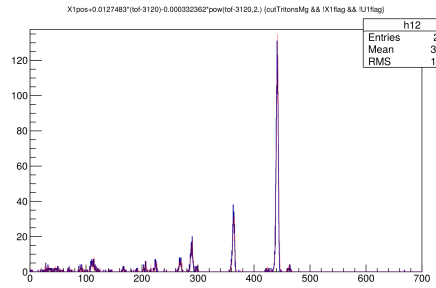


Figure 2.22: *Comparison between the focal plane position ($X1pos$) with the corrected one using the TOF.*

excited state), it is possible then to calculate how many keV per channel the Focal Plane has, this is calculated as follows:

$$\frac{FPV - SPV}{FPC - SPC} = \frac{1.057739 - 0.288}{363.174 - 441.270} = -10.62 \frac{\text{keV}}{\text{ch}}, \quad (2.6)$$

where FPV, SPV are the first and second peak values (from data tables [?]) and FPC, SPC are the centroids from the first and second peak (right to left) of the red spectrum of Fig. 2.22. Once the correspondent value between channel number and keV is known it is possible to make the conversion, assuming the selected peaks are the correct ones, a spectrum in terms of the excitation energy in ^{26}Al is obtained as shown in Fig. 2.23. From here, the identification of the rest of the peaks is possible, it is only matter of fitting them and get the centroid value.

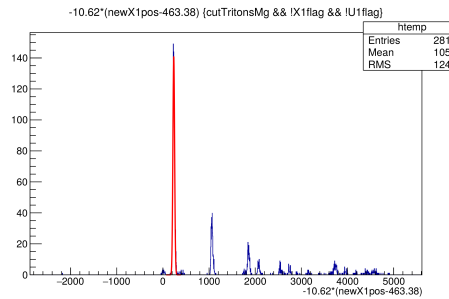


Figure 2.23: *Excitation energies of the populated states in ^{26}Al obtained by a rough calibration.*

An easy thing to do in "root" is rename something to make the writing easier, for example:

```
Data->SetAlias("newX1","X1pos+0.0127483*(tof-3120)-0.000332362*pow(tof-3120,2.)")
```

For which:

```
"newX1" = "X1pos+0.0127483*(tof-3120)-0.000332362*pow(tof-3120,2.)"
```

In order to make te conversion from channel number to keV, in the command line is typed:

```
DATA->Draw("-10.62*newX1","cutTritonsMg && !X1flag && !U1flag","col")
```

For which -10.62 keV, the value obtained above per channel number. The fitting of each peak of Fig. 2.23 is done, and the comparison of the centroid values with those from the literature are shown in Table 2.2, showing a good agreement.

Literature (MeV)	Fitted (MeV)
0.288	0.233
1.058	1.060
1.810	1.850
2.072	2.070

Table 2.2: *Comparison between the values of the peaks (taken from NNDC) and the obtain ones from the rough calibration.*

2.9.4 Calibration using Magnetic Rigidity

Once the peaks have been identify, it is possible to calculate the Magnetic Rigidity $QB\rho$ of the corresponding tritons. For this matter, **SPANC** was used with the following specific parameters:

- Target ^{26}Mg
- Beam ^3He
- Projectile ^3H
- Residual ^{26}Al
- Q-Value = -4.02302412118 MeV
- E_{beam} = 50 MeV
- $T_{thickness}$ = 600 μ/cm^2

The values of the rigidity of the corresponding tritons are listed in Table 2.3 and by plotting the rigidity values versus the corresponding excitation energy we obtain Fig. 2.24, for which a polynomial of order two is fitted in order to obtain some coefficients used for the calibration. The plotting and the fitting has to be done similarly as that in Fig. 2.19.

The coefficients obtained from the fitting are $p0 = 1606.16$, $p1 = 0.214814$ and $p2 = -0.0000174212$. These coefficients have to be included in the "X1pos" plot in order to have the triton peaks in terms of their rigidity as shown in Fig. 2.25.

For this, in the terminal it is typed:

^{26}Al Ex (MeV)	Rigidity (Tmm)
0.288	1697.563
1.058	1681.874
1.810	1666.724
2.072	1662.474

Table 2.3: Identified peaks (left) and their corresponding rigidity (right) [?].

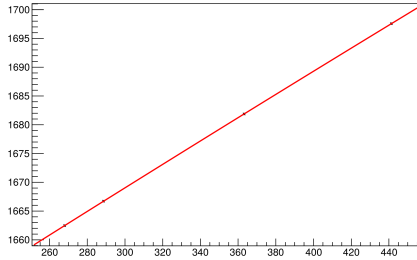


Figure 2.24: Rigidity values v.s. excitation energy of the identified peaks[?].

```
DATA->Draw("1606.16+newX1*0.214814-0.0000174212*pow(newX1,2.)",
    "cutTritonsMg && !X1flag && !U1flag","col")
```

And one more time, we rename it as:

```
DATA->SetAlias("QBrho","1606.16+newX1*0.214814-0.0000174212*pow(newX1,2.)")
```

2.9.4.1 Tritons Momenta and Energy

With the rigidity values it is possible to calculate the momentum of the tritons by:

$$P_t/q = B\rho c, \quad (2.7)$$

for which P_t is the momentum of the tritons, B the magnetic field, ρ the radius of curvature and c the speed of light. In the command line it is typed:

```
DATA->("(Brho/1e3)*(TMath::C()/1e6")
```

Note that $\mathbf{Q}\mathbf{B}\rho$ is divided by 1000, this in order to convert the units from Tmm to Tm. Fig. 2.26 shows the tritons in terms of their momentum.

Finally the energy of the tritons is calculated using:

$$E_t = \sqrt{P_t^2 + m_t^2} - m_t, \quad (2.8)$$

for which E_t is the kinetic energy, P_t the momentum and m_t the mass of the tritons respectively.

In the command line it is typed:

```
DATA->SetAlias("Ptritons",""(Brho/1e3)+(TMath::C()/1e6")
```

```
DATA->Draw("sqrt(pow(Ptritons,2.)+pow(2809.43210768,2.))-2809.43210768","cutTritonsMg &&
```

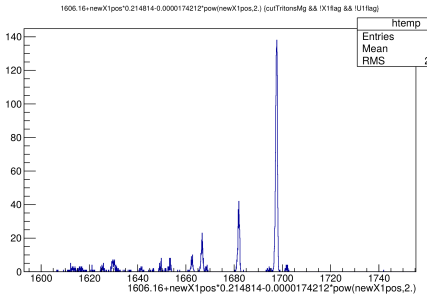


Figure 2.25: *Rigidity values for the tritons.*

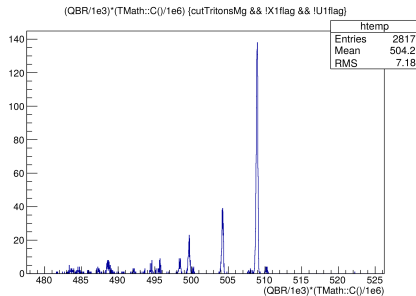


Figure 2.26: *Momentum of the tritons.*

In Fig. 2.27 is shown the obtained triton energy values for which a fitting was done in order to compare and corroborate the values with those calculated ones using a kinematics code. The comparison is shown in Table 2.4.

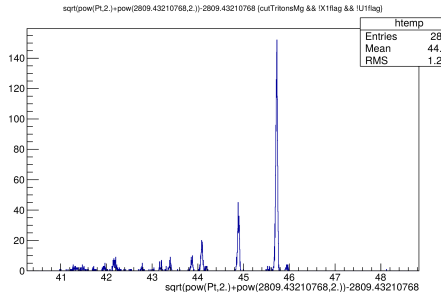


Figure 2.27: *Tritons kinetic energy calculated through the rigidity.*

^{26}Al Calculated E_t (MeV)	Fitted E_t (MeV)
45.73	45.72
44.90	44.88
44.10	44.08
43.88	43.86

Table 2.4: *Identified peaks (left) and their corresponding rigidity (right).*

2.9.4.2 Excitation energy from Kinetic Energy

Quick summary:

1. calibrate rigidity against position;
2. now for any X you can extract rigidity;
3. from rigidity you get momentum, assuming you know what particle type is;
4. from momentum you get kinetic energy of particle in K600;
5. now you can calculate energy of recoil, from knowledge of the different masses and kinetic energies of the beam and the particle in the K600;
6. now you have everything to can calculate Ex.

IMPORTANT: WHAT FOLLOWS HERE IS VALID ONLY IF YOU USE THE SAME UNITS FOR RIGIDITY, THE SAME CALCULATOR FOR RIGIDITY, YOU ARE USING 3He,T REACTION, ETC, the same. If you e.g. use *relkin* the the rigidity is given in kG/cm. To go from that to momentum you need

```
rigidity = momentum(in MeV/c) * charge (dimensionless) * 10 /2.998
```

It is possible to obtain the excitation energy of those states populated in the $^{26}\text{Mg}(^{3}\text{He},\text{t})^{26}\text{Al}$ reaction by using:

$$E_x = E_{target} + E_b - E_t - E_{recoil} - Q_v, \quad (2.9)$$

$$E_x = (m_{target}) + (T_b + m_b) - (T_t + m_t) - (T_{recoil} + m_{recoil}) - Q_v, \quad (2.10)$$

for which E_x is the excitation energies of states in ^{26}Al , T_b the beam kinetic energy, T_t the tritons kinetic energy, T_{recoil} is the kinetic energy for the recoil nucleus, and Q_v the Q-value of the reaction.

What follows should be good in principle, but the details of the definitions may need to some work. In the terminal it is typed:

```
DATA->SetAlias("masstriton","2809.43210768")
DATA->SetAlias("massrecoil","7809.43210768")
DATA->SetAlias("Erecoil","sqrt(pow(Pbeam,2.) + pow(Ptriton,2.)
- 2*Ptriton*Pbeam*cos(theta) *pow(massrecoil,2))")
DATA->SetAlias("Etritons","sqrt(pow(Ptritons,2.)+pow(2809.43210768,2.))-2809.43210768")
DATA->Draw("Ebeam-Etritons-Erecoil -Q","cutTritonsMg && !X1flag && !U1flag","col")

DATAChain->SetAlias("QBrho","1888.13+0.18509*X1posC-0.00000812157*pow(X1posC,2)")
DATAChain->SetAlias("PAlphas","(2*QBrho*2.998/1e1)")
DATAChain->SetAlias("EAlphas","sqrt(pow(PAlphas,2.)+pow(3727.04258,2.))-3727.04258")
DATAChain->SetAlias("Pbeam","sqrt( pow(200+3727.04258,2) -pow(3727.04258,2) )")
DATAChain->SetAlias("Precoil","sqrt(pow(Pbeam,2.)+pow(PAlphas,2.)-2*200*PAlphas*cos(theta))
DATAChain->SetAlias("Erecoil","sqrt(pow(Precoil,2.)+pow(3727.379,2.))-3727.379")
```

```
DATAChain->Draw("200.-EAlphas-Erecoil",CUTbasic && CUTlimits,"")
```

The energies obtained are shown in Fig. 2.28

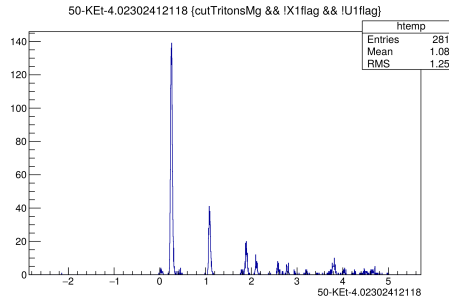


Figure 2.28: *Excitation energy spectrum of ^{26}Al corrected using the magnetic rigidity of the tritons detected at the Focal Plane.*

The comparison of the calculated kinetic energy values with those obtained from the calibration are shown in Table 2.5.

Literature (MeV)	Fitted (MeV)
0.288	0.256
1.058	1.089
1.810	1.890
2.072	2.110

Table 2.5: *Values of the ^{26}Al excitation energies from the literature (left) compared with those values obtained from the calibration (right) [?].*

2.9.5 Calibration of the Excitation Energy of ^9B using the ^{26}Al Calibration

For the $^9\text{Be}(^3\text{He},t)^9\text{B}$ it is required a calibration of the focal plane, for this purpose, the coefficients, flags, and a new cut are used. The cut for selecting the tritons is that shown in Fig. 2.15 corresponding to a ^9B run (**cutTritons9B.C**). The ground state should be sitting at zero MeV, but its centroid is at 0.052 MeV (**why the shift?**), on the other hand, the 2.361 MeV has a fitted centroid of 2.413 MeV. The Fig. 2.29 corresponds only to one RUN (run52.root), and an extra gate (time-gate) has been applied in order to reduce bad coincidences as shown in Fig. 2.30.

Then, for the excitation energies it is typed:

```
DATA->Draw("50-Et-4.02302412118","cutTritons9B && !X1flag && !U1flag","col")
DATA->SetAlias("ExB","50-Et-4.02302412118")
```

Note that the Q-value corresponds now to that of the $^9\text{Be}(^3\text{He},t)^9\text{B}$ reaction.

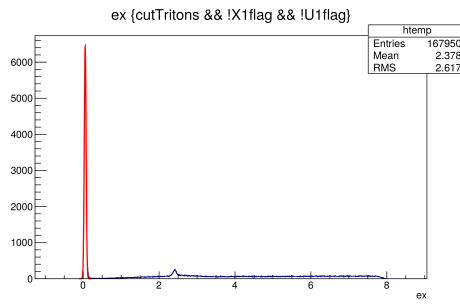


Figure 2.29: *Excitation energy spectrum of ^9B corrected using the magnetic rigidity of the tritons detected at the Focal Plane for ^{26}Al .*

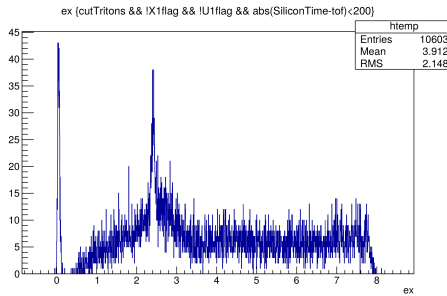


Figure 2.30: *Time-gate applied to the plot in Fig. 2.29 in order to reduce bad coincidences.*

As mentioned before, all the previous procedure has been applied to a single $^{26}\text{Al}/^9\text{B}$ run, but is not limited to that, as well it is also possible to chain all the runs for the $^9\text{Be}(^3\text{He},\text{t})^9\text{B}$ reaction, and it is done using a script ("**mergefiles.cpp**") as follows:

```
TString Treename = "DATA";
TChain * dchain = new TChain(Treename);
dchain-> Add("file1.root");
dchain-> Add("file2.root");
dchain-> Add("filen.root");}
```

For loading the script in the terminal: **.x mergefiles.cpp** and the result is shown in the spectrum of Fig. 2.31.

2.9.6 Silicon Energy V.S. Excitation Energy

Once the Focal Plane has been calibrated and the excitation energy obtained as described above, it is possible to plot different values versus others, for example, one of the most important and robust two-dimensional plot for a K600 experiment in coincidence with a silicon detector array is that shown in Fig. 2.32 in which the energy of the detected particles in the silicon detectors is plotted versus the excitation energy (calculated and calibrated previously from starting with the focal plane position), in which it is possible to observe different loci, which are those coincidence

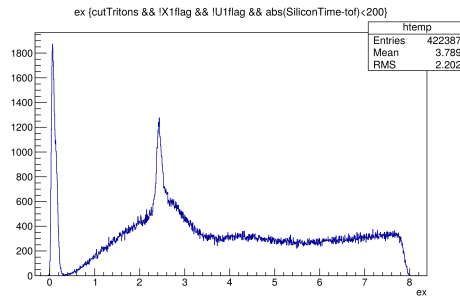


Figure 2.31: Low excitation energy region in ${}^9\text{B}$ (all runs).

events between the focal plane and the silicon detector array, being each of them a different channel of decay. As well, in this two-dimensional plot, it is possible to make cuts in order to select those regions of interest, for example, to select events coming specifically from a proton decay (diagonal locus) or those coming from an α -particle decay (small vertical locus) as shown in Fig. 2.32.

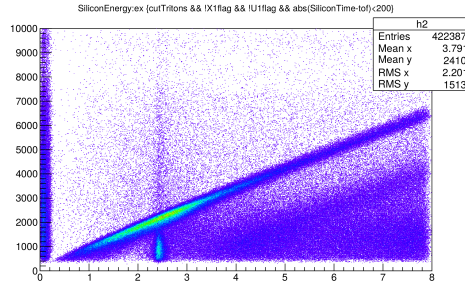


Figure 2.32: Coincidences between excitation energy v.s. those events detected in the silicon detector array. Solid-line box shows the proton decay locus, which has been selected as a "cut" for further analysis (**draw the box!!**).

In the terminal it is typed:

```
DATA->Draw("SiliconEnergy:ExB>>h2(800,0,10.,800,0.,10000)", "cutTritons9B && !Xiflag && !Uiflag && abs(SiliconTime-tof)<200", "col")
```

The proton-decay locus cut can be loaded in the terminal similarly as other cuts: **.x diagonal.C**. With this, it is now possible to project onto the x-axis those selected events by the cut and even better, plot them in the same one-dimensional plot of the excitation energy for comparison purposes as shown in Fig. 2.33.

Or also it is possible to subtract the proton-decay locus contribution from the total spectrum as shown in figure Fig. 2.34.

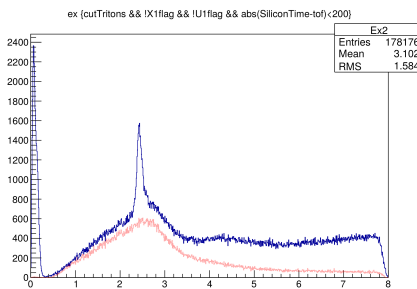


Figure 2.33: Comparison of the total excitation energy spectrum in 9B (blue-colour-line) with that selected region (proton-decay channel) selected in Fig. 2.32 (red-color-line).

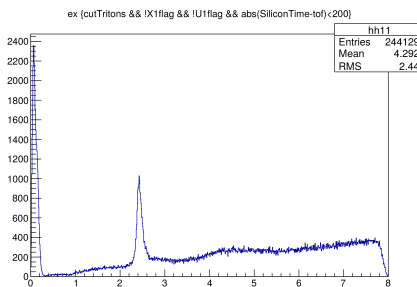


Figure 2.34: Excitation energy spectrum with the subtraction of the proton-decay locus of Fig. 2.33.

Chapter 3

The K600 magnetic fields

The magnetic fields of five magnetic elements of the K600 are controlled from the PC in the middle of the left-most rack in the data room. The non-linear relation between the current setting and the magnetic field for each dipole (the excitation curve) is illustrated in Fig.3.1. It is important to note that this measurement was performed under so-called medium dispersion mode conditions, i.e. the ratio between the two dipole fields was kept to 1 during the measurement. Under different dipole ratio conditions the relation between magnetic field and current setting will be slightly different.

3.1 Setting the spectrometer fields

3.1.1 Theory

When a ferromagnetic material is magnetized in one direction, it will not relax back to zero magnetization when the imposed magnetizing field is removed. It must be driven back to zero by a field in the opposite direction. If an alternating magnetic field is applied to the material, its magnetization will trace out a loop called a hysteresis loop. The lack of retraceability of the magnetization curve is the property called hysteresis and it is related to the existence of magnetic domains in the material. Once the magnetic domains are reoriented, it takes some energy to turn them back again. This property of ferrromagnetic materials is useful as a magnetic "memory" [web10].

In order to travel through the hysteresis curve of the dipole and quadropole magnets in a careful, well-defined and reproducible manner a setup procedure, referred to as the *SET FIELD* procedure (see subsection 3.1.2), was devised after careful studies by Garret de Villiers and other staff members. Parameters that had to be decided upon include the rate of change of the currents, the duration of the waiting points and the size of the so-called overshoot current. Refer to Figs. 3.3, 3.4, and 3.5. The result is repeatability to the level of 10^{-5} and stability to the level of 10^{-4} [Gar10]. Furthermore, it was found that the final, stable, field is achieved after 15-35 minutes. All of this of course assumes temperature stability of the cooling water and atmosphere.

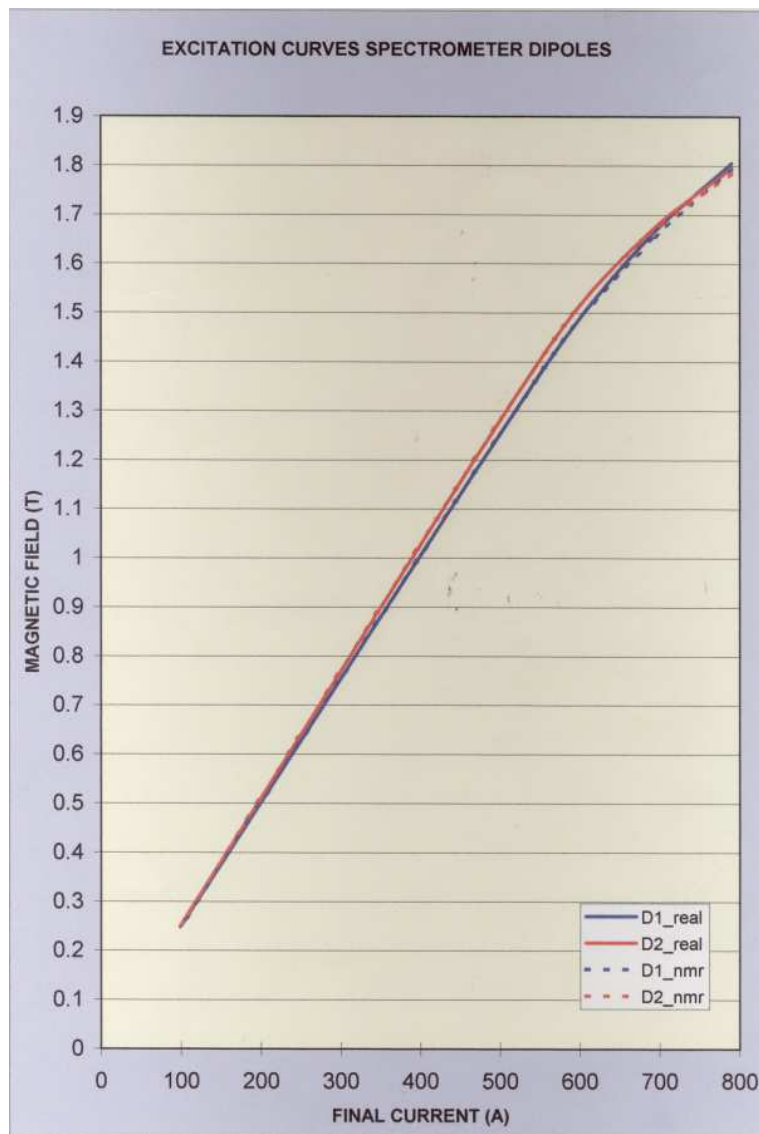


Figure 3.1: The relation between the current setting and the magnetic field of the 2 K600 dipoles for the medium dispersion magnet setting scenario of $D1/D2=1$.

3.1.2 The SET FIELD procedure

Important Precaution: Do not set the magnetic fields while there is beam on target.

If the page displayed on the monitor is the spectrometer power supplies, then a table of the magnetic elements should be displayed. To set the quadrupole, for example, move the cursor with the mouse onto "quadrupole" and click the left front pad of the mouse. This selects the quadrupole and displays the controls of the quadrupole on the right of the screen. The three horizontal boxes with the sliders in the middle are used to set a value for the quadrupole. Clicking with the cursor on the right or the left of the slider will increase or decrease the

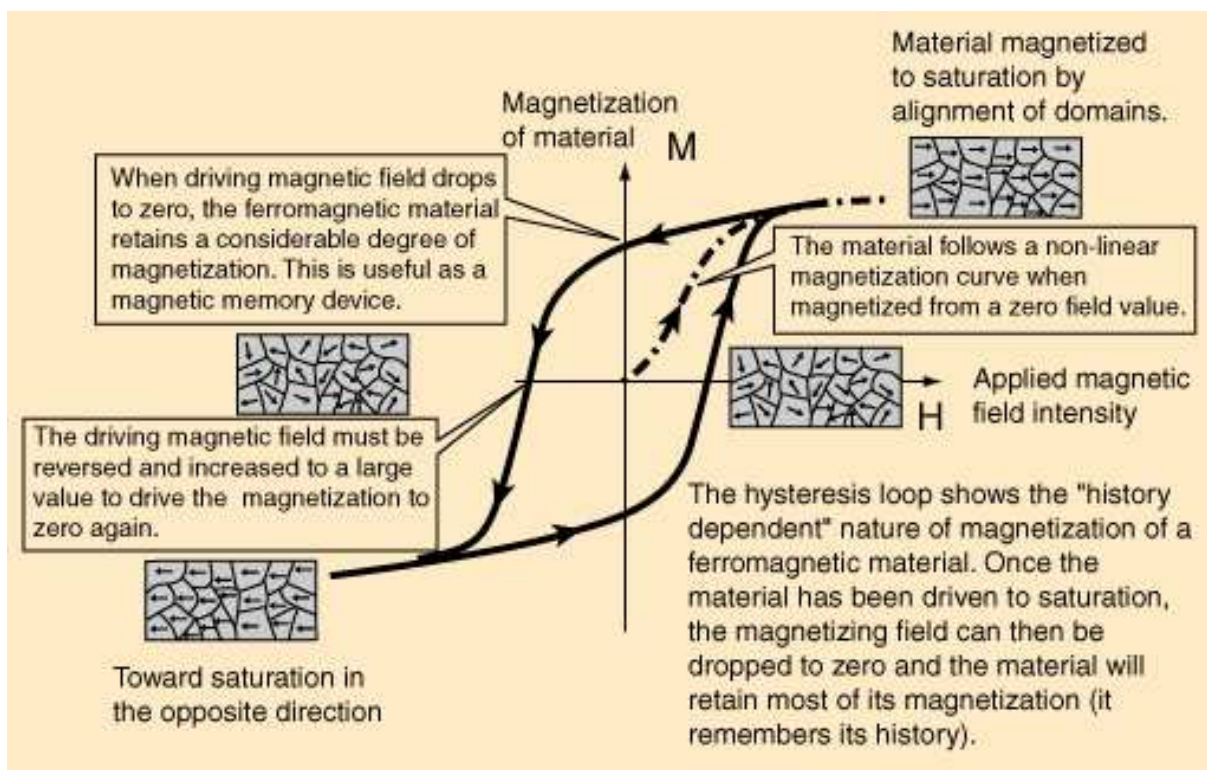


Figure 3.2: The hysteresis loop [web10].

present reference value of the current in amps. Each box has an order of magnitude difference in sensitivity. From the bottom up are ones, tenths and hundredths of an amp. Clicking on the slider and keeping it depressed allows one to move the slider to the left and the right, changing the values at an accelerated rate. Once the desired reference value has been dialed up, the power supply can be set at this value by either clicking on the ENTER button, which will set power supply to this value immediately, or by clicking on the *SET FIELD* button, which will start a program running to erase the memory in the steel of the old value and set it to the new value in a reproducible way. A setting status will be given to the element while the process is in progress. The latter method must be used for the quadrupole and the two dipoles. It takes ten minutes to set the field of the quadrupole and 20 minutes for the dipoles. The setting of the quadrupole should be complete before the setting of the dipoles is started. The dipoles should be set as close to simultaneous as possible.

The *SET FIELD* procedure is not used at RCNP. They simply adjust the currents of the magnets until the desired magnetic fields (as read from NMR probes) is reached. At iThemba LABS we cannot do the same thing. The NMR probes inside the K600 are on the edge of the magnetic field. They can therefore not be used for accurate measurements of the magnetic fields since the measurement depends on the actual position of the NMR probe. The only way to ensure that the fieldsettings are reproducible, and that the ratio of D1,D2 and Q magnetic fields are accurate, is to use the *SET FIELD* procedure.

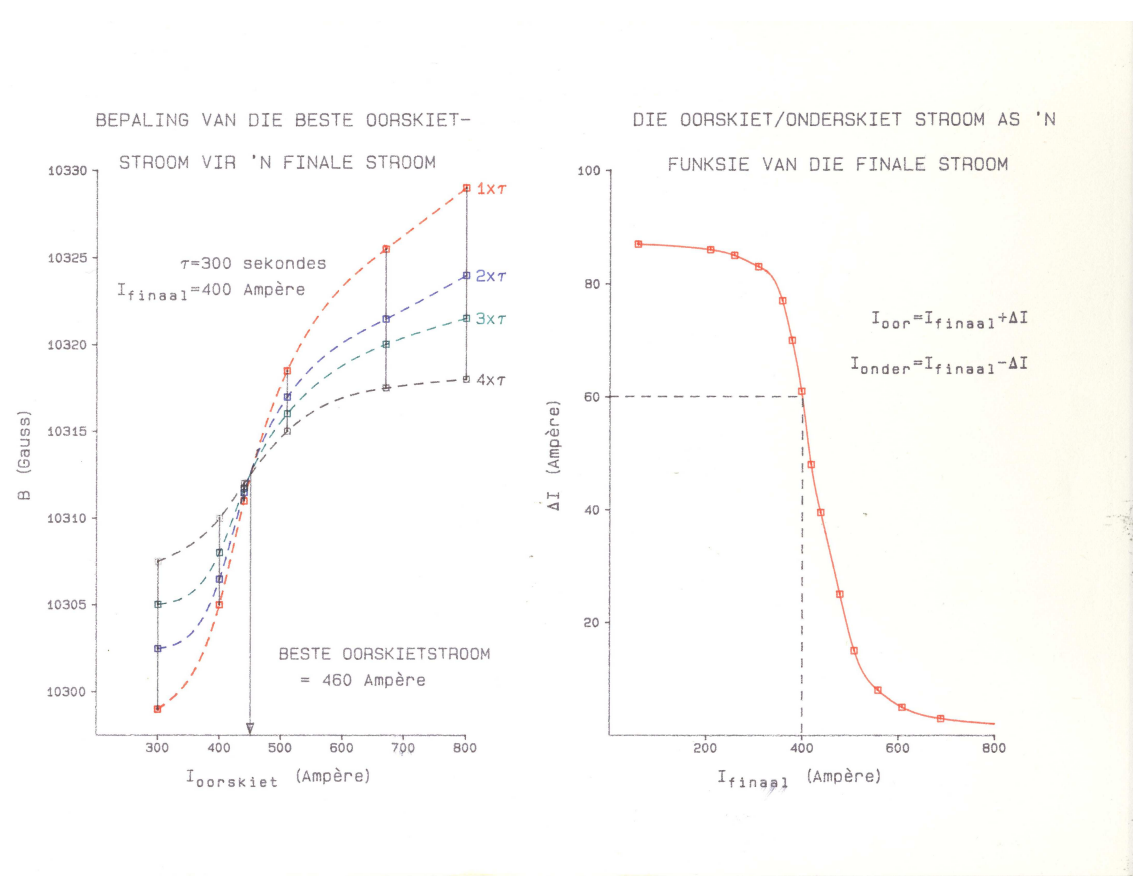


Figure 3.3: The size of the overshoot current was decided by making various measurements of the dipole field after different time constants for different overshoot currents. The final selected overshoot current was selected to be at the waist of the different curves in B versus I [Gar10].

3.2 SPEXCIT

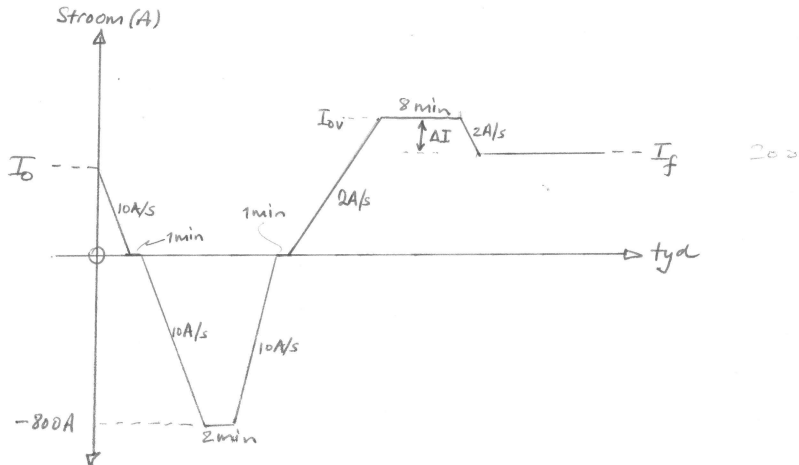
The program SPEXCIT is used to determine the proper electric current of the Q, D1 and D2 magnets of the K600 spectrometer for a specific magnetic field setting. The user selects the type of incident particle, its charge state and kinetic energy. From this information, momentum [MeV/c] and rigidity [Tm] are calculated and proper magnetic fields are estimated. After clicking the "UPDATE MAGNET VALUES" button, current [A] and magnetic fields [T] are shown. The value B_{NMR} should be reflected on the dataroom NMR, while B_{Real} represents the field experienced by the particles in the beam region of the magnets.

The original procedure followed for matching currents to NMR readings and momenta of particles can be briefly summarized as follows:

- Set a current value
- Make NMR measurements of B_{Real} in the beam region of the magnet
- Make NMR measurements of B_{NMR} on the edge of the magnets, in the position where the NMR probes will eventually be positioned permanantly

D1POOL # 1 INSTELPROSEDURE

30-8-1990



Dorskeetsstroomfunksie:

$$\begin{aligned}\Delta I &= 105.0 \operatorname{sech} \left[-1.2142 \times 10^{-7} \times I_f^{2.5835} \right] \\ &\quad + (1.5556 \times 10^{-2}) \cdot I_f \cdot \cos \left[\frac{I_f \times \pi}{170} \right] \cdot \operatorname{sech} \left[\frac{\pi(I_f - 400)}{800} \right] \\ &\quad + (6.0 \times 10^{-3}) \cdot I_f \cdot \cos \left[\frac{I_f \times \pi}{140} \right] \cdot \operatorname{sech} \left[\frac{\pi(I_f - 400)}{450} \right] \\ &\quad + 2.5 \times 10^{-3} \times I_f\end{aligned}$$

$I_{over} = I_f + \Delta I$

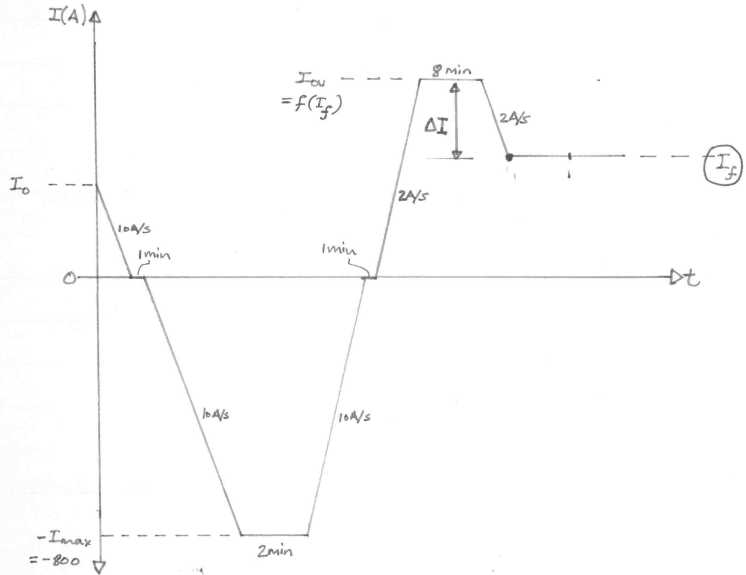
Noorwaarde:

Indien $I_{over} > 800 \text{ A}$ dan is $I_{over} = 800 \text{ A}$.

Figure 3.4: The fieldset procedure for D1, indicating the rate of change for the currents, the duration of the waiting points and the equation to determine the overshoot current [Gar10].

- Find an optimum momentum that associates with the current settings. This was per-

INSTELPROSEDURE OP SPEKTROMETER DIPOL #2



$$\Delta I(I_f) = \frac{C_1}{C_8} \operatorname{sech}\left(-1.2142 \times 10^{-7} \times I_f^{2.5835}\right) + \left(\frac{C_2}{450}\right) \cdot \cos\left(\frac{I_f \pi}{191.25}\right) \cdot \operatorname{sech}\left[\left(\frac{\pi}{2 \times 400}\right)(I_f - 400)\right] \\ + \left(\frac{3I_f}{500}\right) \cos\left(\frac{I_f \pi}{105}\right) \cdot \operatorname{sech}\left[\left(\frac{\pi}{2 \times 225}\right)(I_f - 400)\right] + \left(\frac{2I_f}{800}\right) - 1.0$$

$$\cosh x = \frac{e^x + e^{-x}}{2}$$

$$\operatorname{sech} x = \frac{1}{\cosh x} = \frac{2}{e^x + e^{-x}}$$

Figure 3.5: The fieldset procedure for D2, indicating the rate of change for the currents, the duration of the waiting points and the equation to determine the overshoot current [Gar10].

formed by tracking particles to the focal plane with the code TRACK [Tra02].

A database was thus created for D1,D2 for different current values.

There are 3 versions of SPEXCIT on the iThemba LABS Windows network:

1. **The original.** This is similar to the VMS SPEXCIT version, now adapted to run on Windows with an updated value for the proton mass.
2. **Version Apr2005-OLD.** This version is identical to the original in that it still utilizes the original field maps and parameter sets. In addition this version can be used to calculate K600 magnet settings for the high dispersion focal plane.
3. **Version Apr2005-NEW.** Similar to Apr2005-OLD, but utilizing a new database. During Hiro's tenure Garrett made new field measurements (why? Garrett told me but I forgot) and created a new database used for the SPEXCIT calculations. However, since the NMRs could only be positioned on the fringes of the magnetic fields (by design, due to operational requirements) the fields could not be measured very accurately and consequently this version of SPEXCIT is not as accurate as the OLD version. Note that during the original field measurements the probe was placed both inside the K600, in the beam region of the magnet, as well as on the fringe where the NMRs are currently positioned.

We should use the version "Spexcit_Apr05_OLD". The version "Spexcit_Apr05_NEW" uses different parameters to estimate the current, but "Spexcit_Apr05_OLD" worked better in the first 0-degree beamtime (Hiro Fujita, 2006).

Some notes on the use of SPEXCIT:

- **For the High Disp Plane, the energy you choose in Spexcit is the E of the particle that will exit the K600 at the '0-degrees beampipe position', and not the E of particle in the middle of the focal plane.**
- **For the Med Disp Plane, the energy you choose in Spexcit is the E of the particle that will pass through the middle of the focal plane.**
- The factor of the Q-magnet in the high dispersive mode of 0.968 was estimated for vertical focusing at $E_x=15\text{MeV}$ using a 200MeV proton beam. A more suitable value can be found later.
- Note that the results of the original windows version of SPEXCIT are slightly different from those from the old VAX version of SPEXCIT. This is because proton mass was updated to be the latest value.
- By changing the file ElementData.txt you can add different particles.
- The relative atomic mass used for triton in SPEXCIT is 3.0160497 (see also file ElementData.txt).

This code is available

1. On the spectrometer laptop.
2. From /oberon/users_common/Spexcit.
3. From the Windows machine in the dataroom: log on as labview with password labview.
4. If all else fails ask a Physics staff member or the creator of the program, Garrett de Villiers.

3.3 Measuring D1 and D2 fields

The magnetic fields of D1 and D2 can be determined with the Metrolabs system comprising of a PT2025 teslameter, a 2031 multiplexer amplifier and a collection of 1060-7M NMR probes per dipole:

- 1060-3-7M for the range 0.17-0.52T
- 1060-4-7M for the range 0.35-1.05T
- 1060-5-7M for the range 0.7-2.10T

Refer to table 3.1 to see how these probes are connected to the teslameter. Note that at any given moment only 1 probe per dipole is actually installed. (For some reason the teslameter does not work for a probe installed in channel A in the multiplexer. Had to start at either E or D. Some termination problem?)

According to Garrett de Villiers the NMR probes are not in the central part of the dipole fields, but somewhat on the gradient, which means that the values of the fields are not 100% of what the particles will experience. This is indicated in the output of the computer code *Specxit*

Magnet	Knob	Light	Range (T)
D1	A	5	0.7-2.1
D1	B	4	0.35-1.05
D1	C	3	0.17-0.52
D1	D	2	0.09-0.26
D2	E	5	0.7-2.1
D2	F	4	0.35-1.05
D2	G	3	0.17-0.52
D2	H	2	0.09-0.26

Table 3.1: Information about the NMR probes and teslameter.

3.4 Superknob

The control of the 5 magnets of the K600 by means of one 'superknob' is now implemented. One can choose the ratio of D2, Q, K and H relative to D1, set a value to D1 and then all five magnets will change accordingly in one go. This superknob is on the bottom of the K600 magnet control page.

3.5 Adjusting the K and H-coils

In general, correlation plots of focal-plane angle versus position of rays in the x-plane (horizontal plane) provide one of the most useful diagnostics for determining the ion-optical quality of the K600 spectrometer and its beamline tune. Alternatively, plots of the relative TOF versus position are used to provide similar information.

The K- and H-coils should be adjusted to remove any correlation between the focal plane angle and position of a suitable peak in the middle of the focal plane. The K-coil provides for first-order focusing or correction of the $(x \mid \theta)$ -aberration, and has quadropole and dipole components. The H-coil provides for second-order focusing or correction of the $(x \mid \theta^2)$ -aberration.

The sensitivity of the procedure is enhanced when the horizontal-slit collimator is used. The use of the correlation plots is most suitable for the initial, "coarse" spectrometer tune. The TOF versus position plots do not provide sufficient sensitivity for fine tuning of the K600. Note that after all correlation between x_{fp} and θ_{fp} has been removed, the resolution may still be improved by iteratively performing K and H-coil scans while monitoring the line width.

Fig. 3.6 represent data taken during the K and H coil tuning for experiment PR96a. The data is for elastic scattering of 100 MeV protons from a ^{40}Ca target. The characteristic shape of the elastic locus in the TOF vs focal plane position plot is the inverse of the focal plane angle vs focal plane position plot.

OLD DAQ: The K-coil recipe for the x_{fp} versus θ_{fp} plot: Tilt to the right (left) by making K-coil setting larger (smaller). This is true for positive currents only. For negative currents the locus is tilted to the right by making the absolute value of the K-coil setting smaller.

OLD DAQ: The H-coil recipe for the x_{fp} versus θ_{fp} plot:

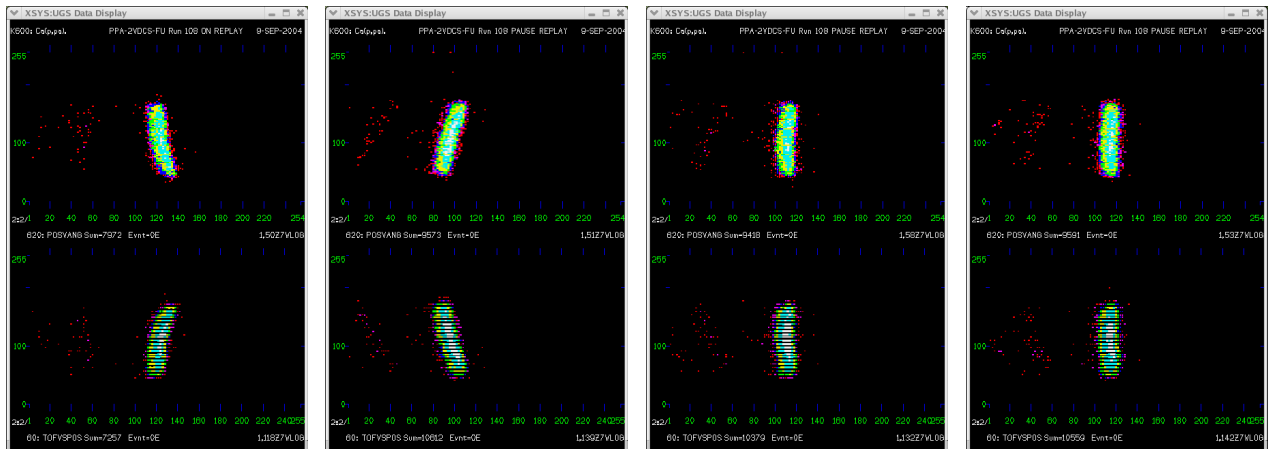


Figure 3.6: (**OLD DAQ**) From left to right: K-coil 0V, H-coil -30V → K-coil 30V, H-coil -30V → K-coil 15V, H-coil -30V → K-coil 15V, H-coil -40V. Top figure: x_{fp} vs θ_{fp} . Bottom figure: x_{fp} vs TOF

3.6 TRACK calculations for the K600

TRACK [Tra02] calculations

Different files for the D1, D2 and quadrupole magnets exists for the nominal setting at 200 MeV (medium dispersion focal plane settings)

de200_d1_2.ext de200_d2_2.ext

and the other is called

de200_d1.ext de200_d2.ext

And also for the quad I have

qe200_hiro.ext

and

qe200_2.ext

For qe200_2 I need the angle in KINETIC to be 308.6 degrees to define the zero scattering angle For qe200_hiro I need the angle in KINETIC to be 310.6 degrees to define the zero scattering angle.

From AUTOCAD files of the K600 it seems as if the angle between the central ray into the K600 (ie in the middle of the collimator) and the face of D2=38.5996 degrees. Thus the TRACK angle in the KINETIC line should be 321.4004 degrees... where am I going wrong here? Is the autocad figure not accurate enough?

The K and H coil fields are calculated. The dipole and quad fields are measured.

3.7 Adjusting the entrance hexapole/sextupole magnet

(*From the original K600 manual. The hexapole/sextupole is not in use at present. Aside from a brief test in Dec 2011 during experient PR183/184 it was not in use since I arrived in Sept 2003 (RN).*)

The entrance hexapole is used to correct for the strongly-coupled (x/ϕ^2) and (x/y^2) -aberrations. Since phi and y focal-plane information is not presently available, suitable correlation plots cannot be generated. By using a vertical slit collimator, however, the shape of peaks in the position spectrum become sensitive to the hexapole field. This is shown in Fig. 3, in which some IUCF position spectra of 120 MeV protons scattered elastically off Au is presented. A hexapole scan should be performed and the line shape and line width monitored. A symmetric line shape usually corresponds with a minimum line width.

Chapter 4

The K600 collimator carousel

The blank collimator should always be in position nr.5, since it forms an integral part of the 0° interlock (refer to section 10.5.2).

The collimator carousel, situated in front of the quadrupole magnet at a distance of 735.5 mm from the target center, can hold 6 collimators. The maximum uncertainty for the solid angle subtended by the spectrometer, due to uncertainties in the collimator radius and distance from the target, is estimated to be 0.3% [New96]. Refer to section 1.2 where it is shown that the K600 transmission is 100% for a 55mm collimator.

The available collimators and inserts are listed in tables 4.1 and 4.2.

Nr	shape	dimensions	thickness
A1	circular	ID=63mm	39mm, with 11mm inserts
A2	circular	ID=63mm	39mm, with 14mm inserts
B1	circular	ID=63mm	51mm, with 7mm inserts
B2	circular	ID=63mm	51mm, with 11mm inserts
C	circular	ID=49mm	51mm, no inserts (see Fig. 4.7)
D	circular	ID=22mm	51mm, uses inserts (see Fig. 4.8)
E	pepperpot		inner 63mm machined 15mm thick
E	multislot		inner 63mm machined 7mm thick
F	multi-hole on x-axis		51mm
G	active collimator slit	32mm	× 7mm
H	solid plug	-	51mm
I	solid plug with cross-hair	-	51mm

Table 4.1: A summary of available collimators. They are all made from brass. (ID≡Inner Diameter)

shape	dimensions	thickness	for collimator
circular	ID=55mm	11mm thick, tapered	A1
circular	ID=49mm	11mm thick, tapered	A1
circular	ID=46mm	11mm thick, tapered	A1
circular	ID=42mm	11mm thick, tapered	A1
circular	ID=49mm	14mm thick, tapered	A2
circular	ID=46mm	14mm thick, tapered	A2
circular	ID=42mm	14mm thick, tapered	A2
circular	ID=42mm	8mm thick Ta	A1 or 2
circular	ID=14 mm	11mm thick	D
circular	ID=63mm	7mm thick	B1
circular	ID=55mm	7mm thick	B1
slot	6mm × 55mm	2 of them, 7mm thick	B1
slot	14mm × 55mm	7mm thick	B1
slot	14mm × 36mm	11mm thick	B2
slot	14mm × 55mm	11mm thick	B2
slot	10mm × 70mm	7mm thick with slotted Ta plate (see Fig. 4.2)	B1

Table 4.2: A summary of available standard inserts with OD (OD≡Outer Diameter) of 78mm. Except where otherwise noted, all these inserts are made of brass. Note that there are also a few non standard inserts available, e.g. with ID=41mm, OD=74mm and 7mm thickness (ID≡Inner Diameter).

diameter mm	solid angle $\Delta\theta\Delta\phi$	horizontal acceptance $\Delta\theta$	vertical acceptance $\Delta\phi$
63 (max)	5.76 msr	± 42.8 mrad , or $\pm 2.45^\circ$	± 42.8 mrad , or $\pm 2.45^\circ$
55	4.39 msr	± 37.4 mrad , or $\pm 2.14^\circ$	± 37.4 mrad , or $\pm 2.14^\circ$
49	3.48 msr	± 33.3 mrad , or $\pm 1.91^\circ$	± 33.3 mrad , or $\pm 1.91^\circ$
46	3.07 msr	± 31.4 mrad , or $\pm 1.8^\circ$	± 31.4 mrad , or $\pm 1.8^\circ$
42	2.56 msr	± 28.5 mrad , or $\pm 1.635^\circ$	± 28.5 mrad , or $\pm 1.635^\circ$
14	0.285 msr	± 9.51 mrad , or $\pm 0.545^\circ$	± 9.51 mrad , or $\pm 0.545^\circ$

Table 4.3: Acceptance with different circular collimator openings.

projectile	material	thickness	E-loss (ELOSS)	E-loss (Lise)
200 MeV proton	brass	7mm	18.730 MeV	18.199 MeV
200 MeV proton	brass	11mm	30.007 MeV	28.152 MeV
200 MeV proton	brass	14mm	38.794 MeV	35.435 MeV
200 MeV proton	tantalum	8mm	33.830 MeV	not calculated

Table 4.4: Energy loss values



Figure 4.1: Clockwise from top left: 11mm thick 55mm diameter (tapered), 7mm thick slot 6x55mm, 11mm thick 55mm diameter (tapered), 7mm thick 63mm diameter.



Figure 4.2: Clockwise from top left: 11mm thick slot 14x36mm, 7mm thick 41mm diameter, 7mm thick slot 14x55mm, 7mm thick slot 10x70mm with 1mm wide slits in 2mm thick Ta??.

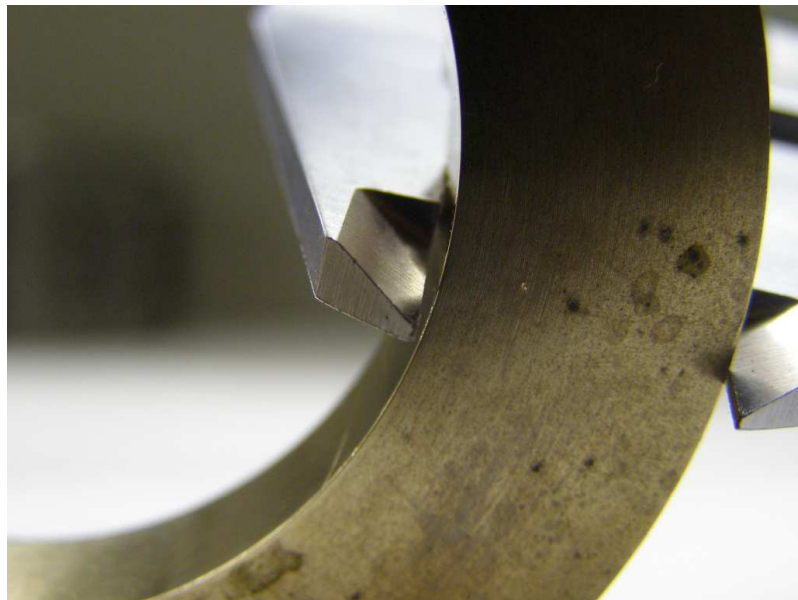


Figure 4.3: The slight tapering of the $\phi=49\text{mm}$ 11mm thick insert can be seen in this picture.



Figure 4.4: A 63mm diameter 39mm thick collimator (type A1): the insert has a diameter of 49mm and is 11mm thick.

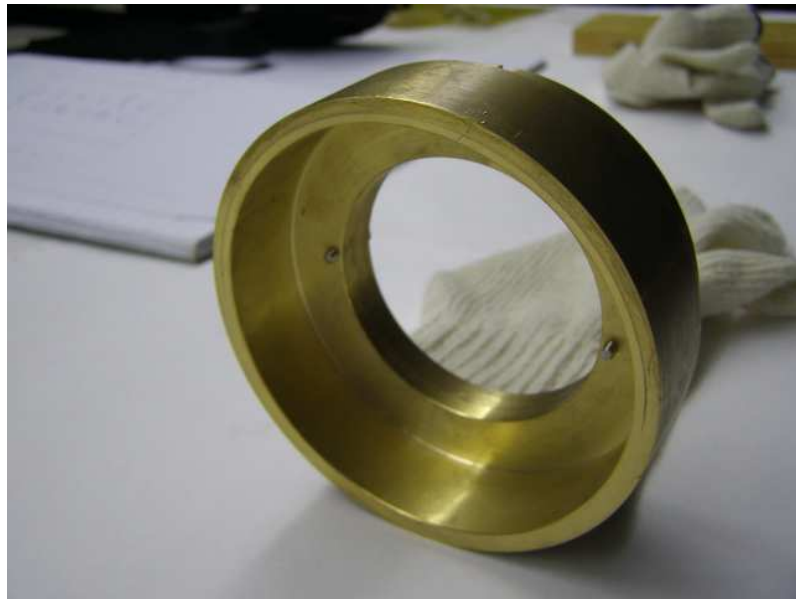


Figure 4.5: A 63mm diameter 39mm thick collimator (type A1 or A2): the insert is not in position in this picture.



Figure 4.6: A 63mm diameter 51mm thick collimator (type B1): the insert has a diameter of 55mm and is 7mm thick.



Figure 4.7: A 49mm diameter 51mm thick collimator with no inserts possible (type C).



Figure 4.8: A small 25mm diameter 51mm thick thick collimator (type C): the insert has a diameter of 14mm and is either 7 or 11 mm thick.



Figure 4.9: A 63mm diameter 51mm thick collimator: the insert is a slot of 55×14 mm and is 7 mm thick.



Figure 4.10: The multihole collimator

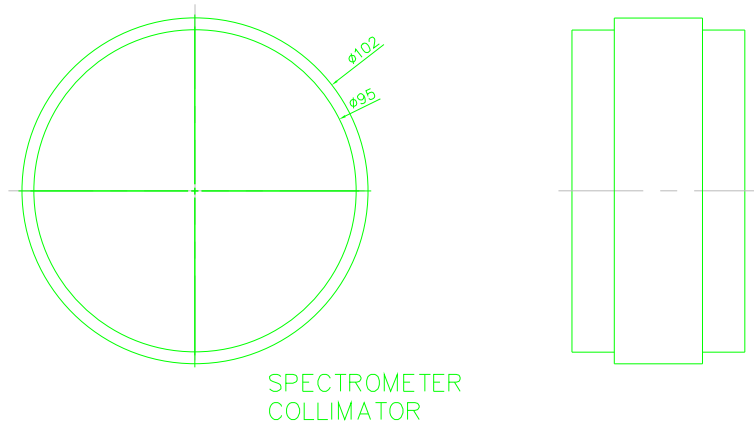


Figure 4.11: The blank collimator



Figure 4.12: A picture of the blank collimator in the carousel: it should not be removed from its present position (in-beam is position nr 5) as it forms part of the interlock system for ZeroDegrees



Figure 4.13:

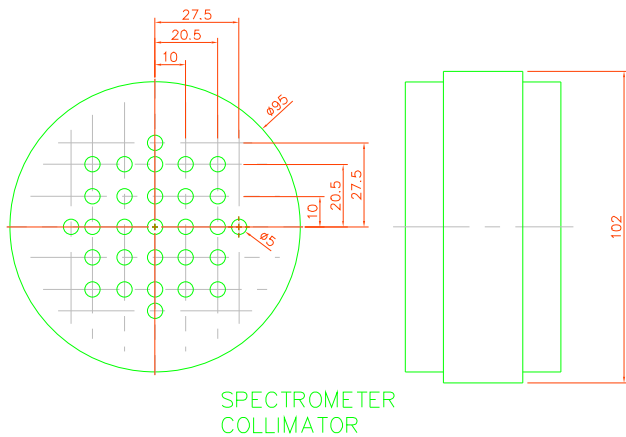


Figure 4.14: A schematic of the pepper-pot collimator. It was modified in April 2005 to be only 15 mm thick for the central region of 63.5 mm diameter (the back of the collimator is therefore 735.5-(51-15) mm from the target, if the pepperpot side is towards the beam; otherwise it is the standard 735.5 mm). Also, an insert was made end 2006 to put in one of the holes to make it smaller, thereby giving a reference point to correlate the picture in the focal plane with the real scattering angles. If the pepperpot is placed such that the holes are on the K600 side, the first hole from the middle on the x-axis/y-axis is at 0.78° (13.6mrad), the second is at 1.60° (27.9mrad), and the third is at 2.14° (37.4mrad). The holes span approximately 0.39° (6.80 mrad), except for the smaller hole which spans approx 0.19° (3.40 mrad).

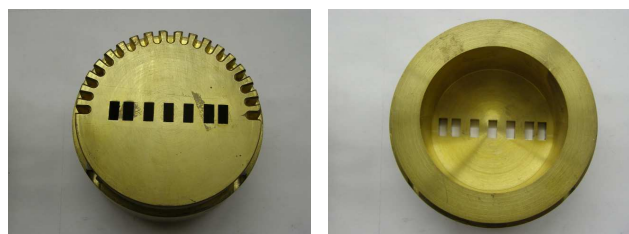


Figure 4.15: The 51mm thick multislot is only 7mm thick for the inner d=63mm. See Fig. 1.17 for dimensions.

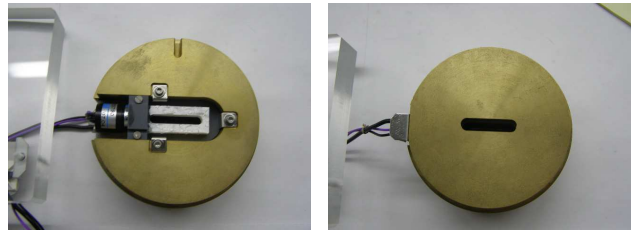


Figure 4.16: The active collimator has a slotted opening ??mm × ??mm.

Chapter 5

K600 angle change and beamstop configuration

There are several different beamstop configurations that can be used.

5.1 External beamstop for $\theta_{K600} > 21^\circ$

With the NIKHEF sliding seal scattering chamber we can reach as small as 22° (maybe even 21° if you are careful) with an external beamstop/Faraday cup.

5.2 Internal beamstop for $5^\circ < \theta_{K600} < 21^\circ$

The scattering chamber can be configured to measure up to 4° with an internal beamstop. However, the smallest angle where reasonably background free (p, p') measurements can be performed with this beamstop is 5° . Realistically this means that the K600 is positioned at 7° and that the 49mm collimator is used for the measurement. Such a setup provides data in the angular range $7^\circ \pm 1.91^\circ$. For (α, α') scattering the minimum angle is 4° , the K600 can be placed at 6° .

Care should be taken when installing this beamstop onto the rotating table to ensure that it will not touch the sliding seal when the sliding seal becomes deformed under vacuum conditions. Do not position this beamstop too close to the sliding seal. Another important thing to keep in mind is that one should be careful not to run this beamstop against the solid part of the chamber and thus lose calibration.

Note that, as indicated in Figs. 5.1 and 5.2, there are 2 permanent magnets in the beamstop. **get a technical drawing as well!!**

5.3 Internal beamstop for angles $2^\circ < \theta_{K600} < 5^\circ$

For even smaller angles there is the small angle beamstop (SABS) which allows measurement between 2° and 5° . Background is however a big problem in this configuration.

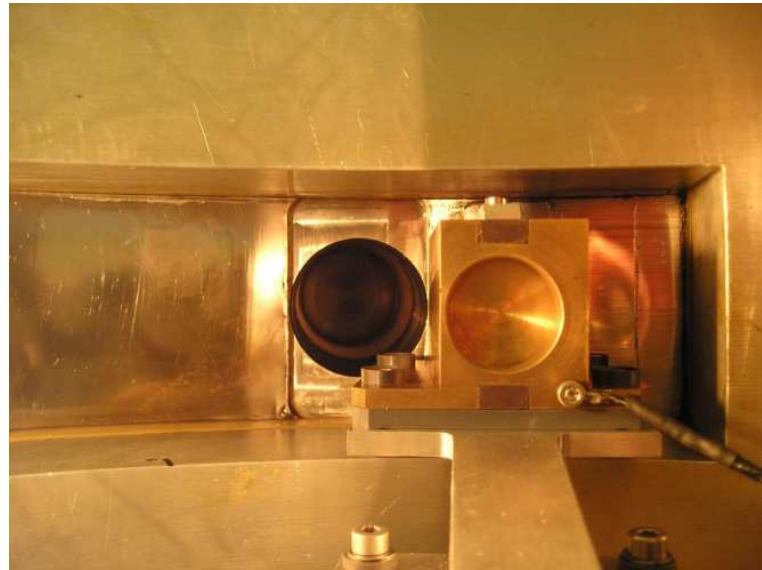


Figure 5.1: The internal beamstop for angles $5^\circ < \theta_{K600} < 21^\circ$ as viewed from the target ladder for the original small sliding seal opening. Note that there are two permanent magnets in the top and bottom of the beamstop.

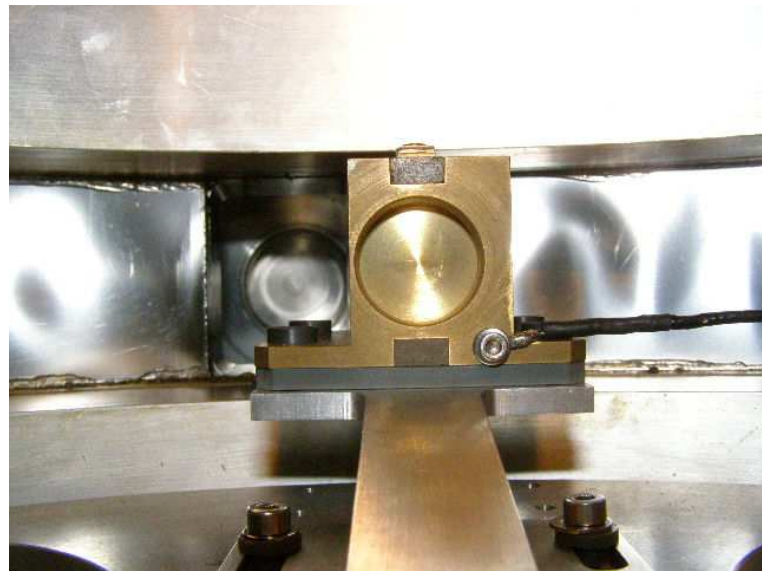


Figure 5.2: The internal beamstop for angles $5^\circ < \theta_{K600} < 21^\circ$ as viewed from the target ladder for the new 64mm \times 64mm sliding seal opening.

5.4 $\theta_{K600} = 0^\circ$ beamstop for (p, p')

For 0° measurements the scattering chamber is rotated so that the beam entrance and exit is through apertures in the sliding seal, not the normal fixed beam entrances and exit. With the big 64×64 mm 2 aperture used in the sliding seal we cannot go to angles bigger than 20 degrees, as the heavier hardware on the sliding seal pulls it away from the chamber as you go to higher

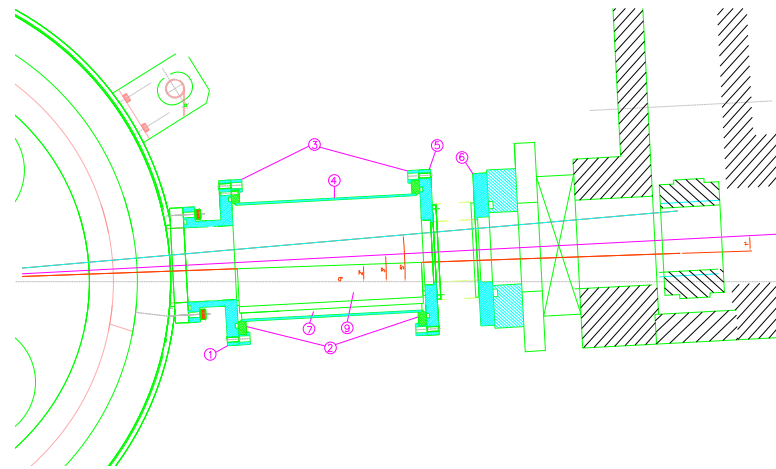


Figure 5.3: An overview of the small angle internal beamstop for $2^\circ < \theta_{K600} < 5^\circ$.

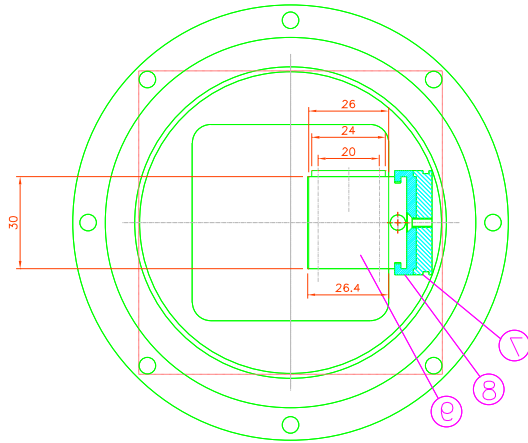


Figure 5.4: The small angle internal beamstop as seen by the beam.

angles, and this creates vacuum leaks.

5.5 $\theta_{K600} = 0^\circ$ beamstop for (p, t)

The (p,t) beamstop as used during PR137 is in the shape of an *L* and is made of brass. A picture of the beamstop is shown in Fig. 5.6. It is designed to be positioned inside the K600 between D1 and D2. The dimensions are provided in Fig. 5.7. A different beamstop, designed to have much less material that could contribute to secondary scattering of particles to the focalplane, is shown in Fig. 5.8. This beamstop was first used during PR170.

Note that similar as stated in the previous section, angles bigger than 20° is not at present possible in this configuration.



Figure 5.5: The 0° beamline and beamstop (2005 version). On the right hand side a section of the high dispersion exit window can be seen. While this picture is good to illustrate the 0° beamstop, note that the beampipe configuration was since changed to have the bellows on the beamdump side, and not just after vacuum valve. Refer to Fig. 10.17.

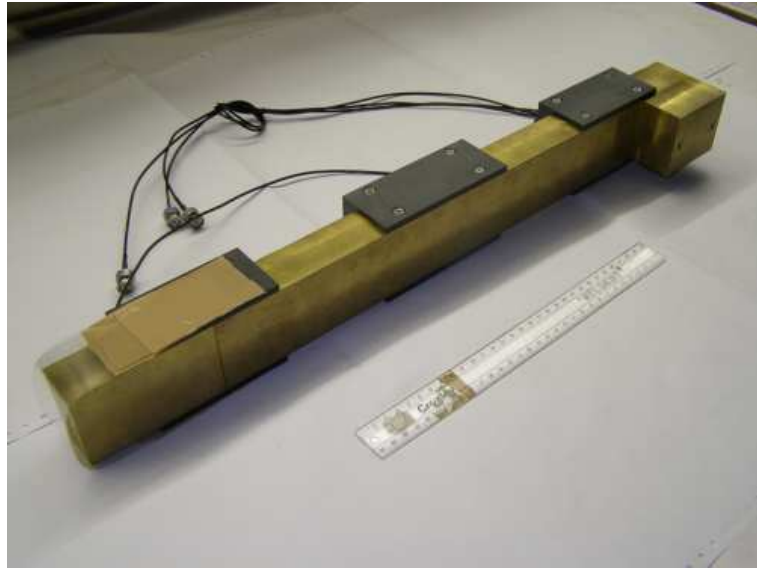


Figure 5.6: The (p, t) beamstop used in PR137. Note that it consists of three separate brass blocks, each with its own cable to go to the current integrator box inside the K600 vault.

5.6 To move the spectrometer

The 524mm diameter scattering chamber presently in use has a sliding seal mechanism. The drive mechanism of the seal in which the scattering chamber exit port is located is coupled

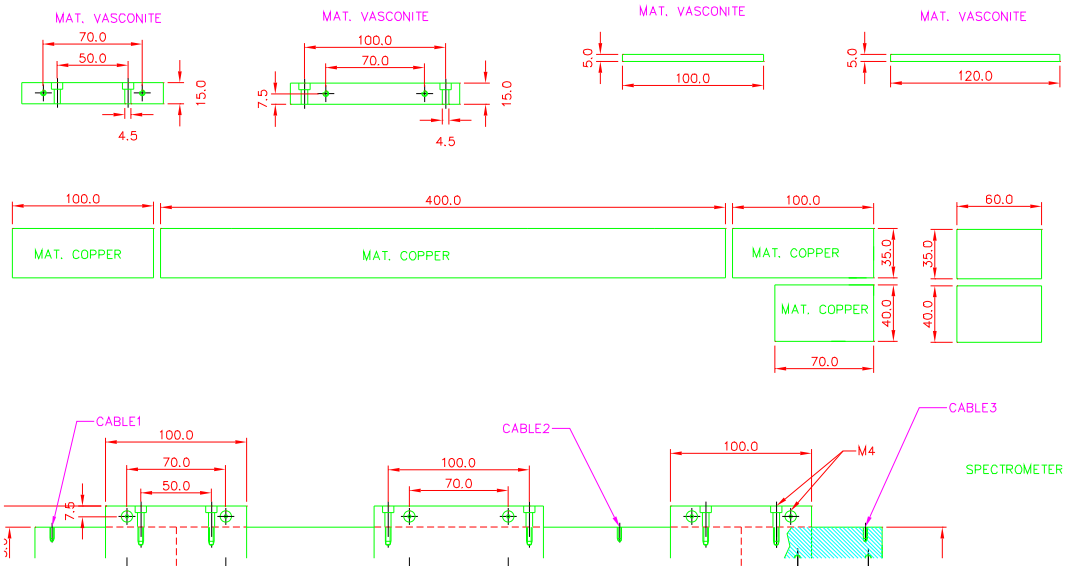


Figure 5.7: The dimensions of the (p, t) beamstop used in PR137.

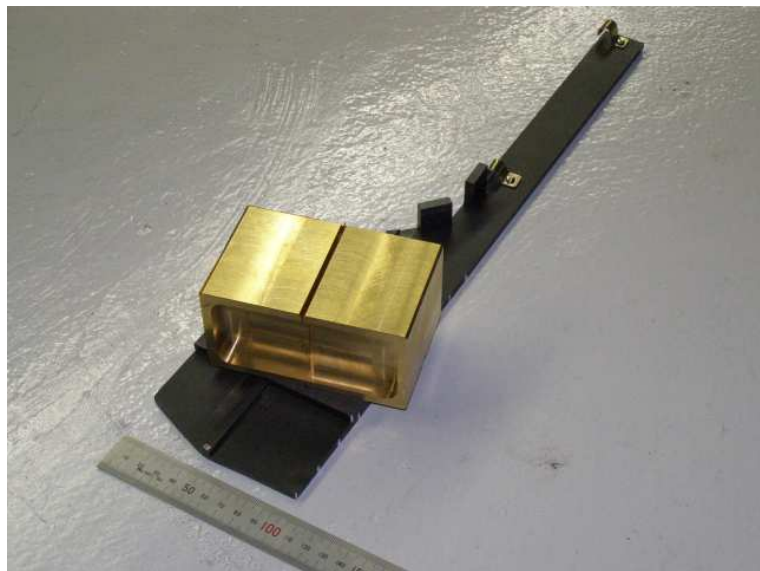


Figure 5.8: The (p, t) beamstop used in PR170. Note that it consists of two separate brass blocks, each with dimensions 70 mm (deep) \times 55.5 mm (wide) \times 55 mm (high). These dimensions includes the lip, which is 5 mm wide and 10 mm deep.

to the drive mechanism of the spectrometer itself. One control system can change both the spectrometer and the the sliding seal exit window to the desired angle setting. However, the system can be also be changed so that only one can be moved at a time.

Always ensure that the movement control tower is on clean earth, or it is unplugged during data acquisition. During PR97 the clean earth was contaminated by plugging the control tower into dirty earth and keeping it plugged in for the duration of the measurement. This resulted in 50Hz noise on the Current Integrator line.

Preferably move the spectrometer when there is good vacuum in the scattering chamber. Lubrication of the sliding seal tends to be better and it immediately becomes clear when a potential leak is forming, which can then immediately be fixed by moving the sliding seal back and forth in small steps.

The procedure requires at least two people.

- Turn down the HV on the detectors inside the scattering chamber (if there are any).
- *Close the valves between the scattering chamber and the K600 as well as between the scattering chamber and the rest of the beamline..* If the sliding seal of the scattering chamber functions perfectly no loss of vacuum should occur, but in reality a sudden loss of vacuum may still occur. A typical cause is inadequate amounts of vacuum grease at some sections of the sliding seal.
- Take the "to move spectrometer" key from the key cupboard and go into the K600 vault. If it is not there then it is most likely already in the vault.
- Check around the spectrometer to make sure there are no obstructions in the way of the spectrometer.
- Ensure that the movement control electronics tower is powered. This includes the Spectrometer Movement unit, the ECS 3 unit and the Digiplan Interface and motordrive unit. Also make sure that a so-called 'dummy break' is connected to the S2 connector of the ECS 3 unit. This is indicated in the top-right of Fig. 5.9.
- Ensure that the trip-switch at the power distribution box on the K600 is in the 'on' position, and that the red door-handle-type knob on the left bottom of this box is in the OUT position. This is achieved by inserting and turning the key. As the key is turned the knob jumps back allowing power on the controls.
- One person remains at the scattering chamber to observe the exit port to the spectrometer. This is to ensure that no unnecessary strain is put on the bellows between the exit port and the spectrometer as the angle is being changed.
- The other person goes to the control electronics tower. The key for the remote-control box is inserted into the red door-handle-type knob. When the key is turned the knob jumps back allowing power on the controls. Both knobs (on the K600 and on the remote control unit) should be in the OUT position.
- Press the OPERATE button together with the clockwise button (C.W.) to move the K600 clockwise, or press the OPERATE button together with the counter clockwise button (C.C.W.) to move the K600 counter clockwise. Both the K600 and the sliding seal will move in the desired direction. However, as the speed of the K600 and sliding seal is not quite equal they tend to get out of step with each other. In order to prevent any damage there are limit switches that will stop the movement of both the K600 and sliding seal

when they are too far out of step. A correction movement by the K600 is then required, since it is easier to move the K600 than the sliding seal. This correction movement is achieved by pressing the big green button on the SPECTROMETER MOVEMENT unit in the movement control electronics tower. This unit will indicate which limit switch was activated.

- The angle of the spectrometer can be read off at the marker at the graduation on the floor on the left of the control box.
- Take the key with you and evacuate the vault.
- Replace the keys in the cupboard.



Figure 5.9: The distribution box on the K600 is indicated in the top left. The bottom right illustrate the electronics in the movement control electronics tower as well as the remote control unit, while the top right show 'dummy break' without which the system will not function.

There is also a way to move the spectrometer manually. Ask the iThemba staff how. This is mostly used to make small corrections to the angle setting that is difficult to do with the motorized system.

I order **to move only the K600** disconnect the cable at the back of the Spectrometer Movement unit labelled *Spectrometer* as well as the cable labelled *Remote* and connect them directly to each other. This now bypasses the logic required to move both the spectrometer and the sliding seal, and allows you to only change the K600 angle.

On 27 January 2006 we put the K600 at 87° for experiment PR96b. This angle is the biggest to date (June 2006).

On 2 February 2005 we found that the K600 angle setting was out by 0.08° (+ or-?). Since when this was the case we do not know. This offset was corrected.

5.7 Small manual K600 angle adjustments

To be performed by hand with a 13 spanner, with 4.5 turns roughly equal to 0.1° .

5.8 Scattering chambers

The choice of K600 angle and where the beamstop is positioned is also connected to the choice of scattering chamber. The scattering chambers used for the K600 are shown in Figs. 5.10 - 5.13.

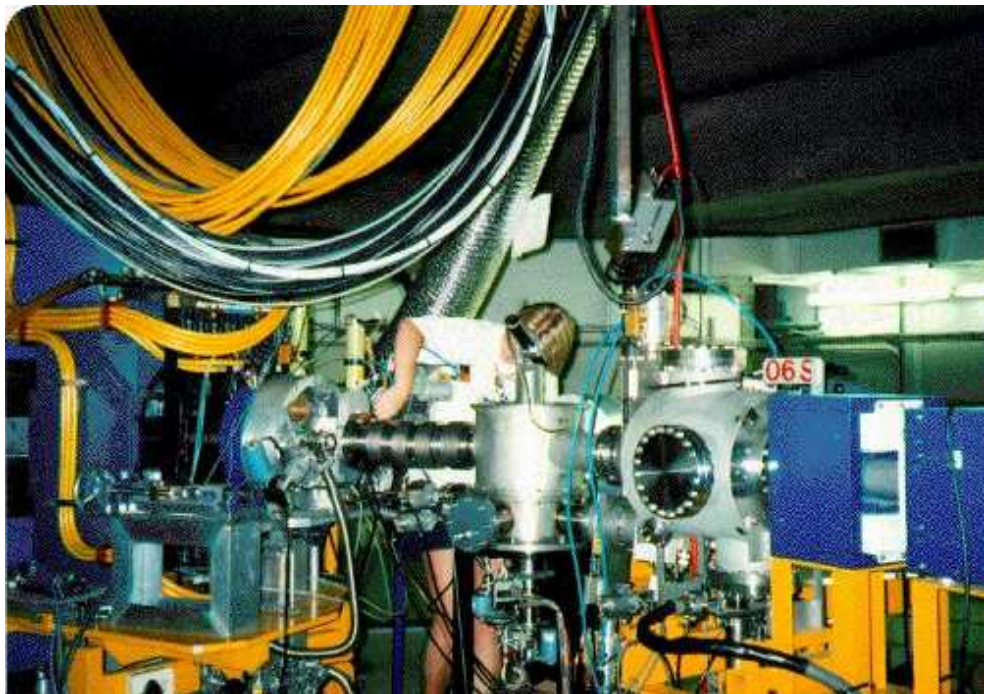


Figure 5.10: An old scattering chamber, from an undated picture. One assumption is that this picture dates from the middle 1990's.

5.8.1 The scattering chamber rotating table

Increasing the encoder reading rotates the table clockwise, and decreasing the encoder reading rotates anti-clockwise.

Typical earlier calibrations yielded roughly 10 steps equals 1 degree; see $(p, p\alpha)$ logbook!



Figure 5.11: An old scattering chamber, from the (p,2p) research of Cowley and Neveling. Circa 1999.



Figure 5.12: The sliding seal scattering chamber (originally from NIKHEF) with the small angle mode from 2015.

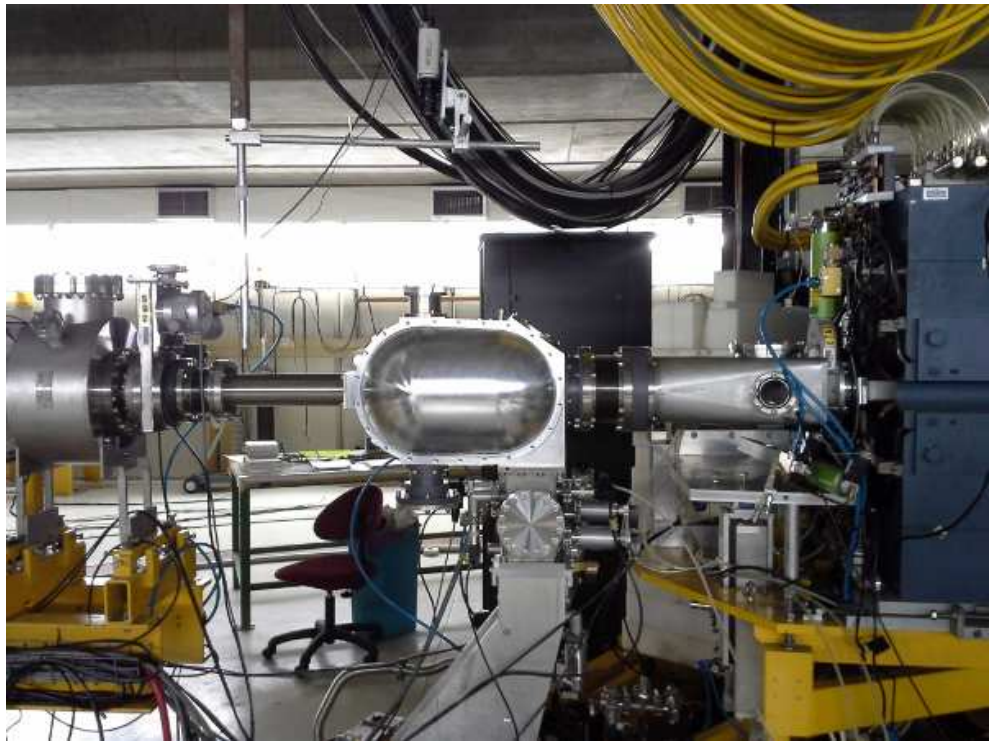


Figure 5.13: The new scattering chamber, designed by Paul Papka, during its commissioning run in 2014.

5.8.2 Sliding seals

- There are 2 different types: one with a big square 64×64 mm opening one with a small round opening of diameter = ? mm.
- The beampipe and bellows between the sliding seal opening and the K600 underwent several changes over time. There is a specific setup for the small round opening and different setups for the the square opening

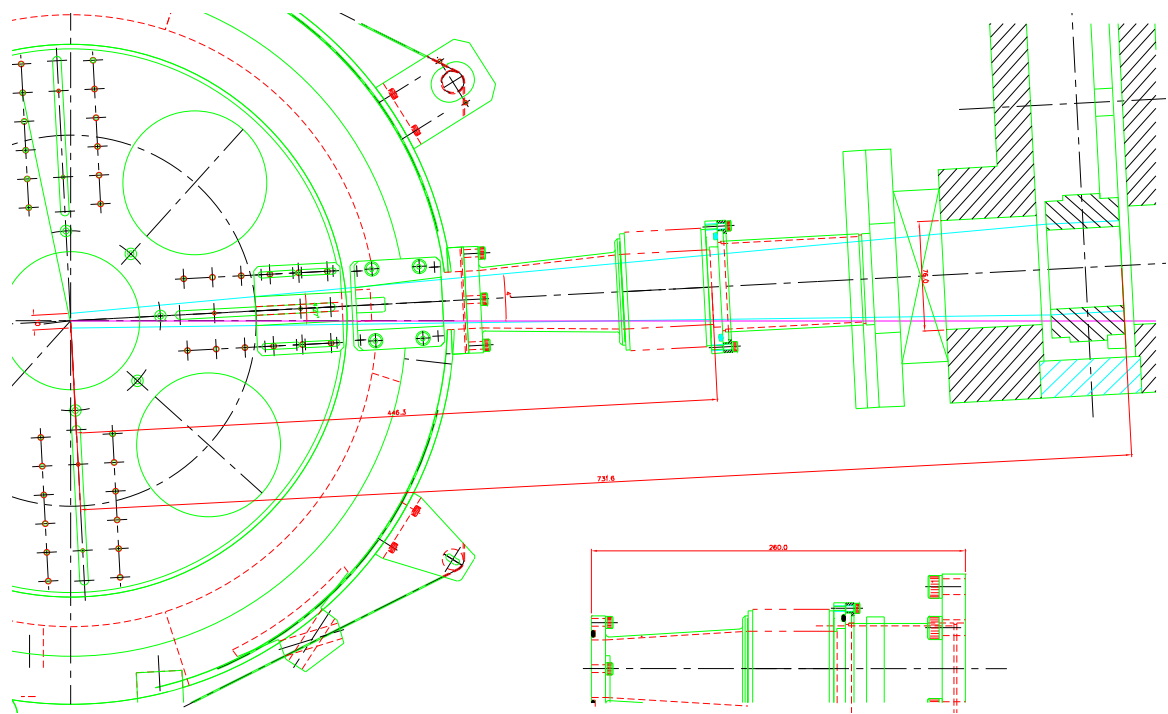


Figure 5.14: The original design for the exit sliding seal.

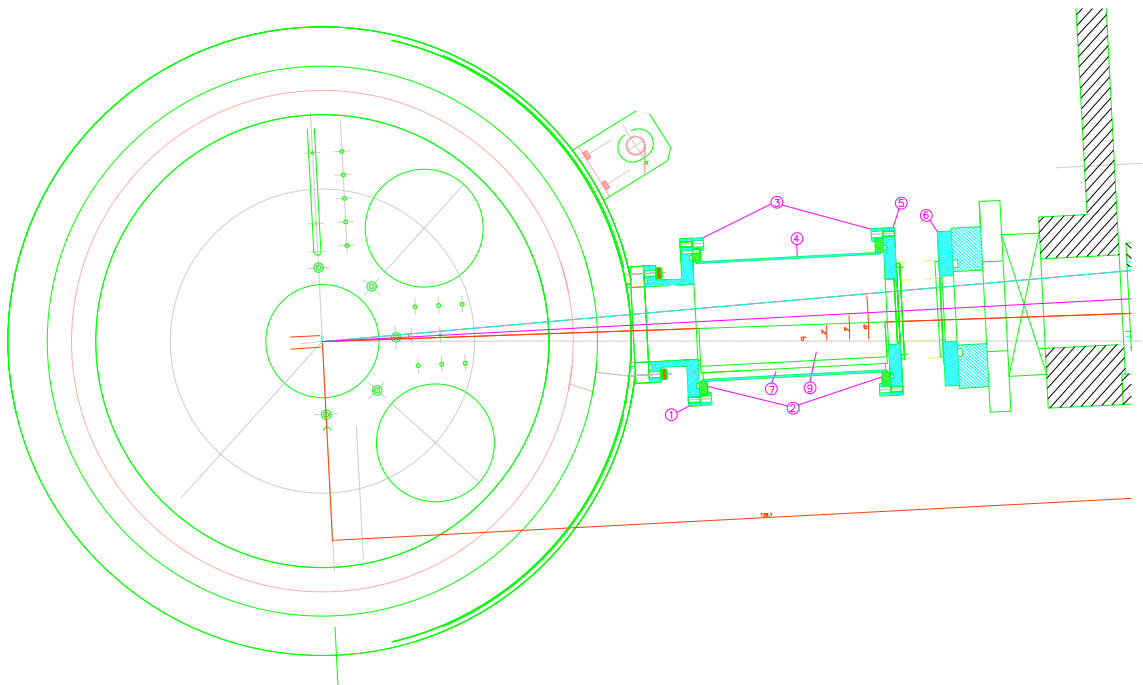


Figure 5.15: The so-called 'Nolan chamber' and the 64 × 64 mm² opening in the sliding seal

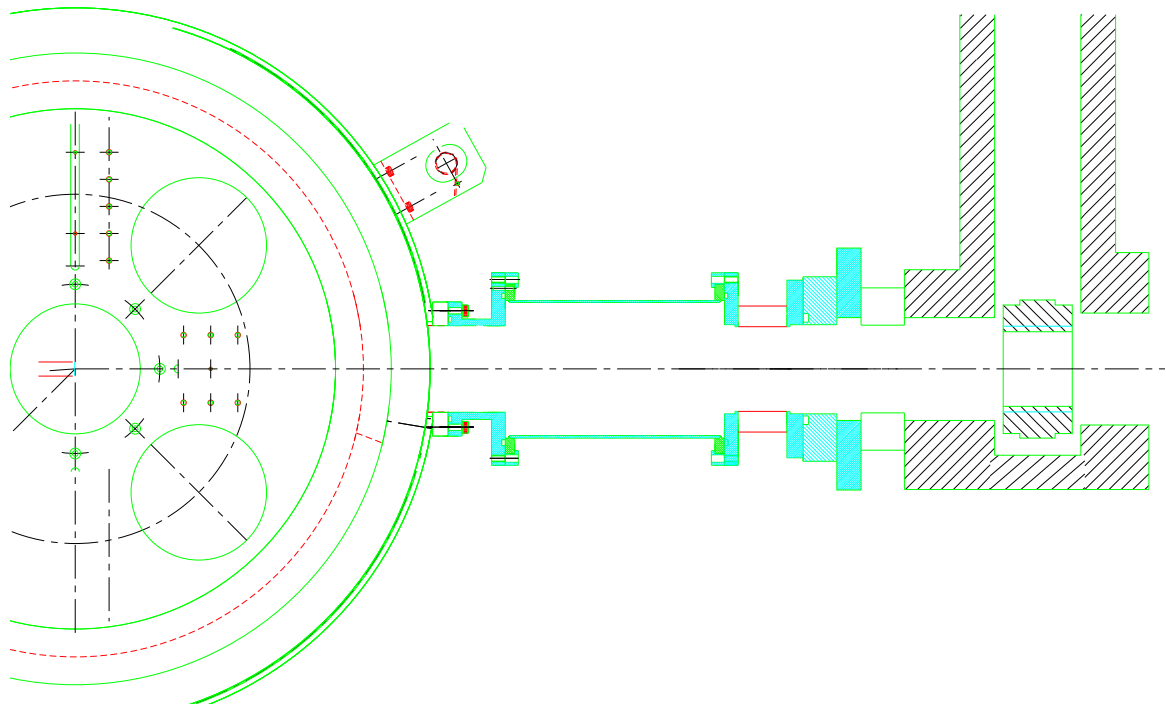


Figure 5.16: The $64 \times 64 \text{ mm}^2$ opening in the sliding seal connected to a new connection between the scattering chamber and the K600. The waist just before the vacuum valve was opened up.

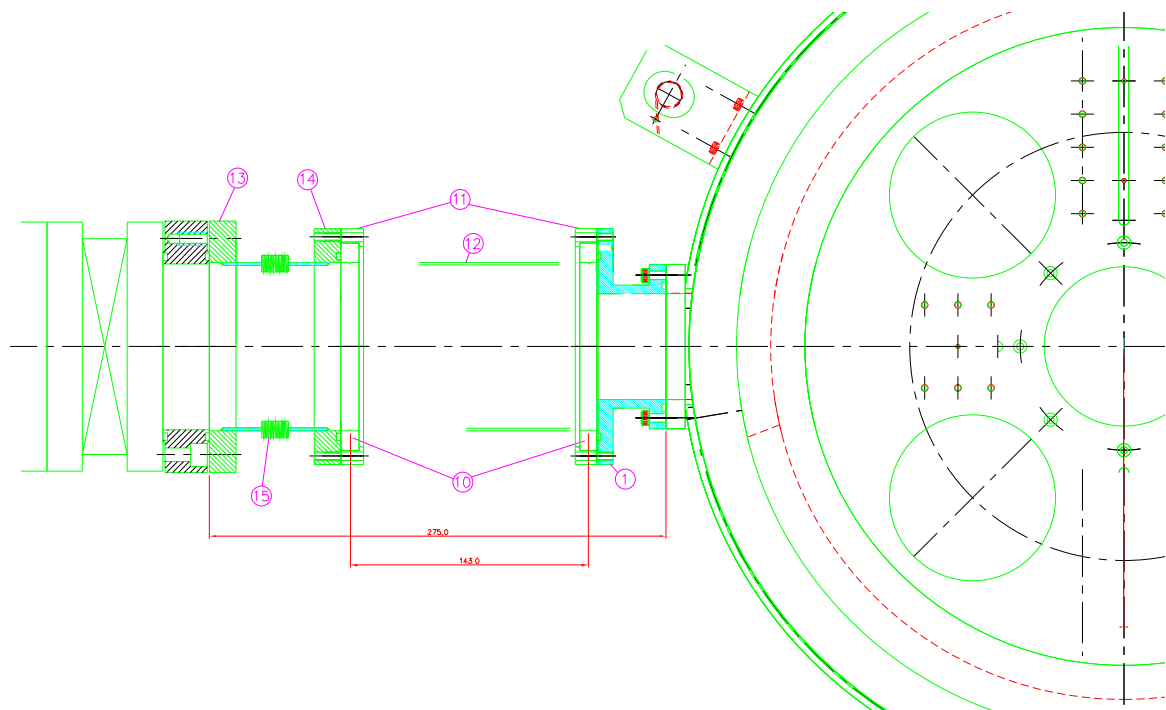


Figure 5.17: An overview of the new begger entrance to the scattering chamber, with a $64 \times 64 \text{ mm}^2$ opening in the sliding seal.

Chapter 6

Miscellaneous hardware

6.1 Hall probes

Monitoring B1P, B3P and Q1S-Q6S. In dataroom, on acc control page. In other words, not yet part of our datastream (March 2011).

6.2 Target ladder and frames

The normal target frames come in different sizes: 25mm diameter, 20mm diameter, 15mm diameter and there are a few that are even smaller. The movement of the target ladder (height and angle) is explained in fig. 6.4.

target	density (g/cm ³)	thickness (mg/cm ²)	thickness (μm)	eloss (keV)	straggling (keV)
C-12	2.253	1	4.44	3.9927	9.8165
Ca-40	1.54	1	6.49	3.5726	9.8789
Au-197	19.311	1	0.52	2.3081	9.0024

Table 6.1: Straggling calculations from LISE++V7.5.10. Is it not wrong that the straggling is more than the Eloss?!



Figure 6.1: An empty target ladder.



Figure 6.2: A semi-filled 0° target ladder, with the material on the low momentum side cut off. Notice that one of the target frames are modified to also have less material on the low momentum side. is



Figure 6.3: Two target ladders filled with varios targets.

6.3 BeamLossMonitors: the halo detectors

The Bergoz Beam Loss Monitor (BLM) consist of two PIN-photodiodes mounted face-to-face to detect charged particles. Coincidence counting make it insensitive to synchrotron radiation

- Active area = 7.34 mm^2
- Maximum count rate $> 10\text{MHz}$
- Output: positive TTL 50 ohm

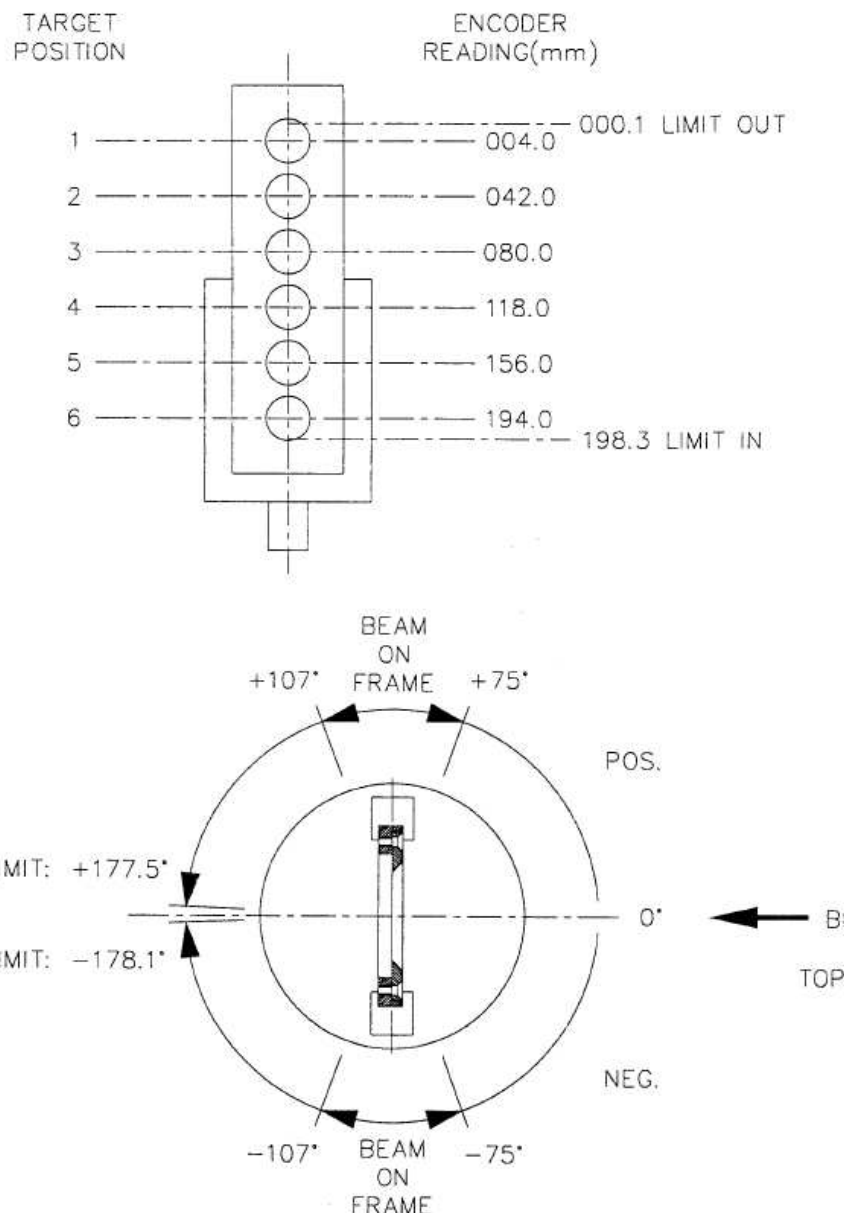


Figure 6.4: Notes on the target ladder height and angle.

- Cabling: BLM connected to the 50 ohm patchpanel to a level adapter (TTL input, NIM output) to a CAMAC scaler.

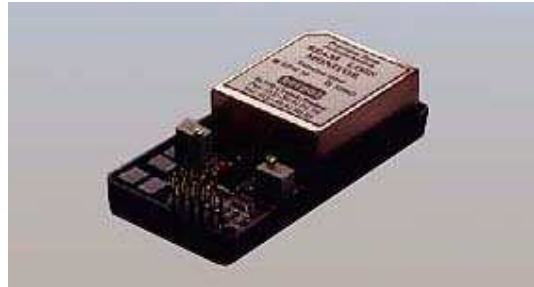


Figure 6.5: The BLM

6.4 Beamviewers

There are three ZnS scintillating viewers in the K600 vault. The first one, which is located just after QS6, is referred to as Hatanaka's mesh¹. The beam image on this viewer should be wide and flat. This viewer is listed as Harp 5S on the operators' control system and is approximately 3.1m from the target center.

NOTE: the *ZnS* is actually most likely phosphor slurry (P22-GN4).

The standard beamviewer at the target position is also made of ZnS. Other than most other iThemba LABS experiments this viewer is a solid screen, i.e. it is not a mesh as Hatanaka's mesh/viewer, and there is no hole in the center as in the case of ordinary 'ruby' targets. Figs.9.1 and 9.3 illustrates how an achromatic beam and a dispersion matched beam should look like on this viewer.

The last viewer is a solid ZnS screen (i.e. not a mesh) that is located in the zero-degree beamline just before the zero-degree beambump. It is 50mm×70mm big, and angled at 45° with respect to the horizontal plane, i.e. for the camera it looks like a square of 50mm×50mm. (At some stage it was harp 6S on the operator's control system).

Typical beamcurrent on these viewers should not exceed 1nA.

6.5 The focal plane beamblocker

There is a 60mm thick movable brass block inside the K600 vacuum-chamber, just in front of the Kapton exit windows, that makes it possible to blank out a section of the focal plane. This blocker can be positioned in front of both the high and medium dispersion planes. There is, as part of the focal plane beamblocker mechanism, a 10mm high (stainless steel?) strip at the bottom of the focal plane (see 1.2) that may adversely influence overfocus mode measurements.

In the Protokolbuch of 29 June 2001 the focal plane blocker encoder calibration for the medium dispersion plane is given as

$$\text{encoder} = 0.348872 \times \text{channelnumber} + 4222.284 . \quad (6.1)$$

At present (September 2005) we do not have control of the beamblocker when the 0° beamline is attached, because there is no electronic feedthrough in this mode. The feedthrough exist only for the small vacuum window and the blank flange.

¹Hatanaka's mesh is named after Prof. Hatanaka from RCNP who provided us with the hardware.

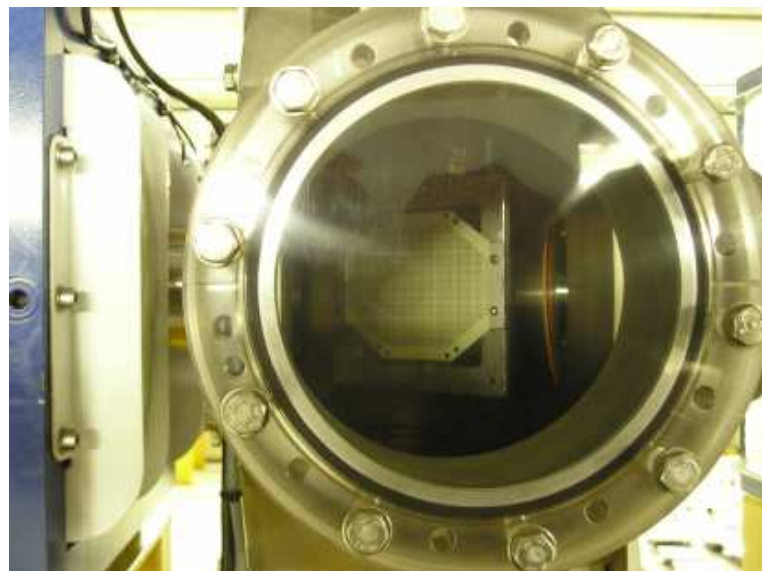


Figure 6.6: The so-called Hatanaka mesh/viewer. It was designed so that viewed from 45° (as it is used in the beamline) the small blocks are 1mm by 1mm. Each bigger block represents 5mm in x and y. The mesh is approximately 3.1m from the target.

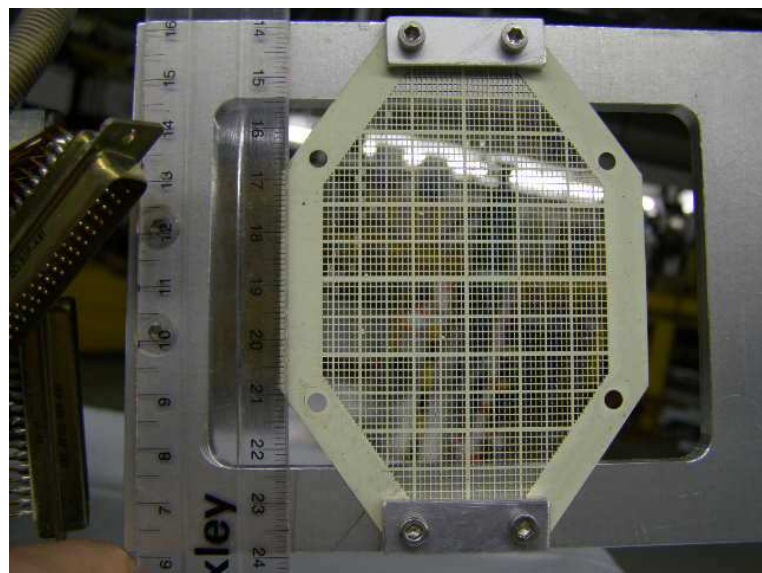


Figure 6.7: The so-called Hatanaka mesh/viewer. It was designed so that viewed from 45° (as it is used in the beamline) the small blocks are 1mm by 1mm. Each bigger block represents 5mm in x and y. The small blocks are 1mm by 1mm. Each bigger block represents 5mm. Note that due to a water leak in the beamline the mesh was replaced and this mesh is smaller, though subdivisions are still same size.

Left on the control system implies movement to the high P side, and right implies movement to the low p side. There is also the possibility to read the charge/bemcurrent on the focal plane blocker. use the bnc connector at the focal plane blocker electric panel on the k600

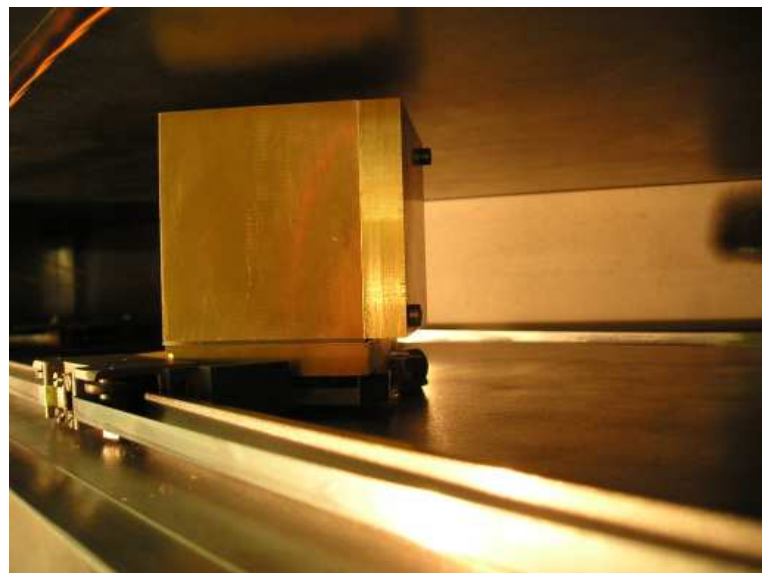


Figure 6.8: A picture of the focal plane blocker. The extra 10mm of brass that was added in 2004(2005?) can clearly be seen

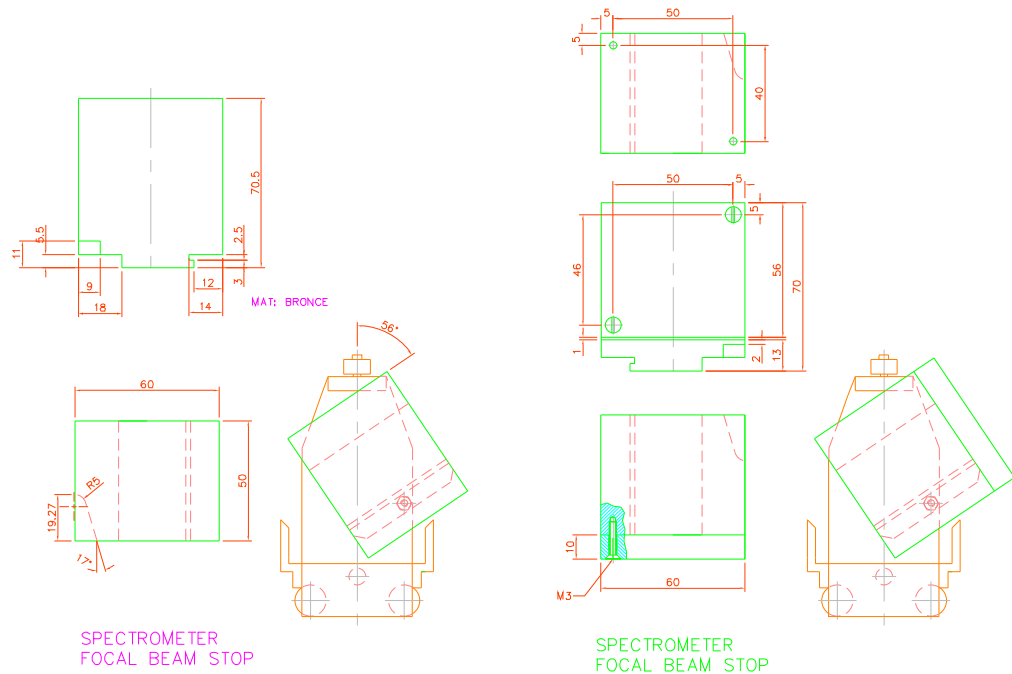


Figure 6.9: The focal plane blocker: then (50mm) and now (60mm).

6.6 Al E-degrader plates for paddles

Hardware exists to place Al plates next to the paddles (both old and new) to act as E-degraders. 3 plates of 0.85mm and 3 plates of 1.18mm thickness.

6.7 Slits at 9X

The X and Y slits were changed from long parallel slits to a new design shown in Fig.6.10. Note that these slits are positioned 150 mm apart, with the closed side of the slit jaw facing each other. The high beam currents used during isotope production made it impossible for the accelerator group to install real thin slits. Current reading from these slits are available. Slit position can be controlled by stepper motors in 0.1 mm steps.

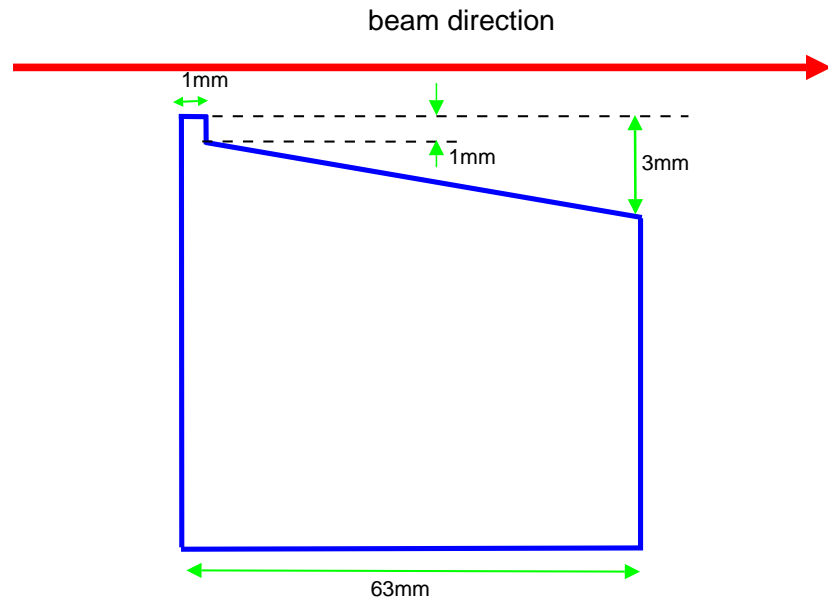


Figure 6.10: The slits at 9X looks like this.

Chapter 7

Gasflow to the driftchambers

The gas handling station is located just to the left of where the beam enters the K600 vault. See Fig. 7.2.

7.1 Gas pipe connections

- The copper pipes are reserved for carrying the gas to the drift chambers.
- The plastic pipes are reserved are for carrying the gas away from the chamber.
- Green taps on the drift chambers are inlets.
- Red taps on the drift chambers are outlets.
- There are unmarked pipes, pipes marked C and pipes marked U. The pipes at the detector end are clearly marked according to the entrance/exit markings at the gas handling station.

7.2 Turning the gas on

The drift chamber gas is a mixture of 10% CO_2 and 90% Ar premixed supplied by Air Products (in the pink cylinders). ¹ Two cylinders of the gas is usually coupled to the gas handling system. Typically one would be in use and the other spare. If the spare bottle is empty it should have an ‘EMPTY’ tag hanging from it. The one in use has an ‘IN USE’ tag hanging from it. A small black valve with one pointed end is at the junction of the pipes from the two cylinders. The valve should be parallel to the pipe and pointing in the direction from which you would like the gas to flow.

The gas line needs to be opened from the outlet to the inlet (and closed in the reverse order). It is a precautionary measure against accidentally over-pressurizing the drift chambers.

¹The decision to use this particular gas mixture was originally taken based on the information in [But90]. NIM A290 (1990) 122.

- Start by ensuring that all the valves between the gas bottles and the gas panel are closed.
- Then connect the output gas line to the oil bubbler, which is in the bottom right hand corner of the gas handling panel.
- Now start to open the valves: situated directly below the drift chambers are the outlet valves (in front) and the inlet valve (at the back). **the same for the HDC?** Open the VDC1 outlet valves and then the inlet valve. The valve is open when the handle is parallel to the pipe. Do this for both VDCs and the HDC.
- The necessary valves on the gas handling panel are normally all left open. Between the cylinders and the gas handling panel are two in-line filters. These two filters, the oxysorb and the hydrosorb, are isolated by the three green valves on either side of them. When their handles are parallel to the pipe the valves are open.
- Between the gas bottles and the filters is a regulator. The horizontal valve is a throttle. Turn this valve anti clockwise to close it.
- ONLY now one can open the valve on top of the gas bottle. The pressure should be indicated on the left hand-side gauge at the regulator, and the right hand-side gauge should be on zero.
- Open the throttle at the regulator slowly. You will notice that the throttle turns with very little resistance. While there is no resistance, the valve is closed. As soon as one starts to feel resistance one should turn carefully while looking at the top left flow-meter on the gas handling panel. The flow should be set at about six on the flow meter. Initially the flow will decrease and needs to be cranked up a bit for about fifteen minutes until the flow has stabilized. There is a slight time delay between the flow meter indicating a flow and bubbles starting to appear in the bubbler.
- Allow the gas to flow for a little while before testing whether the drift chambers can hold HV. This is to the drift chambers from unwanted pollutants which may have leaked or diffused in while the detector was not in use.

7.3 Turning the gas off

The whole process must now be reversed by starting at the gas bottle and working towards the detector.

Firstly the valve on the bottle must be closed. There is some pressure left on the regulator of the bottle. When this pressure has dissipated, the bubbler will stop bubbling. Just before this point is reached the flow indicated on the flowmeter will steadily climb to a maximum before dropping to zero. The horizontal black valve on the regulator in the line can now be closed followed by closing the green valves to isolate the hydrosorb and the oxysorb. Next to close are the valves to isolate the chamber. Always close the inlet first and then the outlet. This way one will not accidentally trap an overpressure in the chamber and pop the windows. Lastly, **and most importantly**, go to the gas panel and uncouple the line at the bubbler. This is done to prevent the oil being sucked into the gas exit lines.



Figure 7.1: The gas handling station

7.4 Replacing a gas bottle

It is important to first bleed a little of the gas-mixture through the pipe connecting the gas-bottle to the T-junction. Otherwise air will contaminate the gas mixture in the drift chamber, and it will take time to purge the detector.

7.5 Specs of a good gas

The volume between the two cathode planes is filled with gas mixture of 90% Ar and 10% CO_2 . The decision to use this particular gas mixture was originally taken based on the information in [But90]. NIM A290 (1990) 122. The following table summarizes specs for a good gas needs. More oxygen or water content will cause ... This follows from a 1993 spec sheet on the gas quality as well as recent experience.

Date	Ar content %	O ₂ content (ppm)	H ₂ O content (ppm)	N ₂ content (ppm)	HC content (ppm)
1993	10	<5	<5	<20	<1
2007	9.5	7.4	0.1	no info	no info
2008	10.2	2.15	0.52	no info	no info

Table 7.1: Specification of good VDC gas

7.6 The hydrosorb and oxysorb

The hydrosorb is used to filter out water particles, while the oxysorb acts as a filter for oxygen.
Replacement procedure:

1. Close all the valves.
2. Start with the hydrosorb. Unscrew on the left, then right.
3. Put in new one first in the right and then the left. Remember to change all the o-rings from the old to the new and put plumber tape on the new 'skroefdraad'
4. Now purge the hydrosorb by letting the gas flow through the detectors.
5. Close all the valves.
6. Replace the oxysorb in the same way as the hydrosorb.



Figure 7.2: The oxygen and water filters.

Chapter 8

Vacuum

8.1 K600 vacuum

Pumping down the K600 was originally done by the lab's vacuum expert. However, over the years the in-house scientists had to take over this function simply due to the workload of the vacuum department, combined with the much more frequent nature of pumping cycles. This increase in the pumping cycle frequency came about due to use of internal beamstops in D1 for zero degree experiments.

This is probably also why we had our first Kapton window implosion on 30 June 2016, with resultant damage to one new XU-VDC.

In light of this it is important to define some operating procedures for pumping down the K600.

- First of all, do not allow a Kapton window to be more than 4 years old.
- If at all possible, take off all the focal plane detectors before starting to pump.
- An Al cover should be in front of the Kapton window when pumping down.
- Ensure that this cover is properly seated so that in the event of an implosion it can block the inrush of air, so that the full force of 1 ATM is not immediately transferred to the pumps. This also giving the vacuum valves time to close.
- If you cannot take off the detectors, at least move the detectors further away from the Kapton window.
- Pump down the K600 from atmosphere to 1 mbar by means of a small fore-pump, preferably one inside the scattering chamber, which can be throttled.
- It should take $\sim 75\text{min}$ to get down to 1 mbar. If it takes longer, then you may have a problem with the Kapton foil. Vent and consult an expert.
- In our (limited) experience of the 2 foils that failed (one damaged a VDC, another broke as part of a test) the Kapton will fail at fore-vacuum pump vacuum levels.
- This means that for each pump cycle, you should allow the vacuum to reach 1 mbar before switching on any turbo pumps. **Do not get impatient and switch on the K600's big forepumps to speed up the process.**

- Pump for 24h with only a fore-pump to make sure the foil is in good shape. Only then switch on one of the 2 big turbos on the K600.
- The Kapton foil should be 75micron thick.

In July 2016, after replacing the Kapton foil, when the vacuum stabilized, the following values for vacuum was attained: meter 8 (at P37) = 1.6×10^{-5} mbar, meter 6 (at P36) = 5.0×10^{-6} mbar, meter 7 (at Kapton window) = 4.25×10^{-5} mbar.

8.2 Scattering chamber vacuum

Two people are required to perform the procedure to pump the scattering chamber. One person must be in the K600 vault at the scattering chamber (*person A*), and the other person must be at the vacuum remote control station in AG1 (*person B*). These two should be in contact per telephone. The telephone number in the K600 vault is 1210, and the number in AG1 is 1200.

- Person A must make sure that there is a hand-valve at the fore-pump, **and that it is closed**. Without this valve thin targets will be destroyed when the fore-pump is switched on.
- Person A must make sure that the green vent-valve on the scattering chamber is closed.
- Person B opens the remote controlled valve ?SV8? between the pumps and the scattering chamber.
- Person B starts the fore-pump while the hand-valve on the fore-pump is closed.
- Person A slowly opens the hand-valve.
- Once the vacuum reaches 1 mbar and the hand-valve is completely open person B can switch on the turbo pump. NOTE that there is a limited time window (after switching on the fore-pump) during which the turbo pump must be switched on. If not, valve ?SV8? closes automatically and the fore-pump is switched off.

When letting up the scattering chamber to air, always close the hand-valve at the fore-pump. This prevents one from forgetting to close it before starting to pump down, which can ruin fragile targets.

To get to the 10^{-5} mbar range takes anything from 20min to 1h20min, depending on how long ago the chamber was pumped down.

Chapter 9

Dispersion matching

According to Wakasa *et al.* [Wak02] the concept of dispersion matching was first demonstrated by Blosser *et al.* [Blo71] after Cohen [Coh59] illustrated that if the beamline and a spectrometer is properly 'matched', the spectral resolution can be better than the beam resolution, up to the limit of the resolving power of the analyzing spectrometer. Proper matching of the incident beam to the K600 spectrometer is thus extremely important if optimum resolution is to be obtained.

A 'normal' or achromatic beam is set up so that the position and angle of protons *on the target* are independent of the momentum of the incident proton, or in Enge [Eng81] notation $(x \mid \frac{\delta p}{p}) = 0$ and $(\theta \mid \frac{\delta p}{p}) = 0$. This is also referred to as **double-achromatic transport**, when we have, in TRANSPORT notation, $b_{16} = 0$ and $b_{26} = 0$ [Fuj02] [Wak02]. For such a beamline setup the inherent momentum distribution of the proton beam limits the energy resolution of detection in the K600 focal plane. To overcome this problem a dispersion matched beam spatially separates the protons according to momentum so that those with the higher momentum will travel a longer distance through the spectrometer than those with smaller momentum, effectively achieving *achromatic focus in the focal plane* [Fuj00] [Fuj02].

9.1 Theoretical background

The following description is an abbreviated version of selected sections from the NIM paper of Hiro Fujita [Fuj02]. It is reproduced here only to serve as a quick reference. The original article should be consulted in order to gain a full understanding of dispersion matching.

Assume that the proton beam enters the beamline system at the source point, which is slit 9X in the X-line at iThemba LABS. The horizontal coordinates at the source point, $(x_0, \theta_0, \delta_0)$, represent the position, angle and fractional momentum deviations from the central trajectory [Wak02]. The beam is transported by the horizontal 3×3 beam transfer matrix $\mathbf{B} = b_{\mu\nu}$ ($\mu, \nu = 1, 2, 6$) to the target position, and then by the spectrometer transfer matrix $\mathbf{S} = s_{\mu\nu}$ to the detector plane, given by the coordinates $(x_{fp}, \theta_{fp}, \delta_{fp})$. The suffixes 1,2 and 6 represent the coordinates of position, angle and fractional momentum respectively. The transformation from the source point to the detector plane is given as

$$\begin{aligned} x_{fp} &= x_0(s_{11}b_{11}T + s_{12}b_{21}) \\ &\quad + \theta_0(s_{11}b_{12}T + s_{12}b_{22}) \\ &\quad + \delta_0(s_{11}b_{16}T + s_{12}b_{26} + s_{16}C) \end{aligned}$$

$$+ \Theta(s_{12} + s_{16}K) \quad (9.1)$$

and

$$\begin{aligned} \theta_{fp} = & x_0(s_{21}b_{11}T + s_{22}b_{21}) \\ & + \theta_0(s_{21}b_{12}T + s_{22}b_{22}) \\ & + \delta_0(s_{21}b_{16}T + s_{22}b_{26} + s_{26}C) \\ & + \Theta(s_{22} + s_{26}K) \end{aligned} \quad (9.2)$$

and

$$\delta_{fp} = K\Theta + C\delta_0 . \quad (9.3)$$

The target function T is defined by

$$T = \cos(\alpha - \phi_T)/\cos(\phi_T) , \quad (9.4)$$

where α is the nominal scattering angle in the lab frame and ϕ_T is the tilting angle of the target. Θ is considered the ‘effective scattering angle’ (in my view a badly named angle, as it only gives an indication of how much the real scattering angle *deviates* from the nominal scattering angle). For a detailed description on the relevant angles refer to [Fuj02]. The kinematic factor, K , is defined as

$$K = (1/p_{out})(\partial p_{out}/\partial\alpha) , \quad (9.5)$$

and is 0 at the nominal scattering angle $\alpha = 0$. The ‘relative momentum ratio’ C is given by

$$C = (p_{in}/p_{out})(\partial p_{out}/\partial p_{in}) , \quad (9.6)$$

and is 1 for elastic scattering. Note that the kinematic factor is defined to be negative when the reaction products are observed on the left of the beamline (see TRANSPORT notes: the sign of K depends on the convention used for scattering angle).

When one considers the first three terms of Eq. 9.1 it is clear that they depend on the beam, target *and* spectrometer transfer matrices. Only the last term depends solely on the spectrometer transfer coefficients. Remember that the aim is to achieve the best possible spatial definition in the focal plane. If one can prevent x_{fp} from being sensitive to the ranges of angles θ_0 and momentum spread δ_0 at the source point as well as the different scattering angles at the target (which plays a role in all four terms), then the range of values for x_{fp} and θ_{fp} also comes down, which means better spatial and angle definition.

The first step towards high energy resolution is achieved by ensuring that $s_{12} + s_{16}K = 0$. This so-called **kinematic correction** is achieved by changing the magnetic spectrometer field in such a way that an upright image of a nuclear state is achieved in the two-dimensional plot of x_{fp} versus θ_{fp} . This is achieved by changing the K coil¹, adjusting $(x | \theta)$ (or s_{12}) for first order focussing, and H coil², which is for correction of $(x | \theta^2)$ (or s_{122}) aberrations. *Please note that the kinematic correction alters the ion optical properties of the spectrometer. It is thus important that this correction be achieved before attempting to adjust the coefficients of δ_0 and θ_0 .*

After the kinematic correction is achieved the aim is to make x_{fp} independent of the momentum spread and angle at the source point. Once the coefficients of δ_0 and θ_0 are adjusted to be zero the remaining term $x_0(s_{11}b_{11}T + s_{12}b_{21})$ will define the smallest possible focal plane image, and thus resolution. For $K < 0$ (i.e. non-zero degree) measurements:

¹The K-coil is a pole face current winding which introduces both a dipole and quadropole component

²The H-coil is a pole face current winding which introduces both a dipole and sextupole component

- the coefficient of θ_0 can be zeroed by shifting the focus on the target downstream of the target. This is referred to as **focus matching**.
- The elimination of the coefficients of the δ_0 term results in **lateral dispersion matching**. Note that the coefficients of δ_0 in Eq.9.1 and 9.2 can also be set to values to simultaneously result in lateral and **angular dispersion matching**. The beamline parameters b_{16} and b_{26} will then have to be

$$b_{16} = -\frac{s_{16}}{s_{11}}(1 + s_{11}s_{26}K - s_{21}s_{16}K)\frac{C}{T} \quad (9.7)$$

and

$$b_{26} = (s_{21}s_{16} - s_{11}s_{26})C. \quad (9.8)$$

This is in contrast to achromatic focus at the target where $b_{16} = 0$ and $b_{26} = 0$.

Angular dispersion matching is required only if angle information is critical, such as the case of a zero degrees experiment. See Chapter 10 for more on measurements at zero degrees.

In order for lateral dispersion matching to be successful a dispersive monochromatic focus of beam on target is required, which means that rays with different δ_0 are focussed at different positions on the target [Fuj02].

Finally, it is important to note that the resolving power of the matched system is dependent on the inverse of the beamsize at the source point:

$$R = \frac{1}{2x_0} \cdot \frac{s_{16}}{s_{11}b_{11}T + s_{12}b_{21}}. \quad (9.9)$$

The final dispersion matched condition as represented by Eqs. 9.7 and 9.8 as well as the focus matching condition was achieved by taking specific spectrometer coefficients $S=s_{\mu\nu}$ into account. These spectrometer coefficients were determined by the kinematic correction procedure with the K and H-coils. **Strictly speaking this means that especially the K-coil settings should not be touched after focus matching and lateral and angular dispersion matching was achieved. If K coil settings are changed after achieving dispersion matching, then you should at least verify by changing Q6 and Q5 that the best possible dispersion matching conditions still prevails.** Dispersion matching concerns only the first order matrix elements. Therefore, in principle, one can change the H-coil even after dispersion matching was performed since it affects the second order matrix term ($x \mid \theta^2$). The same is of course not true for the K-coil as it changes the ($x \mid \theta$) matrix element. Consider the following as an example: During the Nov08 66 MeV beamtime of PR146 we achieved a dispersion matched condition with energy resolution of about 20 keV (see p133 of logbook). After dispersion matching was achieved it was decided that additional kinematic correction is needed. Some K-coil and H-coil changes were made (see p137 of logbook). Following this a quick scan of Q6S was performed, but we could not regain the 20 keV energy resolution. At best we could achieve 26 keV (see p137). What happened here was that after the K and H coil changes the beam and K600 were no longer dispersion matched. To get them matched again a much more elaborate dispersion matching procedure was needed than a quick Q6S scan. After we changed everything back to the original settings (K, H and Q6S) we recovered the 20 keV resolution. **Let this be a warning. Do not mess with the K and H coil after dispersion matching!!!!**

Emittance of the beam: the proton beam obey the conservation law of phase space known as Liouville's theorem, which states that the area within the phase space contour is conserved. The area of this contour, usually an ellips, is called the emittance of the beam. The emittance (the area of the ellips) will be conserved as the beam passes down the transport line irrespective of the magnet focussing or the bending operations performed on the beam. At any given point all the particles that makes up the beam fill the ellips. The ellips can change in shape, but must always conserve the area.

9.2 Comment on Beam-line elements

- The last three quads in the S-line, Q4S-Q6S, were changed from 75mm to 100mm diameter quads somewhere in 2007, before Sept07 (in the Sept 2007 run the operators wrongly used the old values. See Acc archives of 15 Sept 07).
- The first three quads in the S-line, Q1S-Q3S, were changed from 75mm to 100mm diameter quads somewhere in 2009. Most likely after PR137 but before PR138, during the mid year shutdown.
- the last three quads in the N-line before B3P bending magnets, referred to as Q1N-Q3N, are not used in either dispersive or achromatic beamline modes. They were installed for

the neutron TOF facility. The same powersupply is in any case used by Q1S-Q3S or Q1N-Q3N. So it is not as if these can be accidentally be switched on.

-

9.3 Comments on practical matching for $\theta_{K600} \neq 0$

where to put this info: from SPC2 we have higher emittance (as measured in the S-line) than with SPC1. If you have SPC1 and measure 7-ish pi mm rad for x emittance, then that is not good some attention is needed to SSC tune or SPC1 to SSC beamline

In an ideal world (i.e. where we have SSC and injector flattopping for all beam energies one should always start the weekend with an achromatic beamtune. The aim is to ensure that the inherent beam quality from the *accelerator* is good, i.e. small energy spread in the beam and as little as possible halo originating from anywhere before slit 9X. This helps one to test the beam quality independent of the K600 characteristics. E.g. in dispersion matched conditions it may be uncertain whether the bad energy resolution is due to a bad beam out of the SSC or due to bad dispersion matching of the beam to the K600. And since the beam profile of the dispersion matched beam is bigger than the achromatic beam, valuable hours may be lost trying to 'tune the halo' in the P or S-lines when in reality the source of the halo is further upstream.

However, in the real world where we do not have flat topping at experimental energies and where the SSC is in need of the electrostatic channel at injection which was removed for the 66 MeV flattopping we should not start with an achromatic beamtune. At RCNP the flat-topping available to them on both the injector and RING cyclotron results in very good beam quality at the RING extraction with small beam size and divergence. This makes it possible to work without slits from the object point after the RING cyclotron to the target. At iThemba LABS we can 'tune' the accelerator only to a limited level by looking at the achromatic beam as the operators HAVE TO use slit 1P in the P-line to cut the beam dispersion. This slit gap is typically anywhere between 6 and 10mm. WE CAN NOT OPEN 1P ALL THE WAY AND HOPE TO HAVE GOOD ACHROMATIC RESOLUTION. The beam energy spread is simply not small enough, and single turn extraction at e.g. 200 MeV is not that clean. And since we HAVE to use slit 1P, that also means we HAVE to use cleanup slits in the beamline after slit 1P. Finally, the only time when it may be worthwhile to start with an achromatic tune is if the beamenergy is significantly lower than 200 MeV (protons). We achieved some success with the 100 MeV proton beam of PR137.

Here follows a few guidelines to help to achieve a dispersion matched system when $K \neq 0$, i.e. for finite angle measurements:

- As mentioned above the classical reasons to start with an achromatic beamtune does not really apply to a 200 MeV proton beam experiment. But there may be other reasons one wants to start with an achromatic beamtune. One example is the need to obtain good angle calibration spectra. This should be done with the pepperpot and an achromatic beam.

- Beam transmission through the SSC should be maximized. At lower energies one can get very good transmission, but at 200 MeV at least 50% transmission is the norm. During PR138 we had 160nA on FC19J and 100nA on FC1X for 200 MeV protons. During PR137 (logbook1 p97) we had 1.4nA on FC19J and 1.1nA on target for 100 MeV protons. From logbook2 p131 we had virtually 100% transmission from FC19J to FC1X.
- The size of the object point at slit 9X should be 1mm in the X direction and 2mm in the Y direction. Beam transmission through the object slit must be maximized. We do not want a big blob of beam dumped on the slit, and then select only the central part of the beam. Nevertheless, due to the beam quality from the SSC, especially at 200 MeV, it is not possible to focus the beam through these slits without creating a lot of halo at the divergence slits 12X. During PR138 the 100 nA on FC1X became 38nA on FC11X, and 1nA on FC11P. Transmission should be better for lower energy beams, as seen in PR137 where 78% of the beam on FC19J reached the target.
- Ask the operators to provide a nice small, centered beamspot (<1mm in diameter) on the target. Refer to Figs. 9.1 and 9.2 for typical achromatic beamspots. For dispersion matched beams the horizontal size can be up to 10mm. For a zero degree experiment the vertical size is very important and should be minimized.
- Should you choose to start achromatically, ask the operators to optimize the achromatic beam resolution. As an historical example: a phase change of 0.6° of the SSC RF was effective to decrease the E-spread in the beam, resulting in achromatic beam resolution of the faint beam going from about 60keV to 54 keV. (See 2007 logbook p114, run 532).
- Be careful when using the elastic peak of ^{12}C for fine tuning. The elastic peak of the contaminant, ^{16}O , may also be present in this peak if the angle at which you do the measurement is such that the peaks are not kinematically separated.
- Make the kinematic correction with the H and K coils (see section 3.5). This should be performed with the target that will be used to make the measurement with (especially for light targets), and at the angle for that measurement, in order to have the correct kinematical correction implemented. It is best to do this with an achromatic beamtune, but not essential.
- The operator should make as little as possible use of steerer magnets. **And under no circumstances should steerers S3 and S4 in the S-line be used.** At present (end 2009) there are still alignment problems in the S-line. Possibly the quads are to blame. While we always requested no steering in the S-line, necessitating steering in the P-line, I now think it prudent to rather allow steering (small amounts) in the S-line, but only with steerers S1 and S2. We still have the beamviewers to ensure proper alignment of beam on target. When one steers too far upstream you run the risk of not going through the center of quite a few quads, with all kinds of adverse steering effects when you adjust quads to obtain dispersion matching conditions.
- **Q4S, Q5S and Q6S:** With the beamline set up in the dispersive mode, use Q4S, Q5S and Q6S to optimize the resolution of the elastic scattered proton peak by changing the current setting of these magnets.
- **QS5 is used to change vertical focus and**

QS6 changes horizontal focus and dispersion.

Change Q5S and then scan with Q6S until a local minimum is achieved. Do a few iterations for different Q5S values. Additionally Q4S can also be changed, followed by Q5 and Q6 scans. Typical changes to the magnet current settings are of the order of 1% (or 0.2A). This part of the procedure is usually performed in the Control Room.

- **QS0:** a quadrupole was installed between bending magnet B2P and the first S-line quadrupole triplet to be used in angular dispersion matching. This quadrupole was originally Q16J, as used in the J-line (refer to Fig. 9.4). Note that it was not placed exactly at a focus point since slit-2S is positioned at the focal point.
- **Q18P, Q19P, Q21P:** during PR97 the focus condition in the P-line was changed by changing the settings of Q18P and Q21P (see the PR97 logbook p 57 and 59). This had the effect of moving the focus upstream, which resulted in a wider beamspread in the bending magnet between the P and S lines, B3P. During the PR116 test weekend Q19P was used for the same reason, and had drastic effect on resolution (See PR116 logbook p13). **It would be best to change these elements starting with those furthest downstream and work your way upstream.**
- **Q10X:** the beamline object point at 9X can also be tuned by changing the settings of Q10X.
- **9X slit sizes:** investigate whether a change in the object slit sizes (both vertical and horizontal) have an effect on the resolution. Ideally the beam should be focussed through slit 9X, and opening up the 9X slits should not affect the resolution. **This was proven in the test-beamtime of 22-24 September 2006.**
- If the momentum range of interest does not include the elastic peak, you are always faced with the predicament of making the dispersion matching optimization for the elastic peak since the count rate is high enough to allow the optimization procedure to be made in a reasonable time. But then you must change the magnet settings afterwards again, which opens up the possibility of making mistakes. One such mistake concerns the kinematic correction. **If the K and H coil values were determined for a different field setting than the one used in the experiment, change the current settings of the coils in the same ratios as the ratio of the D magnets for the two different fieldsets.**
- If accurate information from ϕ_{target} is required (**but that should only be in the case of over- or under focus modes at 0°**) care must be taken to ensure that the beamspot on target is always quite flat. This would then require making a table of QS5 and QS6 while the beamspot is observed to ensure a flat beamspot is always achieved before attempting to look at the resolution of the different settings. In short, one must be absolutely sure that the Y-focus on target is not disrupted during the Q e then I have not received any communication whatsoever from the NRF informing us if they received the information, or if they require additional information.
strength search.
- **To test the matching condition:** close down slit 1P (which reduces energy spread) and see if the resolution of the peak changes. If there is no change then the dispersion matching is good.

- **Collimators:** Use the 49mm collimator with an appropriate lip. The thickness of the lip of the collimator will depend on the energy at which the measurement is performed. The lip is in general useful to prevent slit scattering by degrading these particles enough to be swepted out of the focal plane. The thickness should be optimized to achieve complete removal outside of the focal plane area.
- Ask the operator to provide you with a printout of the settings of the S-line.
- Gold as a target is popular for resolution tuning as it is mono-isotopic, readily available and it is easy to make very thing target foils. The first excited state of Au is at 77 keV.
- The effect of the size of the gap at slit 9X on resolution may not as big as initially thought. According to Hiro's calculations (refer to the appendix) ($x|x$) of the beamline is 0.3. Thus for a 1mm gap at 9X you have 0.3mm on focal plane. For a 100 MeV tune at 22keV/mm a position resolution of 0.3mm is already very good. At 200 MeV we probably have 40keV/mm, but 0.3mm in the focal plane is still a lot better than we ever had so far. So DO NOT bother to try to make 9X smaller than 1mm. BUT DO go to a lot of effort to make sure transmission through it is good at 1 or 2mm.
- Notes from 2011 experience:
 - fix K and H
 - with Lowry's procedure, ensure proper quads settings for Q1S-Q3S.
 - Q6S. Then Q5S for good Y focus
 - finetune and investigate: Q21P, slit 1P, K600 quad, Q10X, slit 9X size
 - somewhere I had written down emittance = $0.54 \pi \text{ mm}$ yields 50keV/mm??!?!?
 - what does Lowry mean when he talks about kinematic defocussing?

9.4 The faint beam method for $K \neq 0$ experiments

A faint beam is achieved by putting the faint beam meshes (see section 10.3.1), situated between the external ion source and SPC2, into the beam. The faint beam method was originally conceived for use in a zero degrees experiment to aid in dispersion matching, as seen in section 10.3. But it can also employed in $K \neq 0$ experiments. As used in PR120, the faint beam method can be used to check the quality of the achromatic beam by looking directly at the beam energy spread. Additionally the faint beam method can be used to help in the dispersion matching procedure.

It may not seem practical to employ the faint beam procedure to achieve dispersion matching for non-zero degree experiments, as the procedure results in dispersion matching for $K=0$ conditions. This implies specific values for the spectrometer matrix elements $s_{\mu\nu}$, which in turn will determine the beamline matrix elements that are required for dispersion matching (see equations 9.7 and 9.8). At non-zero angles the kinematic correction required is different, and accordingly the beamline matrix elements will be different.

However, the K and H coil settings are not important when looking at the faint beam, since the beam angle spread is minimal. **This was proved during a Sept 2009 test run for project PR138. Please refer to p34 of the logbook for this test weekend for**

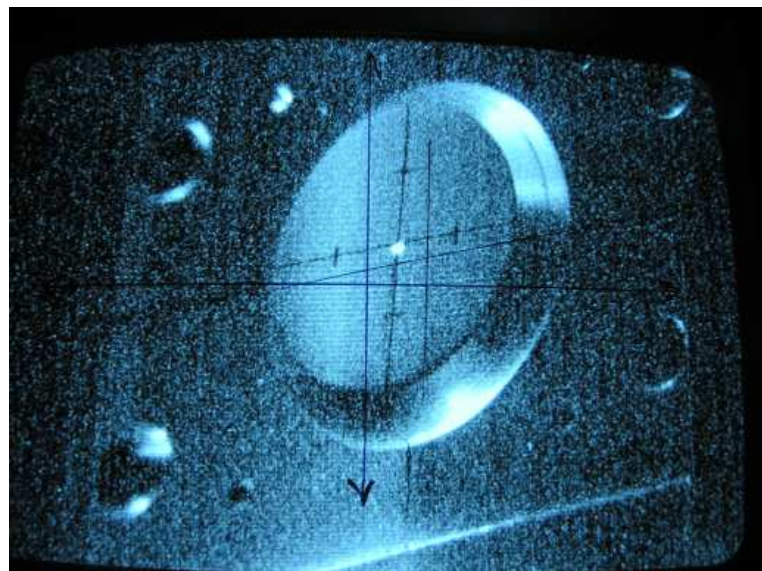


Figure 9.1: A typical target beamspot for an achromatic beam, as seen in the October 2004 development run. The lines on the ZnS screen are at 5mm from the target center.



Figure 9.2: The target beamspot for an achromatic beam, as seen in the July 2009 (p,t) run PR137. The lines on the ZnS screen are at 5mm from the target center. This beamspot is not small enough, and definitely bigger than in Fig. 9.1.

proof, as well as section 10.3.4 of this manual. It is thus advisable to do first do the kinematic correction at the angle and energy settings where the experiment will be performed. If the magnetic fields needs to be changed in order to see the faint beam at zero degrees simply change the current settings of the coils in the same ratios as the ratio of the D1 magnet for the two different fieldsets.

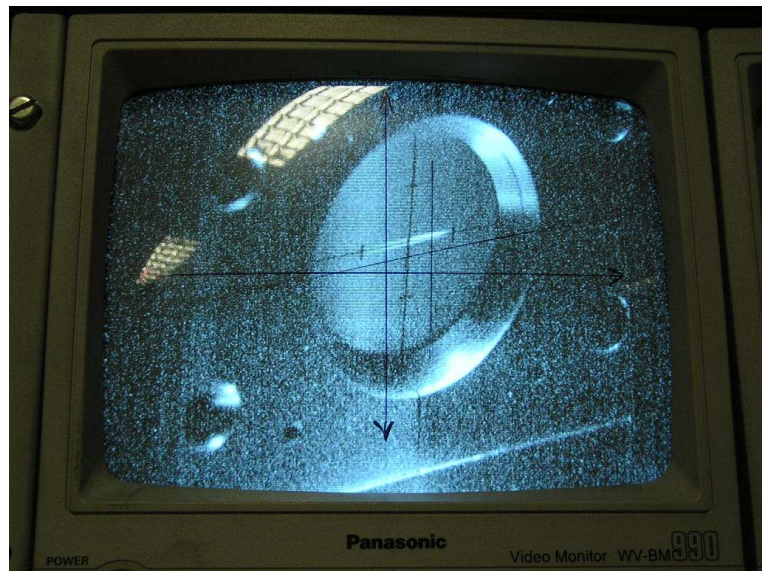


Figure 9.3: A typical target beamspot for a dispersion matched beam, as seen in the October 2004 development run.



Figure 9.4: The S-line quadrupole (still showing its original label Q16J, but since then relabeled Q0S) in front of the 2 triplets, to be used for angular dispersion matching.

9.5 Kinematic factor: some numbers

The kinematic factor K is given as

$$K = \frac{1}{p_3} \cdot \frac{\partial p_3}{\partial \alpha} , \quad (9.10)$$

where α is the nominal scattering angle in the lab frame and p_3 represents the product particle momentum (as opposed to incident particle momentum p). From the NAC report [NAC92] one

can make an estimation of this factor with the non relativistic equation

$$K = \frac{\sin(\theta)}{\sqrt{R^2 - \sin^2(\theta)}} , \quad (9.11)$$

where θ is the scattering angle and

$$R = \frac{m_{target}}{m_{proton}} \quad (9.12)$$

for elastic scattering. For reactions other than elastic scattering

$$R = \left[1 + \frac{m_0 + m_t}{m_t} \cdot \frac{Q}{E_0} \right] \times \left[\frac{m_t m_r}{m_3 m_0} \right] , \quad (9.13)$$

where m_0 , m_t , m_3 and m_r represent the mass for the incident, target, outgoing and recoil particles. E_0 represents the incident energy and Q the reaction Q -value. *K is negative for positive values of α .* A few kinematic factors were calculated for proton elastic scattering and are tabulated in Table 9.1.

Target	angle	KF
¹² C	5	-0.00731
¹² C	10	-0.0146
¹² C	15	-0.0217
¹² C	20	-0.0287
⁴⁰ Ca	7	-0.00307
¹⁹⁷ Au	20	-0.00175
¹⁹⁷ Au	8	-0.00071

Table 9.1: Kinematic factors for proton elastic scattering as calculated with equation 9.11.

9.6 Good resolution records

Refer to the logbooks listed in Table 9.3 for beam conditions when good energy resolution was obtained.

Logbook	Beam E	page	resolution	comment
NAC Annual Report 1992	66	p28	17 keV	achromatic
NAC Annual Report 1995	66	p22	11 keV	unknown beam
Protokolbuch 934 (Oct 2002)	66	~p175	5 keV	faint, BEST EVER
Protokolbuch 934 (Oct 2002)	66	~p175	9 keV	^{197}Au
PRC 80 (2009) 041393(R)	66		24 keV	PR146; Hoyle state
NAC Annual Report 1992	200	p28	42 keV	achromatic
NAC Annual Report 1995	200	p22	26 keV	disp matched, $0.48\text{mg}/\text{cm}^2$ ^{197}Au
Protokolbuch 934, ?	200?	p39	28 keV	^{208}Pb at 8° , 14mm collimator
Protokolbuch 935 (Aug 2003)	200	p21	17 keV	faintbeam, BEST EVER
Oct 2003 logbook	200	p30		
PR101 logbook 1	200	p135-137		
PR101 logbook 1	200			
PR101 logbook 2	200			
PRL 99 (2007) 092503	200		35 keV	PR90
PR146 logbook	200	p42	30 keV	Hoyle state, Febr 2008
PRC 79 (2009) 044305	200		35-50 keV	PR64; ISGQR fine structure
Iyabo PhD thesis	200		38 keV	Ca, C, Exp PR120
Iyabo PhD thesis	200		25 keV	Si, Exp PR120; logbook2 p5 mentions 22 keV!
PR167 (2010) logbook p151	200		33 keV	Au, VDC voltage dependent!

Table 9.2: Historical good resolution conditions. For the Oct 2002 results refer to the subsection 9.7.1

9.7 SSC transmission: historical numbers

Logbook	Beam	page	10J	19J	1X	11X	Pline	Sline	comment
PR183/184 7°, Dec 2011, p103	200 MeV p	890	405	150	19	1.2	1.1		
PR183/184 0°, Jan 2012, p41	200 MeV p	?	230	178	85	1	?		
PR210 logbook2, Jul 2014, p53	200 MeV p	4100	87	19	4.7	0.5	0.5		
PR217 logbook2, Jun 2015, p3	200 MeV p	?	210	45	7	0.6	0.6		
PR242 logbook 2, Oct 2015, p46	100 MeV p	230	15	15	12.7	1.3	1.3		

Table 9.3: Historical good resolution conditions. For the Oct 2002 results refer to the subsection 9.7.1

9.7.1 66 MeV protons

During experiment PR146 in November 2008 we achieved 27 keV achromatic resolution (see logbook p103) but could only achieve 20 keV resolution when dispersion matched. (see logbook p133). This measurement was performed with SPC1, and therefore the faint beam was not available. Flat topping for both SPC1 and the SSC was switched on, and we are baffled as to why we could not achieve better energy resolution. Maybe the relative phase of the flat-topping was not constant enough?

On-Line Spectra 66 MeV Protons, Au target, 10 deg.

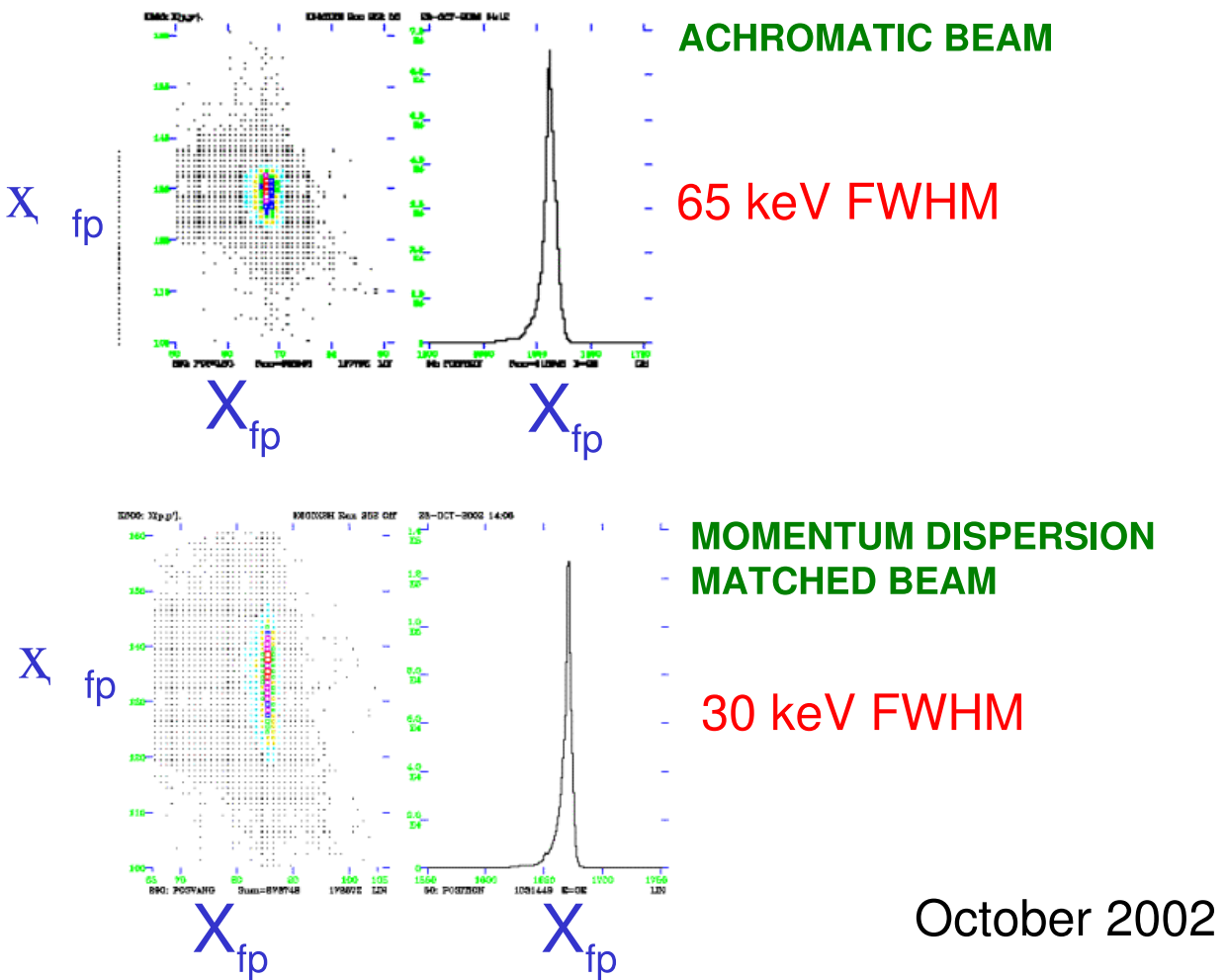
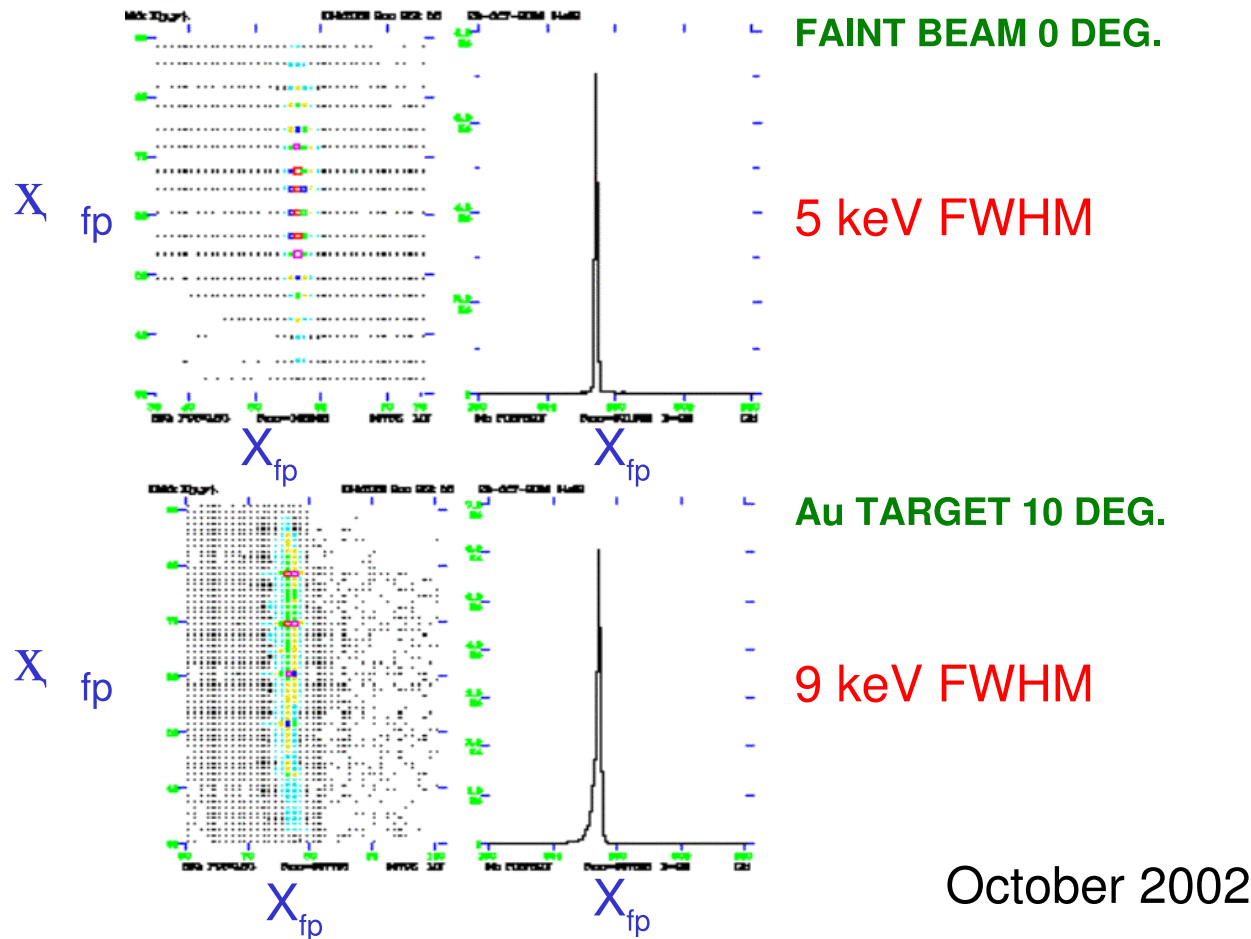


Figure 9.5: October 2002, 66 MeV beam. Normal resolution conditions, before attempting dispersion matching with the new faintbeam method.

On-Line Spectra 66 MeV Protons



October 2002

Figure 9.6: October 2002, 66 MeV beam. Resolution after doing dispersion matching with the faintbeam method. Refer to the Protokolbuch 934 ~p175,

9.8 α beam

Experiments performed with α beams in November 2005 (see PR102 logbook), July 2010 (see PR166 logbook).

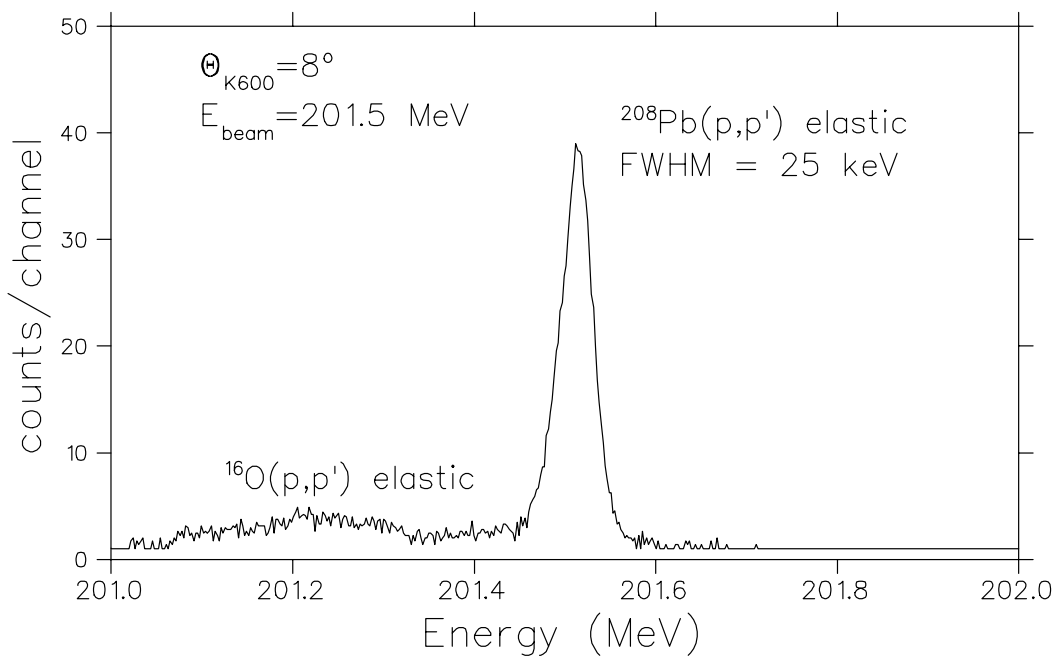
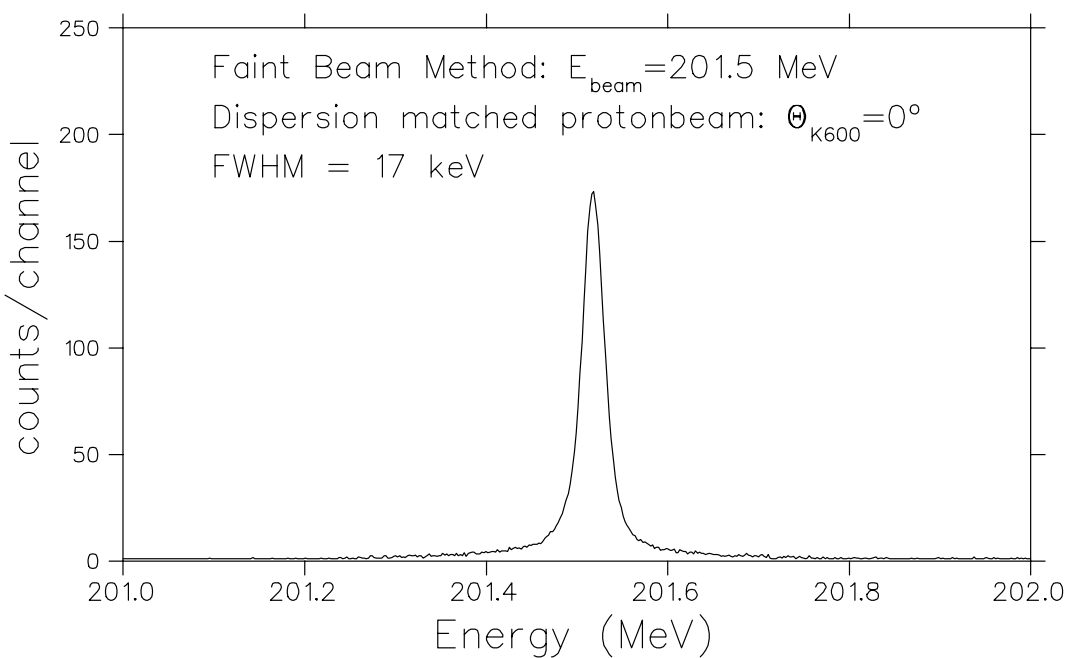


Figure 9.7: Refer to the Protokolbuch, entry at 6 June 2003 for the data 200 MeV scattering data as well as the 8 August 2003 faintbeam data.

Chapter 10

The 0° and 4° modes

NEXT TIME TO DO: be sure to ask for smaller **9X-Y slit setting to try to get a smaller beamspot in the vertical direction!!!**

The beam tuning philosophy for a zero degree experiment is to start at a finite angle and optimize the achromatic beam. Consider the whole accelerator and beam-transport system as consisting of 2 main sections: everything before slit 9X (i.e. the ion source, SPC2 and the SSC), and everything after slit 9X (beamlines P1, P2 and S). Let us refer to these as the *accelerator* and the *HiE beamline*. The aim of achromatic tuning at finite angles is to ensure that the inherent beam quality from the *accelerator* is good, i.e. small beam E-spread and good beam halo conditions. The goal is to achieve, with minimum background, \sim 60keV resolution for the elastic peak from a heavy target (preferably Au) for a 200 MeV proton beam. Once this is achieved one can move the spectrometer to 0° , transport the beam through the K600 and get the 0° *background* with an empty target frame to be below 100 Hz at 1nA. Upon reaching this goal the beamline elements can be changed to the dispersion matched settings. Dispersion matching of the beamline to the spectrometer can now be achieved through the faint beam method. Measurements can commence if the beam halo conditions are still below 100 Hz at 1nA.

Another reason for starting with an achromatic beam tune is that in the dispersion matched mode it is difficult to say whether bad energy resolution is due to incorrect dispersion matching, or because the beam quality and energy spread in the beam from the SSC is not good enough.

The question can be asked why one does not go straight to zero degrees and optimize the achromatic beamtune with the faint beam method? The short answer to that is that while the faint beam method can be used to optimize the beam energy spread, it cannot be used to optimize beam halo conditions.

- Adverse halo conditions caused in the *HiE beamline* are not considered to be a big problem at the achromatic stage of the beam tuning excercise, as the beamline setup will change completely when dispersive mode settings are employed. However, this halo must still be tuned away before the experiment can enter into the next phase.
- On the other hand, if halo originates from the *accelerator*, then the achromatic beam represents the best beam-tune to try and reduce it, as the beam profile in the *HiE beamline* is smaller for an achromatic beam. This makes it easier to achieve low *HiE beamline* halo conditions, allowing one to concentrate on the halo caused by the *accelerator*.

- There is no sensitivity to halo under faintbeam conditions. Instead of the normal $\sim 1\text{nA}$ (i.e. 6.25 billion protons per second) of beam, faint beam results in just 1000-2000 protons per second. Since the beam is so small, the halo is not measurable.

The next question could then be: can one not do achromatic optimization at zero degrees by looking at some excited state? In this way one can do halo optimization as well since the faint beam technique is not used, and you do not have to bother to start at a non-zero degree position for the spectrometer.

- Part of the problem is to get a state that for which the cross-section is high enough to allow for a reasonably small time between a beamline/accelerator adjustment and the measurement of the influence of this adjustment on peak resolution. So far (until November 2008) the only useful state turned out to be the 15.11 MeV excited state of ^{12}C . While it is certainly possible that there could be other nuclei that are better suited for such a procedure, our experience is that the peak/background ratio for heavier targets deteriorates rapidly for increase in target mass due to more secondary scattering of the coulomb cone. In addition, the natural width of this state is given as ~ 43 keV. It is therefore not ideal to optimize the achromatic beam under these circumstances.
- Kinematic spread presents an additional problem when attempting achromatic optimization at zero degrees. It was established above that, so far, the only useful target for a zero degrees optimization procedure with an excited state is ^{12}C . For a light target such as ^{12}C kinematic spread is problematic, even at very small angles. The kinematic spread for a 200 MeV incident beam is about 26 keV between 0° and 2.14° , which is the opening angle of the 55mm collimator. While this spread can be corrected in the horizontal plane by means of the K and H coils, the only thing to be done to correct for the vertical kinematic spread is to use a smaller collimator. A smaller collimator would unfortunately also cause an even smaller countrate, which is already quite as we cannot measure the elastic peak.

It is therefore not a good idea to optimize the achromatic beam by only using the faint beam technique, as this does not allow for halo optimization. It is furthermore also not recommended to tune the achromatic beam by only looking at some excited state at zero degree, as too much time is required and because the peak resolution is inadequate.

However, as pointed out in the previous chapter, especially for all experiments with 200 MeV protons, there is an important difference between how we at iThemba LABS approach the zero degree dispersion matching procedure, and how RCNP does it. At RCNP the flat-topping available to them on both the injector and RING cyclotron makes it possible for them to have no slits whatsoever between the object point and the target. At iThemba LABS we do not have flat-topping available for experimental beams. We can only 'tune' the accelerator to a limited level by looking at the achromatic beam as the operators HAVE TO use slit 1P in the P-line to cut the beam dispersion. This slit is typically anywhere between 6 and 10mm. WE CAN NOT OPEN slit 1P AND HOPE TO HAVE GOOD ACHROMATIC RESOLUTION. The beam energy spread is simply not small enough, and single turn extraction at 200 MeV is not that clean. And since we HAVE to use 1P, that also means we have to use cleanup slits later in the beamline.

10.1 Notes on zero degree beam-tuning

10.1.1 The RCNP experience

An outline of the RCNP experimental procedure for 0° (p, p') experiments:

1. Start with achromatic beam with the spectrometer at a finite angle. Tune the beam-spot to be as small as possible and focused at the target.
2. Check that all spectrometer detectors and subsystems are working properly and accumulate a white spectrum.
3. Optimize achromatic resolution with a ^{197}Au target and the spectrometer positioned at a finite angle (typically 8°).

On the one hand this step requires kinematic correction using the multi-pole magnet of the spectrometer in order to make hardware or *ion optical* corrections for the curvature and/or slope of the line-shape in the x versus θ plot. On the other hand this step requires beam optimisation by the beam operators to ensure that the inherent energy resolution of the beam is minimized. One should keep in mind that as the inherent beam resolution improves the kinematic correction may require further fine tuning. Also, to ensure that uncorrected line-shapes in x versus θ does not negatively influence the measured resolution during the optimisation D1 procedures the position x can be plotted for only a very small θ range.

For the case of (p, p') measurements at RCNP the multipole is used as a quadrupole, and therefore it affects the $(x | \theta)$ matrix element of Grand Raiden. For this reason no changes should be made to this magnet after the dispersion matching procedure, as dispersion matching concerns the first order matrix elements. In the case of ($^3\text{He}, t$) the multipole is used as a sextupole ¹, and therefore it does not affect the dispersion matching. For such experiments the multi-pole magnet may be changed again during dispersion matched mode by looking at a target such as Mg (natural or ^{26}Mg) ².

4. Move the spectrometer to 0° and transport the beam to the zero-degree beam-dump.
5. Do halo tuning with the achromatic beam to ensure a countrate of $<100\text{Hz}$ at 1nA .
6. Look at the line-shape in the x versus θ plot of some excited state. If necessary, make slight changes to the multipole of Grand Raiden (used as a quadrupole for (p, p') work) to make hardware corrections to the second order focusing conditions.
7. Change to the faint beam mode and do dispersion matching.
8. Check that the beam-halo with an empty target is still at the same acceptable levels as with the achromatic beam ($<100\text{Hz}$ at 1nA). At the RCNP halo optimization is usually not required in the dispersion matched mode.

¹During ($^3\text{He}, t$) measurements the magnetic fields of Grand Raiden are much higher than during (p, p') measurements. The dipoles saturate at these high fields and second order aberrations become quite severe when compared to the (p, p') case.

²Mid Dec 2008 Retief put in a tgt request for a natural Mg target, for future use on (p, p') K600 zero degrees measurements

9. Start measurements.

About their beam tuning procedures [Nev08]:

1. One thing that they do that is vastly different from iThemba LABS is that they *visually* verify the beam focus conditions at the various focus points (at least at 11 places) along the beamline by means of viewer meshes similar to the ‘Hatanaka mesh’ in use in the S-line. This is especially effective at the source point (BV-EXT), where they can visually verify that they achieve sharp focus and that the size of the object of the ion optical system is very small. Also important is that they not use any slit to constrain the size of the source point.
2. They employ flat topping only in the RING cyclotron (my understanding is that the flat topping in the AVF injector cyclotron is not yet fully functioning), and the FT phase relative to the phase of the main cavities is kept very stable. According to Hatanaka this stability is key to achieving very good energy resolution.
3. They achieve up to $\sim 95\%$ transmission through the RING cyclotron.
4. Halo optimization is achieved with slits inbetween the AVF and the RING cyclotrons.
5. The stability of the beam at RCNP is quite impressive, i.e. stability in terms of both energy resolution as well as halo conditions. Prof. Tamii believes that the *halo stability* can be attributed to the fact that they do not use any slit after the RING cyclotron. Drifts en beam energy does thus not translate in drifts of the beam onto the sides any slits, which would cause beam halo.
6. Once or twice a day the beam-spot on target was found to be shifted a few mm to one side. This was *usually* corrected by making small adjustments to cavity-voltage of either the AVF or the RING.
7. Beam halo conditions of 100Hz is considered a good beam halo condition.
8. Feedback loops are in place to ensure RF stability as well as temperature stability. However, no feedback control is used to ensure beamline magnet stability. At the start of the experiment a PID feedback loop was used to ensure stability of the magnetic fields of the Grand Raiden spectrometer. However, this feedback made things worse, adding a 12keV width to the energy resolution by changing the magnetic field by 2×10^{-5} Tesla. The PID loop was not sensitive enough since the smallest possible increment in magnet current caused much bigger field changes than the drift in magnetic field.

10.1.2 iThemba LABS: PR137 (p,t) at 100 MeV

This experiment was conducted over an extended beamtime of one week. Note that even though this was a (p,t) experiment we optimized the resolution of the K600 and accelerator system with (p, p') scattering.

1. All the standard procedures used in low energy non-zero degree dispersion matched experiments were used at zero degrees. Start the experiment at a non-zero degree angle with an achromatic beamtune. Ensure that the transmission through the SSC is optimized and

that the transmission through a 1-2mm opening for slit 9X is optimized. Focus the beam to a beamspot diameter on target of <1mm and measure the resolution of the elastically scattered peak.

2. The achromatic resolution was tested with slit 1P wide open. Note that the beam energy was 100 MeV and that slit 1P cannot be open for a 200 MeV experiment. Also important to note that the achromatic resolution achieved in PR137 was around 75-100 keV (WE1, logbook p24,44, WE2, logbook p116).
3. The effect of the size of the gap at slit 9X on resolution may not as big as initially thought. According to Hiro's calculations (refer to the appendix) ($x|x$) of the beamline is 0.3. Thus for a 1mm gap at 9X you have 0.3mm on focal plane. For a 100 MeV tune at 22keV/mm a position resolution of 0.3mm is already very good. At 200 MeV we probably have 40keV/mm, but 0.3mm in the focal plane is still a lot better than we ever had so far. So DO NOT bother to try to make 9X smaller than 1mm. BUT DO go to a lot of effort to make sure transmission through it is good at 1 or 2mm.
4. It takes a long time before the beam is stable. It is not necessarily useful to go to dispersion matched beam setting too soon, as the drifts in the beam is bound to force you to go back to achromatic beam settings again.
5. Good transmission is essential. Best values for PR137: 1.4nA on FC19J and 1.1nA on target (logbook1 p97). As far as is possible the beam must be focussed through slit 9X. The normal procedure of putting a lot of beam on 9X and then only selecting the central part with slit 9X should not be used for a zero degree experiment. This also means that if we only have 1nA on the target, then only about 1nA should be extracted from the SSC, and ideally only 1-2 nA should enter into the SSC. From the RCNP experience this is very important. During PR137 we showed it is possible for a 100 MeV proton beam.
6. Angular calibration must be performed with the pepperpot with achromatic beam tune at finite angles.
7. If you have a new *accelerator* beamtune, i.e. there was major retuning of the beam before 9X, then you need to redo the angle calibration measurement. The beam direction, which defines the scattering angle, needs to be established after every change in the beamline tune. This means a faint beam measurement when one is at zero degrees.
8. Once we have stable conditions (after 2 days or so) and we have a good dispersion matched beam, beamline elements such as steerers or quads or bending magnets **should not** be changed to correct for drifts in beam energies! Energy shifts from the cyclotron should rather be corrected with small D-voltage and phase adjustments. You can also make phase adjustments on the bunchers. This we saw in action during PR137. We achieved a good dispersion matched condition on the Sunday and experimented for 175h without making changes to steerers, quads, bending magnets or any slit except the slits used to change beam intensity (at SSC entrance) and P and S-line slits to optimize halo; mostly slit 2S was used, with the rest wide open. **The position of slit 9X was never moved to optimize beam intensity.** Also, the magnetic fields of the SSC was not touched.

9. To reiterate: once we achieved stable running conditions the *only* elements tuned *before slit 9X* were the phase and voltage of the AX, K-line and J-line bunchers and the SSC. To increase the beam the slit in front of the SSC was regulated.

For typical phase changes see PR137 logbook p186:

- (a) SSC: 100 V and 1-2 degree phase changes were not uncommon
 - (b) J-line buncher: 40 steps in phase, 2000V
 - (c) K-line buncher: 20 steps in phase, 2000V
 - (d) AX buncher: 200 steps in phase
10. To reiterate: once we achieved stable running the *only* elements tuned *after slit 9X* were the S and P line slits to minimize halo. You may also consider looking into slit 12X position, as during PR138?

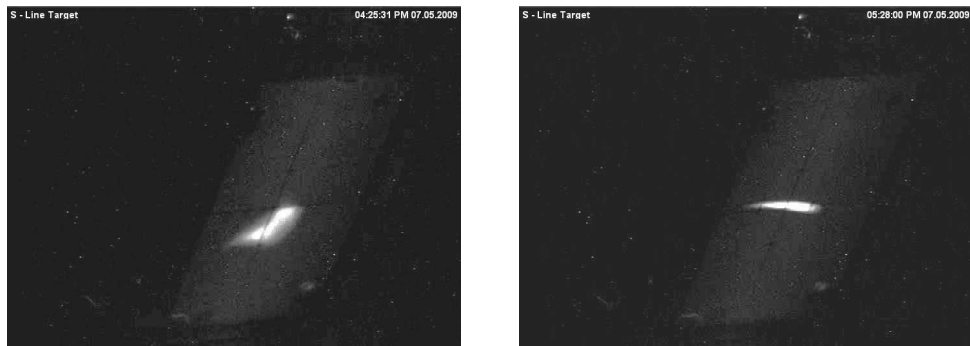


Figure 10.1: PR137: After dispersion matching optimization with faintbeam we had the beamspot on target indicated on the left of this figure. As PR137 was a zero degree experiment it was important to have a flat beamspot on target. After recursively tuning Q5S and optimizing the resolution with faintbeam we eventually ended with the beamspot on the right.

10.1.3 iThemba LABS: the PR138 (p, p') experience

This experiment was performed during October 2009.

1. On the 2nd weekend we decided to start with the K600 at 0 degrees and with the beam set up in the dispersion matched mode, as delivered by Lowry. No achromatic tuning was attempted.
2. We typically found that the final beam tuning before beam conditions were stable enough to allow data acquisition was performed between Saturday night 24:00 and Sunday morning 05:00. Note that this was after the SSC fields were 'run' the Friday from 7am. The detector and beam setup first achieved good energy resolution (33 keV) on Sat morning 2am (with conditions still slowly drifting). Halo tuning then achieved 50-60Hz at 0.7nA. In the 1st 12C run resolution of \sim 54keV was achieved. Refer to the logbook1 of PR138 (p114-p120) as an example of the tuning procedure:
 - Sunday morning 00:15 it was decided to relook at the SSC extraction and beam alignment in the X, P1, P2 and S-lines.

- Charles adjusted the SSC main coil upwards by 1/10000'th of its current strength (.2A on 1495.250). This resulted in better shaped peaks in the SSC and better SSC extraction.
- He then made sure that the alignment in the X, P and S lines is good with the harps.
- When we looked at the beamviewer we saw the beam was high in Hatanaka and low on the target. This was corrected with the combined use of steerers in the P line (ST 3,4,5,6). This means that the alignment can be good according to the harps, but based on the beam viewers it is not. This is mostly an S-line alignment problem. (In discussions with Lowry afterwards it became clear that although the B3P height adjustment improved things, there is still outstanding S-line alignment issues, mainly to do with the quadropoles. *The mistake we made during the weekend was to steer in the P-line. We should steer in the S-line between B3P and the first quad triplet.*)
- The beam was transported to the 0degree beamdump.
- Halo was optimized: starting value 110Hz at 1nA (already quite good). The main item was the positions of slit 9X in X and Y. The result was 30Hz at 0.9nA.
- Next followed faint beam energy resolution optimization: starting value 63 keV. We started with the elements closest to the beamline and worked our way toward the SSC. Q6S and Q5S did not have much of an effect, so we kept them at the same place. The next element to tune was Q21P. Here we could optimize the resolution all the way to 29.1 keV. In the process we increased Q21P to almost the same level as Q19P, which is the way it is supposed to be (it was initially 22.8A, finally 29.1A)
- After resolution optimization we looked at halo: was 500 Hz at 1nA. Setting Q21P back to its original, bad resolution, value made halo go away, so it was clearly the source of new halo, no beam instabilities
- Now we decide not to touch 9X, or any quads, but try to optimize the halo with other slits downstream from 9X. Slit 12X position helped a lot, and slit 1P a little. Halo with the 0degr beamdump viewer = 140 Hz at 1nA. Halo without the 0degr beamdump viewer = 70 Hz at 1nA. *So the beamdump viewer does have a small but non-negligible effect on the halo count!*
- Back to beam viewers: again the beamspot was not quite center on the target: see logbook p 116,117 and Fig.10.2. This was corrected with B3P and ST1SX. This was to be expected, since we steered in the P-line. And then changed a P-line quad. This is more reason for not steering in the P-line, but only in the S-line.
- Halo check 40 Hz at 0.6 nA; good enough.
- Faint beam check (have to give magnets a while to settle), find 30.4 keV resolution → conclusion: final small steering in the S line did not hurt us!
- Transmission numbers for this setup:
FC10J 343 nA
FC19J 28.6 nA
FC1X 15 nA
FC11X 3nA
FC4P 1nA
FC11P 0.7nA
FC4S 0.7nA

- Slit gap sizes: 9X-X = 0.9mm, 9X-Y = 2mm, 1P-X = 7mm.

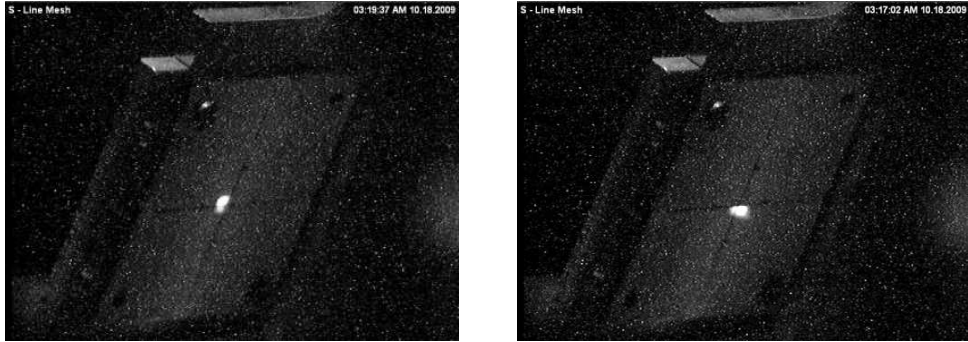


Figure 10.2: PR138: Due to wrong alignment procedures where we steered too much in the P-line we found that the settings of Q21P affected steering. The left figure shows the beamspot on target with Q21P=29.1A, and the right figure shows the beamspot with Q21A=22.8A.

3. Discussions with Lowry

- Focus at 9X: the beam from the accelerator has a specific emittance. This is a constant for the beam, and also an indication of the beam quality. If you focus more at 9X, the beam divergence will be more, and hence you will have more of a problem downstream at slit 12X to handle this divergence. If the operators focus the beam more at 9X, more halo will be created at 12X.
- The alignment problem mentioned above where changes to Q21P was needed for better resolution (but causing steering problems) is due to our usual insistence that no steering may be done in the S-line. There is a known steering/alignment problem in the S-line. This was fixed largely by the height adjustment of B3P, but there are some remaining, mainly Y alignment, problems with the quads. For now, we should allow the operators to fix the alignment problem with the first 2 steerers in the S-line. These are in front of the quads of the S-line, so if the problem is fixed here then hopefully we can go straight through the s-line quads.
- Temperature: the red line in the temp plot is the average between SSC ingoing and outgoing temperatures. At RCNP the fluctuation of the SSC temperature is 0.1 degree. It is not clear what it is here.
- Accelerator To Do list: Efforts should be made to see what the SSC vault temperature oscillations are.
- Accelerator To Do list: The electrostatic channel in the injection point of the SSC was removed when the SSC flattopping resonator was installed. This has a negative effect on the beam quality. See Lowry's PhD thesis. Maybe we should try and put this electrostatic channel back during end of year shutdown next year; must push for development during next year?
- Accelerator To Do list: better RF monitoring.
- Accelerator To Do list: fixed phase probes. these new ones should be more sensitive and should be usable even with as low as 30nA.

- (h) Beam tuning procedure for the 3rd weekend of PR138 2009. SSC main fields: if the phase at extraction is more than 1/2 ns out compared to phase at injection some intervention is required. Lowry suggests that especially at the beginning of the weekend we should give the beam to the operator every 30min so that he can put in the cups, increase the beamcurrent and check the SSC phase probe at extraction. If the phase was drifting then small magnet corrections should be made (on the order of 0.02A) after which 3-5min should be allowed for the magnetic fields to settle.
- (i) On the big Y size of beamspot: possible Q2S alignment in Y is out.
4. Startup procedures/runplan for weekend 3 of PR138 2009, starting at zero degrees:
- (a) cycle the magnets to D1=431 (merely a starting value, not particularly magic)
 - (b) align beam on tgt and hatanaka (no p-line steering, only s1 and s2 and B3P steering)
 - (c) transport beam through K600: D1/D2=1.5233, Q+3%
 - (d) get halo down to reasonable values, with only the scintillators switched on. Now we can still change 9X position and size. (see again bullets 9 and 10 in section 10.1.2 Once good halo is established, 9X **should not** be changed again to optimize beam throughput or resolution or anything else, since you will only change the halo conditions for the worse.
 - (e) look at beam on viewers and re-align. Re-optimize halo.
 - (f) If realigned, look at halo again.
 - (g) switch on detectors, look at ^{12}C spectrum; do kinematic correction with K&H coils
 - (h) faint beam resolution optimization; change fields with superknob
 - (i) test halo and optimize if necessary
 - (j) look at beam on viewers and re-align
 - (k) if any changes were made in above 2 steps, test faintbeam again
 - (l) if all is well cycle the magnets to prepare for data acquisition
 - (m) calibration and resolution check with ^{12}C
 - (n) take data
 - (o) log beam transport through SSC and from X to P-line
 - (p) look at SSC transmission when the beam start to get unstable

10.1.4 iThemba LABS: the PR183/184 (p, p') experience

This experiment was performed during a weeklong beamtime in January 2012.

1. The correct order for tuning 0 degree is
 - look at beam on tgt viewer + hatanaka
 - transport beam through K600: look at beamdumpviewer
 - check and tune halo
 - do faint beam for high res

- look at beam on viewer + hatanaka
 - test halo
 - if all well, take data
2. slit 12X Xpos makes res diff and background diff!! must be centered!?
 3. slit 9X Xpos makes res diff!
 4. sometimes Q21P makes a diff; not always. When it does, also, after tuning Q21P, tune its partner in the triplet: Q19P
 5. flat in Y is realy important: if not flat then in focus mode you can see substantial increase in Y size of events in focal plane
 6. it is really important to use the emmits program via DOSBOX!!!! to get good Sline tune ask for 1.5mm on tgt X and 1.1mm on tgt Y
 7. halo tuning: sometimes the J line slit 18 and K line slit 7 can help to take halo down.
 8. in previous experiments i believed that there are lots of rules that should not be broken/ beamline elements thay may under no condition be changed. I no longer believe the rules are so clearcut.
 9. The operators MUST tell us everytime they tune phase and voltage, as this can slightly change the beam energy!! I see up to 20 keV shifts in E calibration!
 10. MUST find a way to visualy verify that we have as flat a beamstop as possible. at IUCF they used 0.2mm wide strip targets? See 1993-1994 report p106.
 11. at iucf they went to a lot of effort to determine the beam pos we need to think about this for next time!!!!!!
 12. FOR THE NEXT 0 DEGR BEAMTIME: look at K600 book nr 8 p 110

10.1.5 iThemba LABS: summary of what we know so far and what you should do:

1. Start from closest to the target: Q65, Q5S If beamspot is big in Y try using Q5S together with Q2S to get it flat, then recover dispersion matching with Q4S and Q6S.
2. Q21P: change focus before B3P
3. Q20P: change focus before B3P
4. Q18P: change focus before B3P
5. See if resolution changes when slit 1P is closed. If not, then you are dispersion matched
6. Q10X: change focus going into slit 9X
7. Slit 9X: change size and see if it has effect on resolution.

8. Once we achieved stable running conditions the *only* elements tuned *before slit 9X* were the phase and voltage of the AX, K-line and J-line bunchers and the SSC. To increase the beam the slit in front of the SSC was regulated.
9. Once we achieved stable running the *only* elements tuned *after slit 9X* were the S and P line slits to minimize halo. You may also consider looking into slit 12X position, as during PR138?
10. What is the beam transmission? It will give a clue to the beam quality. Note down the beamcurrent on FC10J, FC19J, FC1X, FC11X, FC4P, FC11P, FC4S, experimental FC.
11. Is 9X slit size really as small as we think? If all else fails, try to close 9X a little more
12. what else?

Things to look at when experiencing problems:

1. How good is the transmission through SSC and X and P lines?
2. Are we still well aligned in P-line?
3. Was 9X changed after halo optimization finished? If so it will most likely be very bad for halo conditions
4. When optimizing faintbeam resolution, rather work from Q6S upstream than trying to change quads in P-line first. Work your way back up to the SSC.
5. Are the P-line quad settings the same than it was for previous good conditions? Did you make a printout of beam settings when things were good?
6. For halo optimization: before SSC you can only change buncher phase, SSC phase and voltage and SSC B-field. **Not** bending magnets, quads or 9X.
7. For halo optimization: after the SSC you can only change the slits. **Not** bending magnets, quads or 9X.
8. Sometimes I find that slit 1P position is important: changing X position by only 1mm can be decisive for halo tuning

10.1.6 iThemba LABS: experience from other runs

1. The beam viewer in front of the zero degree beamline does have an effect, though small, on the trigger rate. During the Sept 2009 test weekend we saw under good halo conditions (30 Hz at 0.7nA) the trigger rate increase to 100 Hz when the beamviewer was in the beam. Initially (Sept 2007) we thought that the effect is small enough to allow us to have the beam viewer in permanently, but that is no longer the case.
2. Suggestion: do the 7degr angular calibration at the end of the weekend once we know what K600 ion optics it is we used?

3. The Q-line slit after the first bending magnet of the SPC2 ECR source (slit 3Q?) can be used to select a good section of the beam. These slits are between the ECR source and the Hatanaka meshes, with 2x2mm opening typical (correct?). Good Q-line slit position will allow good peak separation in SPC2. For a set of good Q-line slit settings, see the K600 Zero Degree development logbook for August/September 2007 p39-40.
4. See Sept07 Logbook p39,40 for important injector tuning settings (look at these values again!!)
5. SPC2 Radax and radial slit 2; Used as a phase slits.
6. The K-line slit 7X is an energy selection slit.
7. Slit 18J is used for divergence adjustment.
8. Sept07 logbook p47: Beam-line adjustments to achieve good beam resolution
9. Sept07 logbook p99!!!!!!
10. Vertical kinematic effect:
we should be careful that we cannot use the position-TOF or position- θ plot for K and H coil tuning at zero degree and think all is well. Do not forget about the vertical kinematic effect (difference of recoil energy of target nuclei in the spectrometer acceptance), which cannot be neglected at zero degrees. This effect can be corrected only by software, provided you have the proper vertical scattering angle resolution.
11. Use of different collimator, Sept 2007:
In the end of the 2nd and 3rd weekend, we took data with different collimators, with the following results:
 - collimator without lip (63mm diameter): This widest collimator gave us reasonably clean spectra, however, the background distributions were not flat, but tilted.
 - collimator 49mm diameter+11mm lip and 42mm+8mm lip: gave us rather flat background distributions. However, energy loss in these lips are not enough so degraded protons generated many triggers though the medium-dispersive exit window of the spectrometer. We need better shielding here to reduce trigger rate.
 - collimator 55mm+11mm lip: shows tilted background like 63mm.
 - no collimator/empty collimator: spectrum shows big bump in the middle which is independent of the target being used, probably scattered particles degraded somewhere.

10.2 K and H coil settings for measurements

Once stable background conditions are achieved the drift chamber high voltages are switched on and the proper values for the K and H trim coils are determined to remove the correlation between the focal plane position and angle. At finite angles this ion-optical correction differs according to target mass due to the correlation between momentum and scattering angle. However, within the angular acceptance of the spectrometer the difference in kinematic factor $k = 1/p_{out}(\partial p_{out}/\partial \alpha)$ between light and heavy nuclei, e.g. ^{12}C and ^{208}Pb , is quite small when the spectrometer is positioned at 0° . This procedure is used firstly to correct the ion optics of the spectrometer when using the high dispersion focal plane for $R=1.49$ (a few hundreds of keV), and secondly to perform the slight kinematic correction needed for different targets (a few tens of keV). Since the accessible excitation energy range during 0° (p,p') measurements at $E_p=200$ MeV starts from ~ 8.5 MeV this correction is performed with the relatively strong 1^+ state in ^{12}C at $E_x=15.110$ MeV.

10.3 The faint beam method for K=0 experiments

The faint beam method was initially conceived as a method to achieve both lateral and angular dispersion matching when $\theta_{K600} = 0^\circ$ and thus $K = 0$. See reference [Fuj02] for a detailed explanation. A faint beam is obtained by putting the faint beam meshes (see Figs.10.3 and 10.4), into the low energy beam from the ion source. The faint beam method is used mainly in zero degree experiments, but can also be of use in $K \neq 0$ experiments (see section 9.4).

10.3.1 Beam attenuation meshes

The beam attenuation meshes are located between the ECR ion source and SPC2, between B1Q and L2Q (see Fig. 10.3). These meshes are made of special perforated copper plates and are shown in Fig. 10.4. They are used to drastically reduce beam intensity without changing the beam profile, as happens when beam intensity is reduced by means of slits. The meshes are listed as APP1 and APP2 on the accelerator control system. APP1 attenuates the beam by a factor 10^2 , and APP2 attenuates the beam by factor 10^4 . **April 2011: it seems as if the meshes were swapped around. Make 100% sure what the current status and do not assume the above is correct**

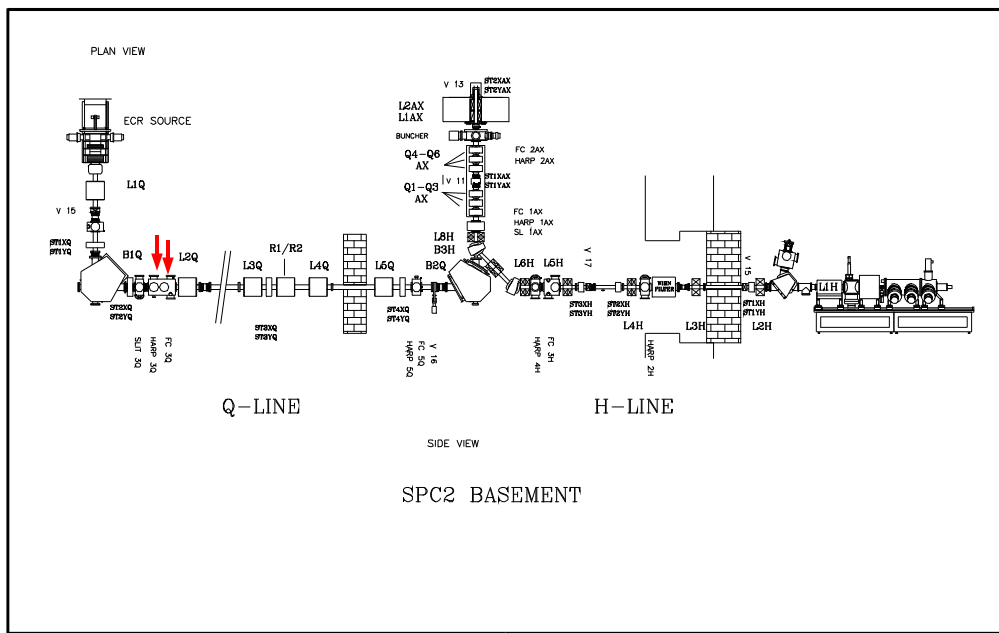


Figure 10.3: The red arrows indicate where the beam attenuation meshes are located.

10.3.2 Faintbeam: original DAQ and VDCs

The record for FWHM of the faint beam at iThemba LABS is 17 keV which was achieved during the Aug 2003 development run. For the evolution of the beamspot in $x-\theta$ refer to Fig.10.5.



Figure 10.4: The mesh on the left hand side only allows through 1/100'th of the beam, and the two meshes on the right hand side (factors 10 and 1000) collectively allows through 1/10000'th of the beam.

10.3.3 Faintbeam: PR137

No effort was made during PR137 to optimize the angular dispersion. Some plots of the focal plane position and angle of the faintbeam are shown in Fig.10.6. At the end of the faint beam process the horizontal angular resolution for the focal plane scattering angle was $\sim 0.5^\circ$ FWHM. For the K600 we have that $(\theta \mid \theta) = -1.9$ ($=1/(x \mid x)$) for the medium dispersion focal plane. Therefore the scattering angle resolution is $\sim 0.26^\circ$ (4.5 mrad) FWHM.³

10.3.4 The myth of the K-coil during faintbeam tuning

Sometimes in the middle of the nightshift people convince themselves that the K-coil should have an effect on the resolution of the achromatic faint beam. **It does not.** Refer to Fig.10.7. The data was taken September 2009 with the detectors in the high dispersion focal plane. Faint beam setting of 215 MeV (D1=448.32, D2=285.32, Q=-493.10) was used. Remember that while it is true that the energy spread in the achromatic beam is significant (100keV or more) the angular spread of the beam is small. The K-coil is a quadropole focussing element (with an additional dipole component) that can only influence the first-order kinematic variations of momentum with angle, i.e. the $(x \mid \theta)$ term. If there is no angle spread to speak of, then you cannot expect position sensitivity.

³From the analysis we see that the angular range at the focal plane is roughly $\times 1.6$ bigger than the horizontal scattering angle since the ± 2.14 degree range of the pepperpot translates to $\sim 7^\circ$ in the focal plane. Horizontal scattering angle resolution was thus $\sim 0.3^\circ$ FWHM.

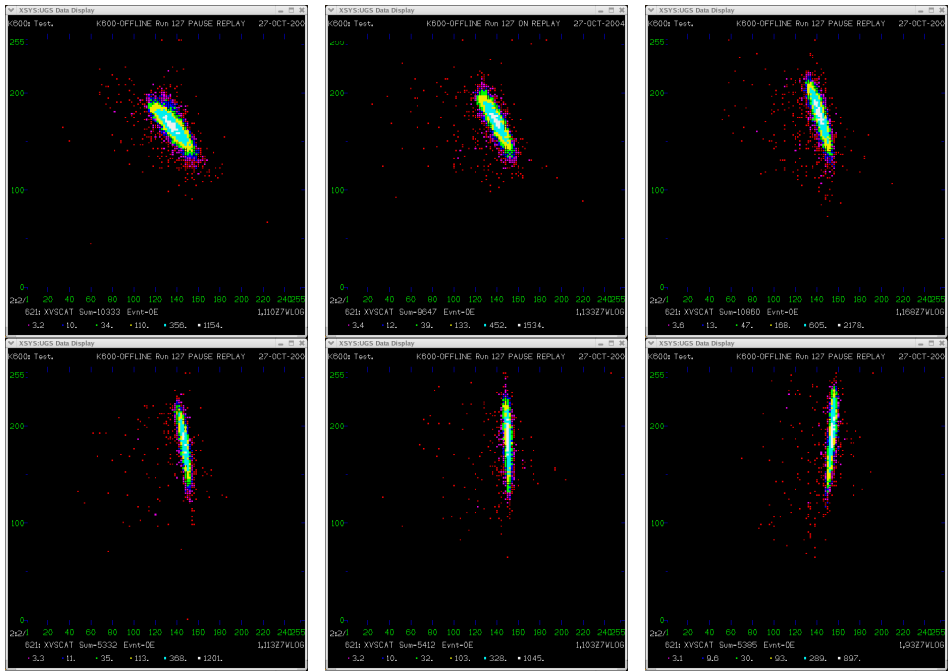


Figure 10.5: Q4=18.43 with Q5 and Q6 search: faint beam DM, Overfocus +15%, 49mm collimator, Run 127 of the October 2004 development period. Final resolution was 24 keV

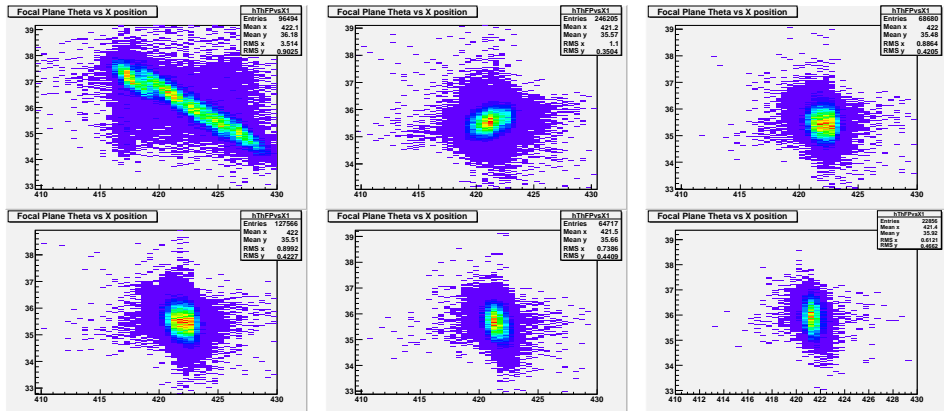


Figure 10.6: Some plots of the faint beam tuning process for dispersion matched beam, overfocus mode +15%, with no collimator (PR137 logbook p143-155).

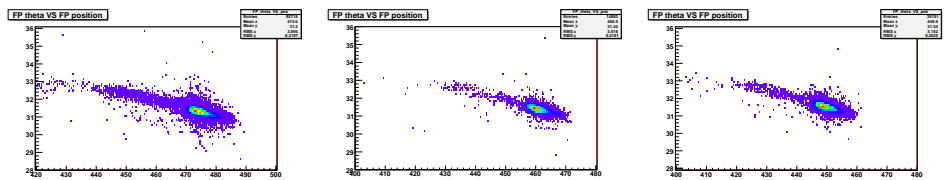


Figure 10.7: Faint beam for achromatic beamline settings. From left to right, K coil =20, 40, 55 (PR138 test weekend runs 4032, 4028, 4030 respectively). Note that the only effect is the shift in position. The general shape of the x-theta locus stays the same (take into account the different total counts in each run). In the position spectrum the sigma of a gaussian fitted to the faint beam peak was 2 mm for all three runs.

10.4 Scattering angle calibration and resolution

10.4.1 Over and under focus mode

For a comprehensive description see reference [Fuj01]. Good Y focus on the target as well as good Y determination in the focal plane is necessary before the use of these off-focus modes becomes a profitable excercise.

- Atsushi Tamii from RCNP says that they applied 'mild' under-focus mode in their early years. After establishment of a suitable analysis procedure, they now sometimes use a 'full' under-focus mode. For the 'full' mode, compared to the 'mild' mode, - Vertical scattering angle resolution becomes better. - The reconstructed vertical scattering angle becomes less sensitive to the vertical beam position on target. - Vertical angular acceptance becomes smaller. - Signal to noise ratio in the background subtraction method becomes worse (due to larger distance of the focusing position from the detector).
- At iThemba LABS we have not clear preferance for a particular focus mode. Originally our conclusion was as follows:
 1. Over-focus mode is better to reduce background produced in the spectrometer.
 2. Over-focus mode is better to realize a good focusing at the focusing position (better S/N in the background subtraction method).
 3. Under-focus mode is better in the sense that the ion-optical parameters in the vertical direction, i.e. vertical scattering angle resolution and vertical angular acceptance, becomes less dependent on x (horizontal position) and theta (horizontal angle).
- In experiment PR137 (100 MeV pt reaction, MDFP) we used the overfocus mode. The comparison in these modes are shown in Fig. 10.8
- In experiment PR244 (200 MeV inelastic α -scattering, HDFP) we used the underfocus mode. See run 48. Note that in this experiment 2 horizontal rows of the pepperpot were blanked out, as we used only a mild underfocus mode.
- In experiment PR242 (100 MeV pt, MDFP) we used the overfocus mode. See run 2028. A full overfocus mode was used, since there is not need for the same background subtraction procedure as is required in inelastic scattering at small angles, including zero degrees.
- From a quick glance at the data it would seem as if we got better Y-information overfocus mode in PR242 compared to the underfocus mode in PR244. for the (p,t) than for the (a,a') . See the attached plots in Fig.10.9 for examples. However, one can only come to a conclusion once you know how big the beamspot was. Also shown in the above-mentioned figure is the image of the beamspot on the scintillating target. Even though the quality of the picture in PR244 is not as good as in PR242, it is clear that the vertical focus was much better for the pt measurement of PR242, and it is therefore easier to get good vertical Y information in the focal plane.
- In experiment PR183 (200 MeV inelastic protons scattering, HDFP) we used the under-focus mode.

- A comprehensive comparison between different overfocus and underfocus modes for inelastic protons scattering during PR183 is shown in Figs.10.10 and . Note that in this experiment the detectors were located on the high dispersion focal plane. The focus mode percentage is defined by the kinematics in the medium dispersion focal plane (via SPEX-CIT) and are therefore not to be taken literally. For example, the true focus is achieved at the nominal setting for a slight focus mode of 4%.
- The sensitivity of a particular focus mode during inelastic proton scattering measurements of PR183 is shown in Fig.10.12.

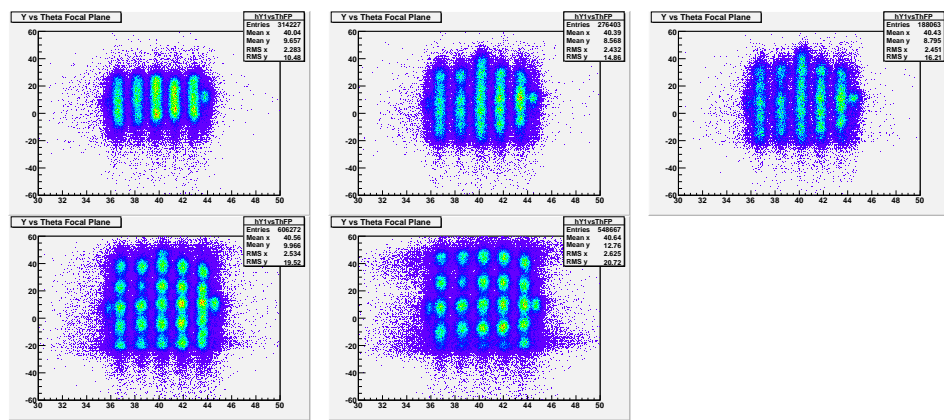


Figure 10.8: Pepperpot collimator during weekend 1 of PR137: from top left to right, first row then second row: underfocus -6.5%, overfocus +7.5%, +8.6%,+11.9%,+15%, PR137 logbook p30-32

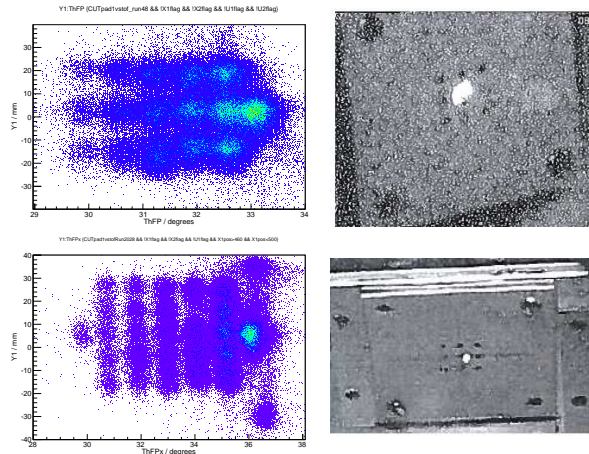


Figure 10.9: Pepperpot collimator calibration runs from experiments PR244 (top left) and PR242 (bottom left). PR244 utilized underfocus mode, and PR242 overfocus mode. A typical beamspot image for experiment PR244 (top right) and PR242 (bottom left) is also shown.

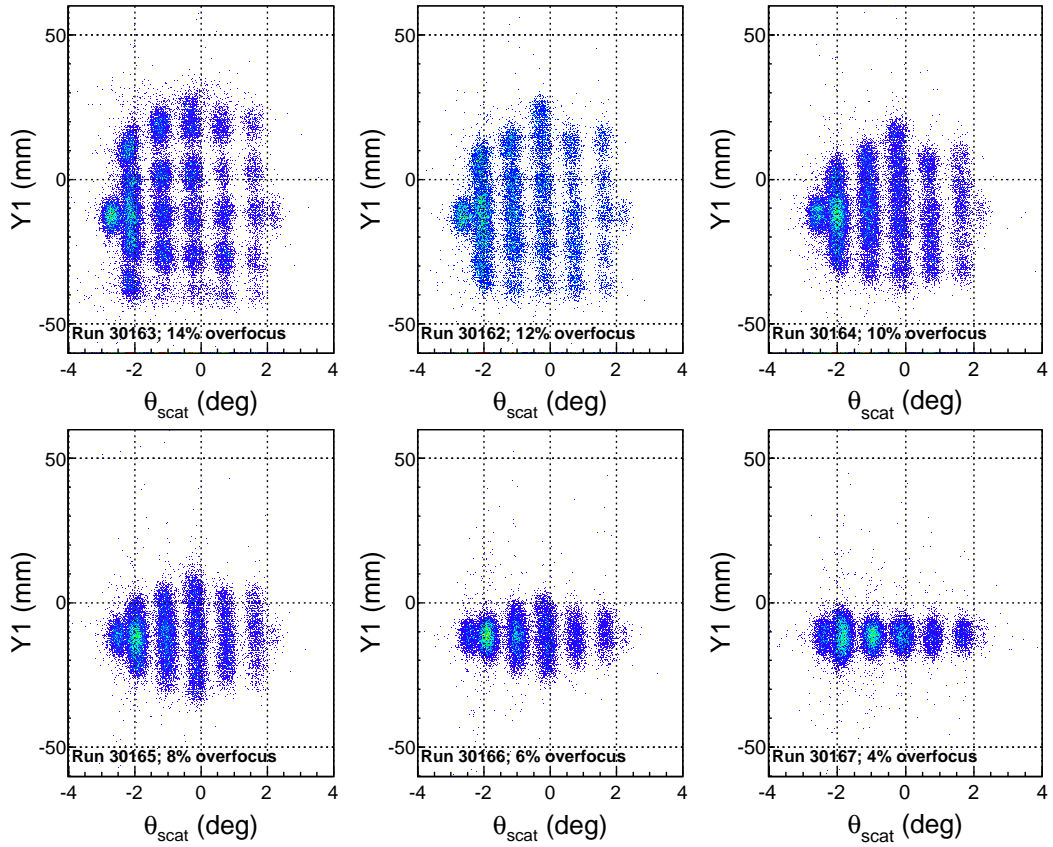


Figure 10.10: Pepperpot collimator for different overfocus modes during experiment PR183. Note that the nominal setting of 4% overfocus mode is the real focus mode.

10.4.2 Vertical scattering angle resolution

The reasons why one wants good vertical scattering angle (sometimes referred to as ϕ) resolution at 0 degrees are:

1. you can get different angle bins and thus finer grained angular distributions
2. some reactions may require that you have accurate scattering angle determination to help distinguish between M1 and E1 states and states with higher l values.
3. if there is significant kinematic E spread then you can only fix if you have good ϕ resolution. ^{12}C has 23 keV E difference between 0° and 2° . Without good phi resolution you cannot correct for this in software.
4. good ϕ resolution may help in background subtraction procedures.

10.4.3 Horizontal scattering angle resolution

Angular dispersion matching is essential for accurate reconstruction of the horizontal scattering angle θ under dispersion matched beam conditions. Under lateral dispersion matched conditions there exists an ambiguity in the horizontal scattering angle as determined from θ_{fp} , as illustrated in Fig.10.13.

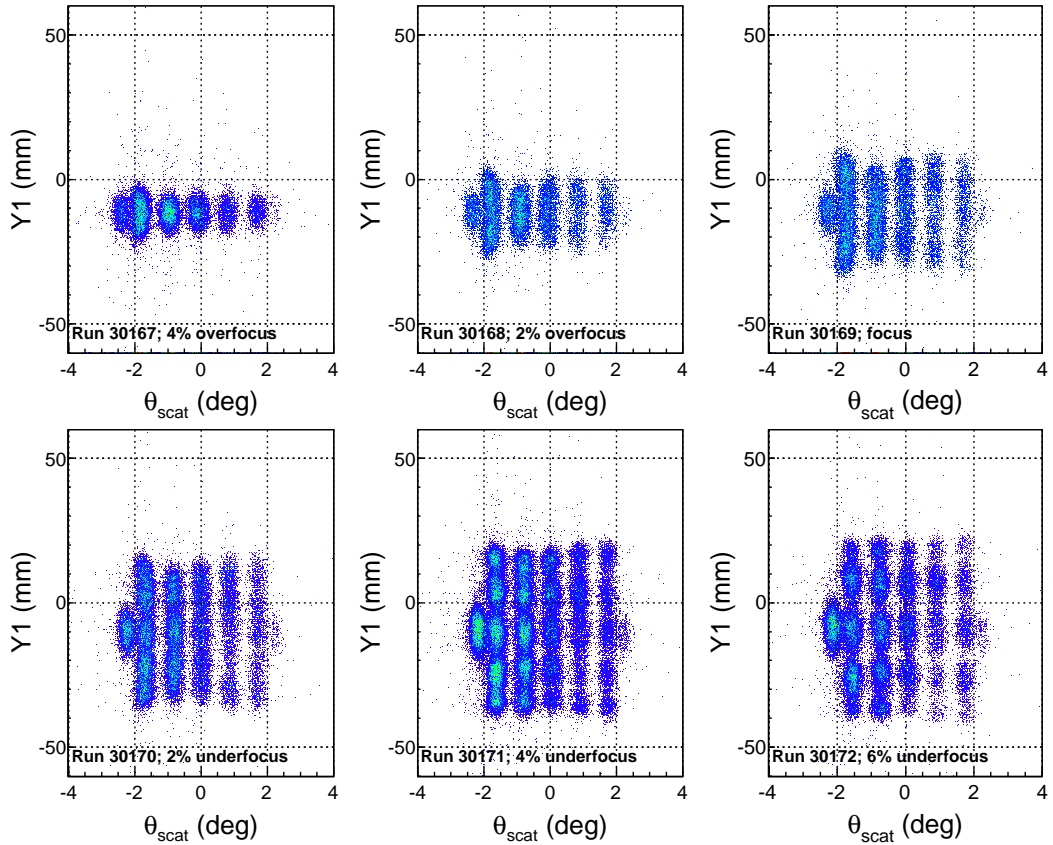


Figure 10.11: Pepperpot collimator for different underfocus modes during experiment PR183. Note that the nominal setting of 4% overfocus mode is the real focus mode.

By way of example, as reported in section 10.3.3 a horizontal scattering angle resolution of $\sim 0.26^\circ$ (4.5 mrad) FWHM was achieved during PR137 (a 100 MeV pt experiment).

At RCNP the horizontal scattering angle resolution achieved is around 0.15° (2.6 mrad) FWHM [Tam09]. According to Hiro angular dispersion presented a serious problem at RCNP, but not at IUCF. This is because the Grand Raiden spectrometer requires a huge beam dispersion at the target ($\sim 37\text{m} (=D/M_{xx}$ of Grand Raiden)), which is considerably more than the $\sim 14\text{m}$ of the K600), which forced RCNP to enlarge the beam strongly just before the target. Hiro believes that angular dispersion was almost naturally matched at IUCF, and possibly at iTL as well. **SOME DAY SOMEONE SHOULD USE TRANSPORT AND TRACK TO CALCULATE THE BEAM AND THE K600 MATRIX ELEMENTS TO NUMERICALLY VERIFY THIS POINT.** To proof this point, refer to Fig.10.15 where a pepperpot spectrum for a dispersin matched beam was obtained for a 200 MeV proton beam and the K600 quad setting for 7% underfocus mode. If the angular dispersion was not 'naturally' matched then the horizontal distinction in scattering angle would not be clear at all.

10.4.4 Calibration

In order to determine the vertical scattering angle ϕ the focal plane detectors must be capable of provinding Y_{fp} information to a reasonable degree of accuracy. At iThemba LABS this is

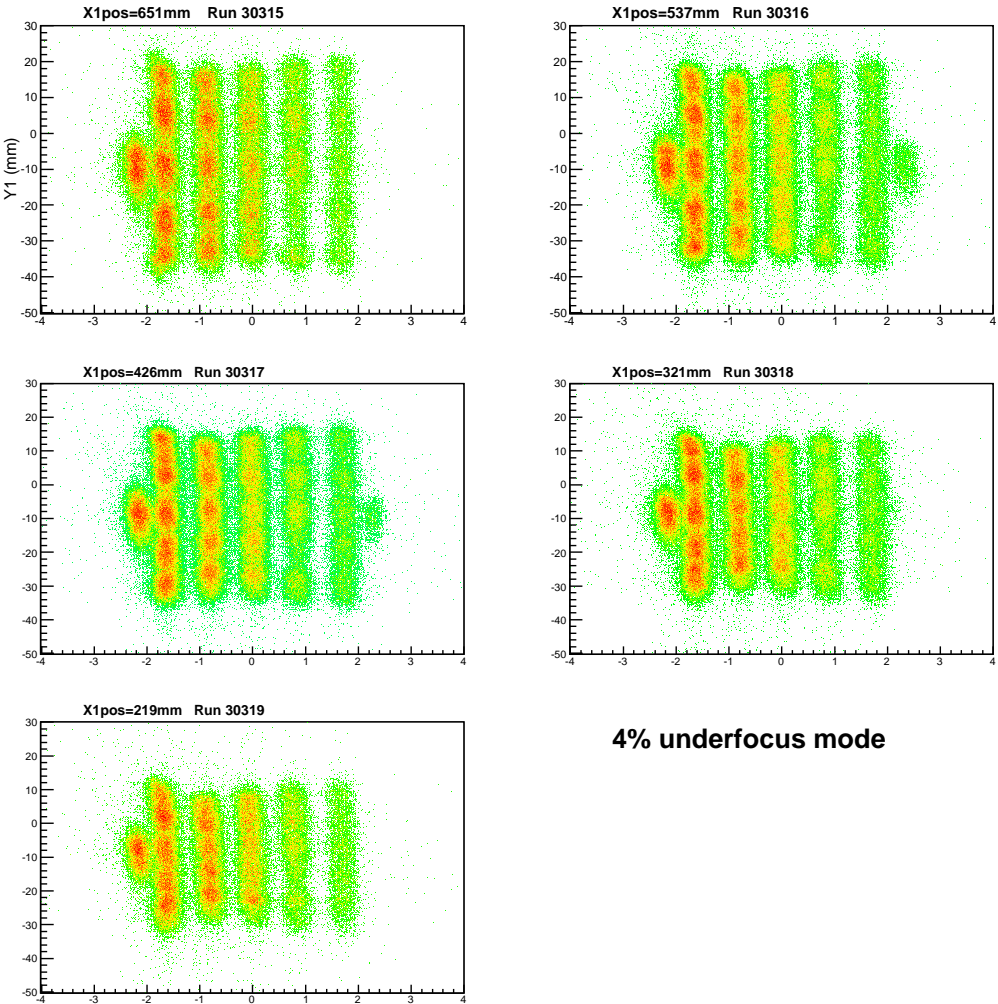


Figure 10.12: Position sensitivity of the pepperpot collimator plots for 4% underfocus mode (which is in reality a 8% underfocus mode) during experiment PR183.

now possible with the new XU vertical drift chambers.

Scattering angle (horizontal and vertical) calibration data is acquired under achromatic beam conditions. This calibrates the ion optics of the K600, which remains the same for both achromatic and dispersion matched beam settings. It should be done after establishing the ion optics of the K600, in other words for the final K and H coil settings that will be used during the measurement. A different calibration is required for the different ion optical modes of the spectrometer, such as the medium dispersion mode, the high dispersion mode and for different and over-focus and under-focus modes.

- Move the spectrometer to a reasonable angle to view the elastic scattered particles. With detectors on the high dispersion focal plane this angle is $\sim 7.3^\circ$ (see section 10.5.4).
- Put in the appropriate collimator: the pepperpot (for ϕ and θ) or the multislot (for θ calibration only).

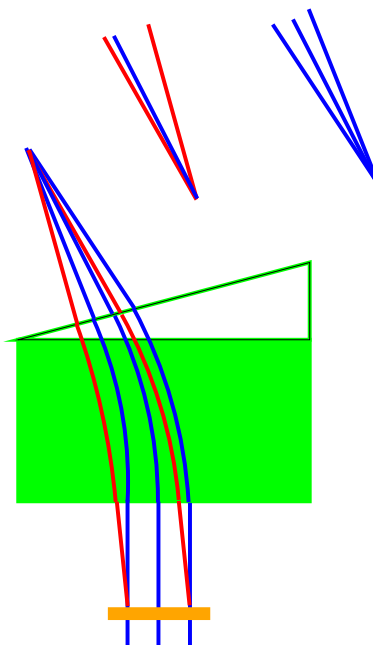


Figure 10.13: With a lateral dispersion matched beam there exists an ambiguity in the horizontal scattering angle. This very rough figure illustrates that 0 degree scattering has a certain focal plane angular range, which is not that different from the focal plane angle range experienced by small non-zero angle scattering, represented by the red lines.

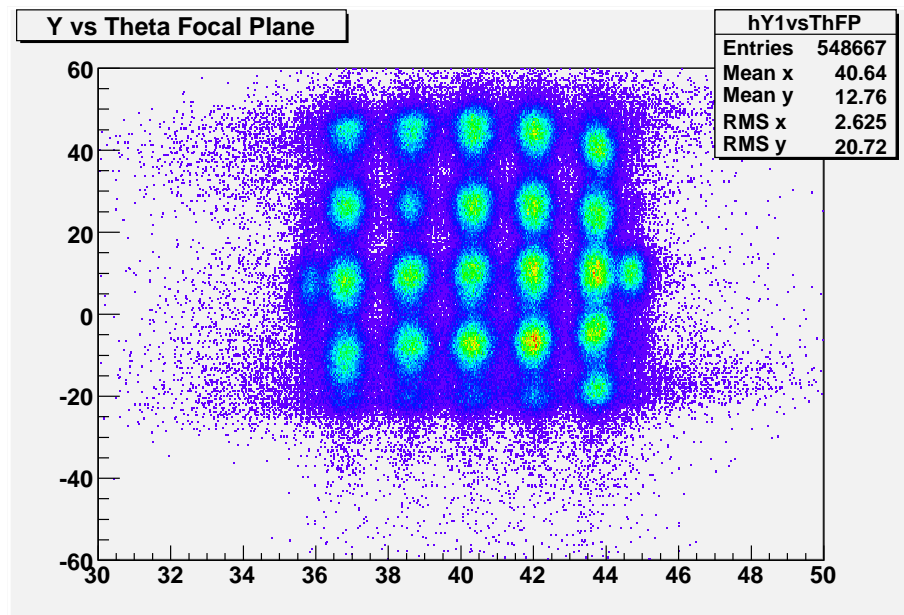


Figure 10.14: Pepperpot collimator during weekend 1 of PR137 +15% overfocus mode, PR137 logbook p32

- Take data for different field settings (without changing the basic ion-optical character, so the ratios of Q,D1,D2 and K and H coils should stay unchanged; use the new superknob

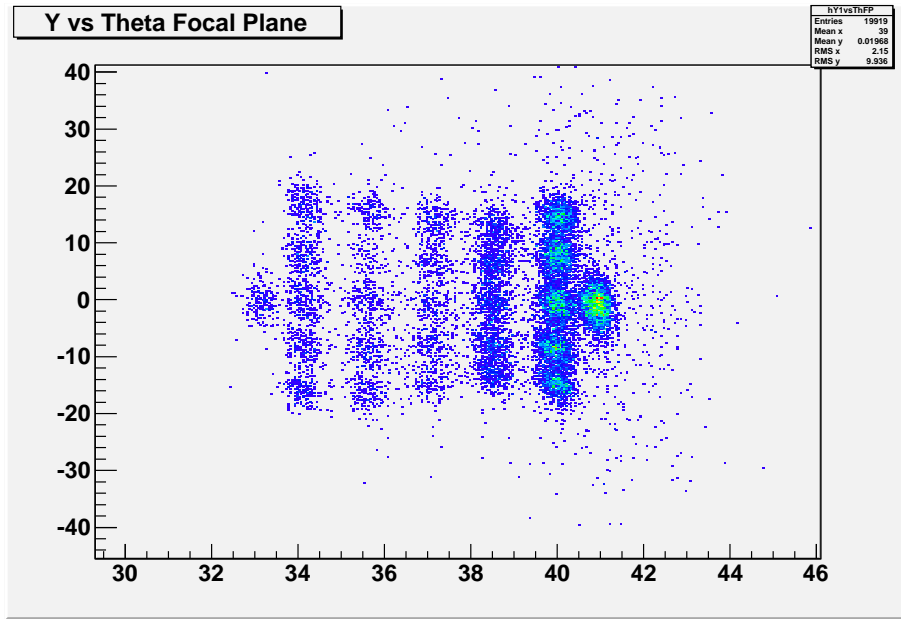


Figure 10.15: Pepperpot collimator for run 21336 of PR170 (PR170 logbook p8): 200 MeV proton beam, dispersion matched beam, K600 quad in -7% underfocus mode, $\theta_{K600}=10^\circ$.

to do this) so that you can 'drag' the elastic locus across the θ_{fp} versus x_{fp} .

Offline analysis of this data will allow the determination of the transformation parameters from focal plane angle to scattering angle.

Irrespective of whether the beam is in the achromatic or (angular dispersed) dispersive mode, the calibration of the K600 should hold true. This however assumes that the calibration is independent of the exact location of the beamspot, which may or may not be true. Indeed, in their zero degree NIM paper (section 3.4) Tamii *et al.* mentions that calibration data was acquired for beamspot at different X and Y positions on the target to analyze the position dependence of the calibration.

The standard figures such as Fig.2 of Ref [Fuj02] has been the cause of some confusion on my part. It is always said that the reason for angular dispersion matching is to get rid of the angular uncertainty you have under normal lateral dispersion matching conditions. But, at least on the scale of the figure, the angle uncertainty for achromatic beamtune is also terrible. Maybe the problem with these figures is the relative scale? The angle spread for an achromatic beamtune is equivalent to, for argument sake, 100 keV. For a calibration value of the focal plane of ~ 40 keV/mm this translates to 2.5 mm position difference over 8 m flightpath, or approximitaly 0.02° . And we know from PR137 a typical dispersive mode focal plane angle resolution of $\sim 0.5^\circ$ FWHM was obtained, which is equivalent to scattering angle resolution of $\sim 0.26^\circ$ FWHM. Therefore, the angular spread in Fig.2a of ref [Fuj02] is in reality a lot smaller than in Fig.2b. Finally, the fact that the central ray of Fig.2a and 2c is the same makes it clear to me that you can use the calibration of Fig.2a to determine the horizontal scattering angles in Fig.2c.

10.5 Miscellaneous for Zero Degrees

10.5.1 Zero degree beamline to beamdump

Figs. 10.16 and 10.17 illustrates the positioning of the detectors in the high dispersion focal plane as well as the zero degree beamline to the (p, p') zero degree beAMDUMP. Fig 10.18 shows how the beam looks like at the entrance to the zero degree beAMDUMP.

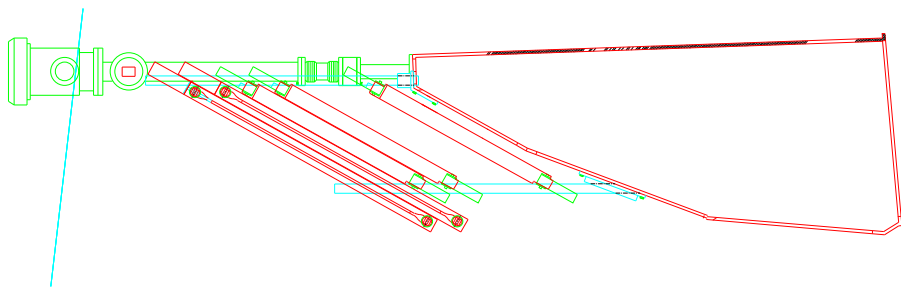


Figure 10.16: The detector setup in the high dispersion focal plane, with the 0-degree beamline (2005 version). Notice the beamviewer just before the beAMDUMP entrance. In this scenario the old VDCs were still used in the focal plane. Since then the bellows was moved towards the beam viewer side and the detector support rod on the low momentum side was shifted. See Fig.10.17.

10.5.2 0° interlock

In the 0° mode the beam interlock system is designed to protect the K600 focal plane. Under no circumstance should the full beam be allowed to impinge on the focal plane vacuum window and detector system. It is activated by turning the key at the back of the collimator box from non-zero to zero, and by activating the interlock on the magnet control page *SP Interlock Control*.

At any stage at least one of the following conditions must be true to allow for beam delivery (FC4S will stop beam delivery to the vault):

- *The solid collimator (which should be in collimator position 5) is in the inbeam position.*
At the back of the control box for the collimator carousel in the dataroom there is a key used to select either a 0° mode or a normal mode. Once the key is switched to the 0° mode (which will be indicated on the frontpanel by a LED light) the interlock condition for the collimator is activated. With the key in the non 0° mode this condition is not needed for beam delivery. Refer to Fig. 10.19.
- *The beam attenuation meshes must be in the beam.*
See section 10.3.1.

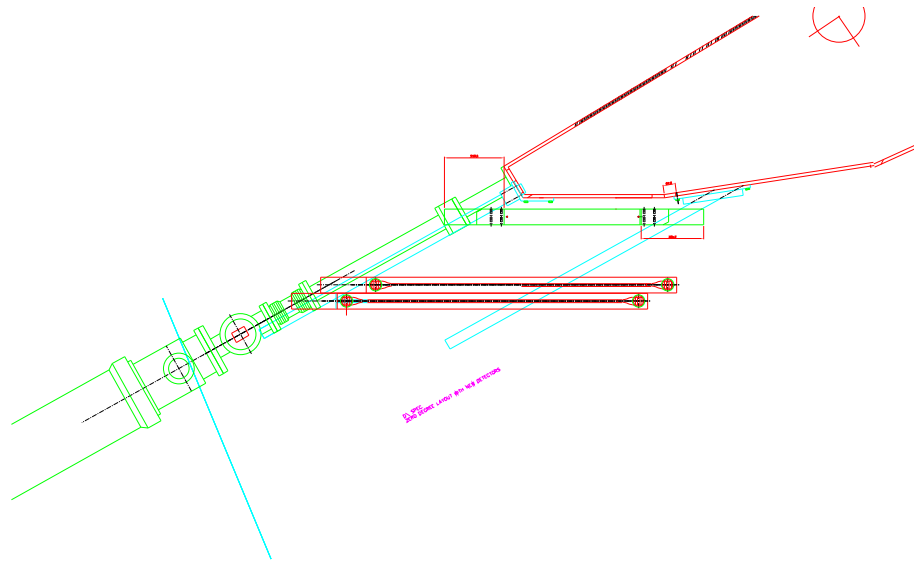


Figure 10.17: The new detector setup in the high dispersion focal plane, with the 0° beamline. Notice the beamviewer just before the beadmump entrance. The support rod on the low momentum side was moved to accomodate the new shorter detector. Also, the bellows was moved further downstream compared to Fig. 10.16. The angle between the 0° beamline and the detectors is 29.15° .



Figure 10.18: The proton beam as seen on the viewer (left of the two shown) just in front of the zero degree beadmump, during experiment PR101 in 2005. The blue line represents the full size of the viewer ($50\text{mm} \times 70\text{mm}$).

- *The magnetic fields of the K600's dipoles must be within predefined ranges.*
These ranges are defined with the same system that is used to set the currents of the magnets. Refer to Fig. 10.20. The following limits were used in PR101:



Figure 10.19: The control box for the collimator carousel, with the new indicator lights that indicate whether the key at the back of the control box (see inset) is set to zero or not. (apologies for quality of picture)



Figure 10.20: The display of K600 magnet settings. The interlock settings for the K600 magnet settings are displayed at the bottom of the screen, as well as the status of the zero-degrees interlock.

10.5.3 Small K600 angle adjustments

In 2005 we found that to align the K600 zero degree beamline with the beambump we had to put the K600 at -0.14° .

What is the case for the new zero degree beamline?

The K600 angle can be adjusted by about ± 0.2 degrees. **This should only be attempted with the manual method of moving the K600.** 4.5 turns is about 0.1 degrees.

10.5.4 Maximum angle of K600 with detectors in high dispersion focal plane

For the detectors in the high dispersion focal plane the maximum angle is quite small.

Should you like to move to a non-zero angle, remember that the maximum angle the K600 can be moved to is only $\sim 7.3^\circ$ before the support rods run into the wall of the vault.

10.5.5 Historical numbers

IUCF:

- DAQ alivetime of 80% for a trigger rate of 800Hz [Berg05].
- beam related halo date was 100 Hz at 2nA [Berg05].

For PR137:

- 223h continuous run.
- Stable running conditions after 48h.
- Stable running for remaining 175h; only SSC phase optimizations required from time to time.
- Excellent beam transmission. Best values: 1.4nA on FC19J and 1.1nA on target (logbook p97)
- Resolution: achr = 78 keV (Au gs peak, logbook p116); disp = 24 keV (faintbeam, logbook p155)
- gas target worked well: resolution = 46 keV (logbook p83; resolution will improve in offline analysis)
- DAQ needs attention before next experiment: deadtimes limits rate to ~ 300 Hz

10.6 Historical high dispersion focalplane magnet settings

Refer to the EXCEL file *hidispplane-magnet-ratios.sxc* in /home/neveling/K600/ZEROD/MAGNET/ for notes on magnet settings. Also, the TRACK figures in the Sept 2009 test weekend logbook make for informative reading. The following three tables contain some reference material for zero degree magnet settings.

Logbook	Run	E_{beam}	D1	D2	Q	K-coil	H-coil	comment
p72	-	197.66	427.51	278.27	-480.03	0?	0?	from SPEXCIT_fake.sxc
p87	399	197.66	427.81	278.73	-481.820	0	0	unclear origin
p103	-	197.95	429.374	279.51	-481.820	28	-100	finetuned by hand
p109	-	198.32	429.374	279.51	-481.820	28	-100	

Table 10.1: Sept 2007: zerodegree settings to get the beam through the K600. Fieldstrengths indicated represent the current, not the magnetic field value.

origin	D1	D2	Q	D1/D2	D1/Q
Sept07	427.51	278.27	-480.03	1.5363	-0.8906
Sept07	427.81	278.73	-481.820	1.5349	-0.8879
Sept07	429.374	279.51	-481.820	1.5362	-0.8912
Sept07	429.374	279.51	-481.820	1.5362	-0.8912
Sept09	428.5	282.390	-471.501	1.5174	-0.9088
Oct09	431.0	282.96	-488.5	1.5231	-0.8823
SPEXCIT 200 MeV MDP std	391.99	389.71	-484.59	1.0059	-0.8089
SPEXCIT 200 MeV HDP std	430.6	282.67	-473.82	1.5233	-0.9088
SPEXCIT 200 MeV HDP mod	427.51	273.66	-470.83	1.5622	-0.9080

Table 10.2: Comparing SPEXCIT settings and experimentally determined settings. Values indicated represent currents (amp). It is important to realize that the ratio between the magnets that is specified in SPEXCIT applies to the REAL MAGNETIC FIELD, and not to the currents. There is a subtle, but real, difference between the two.

origin	D1	D2	Q
SPEXCIT 200 MeV MDP std	391.99	389.71	-484.59
Sept07	427.51	278.27	-480.03
ratio: setting vs std setting	1.091	0.714	0.991

Table 10.3: The third row indicates the ratio that should be used in the TRACK calculation to be able to follow the particle track through the K600, since the fieldmaps we have are valid at the 200 MeV (p, p') settings in the medium dispersion focal plane.

Appendix A

Software notes

A.1 SPANC

To get SPANC working from scratch, do the following:

1. Have a working Java installation with the environment correctly set up in `~/.bashrc`.

For UBUNTU users see

```
https://www.digitalocean.com/community/tutorials/how-to-install-java-with-apt-get-on-ubuntu-16-04
```

for very simple, step-by-step instructions. You have to follow all the instructions, except the sections covering Oracle JDK 6,7 and 9.

For RHEL/CentOS/Fedora users see

```
http://tecadmin.net/steps-to-install-java-on-centos-5-6-or-rhel-5-6/#
```

for very simple, step-by-step instructions. RHEL/CentOS/Fedora users should also remember to change their environment variables to be:

```
# Java Environment Variables:  
export JAVA_HOME=/opt/jdk1.7.0_79  
export JRE_HOME=/opt/jdk1.7.0_79/jre  
PATH=$PATH:/opt/jdk1.7.0_79/bin:/opt/jdk1.7.0_79/jre/bin  
export PATH
```

2. Download the .jar from:

```
http://sourceforge.net/projects/nukesim-classes/
```

3. [user@PC download/place]\$ jar xf dwvisser.jar
4. [user@PC download/place]\$ javac dwvisser/*.java

For step 4, you NEED to be in the directory above the dwvisser folder. If the terminal complains when running javac it has conflicting class files; just delete all the old .class files in the dwvisser folder.

5. [user@PC download/place/] java -cp . dwvisser.NukeSimLauncher

For step 5, as in step 4, you NEED to be in the directory above dwvisser. It is due to the way the code is written. Otherwise you will encounter run-time errors and the program will exit immediately.

6. Additional comment: Add the following line to `~/.bashrc`

```
alias run_spanc='cd ~/SPANC && java -cp . dwvisser.NukeSimLauncher'
```

A.2 SPEXCIT

The following is from J.W. Brümmer:

Another useful program to install is Spexcit. These instructions will likely also be found in the appendices of the K600 manual at a later stage.

Spexcit is obviously Windows based so we need a suitable environment for that. I chose Wine. I didn't want to run it on VB because that takes longer to install and significantly more HDD space. Once again, these instructions are for installing Wine 1.7/1.6/1.5 for RHEL 6/CentOS 6 (32-bit and 64-bit) which is useful given that some of the lab computers run Scientific Linux and due to the CERN support for that being downscaled the IT guys at iThemba are starting to switch over some of our PCs to CentOS (as has been done to Arthur).

All the links below have been checked and are functional presently.

For UBUNTU: Install Wine from the Ubuntu Software Center.

```
Installing Wine (32-bit):
(# indicates su access, $ not)
# yum localinstall --nogpgcheck http://download.fedoraproject.org/pub/epel/6/i386/epel-release-6-8.noarch.rpm
# yum localinstall --nogpgcheck http://rpms.famillecollet.com/enterprise/remi-release-6.rpm
# yum localinstall --nogpgcheck http://download1.rpmfusion.org/free/el/updates/6/i386/rpmfusion-free-release-6-1.noarch.rpm
# yum localinstall --nogpgcheck http://download1.rpmfusion.org/nonfree/el/updates/6/i386/rpmfusion-nonfree-release-6-1.noarch.rpm
# yum clean all
# yum update
(wine now loaded into repository and can be installed like other repository items)
# yum install wine

Installing Wine (64-bit):
# yum localinstall --nogpgcheck http://download.fedoraproject.org/pub/epel/6/x86_64/epel-release-6-8.noarch.rpm
# yum localinstall --nogpgcheck http://rpms.famillecollet.com/enterprise/remi-release-6.rpm
# yum localinstall --nogpgcheck http://download1.rpmfusion.org/free/el/updates/6/x86_64/rpmfusion-free-release-6-1.noarch.rpm
# yum localinstall --nogpgcheck http://download1.rpmfusion.org/nonfree/el/updates/6/x86_64/rpmfusion-nonfree-release-6-1.noarch.rpm
# yum clean all
# yum update
# yum install wine
```

Wine is now installed. The Spexcit files are on K600daq:`~/SPEXCIT` but if you are unable to ssh into it or physically access it I have loaded Spexcit (along with the tarball) into my dropbox and it may be downloaded via this link: https://www.dropbox.com/sh/o0q20i2fburpgye/AABw-fM1hf1ffFQk_s6p9vwCa?dl=0

I am going to assume that all the Spexcit files are located in `~/SPEXCIT` in `~/.bashrc` add the line:

```
alias spexcit='cd ~/SPEXCIT/ && wine32 Spexcit.exe &'
```

The `wine32` command is used regardless whether you did the 64-bit installation.

```
in terminal:  
$ source ~/.bashrc  
$ spexcit  
Done
```

Incidentally, if you want to load things into your repository for easier installation (yum install or apt-get install) you can download the desired .rpm file (e.g. to ~/Downloads) and load it into your repository using similar commands as the ones above:

```
# yum localinstall --nogpgcheck ~/Downloads/<filename>.rpm  
# yum clean all  
# yum update  
# yum install <package_name>  
(these commands cannot be combined to e.g. # yum clean all && update)
```

Appendix B

Old Electronics and DAQ: CAMAC and XSYS

The CAMAC electronics and XSYS software that formed the backbone of the K600 DAQ until early 2009. Most of this chapter is now obsolete.

B.1 The autotrim procedure

The autotrim procedure must be performed if the power to the CAMAC crates and/or power to the pre-amp powersupplies in the spectrometer vault has been off since the previous autotrimming exercise.

Each digitizer channel of the Lecroy Model 4291B TDC can be automatically trimmed so that all pedestals and slopes are set to identical values, thus eliminating the need to do computer corrections for these channels. This is the so-called *autotrim* feature of the Lecroy Model 4298 TDC Controller. When autotrimming is initiated the TIME register is alternately set to $t=0$ for the pedestal trimming, and $t=\text{fullscale}$ for the gain trimming. This cycle is performed automatically by the 4298 TDC Controller.

For an *internal autotrim* the wire inputs of the TDCs are disabled and timing pulses are injected after the TDC inputs. In the *external autotrim* procedure the wire inputs of the TDCs are enabled and an external test pulse is created that in turn fires three different pulsers which supply a test signal to all the pre-amp cards on the three drift chambers. This allows trimming of time differences due to different pre-amp channels and cable lengths. As in the case of data acquisition the TDCs operate in the common stop mode during the autotrim procedure.

Some technical notes on the autotrim procedure:

- It is advisable to perform an internal autotrim before doing an external autotrim.
- The *Start 1* connector of the Lecroy 4298 TDC Controller must be connected via a delay of 48ns (at present the signal also goes through a logic Fan-in/Fan-out, why I do not know) to the three HP 8012B pulse generators.
- Make sure the pulser cables from the HP 8012B are connected to the drift chambers. The pulser connectors on the VDC's are the inner of the two LEMO connectors on the high momentum side of the VDCs. For the HDC the pulser connector is the upper of the two LEMO connectors. Also make sure the data highway is connected in the correct way.

- The settings of the HP 8012B pulse generator: Pulse period should be at negative Ext. To have an idea of the required pulse shapes refer to the logbooks of PR64b, PR90 and PR96a. A good starting point for the shape of the pulser for the VDCs is as follows: total width=6.15 μ s, total signal size=10.22V, first slope=10.22V drop in 9ns, final slope=10.22V climb in 296ns. Note that it is possible to have a too big pulser for the VDC. Also ensure that the pulser outputs to the chambers are in sync.
- As in Fig7 of the TDC preamp manual (which is given as fig 4 on p15) the current into the TRA402S is the integrated $I = CdV/dt$ where dV/dt comes from the leading edge of the pulser signal. For a leading edge 10ns wide for 4V drop $dV/dt = 400\text{mV/nsec}$ i.e. 20uA 10ns pulse into the TRA402 chip. Note that the threshold level applies to the OUTPUT amplitude of the TRA402 amp. What is the amplification factor of the TRA402?

- **Internal autotrim:**

Turn off all drift chamber HV and put the preamp thresholds to 2 volts (*Why this? Just due to superstition? I think it is not required, but this theory is not tested yet*). Execute the following XSYS commands in the [online.spectrometer.autotrim2] directory of the online account¹:

`$ @exttest` (define the correct XSYS data areas)

If you get an error message that goes something like *unable to open global section file*, do a `$ amem new`. Otherwise continue as follows:

`$ @extvme` (vmeput etc. You will be asked to press the red button etc.)

Ignore and give then next command)

`$ @exttpe` (tpe setup, open stream and init)

Once these three commands are given you need not do them again in the following iterative procedure...

`$ @autotrim` (command 4298 to do internal autotrim)

Set the preamp thresholds to ~6.8 volts and acquire data where a pulser is sent to all the channels on all the pre-amp cards. This will indicate the effect of the internal autotrim:

`$ vrctl -c begin` (start a run)

`$ vrctl -c halt` (stop a run)

This should show an internal autotrim that is 6 or 7 channels wide in data area 1, with both X chambers and the Y chamber being centred roughly around channel number 182².

- **External autotrim:**

Execute the following XSYS commands in the [online.spectrometer.autotrim2] directory

¹If the default XSYS directory of the online account is set to something else than the directory [online.spectrometer.autotrim2] you **must** log out completely and log in anew, making sure that the default XSYS directory is [online.spectrometer.autotrim2].

²Due to a bug in XSYS the graphics window does not always automatically update. Without this knowledge one may think that the latest run's results are exactly the same as the previous run, and that any hardware changes made had no effect on the autotrim. To avoid this common error make a habit of viewing data area 2 before looking at data area 1 for each new run. In this way you will know that you always view the real data for data area 1

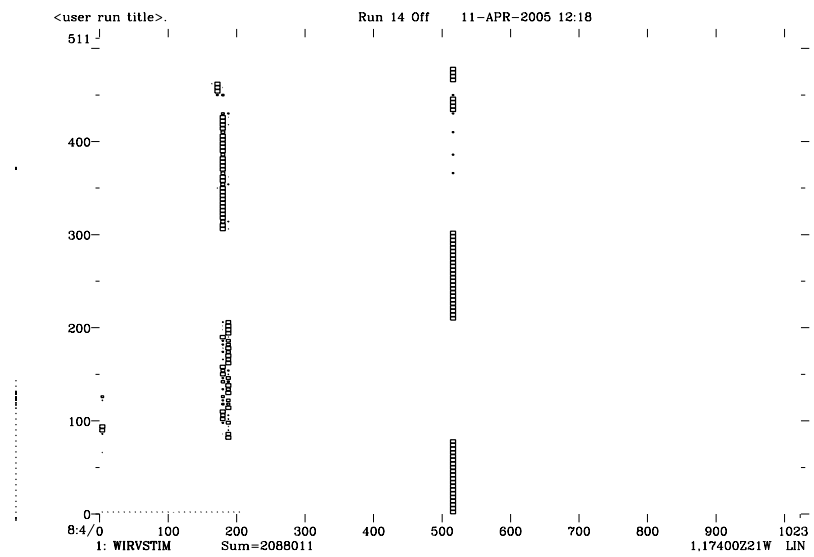


Figure B.1: An overview of typical internal autotrim results for half of the channels for VDC1 and VDC2.

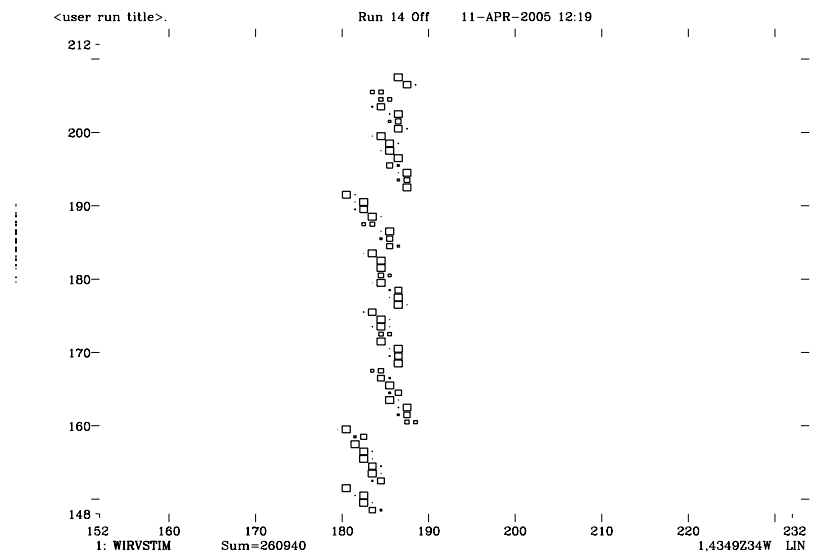


Figure B.2: A close-up view of typical internal autotrim results.

of the online account:

```
$ clear all
$ @autoext          (command 4298 to do external autotrim)

$ vrctl -c begin
$ vrctl -c halt
```

This should give an autotrim that is about 2 channels wide in data area 1, centred around channel nr 256. 256 ns represents the preset time difference for external autotrim between the start and stop signals issued by the TDC controller. See the file *userevents.h*, where the time register is set to the hexadecimal value 0xe010. Repeat with a slightly different threshold if unsuccessful.

B.2 Autotrim problems

Typical problems experienced during autotrim:

- Febr 2008 we found that the external autotrim cable at the TDC controller, between the **STOP 1** and **External Common**, was defective. With this scenario the internal autotrim would seemingly work very well, but once the external autotrim command is performed, the spectrum would look terrible. This is because the signal entering the **External Common** looked terrible, and did not provide a good time-pickoff for the common stop signal.
- Coupled with above, we also found in Febr 2008 that the delay setting (of the HP pulser) between receiving the pulse and producing an output pulse is very important. For a delay of 32ns the external autotrim did not want to work, but with 18ns delay it worked.
- It is very important that the pulser outputs are synchronized. They should pulse at the same time, otherwise the one that pulses first will make it difficult for the second chamber to external autotrim.
- If you experience problems in loading the autotrim software, make sure that you are logged onto the correct computer. Look at the name written on the VME CPU and make sure that you are logged onto that computer. Until further notice that computer is PINCH.
- If it seems as if no matter what changes you make to the hardware that the autotrim results stays the same, read the second footnote from the Internal Autotrim section.
- Electronic noise can be a problem. Observe fig... The only difference between these two is that in the better autotrimming the cables for the focal plane blocker was disconnected. NB remember clean earth and mother earth next to gas box.
- For ideal conditions, switch off the lights in the vault to do away with electronic emissions of the lights.
- Generally if locus is to the left the threshold is too low.
- Totally to the left, no pulser received?
- In Fig. B.3 it is seen that a couple of channels report raw TDC values above 512. This is impossible since the TDC has only 512 ns available. This probably means this channel on pre-amp card or TDC is totally dead. Remember that the TDCs operate in common stop mode. Data in channel 512 probably means that the time measurement was started, but never stopped. It must then mean that the problem is with the TDC, since the start signal comes from the pre-amp card. The stop signal is common to all TDCs. Events in

channel 512 probably refer to overflow events, and all kinds of other errors. Must look into the TDC to find out the detail. Because we see channel 512's for TDC channels with no inputs whatsoever. One can therefore not reason that there was a start but no stop.

- Experience learns that VDC2 thresh is lower than VDC1 thresh.
- As a last resort, try recycling power to the pre-amp powersupplies.
- If there are channels that does not want to autotrim (some channels stay stuck with zero TDC value) then they may be all right. They may yield data.
- The TDC offsets can be corrected by creating a suitable file and putting this in spectrum 1006. The C code for this is on PISTOL as */home/neveling/CPLUSPLUS/create_offs.C*. To get to VDC2 TDC channel nr in spectrum 206,207 subtract 224 from the real TDC channel nr.
- Keep in mind that the drifttime of the 2-dimensional drifttime versus TDC channel nr spectra is divided by 2. Thus 1 channel equals 2ns.
- If one preamp stubbornly does not want to autotrim, even though everything else seems to be fine, see if the ribbon cable orientation is fine.

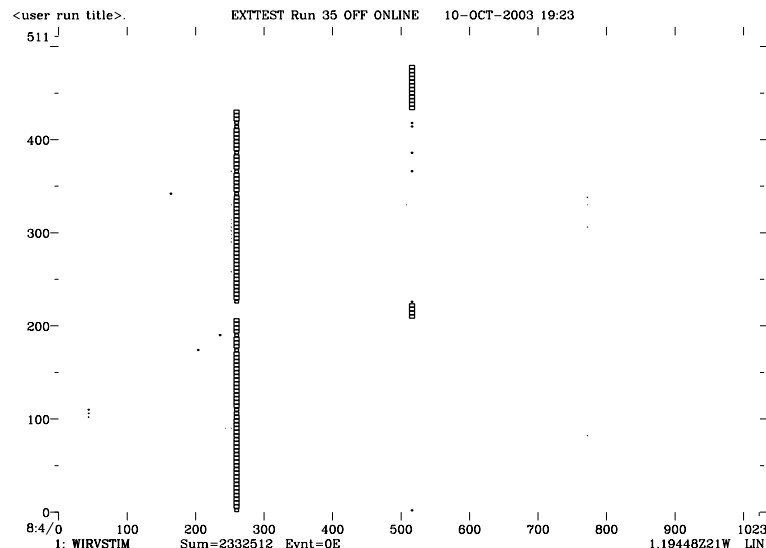


Figure B.3: External autotrim results with suspect datapoints higher than 512ns

B.3 General electronics notes

Take note of the following:

- Always ensure that clean earth is not compromised. During PR97 the clean earth was contaminated because the control system for the sliding seal and

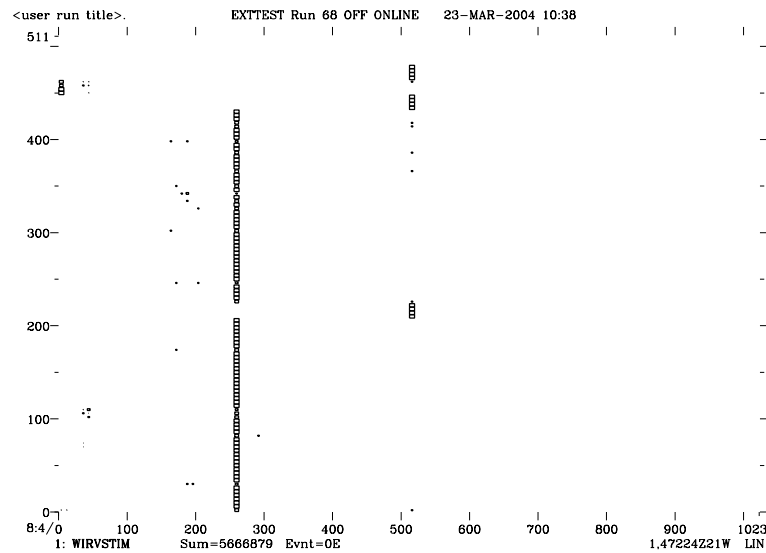


Figure B.4: External autotrim results common to most recent experiments: a couple of TDC channels in the 2nd wire chamber are completely dead (see data at 512ns), and a couple of other TDC channels require software correction to shift them in line with the rest of the channels (see data below 256ns).

Pre-amp card	Signal wire	TDC channel	TDC module
1	-	0-7	1
1	1-8	8-15	1
2	9-24	16-31	1
3	25-40	32-47	2
4	41-56	48-63	2
5	57-72	64-79	3
6	73-88	80-95	3
7	89-104	96-111	4
8	105-120	112-127	4
9	121-136	128-143	5
10	137-152	144-159	5
11	153-168	160-175	6
12	169-184	176-191	6
13	185-198	192-205	7
	-	206-207	7

Table B.1: Preamp card, signal wire, TDC unit and TDC channel numbering of VDC1. VDC1 has 198 wires, connected to TDC channels 8-205. Channels 208-223 represent the second half of TDC unit nr.7, which is unused.

K600 movement was plugged into dirty earth. This resulted in 50Hz noise on the CI line.

- The RS-232 cable for the HV control of the VDC1 cathode plane is numbered 61. Similarly

Pre-amp card	Signal wire	TDC channel	TDC module
1	-	224-231	8
1	1-8	232-239	8
2	9-24	240-255	8
3	25-40	256-271	9
4	41-56	272-287	9
5	57-72	288-303	10
6	73-88	304-319	10
7	89-104	320-335	11
8	105-120	336-351	11
9	121-136	352-367	12
10	137-152	368-383	12
11	153-168	384-399	13
12	169-184	400-415	13
13	185-198	416-429	14
	-	430-431	14

Table B.2: Preamp card, signal wire, TDC unit and TDC channel numbering of VDC2. VDC2 has 198 wires, connected to TDC channels 232-429. Channels 432-447 represent the second half of TDC unit nr.14, which is unused.

Pre-amp card	Signal wire	TDC channel	TDC module
1	1-16	448-463	15
1	-	464-479	15

Table B.3: Preamp card, signal wire, TDC unit and TDC channel numbering of the HDC. The HDC has 16 wires, connected to TDC channels 448-463. Channels 464-479 represent the second half of TDC unit nr.15, which is unused.

the RS-232 cable for the HV control of the VDC2 cathode plane is nr 62.

- At the back of electronics tower on the K600 platform you will find a 50Ω cable patchpanel. Only the cables numbered 16-30 are patched through to the dataroom. Cables 1-15 are patched to a patchpanel in the AFRODITE vault.
- Remember to patch the RF signal through to the K600 vault electronics. It is the RF-ref signal, NOT the BEAM-ref signal.
- The electronics rack in the K600 vault only has power if ‘clean power’ is connected via the dataroom patchpanel (behind the NIM crates)
- Remember that there are two *earth* connections in the K600 vault approx behind the gaspanel: the *clean earth* and the *Mother earth* connections. Make sure that the connector is inserted into the *clean earth* connector.
- For K600 pulser (NOT the autotrim pulser): remember that the signal going into the BNC tailpulse generator must be positive and have an amplitude of at least 1 volt (but the signal input to the Ortec 436 should be negative). For other useful info on the pulser

see the black PR90 logbook p25 and p41, or PR101 the first logbook p? (has a drawing of electronic units required).

- The connectors on the VDCs for the pre-amp threshold are the outer of the two LEMO connectors on the high momentum side of the VDC's. For the HDC it is the lower of the two LEMO inputs, situated at the low momentum end of the HDC.
- When connecting the signal out cables of the paddle PMT's make sure that you use the Dynode Ouput of the PMT, not the Anode output (i.e. not connectors A1 or A2). Even thought the time structures of both these outputs are more or less the same, the Anode signal may be too big for the CAMAC ADC, which has a full scale range of 256 pC?? not true??. **IT SEEMS THAT THIS ISSUE IS NOT RESOLVED: SOME PREFER THE DYNODE, OTHERS THE ANODE. A FINAL DECISION MUST BE MADE AND WE SHOULD STICK TO THAT. RN 26 SEPT 06. THERE SEEMS TO BE NO GOOD REASON TO CHOOSE ONE OVER THE OTHER**
- When doing an experiment with other detectors as well, it is not to be assumed that once you have connected the pre-amp power at the patchpanel that all will be well. You must trace which pre-amp power-supply supplies that power, and you must ensure that the power is on.
- Driftchamber Threshold Supply units: the 50 ohm cables for the units in the dataroom must be connected to the *OUT* connector. In the K600 Vault the cables must be connected to the *Remote* connector
- The ‘Hit-Display’ box must be connected to ‘Charlie’s Electronic Box’ connector *Serial OUT*. The other connector labeled *HIT OR* was used in some initial K600 experiment. For detail approach Ricky Smit.
- The Y-chamber wires: bottom wire on the pre-amp card goes to TDC channel 15, and the top wire on the pre-amp card goes to TDC channel 0. **BUT WHICH WIRE IS CONNECTED TO WHICH PRE-AMP CARD CHANNEL?**
- Nieldane and Shaun tested the propagation time of a signal between the dataroom and the K600 vault, and found it to be 300ns (Dec 2005).
- When the HV on the drift chamber HV planes is too high you start to see junk on the low side of the usual drifttime spectrum.

B.4 Focal-plane detector trips

- Drift chamber trips will occur when e.g. the dipoles are being cycled through the hysteresis loop (SET FIELD procedure) and the changing magnetic field induces a current in the VDC wires. It will also happen when the particle flux through the detector is too high. Or when the quality of the gas deteriorates and more the spark-through voltage of the gas medium is low enough.
- An alarm will sound in the dataroom from the remote power supply control unit.

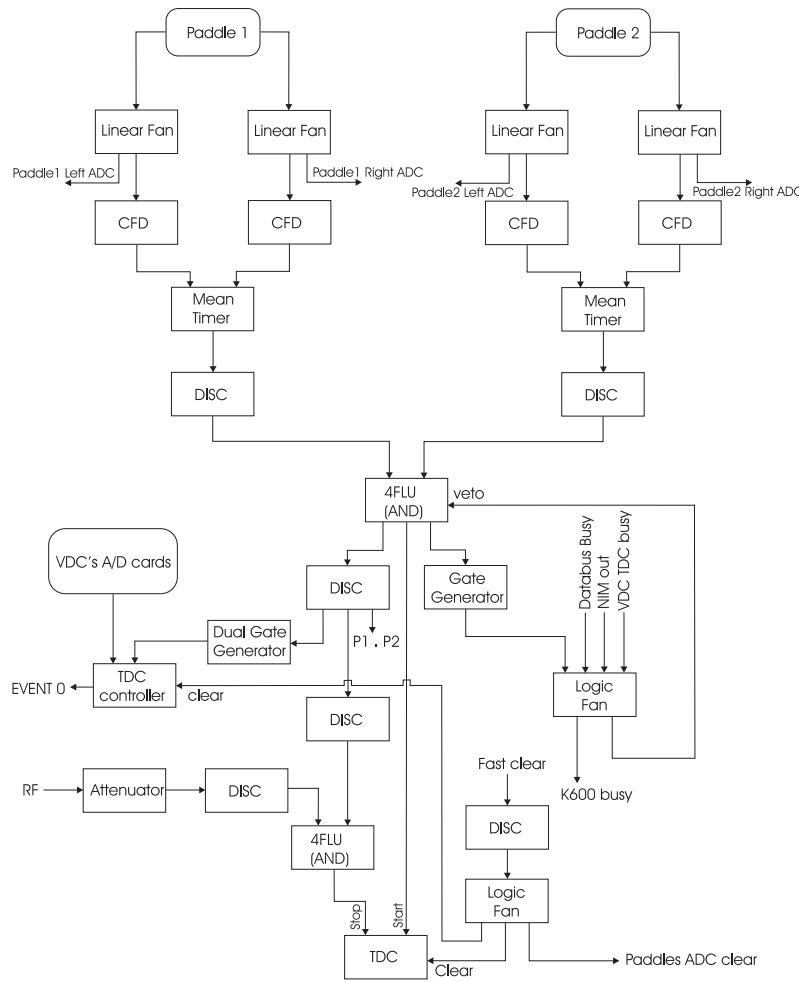


Figure B.5: An overview of the K600 timing electronics in the vault.

- Flicking the on/off switch will switch off the alarm and then ramp up the volts to what it was.
- It is better not to do this ramping up procedure all the way to the set voltage, but rather turn the voltage down two hundred volts or so, let it ramp up to this point and then turn up the volts slowly to the required voltage.
- Sometimes the electronics is set up so that when the detector trips it automatically stops the acquisition. (if the setpoint of the HV control is connected as shown in the Fig.?) This causes a problem because once the ramping is complete the acquisition will automatically be started although the required volts on the detector has not yet been reached and junk might be acquired. Stopping the run before the detector is reset is therefore advisable.

B.5 Data acquisition hardware

- The CAMAC drifttime TDC (Lecroy 4291B) has range of 512 to 2048ns, with corresponding resolution 1ns/bin to 4ns/bin.
- The CAMAC QDC (Lecroy 2249A) has full scale of 256pC.
- The CAMAC TOF TDC (Lecroy 2228A) has a 11 bit binary output (thus about 2048 channels). It is used in the 500ns full scale range, which means 250ps/bin. Thus a 1024 channel spectrum will NOT show all times?!
- The VME QDC (Caen V792) has full scale of 400pC.

B.6 Data acquisition software

Online data acquisition is performed (depending on which VME CPU is used) with either NACDH7 or PINCH (nowdays it is mostly PINCH). To access PINCH you must either use the PINCH terminal or the Linux PC called k600daq. To get the system running from the Linux machine follow this procedure:

- Log onto k600daq as *k600user*, with password *k600pr121*
- Click on the *Terminal Command line* icon on the toolbar
- Type *xhost + pinch* in the terminal window
- Telnet to PINCH (with the command *telnet pinch*) and log on as *online*
- Make sure that the data subdirectory is the one you want.
- Once you get the VMS command prompt, type *@fireup-k600daq*. This off course assumes that this com file exists in this specific directory of PINCH. If not, copy the file from [online.ppa] to the present directory

If all went according to plan you will now have the VMS desktop for the online account. Now you can proceed and load the data acquisition software as follows:

- \$ set def [.vme]
- \$ vmeput
- \$ vrctl -c “restart cold”
- \$ set def [-] (wait until the download to the VME CPU is completed before continuing)
- \$ tpe se *eval-file* “xtcpsort-ucx”
- \$ tpe open stream ‘frontend’
- \$ vrctl -c init
- \$ vrctl -c begin

Some other useful notes on the data acquisition:

- To set the run number to e.g. 200 use the command:
 \$ vrctl -c "set run 200"
- To write data event by event to disk use the command:
 \$ tpe tape ed:
 Wait a few seconds and then press CTRL-C (this is due to a bug in the XSYS software).
 The logical name *ed* is defined for the sake of convenience (in the interest of less typing work) with the command:
 \$ define ed eventdisk:[online.yourdirectory]
- To stop writing event data to disk use the command:
 \$ tpe notape
- When for some reason the buffers fill up too slowly you can always flush out the contents of the buffers in order to view them without having to wait for the buffers to fill:
 \$ vrctl -c flush
- To print a list of the XSYS data areas:
 \$ list mem
 \$ print xsys.lis
- From the Linux desktop, to completely log out of the VMS remember to issue the *xhost - pinch* command before logging off pinch. Otherwise you will not only log out of pinch, but also out of your Linux session.
- The fireup file for the Windows PC used during dispersion matched beam optimization procedures in the control room has a very unlikely name: *fireup_jlab* . Note that recently the PC in the dataroom changed, so that the fireup command now must be *fireup_k600* instead. If the fireup does not work ensure that the fireup file in [online] refers to the correct PC.

B.7 Setting up the lookup table

At the beginning of each experiment, it is necessary to establish the relationship between drift time and particle track distance for the VDC. This relationship may depend on high voltage, the gas mixture, the energy of the particles that cause the ionization and the physical condition of the chamber. A lookup table, proportional to the integral of the average drift time spectrum, is therefore generated. The current procedure integrates using a PLOTDATA macro which runs on (at least) NACDH4 (other platforms not tested or confirmed).

Follow this procedure:

- The spectrometer should be tuned to illuminate the focal plane uniformly (i.e. a white spectrum tune). Data should be collected until reasonable statistics is obtained in the average drifttime spectrum (in present software data area 7)
- The drifttime data area (at present it is nr 107) is then moved out to a file with the following statement:
 move 107 out drifttav.dat nohead

- Logon to nacdhs4 or nacdhs8 or any machine on the cluster that can run PLOTDATA
- Copy the file from the online account to your present account eg.:


```
copy pinch"online online"::[directory]drifttav.dat *.*
```
- Make sure that you have the PLOTDATA macro called lut.pcm in your current directory
 If not look around in all the K600 related directories in the online account for a version of the macro. Or simply ask the iThemba LABS staff for a copy.
- launch PLOTDATA
- @lut
 This PLOTDATA file looks for an input file (without a header) called *drifttav.dat*, and generates a lookup-table called *lut.dat*.
- Copy the lookup-table file to the online account.
- Move the new lookup table into data area 1001, LUT:
`move 1001 in lut.dat`
- To check the lookup table, clear all and start a run.
- Look at spectrum RES2D. It should have a smooth locus running almost horizontally across the spectrum. If there is a break in the locus, the lookup table needs shifting. See Fig. B.6.
- To do this first determine the number of vertical channels between the two sections of the locus. If the section on the right is six channels lower than the section on the left, the lookup table must be shifted by -3 (for a 64x64 RES2D) and vice versa. The successful result is illustrated in Fig. B.7.
- The statements to do this at the \$ prompt are as follows:

`$ TRAN 1001 1002` (Moves spectrum 1001 into 1002)

`$ TRAN 1002 1001 -5` (Shifts the spectrum 5 channels to the right and back into 1001)

or

`$ TRAN 1001 1002`

`$ TRAN 1002 1001 5` (Shifts the spectrum 5 channels to the right and back into 1001)

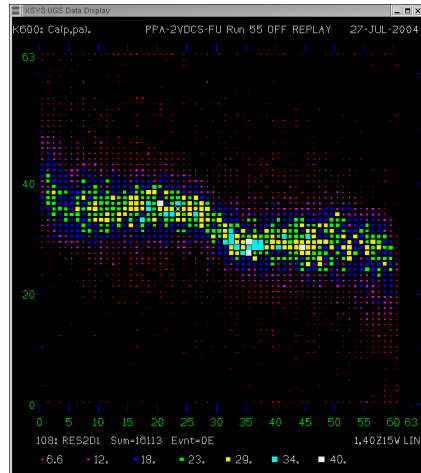


Figure B.6: This RES2D spectrum indicates that a lut shift of roughly -3 is required.

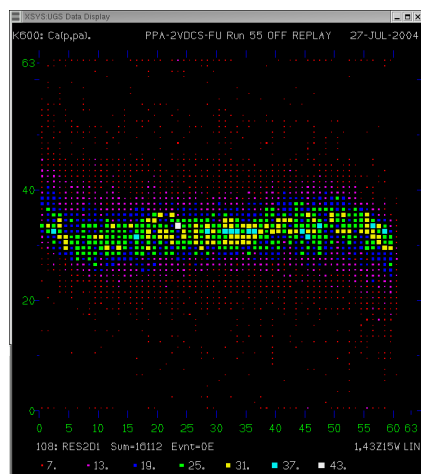


Figure B.7: This RES2D spectrum that results from a properly shifted LUT.

Appendix C

Hiro: beamline comparison between iTL and RCNP

K600 meeting memo 30/08/06

H. Fujita

I. COMPARISON OF ITL AND RCNP

I performed ion-optical calculations using GIOS for two cases, the iTL P- and S-Line with our K600 spectrometer and the RCNP WS course with the Grand Raiden spectrometer. Results of comparison of the transfer matrix elements up to 3rd order are shown in Table I. Matrix elements of iTL which are smaller than RCNP are shown in blue, otherwise in red. From the comparison it was found that most of iTL matrix elements are smaller than those for RCNP.

TABLE I: The calculated transfer matrix elements from the object point of the beamline to the focal plane of the spectrometer of iTL and RCNP, respectively. iTL matrix elements in blue/red are better/worse than RCNP. Estimated image size contributions are also shown in mm.

Matrix elements	RCNP	iThemba LABS	[mm]
$(x x)$	-4.1×10^{-1}	$\textcolor{blue}{-3.1 \times 10^{-1}}$	0.1534
$(x \theta)$	≈ 0	≈ 0	≈ 0
$(x \delta)$	≈ 0	≈ 0	≈ 0
$(x xx)$	$-1.2 \times 10^{+1}$	$\textcolor{blue}{+2.3 \times 10^0}$	0.0006
$(x x\theta)$	$-5.1 \times 10^{+1}$	$\textcolor{blue}{+1.1 \times 10^{+1}}$	0.0111
$(x x\delta)$	$+5.8 \times 10^{+1}$	$\textcolor{blue}{+2.6 \times 10^{+1}}$	0.0011
$(x \theta\theta)$	$-5.5 \times 10^{+1}$	$\textcolor{blue}{+1.5 \times 10^{+1}}$	0.0584
$(x \theta\delta)$	$+9.5 \times 10^{+1}$	$\textcolor{blue}{+7.3 \times 10^{+1}}$	0.0120
$(x \delta\delta)$	$+2.8 \times 10^{+2}$	$\textcolor{red}{-1.8 \times 10^{+1}}$	0.0001
$(x yy)$	$+1.7 \times 10^{+1}$	$\textcolor{red}{-4.7 \times 10^{+1}}$	0.0118
$(x y\phi)$	$-1.4 \times 10^{+1}$	$\textcolor{blue}{+4.3 \times 10^0}$	0.0043
$(x \phi\phi)$	$+4.1 \times 10^{-1}$	$\textcolor{red}{+7.4 \times 10^0}$	0.0296
$(x xxx)$	$-5.2 \times 10^{+2}$	$\textcolor{blue}{-2.4 \times 10^{+1}}$	0.0000
$(x xx\theta)$	$-2.6 \times 10^{+3}$	$\textcolor{blue}{-2.1 \times 10^{+2}}$	0.0001
$(x xx\delta)$	$-1.2 \times 10^{+4}$	$\textcolor{blue}{+1.8 \times 10^{+2}}$	0.0000
$(x x\theta\theta)$	$-4.4 \times 10^{+3}$	$\textcolor{blue}{-7.1 \times 10^{+2}}$	0.0014
$(x x\theta\delta)$	$-4.1 \times 10^{+4}$	$\textcolor{blue}{+1.5 \times 10^{+3}}$	0.0001
$(x x\delta\delta)$	$-7.4 \times 10^{+4}$	$\textcolor{red}{-3.4 \times 10^{+2}}$	0.0000
$(x xyy)$	$-1.2 \times 10^{+3}$	$\textcolor{blue}{+3.1 \times 10^{+2}}$	0.0000
$(x xy\phi)$	$+6.1 \times 10^{+2}$	$\textcolor{red}{+1.6 \times 10^{+3}}$	0.0008
$(x x\phi\phi)$	$-3.9 \times 10^{+1}$	$\textcolor{red}{-3.3 \times 10^{+2}}$	0.0007
$(x \theta\theta\theta)$	$-2.8 \times 10^{+3}$	$\textcolor{blue}{+1.5 \times 10^{+3}}$	0.0123
$(x \theta\theta\delta)$	$-2.5 \times 10^{+4}$	$\textcolor{blue}{+1.5 \times 10^{+4}}$	0.0049
$(x \theta\delta\delta)$	$-3.1 \times 10^{+5}$	$\textcolor{blue}{-7.7 \times 10^{+4}}$	0.0010
$(x \theta yy)$	$-2.6 \times 10^{+3}$	$\textcolor{red}{-7.3 \times 10^{+3}}$	0.0036
$(x \theta y\phi)$	$+1.6 \times 10^{+2}$	$\textcolor{blue}{+2.2 \times 10^{+2}}$	0.0146
$(x \theta\phi\phi)$	$-8.5 \times 10^{+2}$	$\textcolor{red}{-1.5 \times 10^{+3}}$	0.0120
$(x \delta\delta\delta)$	$+9.6 \times 10^{+5}$	$\textcolor{blue}{+1.6 \times 10^{+5}}$	0.0001
$(x \delta yy)$	$-3.7 \times 10^{+3}$	$\textcolor{red}{+5.8 \times 10^{+4}}$	0.0012
$(x \delta y\phi)$	$+2.0 \times 10^{+4}$	$\textcolor{red}{+4.2 \times 10^{+4}}$	0.0034
$(x \delta\phi\phi)$	$+1.3 \times 10^{+4}$	$\textcolor{blue}{+2.3 \times 10^{+3}}$	0.0008
Total	1st+2nd+3rd =	0.15+0.13+0.06	= 0.34

By using these matrix elements, I estimated image size

of the beam from the image size at the object point of the beamline. Assuming x_0 and y_0 (half x/y width at Slit 9X) of 0.5 mm, θ_0 and ϕ_0 (half horizontal/vertical angle spread at Slit 9X) of 2 mrad, and momentum spread δ of 0.00015 (corresponds to 60 keV energy spread at 200MeV), half image size in the K600 focal plane should be 0.34 mm. Applied beam emittance was estimated from the drawing of the X-line slits. By applying 40 keV/mm, this image size corresponds to energy resolution of 27 keV ($0.34 \times 40 \times 2$), which is consistent with our experiences. From this results I think these initial parameters are not far from the realistic values.

I did the same calculation for the RCNP (${}^3\text{He}, t$) reaction at 420 MeV with the same beam emittance parameters (x_0 , θ_0 , y_0 , and ϕ_0). The momentum spread δ was estimated from 100 keV energy spread, which was realized at Nolan's experiment. Resulting half image size is 0.58 mm. This corresponds to 39 keV resolution, but in reality we could achieve 22 keV in this experiment.

From the same calculation for (p, p') at RCNP using 295 MeV with 40 keV energy spread, image size of 0.57 mm was obtained. Applying the focal plane dispersion of 23.0 keV/mm, this image size corresponds to 26 keV. However, they could achieve 17 to 20 keV.

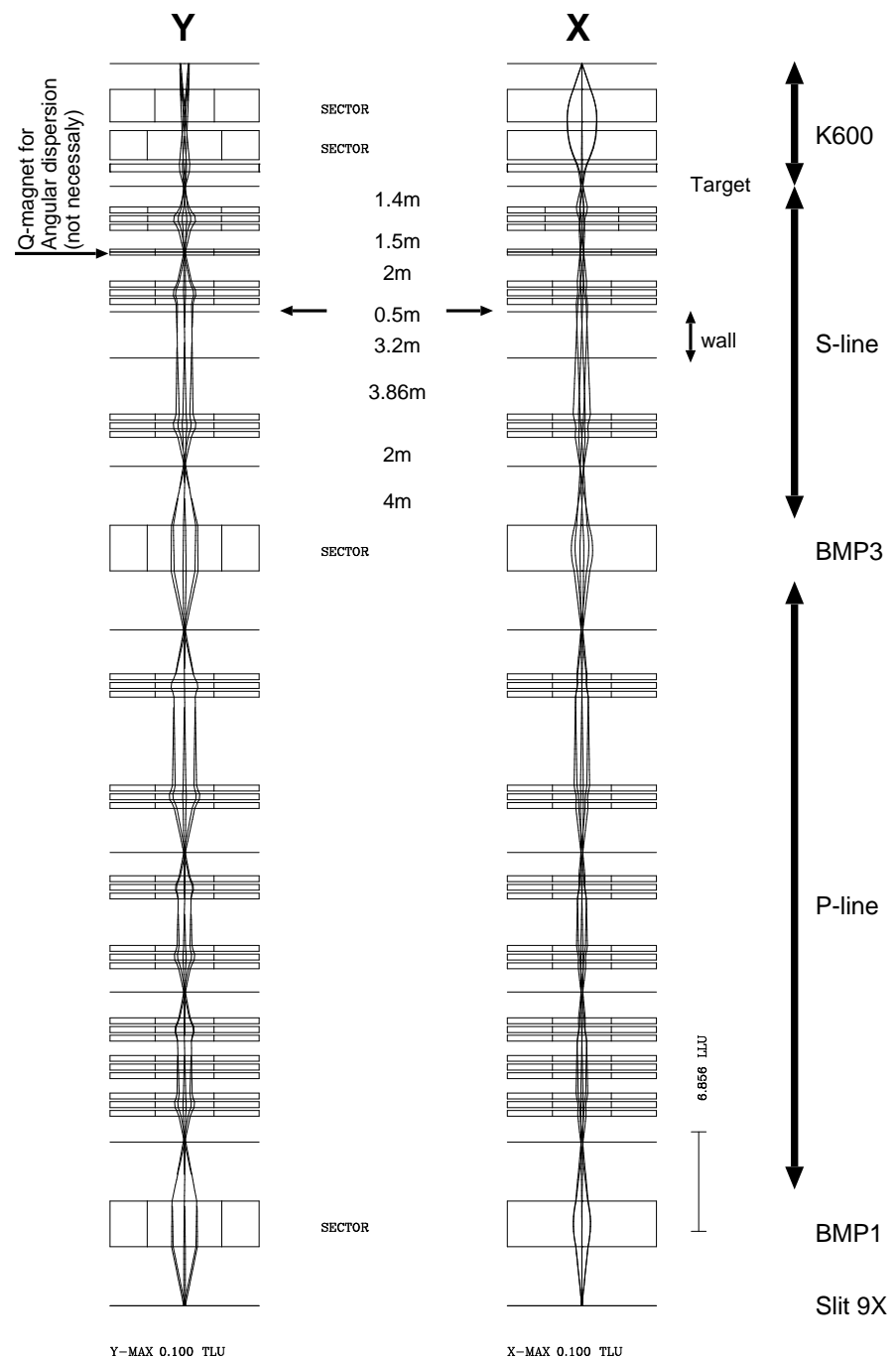
These facts suggest that their image size and emittance of the beam may be smaller than assumed (our) values. For me it is great pity if our well designed accelerator, beamline and spectrometer cannot show their best performance simply due to the bad focusing at the object point.

It should be noted that even with their larger image size in mm in the RCNP focal plane, their energy resolution is better because their spectrometer is much larger than our K600. Therefore if we achieve better resolution in keV then the image size in the focal plane will be much smaller. However, at least we know we can measure 17 keV resolution, which corresponds to 0.4 mm in the focal plane, from the measurement of the faint beam image.

II. THE NEW S-LINE CONFIGURATION

Following Lowry's suggestion, I performed another optics calculation for the new configuration of the S-line. One Q-triplet is added and point-to-point focus was realized by the two triples like the P-line. Results of the calculation is shown in Fig. 1. In this calculation the concrete wall between the beamline area and the K600 vault is roughly taken into account.

From the point of view of energy resolution, this beamline is equivalent to the present beamline. Main difference is smaller width of beam envelope in the S-line,



28-Aug-2006 14:57

FIG. 1: Results of optics calculation for the possible new configuration of S-line with one more Q-triplet. Left/right plot gives the vertical/horizontal beam envelopes.

which is better to reduce background from beam scattering on the beam pipe. However, stronger fields in Q-magnets are required. In Table II, assumed configuration and estimated Q strengths are shown.

TABLE II: Configuration of the new S-line. Effective length and estimated field strength of the Q-magnets are also shown.

Element	Length (m)	Field (KG/cm)
BMP3		
Drift space	4.0693	
Focus point		
Drift space	2.0	
Q-magnet	0.4111	0.384354
Drift space	0.1889	
Q-magnet	0.4111	-0.713818
Drift space	0.1889	
Q-magnet	0.4111	0.384354
Drift space	3.8596	
Drift space	3.2	Concrete wall
Drift space	0.5	
Q-magnet	0.4111	0.384354
Drift space	0.1889	
Q-magnet	0.4111	-0.713818
Drift space	0.1889	
Q-magnet	0.4111	0.384354
Drift space	1.8	
Q-magnet	0.4111	0.329443
(Effective for angular dispersion)		
Drift space	1.3	
Q-magnet	0.4111	0.557119
Drift space	0.1889	
Q-magnet	0.4111	-1.129770
Drift space	0.1889	
Q-magnet	0.4111	0.895752
Drift space	1.4271	
Target		

Appendix D

Single-turn extraction from the injector cyclotron 2 (SPC2) and the separated-sector cyclotron (SSC).

Author: Lowry Condarie

To achieve single-turn extraction a combination of a relatively large orbit separation (the distance between successive turns) at extraction, a low energy spread and a small radial emittance are required. A large orbit separation implies a high dee voltage and/or a large extraction radius. Unless a flat-topping system is used the beam pulse length has to be short to obtain a low energy spread. To maintain a low energy spread over a period of hours, and preferably days, the magnetic field has to be stable. The required magnetic field stability depends on the number of turns in the cyclotron. A high dee voltage, and therefore a small number of turns, alleviates the required magnetic field stability. It is also easier to maintain a low energy spread, and therefore single-turn extraction, over long periods if the magnetic field has from the start been isochronized to within a few RF degrees over the full radial range of the cyclotron and up to extraction. This means that the beam has to be extracted before the region where the magnetic field drops off with radius is reached, although extraction would be easier in this region. For extraction at high energies in the isochronous region of the magnetic field a narrow magnetic pole gap is advantageous to obtain a sharp magnetic field drop-off for easy extraction. If the beam from an injector cyclotron is injected into a second cyclotron, the rf phase of the second cyclotron, and of any rebunchers in the beamline between the two machines, have to be optimized for minimum energy spread, and stabilized with respect to the dee voltage of the first cyclotron. It is much easier to achieve the required rf phase stability than the magnetic field stability. The rebuncher voltages have to be adjusted for minimum pulse length at injection in the second machine.

Considering the k-value of 8, SPC2 has been designed with a low average magnetic field and therefore a relatively large extraction radius. The beam is extracted before the edge field is reached. The central region of SPC2 has been designed for operation with 8, 16, and 32 turns. The turn number is determined by the charge-to-mass ratio of the ion, the extraction energy and the limitation of the dee-voltage to between 20 kV and 64 kV. Single-turn extraction can easily be obtained due to the relatively large orbit separation of 28 mm, 14 mm and 7 mm at extraction, for the three orbit geometries. To ensure single-turn extraction, despite the above-mentioned orbit separations, the following measures are taken during beam development:

1. The emittance of the beam from the electron cyclotron resonance ion source is defined by various horizontal and vertical slits in the beam line between the ion source and SPC2.
2. The voltage of the buncher, upstream from SPC2, is adjusted for minimum pulse length at injection in SPC2.
3. The phase of the SPC2 dee voltage is adjusted for optimum acceleration and therefore also for minimum energy spread
4. The beam width and height are defined in the central region of SPC2 with channels in the dees and slits.
5. The channels and the horizontal slits also limits the beam pulse length for low energy spread, and consequently small radial width, at extraction.
6. The horizontal slits also reduce the energy spread in the beam that is passed through for acceleration.
7. The current of the main and trim coils are initially set to the calculated values. The main and trim coils are further fine-tuned to isochronize the magnetic field, which results in well-defined orbits with minimum energy spread, as shown if figure 1.

Considering the k-value of 200, the SSC has been designed with a low average magnetic field and therefore a relatively large extraction radius. The beam is extracted before the edge field is reached. The cyclotron is operated with a variable number of turns, depending on the required ion specie and beam energy. The maximum dee voltage is 200 kV. Single-turn extraction can be obtained due to the relatively large orbit separation, even without the use of an electrostatic extraction channel. To optimize the beam quality from the SSC the following procedure is followed:

1. The beam intensity and emittance are reduced with horizontal and vertical slits in the transfer beam line between the SPC2 and the SSC.
2. Horizontal slits in the beamline limits the energy spread in the beam and also the increase in the beam pulse length in the beamline section up to the first rebuncher.
3. The voltages of both the rebunchers in the transfer line are optimized for minimum pulse length at injection.
4. The rebuncher phases are optimized for minimum energy spread at injection.
5. The magnetic field of the SSC is isochronized to ± 8 rf degrees by measuring the beam phase with a movable phase probe over the entire radial region of the cyclotron, and adjusting the trim coil currents to newly calculated values.
6. The rf phase of SSC relative to that of the second rebuncher is optimized. The rf phase is optimized by monitoring the orbit pattern at extraction in the SSC with a moveable harp which displays 5 turns simultaneously
7. The current of the injection elements, last horizontal steering magnet in the beamline in front of the SSC, two injection bending magnets and magnetic channel in the nose of one of the sector magnets are optimized for maximum orbit separation at extraction in

the SSC. The orbit separation can be doubled with appropriate settings of the injection element currents.

8. The rf voltage is optimized for the best extraction efficiency.
9. The phase of the SSC is finally fine-tuned while observing the beam profile at the double focusing point in the beamline of the first 90-degree bending magnet in the beamline between the SSC and spectrometer.
10. During the first 24 hours after an energy change small adjustment to the dee-voltage and phase of the rf of the SSC have to be made to compensate for drift in the magnetic field of the SSC. The main coil current of the SSC is also twice during the first 24 hours to keep the magnetic field isochronized.

To optimize the beam quality in the high-energy beamlines the following procedure is followed:

1. The horizontal and vertical beam width and divergence are defined by four slit pairs upstream of the first 90-degree bending magnet.
2. Directly downstream from the first 90-degree bending magnet the energy spread is defined by a pair of horizontal slits.
3. Downstream from the slit used for energy definition various slit pairs, both horizontal and vertical, are positioned around the beam to intercept scattered particles, without stopping particles in the beam core.

A prerequisite condition for a high quality beam is single turn extraction from the injector cyclotron as well as from the main cyclotron. To achieve single-turn extraction a combination of a relatively large orbit separation at extraction, a low energy spread and a small radial emittance is required.

The following measures were taken during beam preparation with SPC2.

- The emittance of the beam from the ECR ion source was defined by various horizontal and vertical slits in the beam line between the ion source and SPC2.
- The voltage of the beam buncher, upstream from SPC2, was adjusted for minimum pulse length at injection into SPC2.
- The phase of the SPC2 dee voltage was adjusted for optimum acceleration and therefore also for minimum energy spread.
- The beam width and height were defined in the central region of SPC2 with channels and slits in the dees. The channels and the horizontal slits also limited the beam pulse length for low energy spread, and consequently small radial width, at extraction.
- The current of the main and trim coils were initially set to the calculated values. The main and trim coils were then fine-tuned to synchronize the magnetic field, which resulted in well-defined orbits with minimum energy spread.

To optimize the beam quality from the SSC the following procedure was followed:

- The beam intensity and emittance were reduced with horizontal and vertical slits in the transfer beam line between the SPC2 and the SSC. Horizontal slits limited the energy spread in the beam and also the increase in the beam pulse length in the beam line section up to the first rebuncher.
- The voltages of the two rebunchers in the K and J transfer lines were optimized for minimum pulse length at SSC injection. Rebuncher phases were optimized for minimum energy spread at injection.
- The magnetic field of the SSC was isochronized to $\pm 8^\circ$ in radio-frequency (RF) by measuring the beam phase with a movable phase probe over the entire radial region of the cyclotron, and adjusting the SSC trim coil currents to newly calculated values.
- The RF phase of the SSC relative to that of the second rebuncher was optimized by monitoring the orbit pattern at extraction in the SSC with a movable harp which displayed 5 turns simultaneously.
- The currents of the injection elements, consisting of the last horizontal steering magnet in the beam line in front of the SSC, two injection bending magnets as well as the magnetic channel in the nose of one of the sector magnets, were optimized for maximum orbit separation at extraction in the SSC. The orbit separation could be doubled with appropriate settings of the injection elements.
- Finally the phase of the SSC was fine-tuned while observing the beam profile at the double focusing point after the first 90° bending magnet in the beam line between the SSC and spectrometer.

Appendix E

List of proposals since November 2004

1. PR96a: (p,p alpha) cluster knockout on 40Ca at 100 MeV
2. PPR101: PAC of November 2004: Study of Isovector Excitations in mass 60,62,64 nuclei
3. PPR102: PAC of November 2004: Identification of stretched high-spin states in 48Ca via high resolution proton inelastic scattering
4. PPR96b: PAC of November 2005: (p,p alpha) cluster knockout on 40Ca at 100 MeV
5. PR97b: PAC of November 2005: An investigation into the nature of M1 transitions in Fe-56 with high resolution inelastic proton scattering at zero degrees
6. PR116: PAC of November 2005: Development of a beamstop for the study: Resonance states in 30S, 34Ar and 38Ca nuclei using the (p,t) reaction and reaction rates in the rp-process
7. PR120: PAC of May 2006: A Global Investigation of the Fine Structure of the Isoscaler Giant Quadropole Resonance: The Low-Mass Region 12j A
8. PR121: PAC of May 2006: Discovering Giant Pairing Vibrations with the (p,t) reaction
9. PR128b: PAC of Oct 2007: Development time for the K600 ZeroDegree facility
10. PR132: PAC of May 2007: An investigation of alpha-clustering in 212Po by using a ($^7\text{Li},t$) reaction
11. PR137: PAC of May 2007: Resonant states in 30S, 34Ar and 38Ca nuclei using the (p,t) reaction and reaction rates in the rp-process
12. PR138a: PAC of May 2007: Fine Structure of the Isovector Giant Dipole Resonance: A survey of the (p,p') reaction at 0 degrees
13. PR142a: PAC of October 2007: Development of forward angle mode using the K600 spectrometer
14. PR143a: PAC of October 2007: Investigation of the ($^3\text{He},^8\text{He}$) reaction

15. PR121b: PAC of April 2008: Discovering Giant Pairing Vibrations with the (p,t) reaction at zero degree
16. PR137: Resubmission: PAC of April 2008: Resonant states in ^{30}S , ^{34}Ar and ^{38}Ca nuclei using the (p,t) reaction and reaction rates in the rp-process
17. PR153a: PAC of October 2008: Analyzing power angular distributions in the excitation of low-lying states in ^{56}Co
18. PR146b: PAC of October 2008: Does the 9.641 MeV 3^- state in ^{12}C hide a state with a 2^+ character?
19. PR128c: PAC of October 2008: Development time for the K600 Zero Degree Facility
20. PR138b: PAC of May 2009: Fine Structure of the Isovector Giant Dipole Resonance: A survey of the (p,p') reaction at 0 degrees
21. PR164: PAC of November 2009: Does the 11.16 MeV state seen with the $^{11}\text{B}(^{3}\text{He},\text{d})$ reaction belong to ^{12}C and if so, does it have a 2^+ character?
22. PR166: PAC of November 2009: First (α,α) measurements with the K600 Spectrometer at Finite Angles and Zero Degrees.
23. PR153b: PAC of November 2009: (resubmission as it timed out) Analyzing power angular distributions in the excitation of low-lying states in ^{56}Co
24. PR167: PAC of November 2009: Fine Structure of the Isoscalar Giant Quadrupole Resonance and 2^+ level densities in spherical to deformed nuclei across the isotope chain $^{142,144,146,148}\text{Nd}$ using the (p,p) reaction
25. PR170: PAC of April 2010: Characterization of cluster states in ^{16}O with the (p,t) reaction.
26. PR166b: PAC of November 2010: A Test of Making (,) Measurements with the K600 Spectrometer at Finite Angles and Zero Degrees.
27. PR164b: PAC of November 2010: Does the 11.16 MeV state seen with the $^{11}\text{B}(^{3}\text{He},\text{d})$ reaction belong to ^{12}C and if so, does it have a 2^+ character?
28. PR184: PAC of November 2010: Fine structure of the Isovector Giant Dipole Resonance using the (p,p) reaction at 0: Effects of strong nuclear deformation
29. PR183: PAC of November 2010: A study of the complete electric dipole response in ^{96}Mo
30. PR185: PAC of April 2011: Investigating the structure of 2^+ mixed-symmetry states in the nuclei ^{70}Zn , ^{96}Ru and ^{96}Mo with high-resolution proton scattering
31. PR193 PAC of November 2011: Development of forward-angle mode using the K600 spectrometer
32. PR194 PAC of November 2011: Development of high energy resolution inelastic α particle scattering at zero degrees

33. PR195 PAC of November 2011: Further characterization of the 2^+ cluster state in ^{12}C
34. PR196 PAC of November 2011: Search for the 0^+ cluster state near the 5 alpha breakup threshold in ^{20}Ne with the (p,t) reaction
35. PR196 PAC of April 2012: Non-resonant triple- α reaction rate at low temperature
36. PR210 PAC of November 2012: Fine structure of the Isovector Giant Dipole Resonance in neutron-rich calcium isotopes using the (p, p') reaction at 0° .
37. PR211 PAC of November 2012: Superdeformed states in ^{28}Si
38. PR203 PAC of November 2012:
39. PR217 PAC of April 2013: Influence of the proton core on the ne structure of the Isovector Giant Dipole Resonance as a function of nuclear deformation across the neodymium and samarium isotope chains
40. PR218 PAC of April 2013: no beamtime approved since Li beam is needed
41. PR226 PAC of November 2013:
42. PR227 PAC of November 2013:
43. PR228 PAC of November 2013:
44. PR231 PAC of November 2013:
45. PR232 PAC of November 2013:
46. PR236 PAC of April 2014: Fine structure of the Isoscalar Giant Monopole Resonance in ^{208}Pb , ^{90}Zr , ^{58}Ni , and ^{40}Ca , using alpha scattering at zero degrees
47. PR238 PAC of April 2014: Testing the Isobaric Multiplet Mass Equation for the $A = 32$ quintet.
48. PR240 PAC of October 2014, October 2015:
49. PR244 PAC of October 2014:
50. PR242 PAC of April 2015:
51. PR249 PAC of April 2015:
52. PR251 PAC of April 2015:
53. PR254 PAC of October 2015:
54. PR259 PAC of October 2015:
55. PR260 PAC of May 2016:
56. PR262 PAC of May 2016:
57. PR263 PAC of May 2016:
58. PR264 PAC of May 2016:

Appendix F

Zero degree experiment run checklist

- Ensure the scattering chamber beamstop is in position, and collimator 5 is in. Look at the target and the Hatanaka viewer, and ensure good alignment. Also note how the beam looks like at this point
- Next ask the operators to measure the beam profile in the S-line with harps 1S, 3S and 4S. This means they have to stop the beam on FC4s to increase beam intensity.
- Put these values into the *emmits* program. The emittance values should be decent. X should be 4-5 π mm rad, Y should be \sim 2-3 π mm rad If you have a good choose good values for Q1s to Q6S remember we need cross-over before the middle harp - look at viewers again - move collim to 3, move beamstop out, empty target - transport beam to beamdump viewer, all detectors still off use the superknob by changing d1 values in small steps - after that put on scintillators and look at halo ask operators to tune halo if halo good, switch on the VDCs - if halo good change to faint beam mode 1. stop beam. 2. ask operators to put in faint beam meshes 3. change field of K600 with superknob to D1=443 4. ask operators to put in 5. if operators verify that meshes are in then ask for 1nA 6. look for beam in CI and visually on viewer. Move with superknob D1 closer to beam left 7. optimize resolution: change Q6S, Q5S, Q21P, SSC phase and voltage 8. verify that slit 9X is narrow: X-gap 1mm or less, 9X y-gap should not be more than 2mm - if good resolution stop beam, operators take out meshes, put in collim 5 and internal beamstop check the tgt and hatanaka viewers again - if happy, then change K600 fields with superknob to beam transmission mode again change to collim 3 and take out internal beamstop check halo

Appendix G

Setting up CAKE

CAKE, the coincidence array for K600 experiments, is a silicon array for use with the K600. In this chapter, the basics of setting up CAKE from mounting the detectors to taking data with the DAQ will be described. In advance of doing anything, I (Phil) urge you to strongly do the following:

1. Get your tools ready and check if there are masks and latex gloves.
2. Go and have a look at the silicon detectors so you have some idea of what you're trying to do.
3. Find the MHV-4, MSCF-16 and MPR-16/32 manuals - these will be referred to in this guide so you might as well have them ready now. They can be found on the Mesytec website and hard copies are usually floating around the vault somewhere.

G.1 Mounting the Detectors

In an ideal world, you will never need to do this as the CAKE is already mounted and on the frame (at the time of writing). However, there should be a guide for it in case it needs to be done. It may be the case that after a few years, the radiation damage of the CAKE detectors is bad enough that they will need replacing.

Note also that there are people at iThemba LABS who have experience of handling silicon detectors. If you are unsure or would like assistance, please ask around and find someone to help you. At the time of writing, the people that you probably want to talk to are Retief, Mathis and Paul.

Required:

1. A detector.
2. A mounting frame.
3. Two plastic nuts and two plastic bolts.
4. Some way of securing the frame while mounting the detector.
5. Gloves and a facemask.
6. A friend, preferably someone who has mounted the detectors before if you have not.

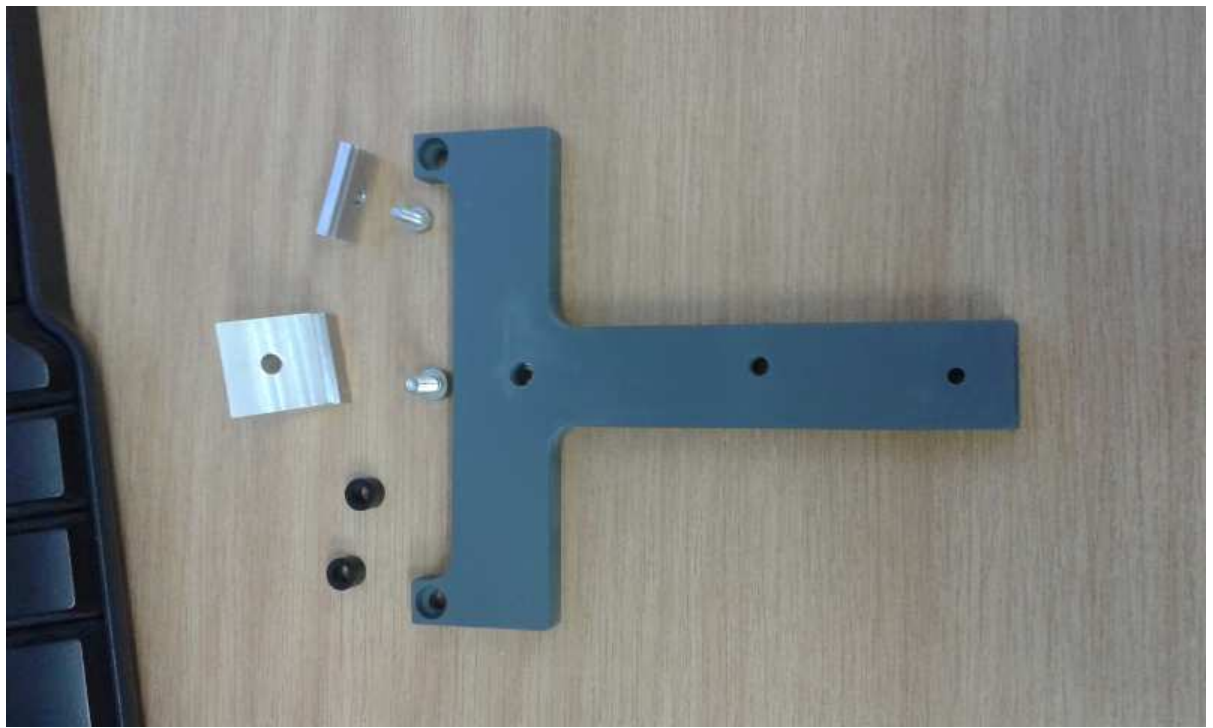


Figure G.1: The parts required for mounting CAKE - the plastic frame, 2 black spacers, the holder for the detector point and the back bracket.

- The first thing to do put your gloves and facemask on. Then look at the detector to locate the bonding wires on the front (which go down one side of the detector) and the back (which go around the outer edge of the detector). These bonding wires must not be allowed to come into contact with any surface. They are very fragile and are extremely easy to break.
- The detector (even the PCB) must never be touched without gloves. A mask should be worn so that there is no contamination from breath or spit. Never touch, even with gloves on, the silicon wafer. You must never allow anything to come into contact with the wafer. Even the lightest touch from a piece of metal will cause a scratch which could destroy the detector.
- Up to 5 CAKE detectors may be mounted at one time. Each of the detectors sits on a cross-shaped stand. The thin end of the detector is placed into the slot in the metal cap on the end of the stand, shown Figure G.1 below. There are two black spacers which are placed within the holes on the cross-pieces of the detector which ensure that the bonding wires on the back of the detector do not come into contact with the stand.
- Two plastic bolts are used to hold the detector in position. These are secured using two plastic nuts. This should be done before the detector is moved.
- Once this has been done, the detector can be put on the frame which goes into the chamber. This frame consists of: the rib which goes around the chamber, two rails and then some connecting parts. These are shown in the Figures G.5, G.6, G.7 and G.8.



Figure G.2: The assembled version of the parts required for mounting CAKE



Figure G.3: Another view of the assembled CAKE mount.

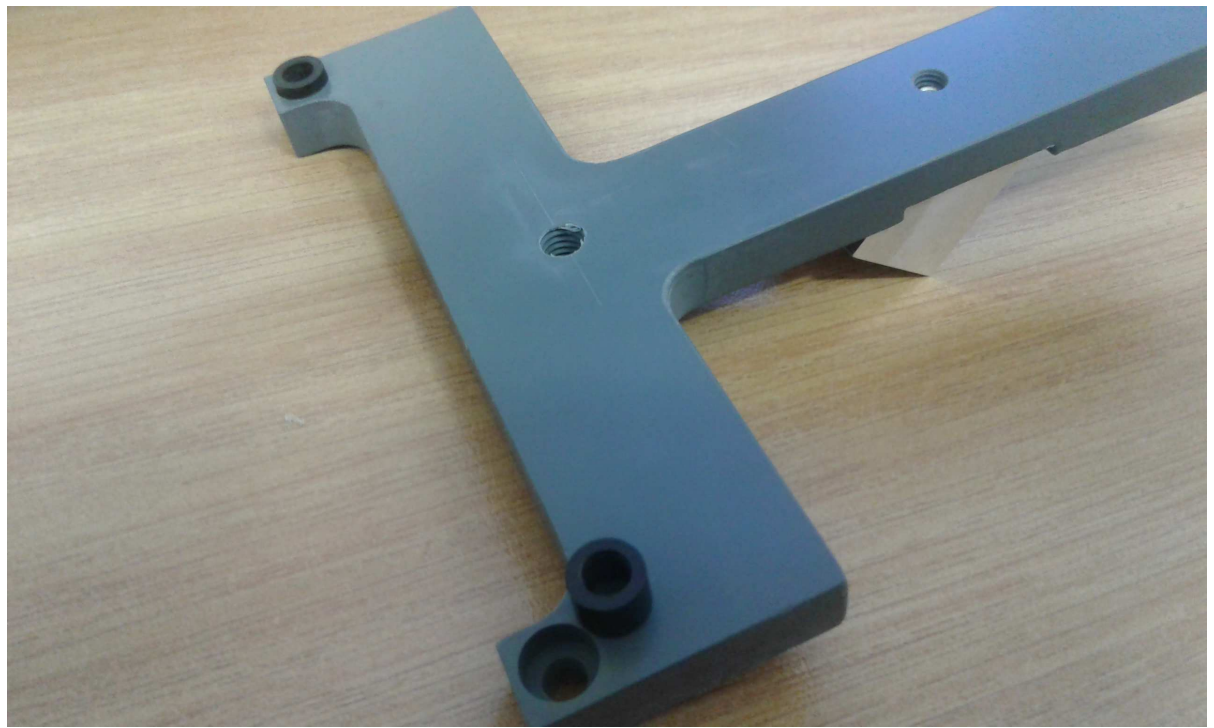


Figure G.4: A picture showing where the spacers go.

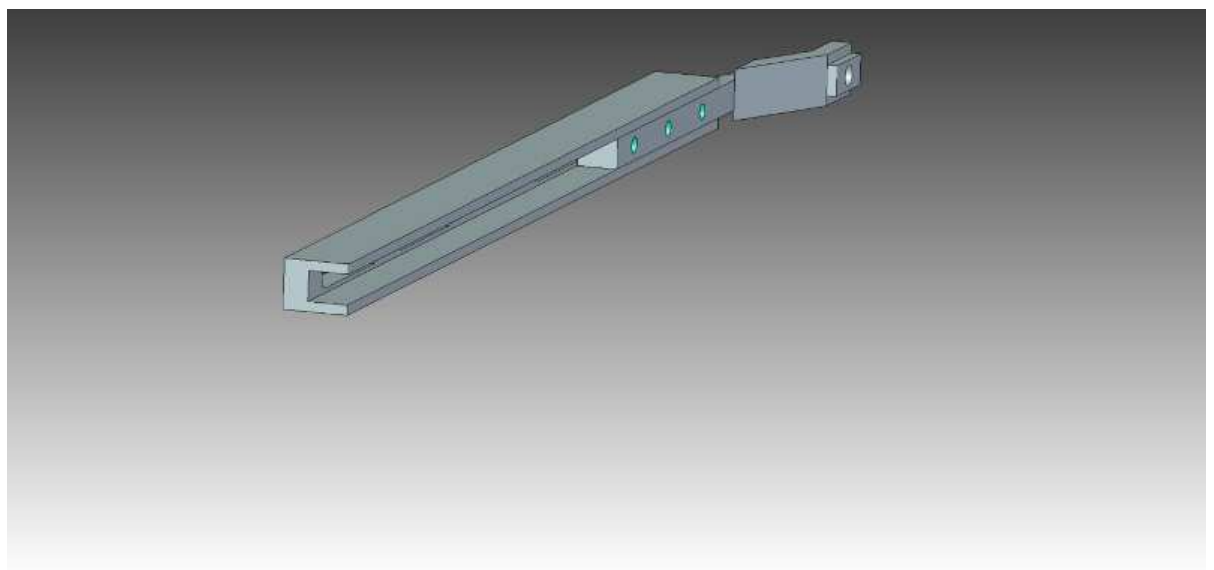


Figure G.5: The corner bracket and the rail: how they fit together.

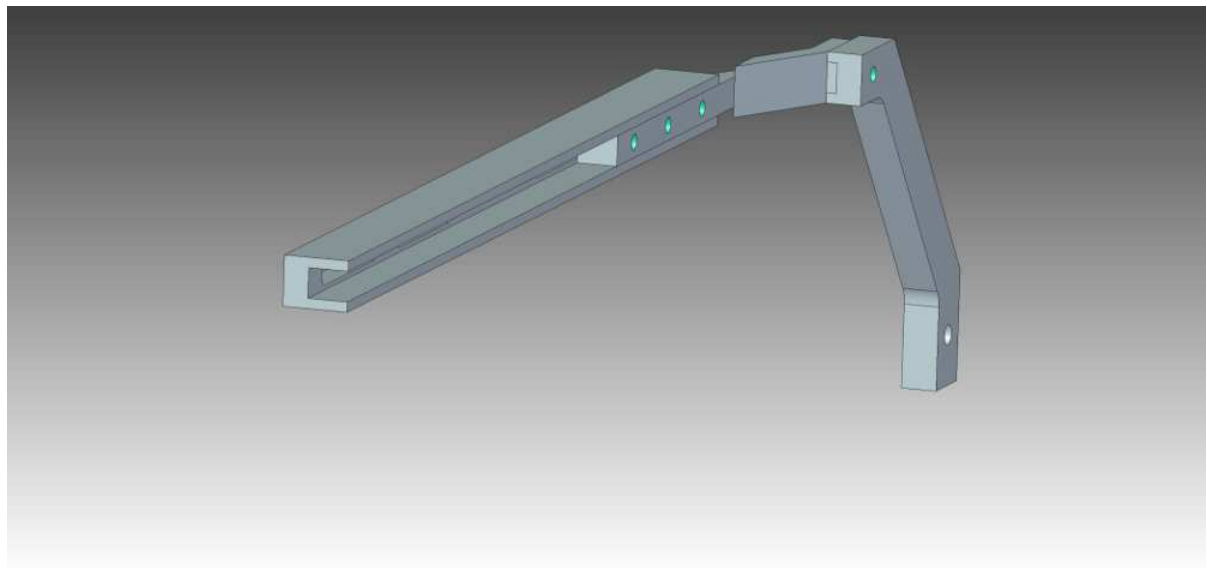


Figure G.6: The corner bracket and rail with the uh... next bracket.

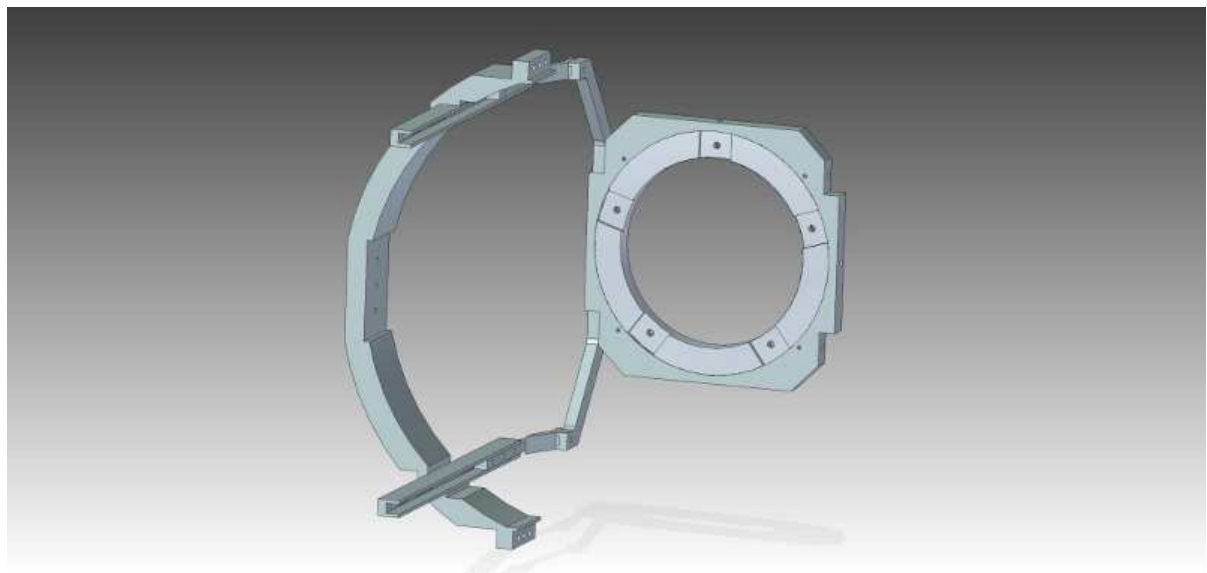


Figure G.7: The rib with the two rails and the mounting plate for the MMM detectors. Note that the circular inset is separate from the metal bracket that comes around and must be secured with two locking nuts before the detectors are mounted.

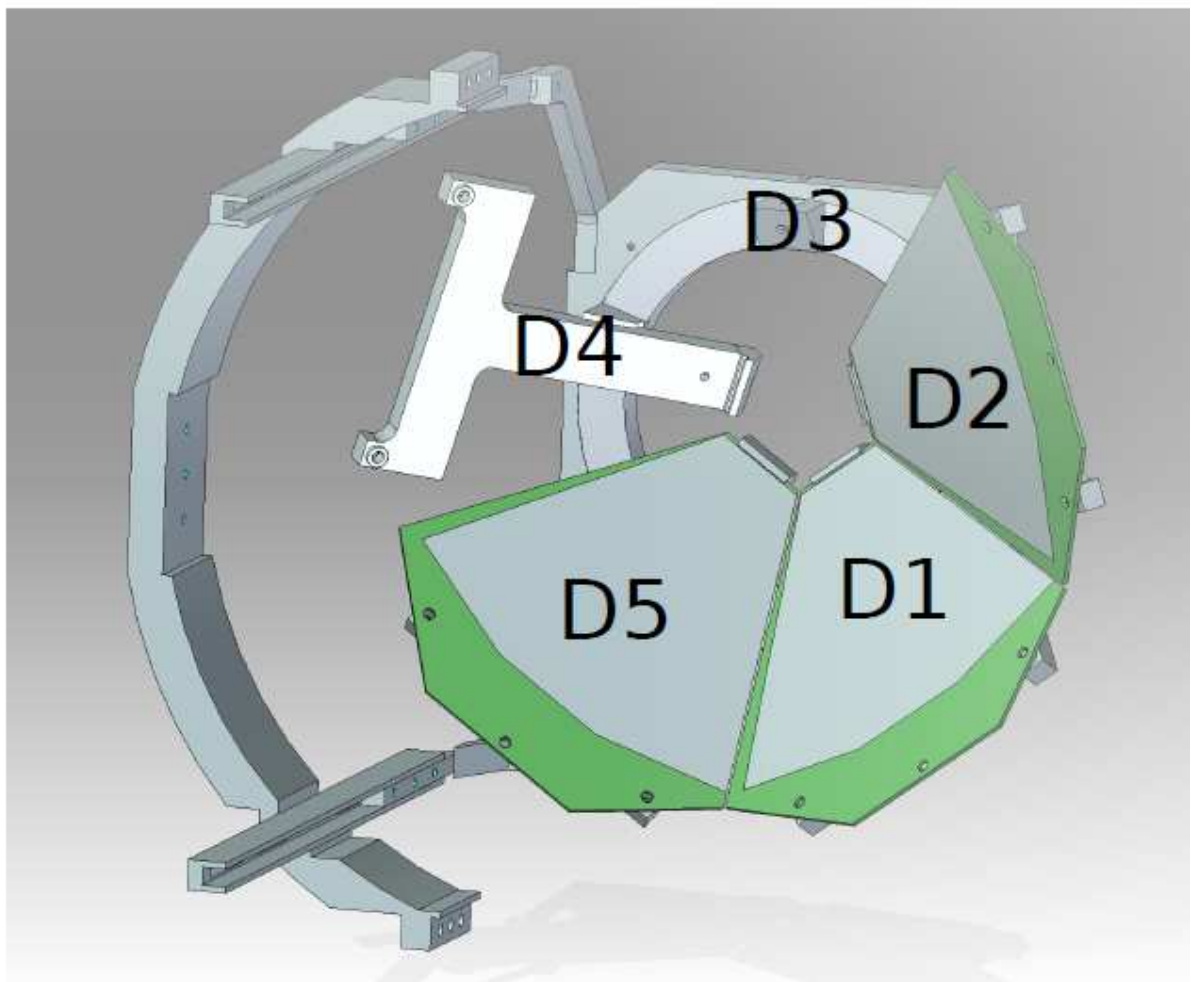


Figure G.8: How the MMM detectors go onto the frame. One detector position has no frame but has the small metal connecting piece shown while another detector position has the MMM frame shown without the associated detector. The detector numbers have been added to this figure.



Figure G.9: MMM detector cable. The upper cable with more wires at the grey connector is the junction (p-side) cable. It carries 16 signals. The lower cable is the ohmic (n-side) cable. It carries 8 signals.

- The detectors are mounted on the ring which sits inside the square bracket. This must be secured into place with two locking nuts before the detectors can be mounted.
- To do this, put one of the large plastic screws into the back of the detector stand. Then, bring the detector to the metal ring and slowly tilt it into place, keeping an eye out for other detectors which may get in the way. They should fit smoothly together without any touching.
- This process is repeated for each detector. When doing this, start at the top and work down. This means that if you drop a detector, you dont break any detector below it when it falls.
- Finally, cables and connectors. There are long 50-way connectors with two cables coming off, one with 8 channels (sectors - ohmic) and one with 16 (rings - junction) - see Figure G.9. The cables have a key and can only go onto the detector in one way. When doing this, try to push the cable connector from the other side for bracing to avoid physical stress on the detector.

I number the CAKE detectors from 1 to 5. 1 is the lower detector on the beam-left side, 2 is the upper detector on beam-left, 3 is the top detector, 4 is the upper beam-right detector and 5 is the lower beam-right detector. I.e. the numbering starts from vertically downwards and then goes around clockwise. I sketch showing this can be found in Figure G.8.

G.2 Putting CAKE in the chamber

- Before you do this: make sure that the spare rib is in place on the beam-left side of the scattering chamber. This is required to guide and secure the cable for detector 3.
- Putting CAKE in is fairly easy. It requires two people (though it's useful to have three to have more spotters) and the right bolts. You should have at least a couple of these bolts holding CAKE onto the storage point in the parking garage. You will need three (3, III) of these bolts.
- Take off the sides of the scattering chamber.
- Pull the storage frame slowly out of the parking garage. If the cables are already attached, ensure that they dont dangle around and scratch something.
- Secure the cables to the rails or the rib using cable/tomato tape - this is the velcro tape which can easily be disconnected. You can use a cable-tie if you cant find the tomato tape.
- Once you are happy that everything is secure: one person should hold the rib of CAKE (and somewhere else for stability) while the other person disconnects CAKE from the temporary stand. Make sure you disconnect the screws at the very bottom and not the screws holding the rail.
- You should now be holding CAKE. Your glamorous assistant should check that the cables are not able to slip out and then you should take CAKE slowly to the scattering chamber. Your assistant needs to make sure that the cables of CAKE do not snag while you position CAKE in the chamber. Generally, try to go in slightly too far downstream and then move back upstream to avoid banging the tips of the detectors on the upstream side of the chamber. This process is made much safer by having a spotter on the other side who is able to make sure that you are not about to hit something with CAKE.
- Once CAKE is in the chamber, you should attach the cables. As a general rule, I prefer to put all of the junctions into one rank of connectors and all of the ohmics into the other. I.e., you have two ranks of five connectors on top and bottom. I use the upstream rank for junction and downstream rank for ohmic. This reduces the chances of accidentally forward-biasing the detector.
- Make sure that all of the cables are clear of the target ladder. This will require you to be a bit careful with the cables for detector 3 (the one at the top). The cables need to go backwards and around ribs on either side and then secured with cable ties. See Figures G.10 and G.11.
- Once this is done, you can put the side of the chamber on. Do this slowly - the o-rings like to fall out. Its helpful to have one person put the side on slowly while the other carefully looks from the side to see that nothing is wrong. I suggest that you put the beam-left side on first because the cable for detector 3 on that side is usually the most problematic.
- Once this has been done, you can test the diode responses of the detectors. Note that the ohmic side only has 8 channels so you might have to look a bit to find one. The 19-pin LEMOs are: one central pin (ground), intermediate ring of 6 channels (these are usually

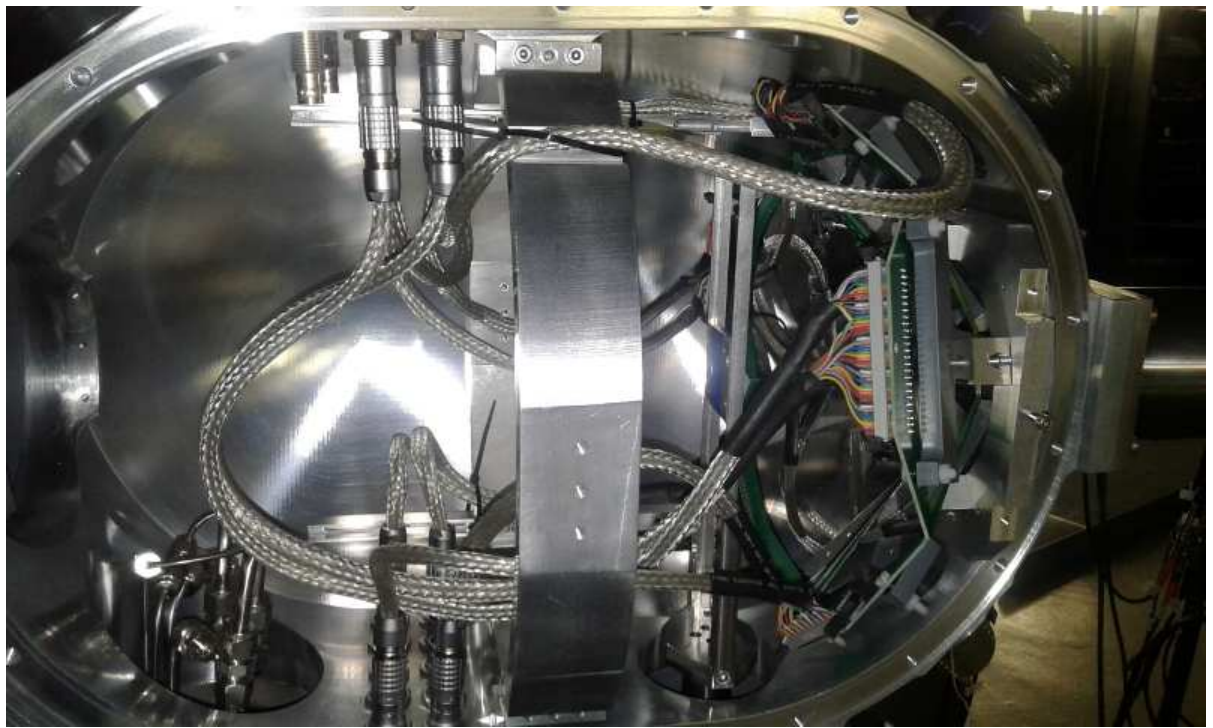


Figure G.10: CAKE cabling inside the chamber. Note the folding back of the cable from detector 3. Make sure that this doesn't flop onto the detector below when you're connecting it or when you are putting the side on the chamber.

all signal channels - some of the channels, especially on the 19-pin LEMOs are blanks as there's no physical strip for them to be connected to) and an outer ring of the rest.

- Junction side: central pin is ground - two empty pins on the outside. See Figure G.12.
- Ohmic side: central pin is ground, intermediate ring is signals and two signals on the outside. See Figure G.13.
- Diode response: multimeter on diode setting. Red lead to junction connector, black lead to ohmic connector. You should see something like 400 mV as the reading. If you do not, make sure you have a signal channel on both sides. If that wasn't the problem, then try swapping the leads. If you now see something, you have probably swapped the junction and ohmic signals, or your labels as to which is junction and which is ohmic are wrong.

G.3 Electronic Gubbins

Now comes the frustrating part: the electronics. You will need:

- Preamplifiers. (MPR-16/32)
- Amplifiers. (MSCF-16)
- High-Voltage (Bias) supplies. (MHV-4)



Figure G.11: A closer-up picture of how the cable for detector 3 is secured on the beam-left side. It's bent back around upstream from the detector and is then secured to the rib before going to the LEMO feedthrough. You have to ensure that that cable isn't going to flop onto detectors 2 or 3 when you're connecting it up or when the side of the chamber is put on.

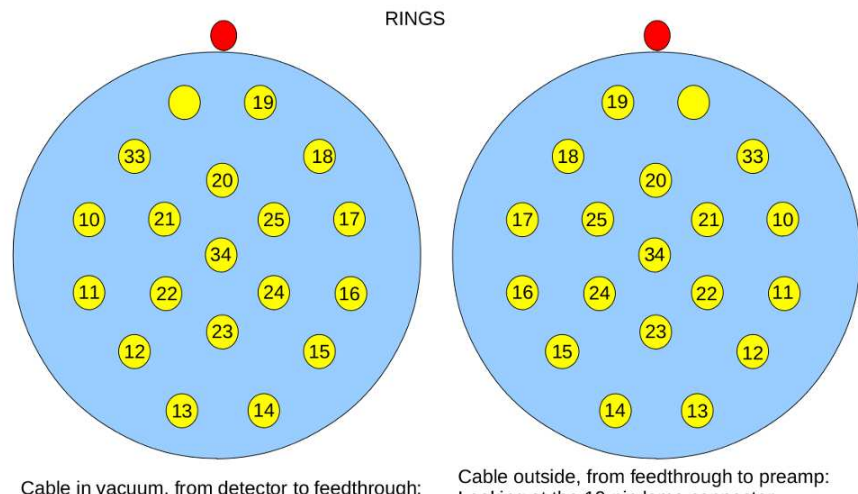


Figure G.12: CAKE Junction LEMO

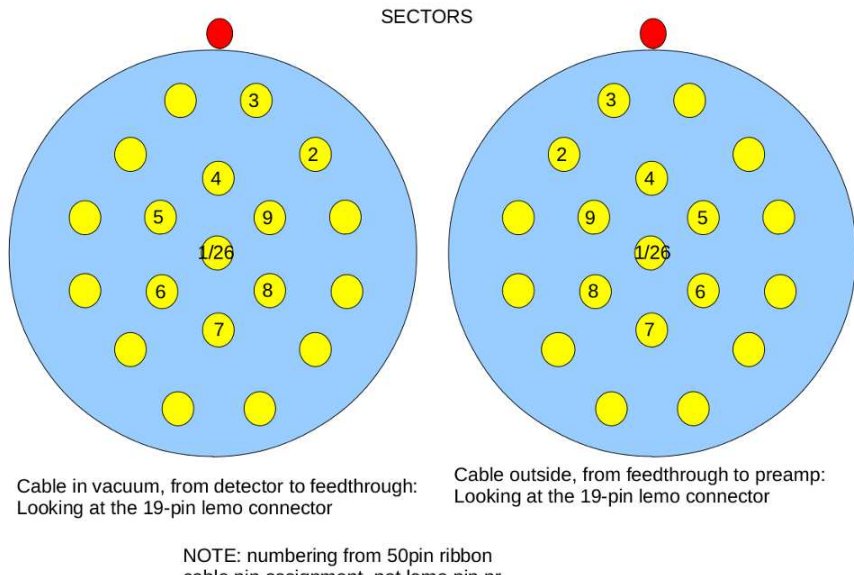


Figure G.13: CAKE Ohmic LEMO

- As the preamp power comes from the amplifiers, it's usually easier to have setup the amps up first. The amplifiers have a jumper in which allows selection of negative or positive input signals. As the signals from the front and back of the silicon detectors have differing directions, this is rather important. Instructions for how to do this are included in the MSCF-16 manual.
- CFD settings may also be changed with the MSCF-16 modules - consult the manual for how to do this. Michael Munch and Alan Howard of Aarhus advised 60 ns and 40% threshold as the optimal settings for the MSCF-16s. PA (foolishly) failed to check that the new MSCF-16s had this setting when they were used in 2016 for PR254, PR259, PR238 (second round) and PR264. Some of the modules were on this setting and some were not.
- The preamps are (usually) Mesytec either 16 or 32 channel. To use them, first decide which side should be connected to the junction side of the detector and which to ground. Then, put the cables from the detector through the flange into the right place on the preamp.
- Having done this, take the LEMO cable that you want to use for biasing the detector and put it into the correct place on the preamp. This is on the output side and is marked HV < 400 V. Note that the bias is limited to 400 V. The HV input on the other preamp for the detector (where the ohmic side is connected) must be terminated. Otherwise the leakage current has no place to go.
- Now, attach the preamp power. There are long off-white cables which go from the back of the amplifiers to the preamps and provide preamp power. Many of these cables are already marked as preamp power cables.

- Now you have everything you need to put bias on the detectors. The power for the preamps must be on before you put bias on the detector as putting power onto the preamp while bias is applied may cause the preamp to blow.
- To put bias on, put the LEMO into one of the connectors on the back of the MHW-4 (you will need a BNC-LEMO adaptor to do this). If possible, look at the signals coming from the preamp on a scope to ensure that nothing is going wrong.
- Now, check that the bias polarity is correct and that the bias is set to 0 V. The polarity is obvious from the front of the module: there are two LEDs which tell you which direction. As we are putting bias on the junction side, the bias must be negative (yellow LED with a - sign). If the bias setting is positive, the next LED (next to a +) is lit and it is green.
- I just want to make this point explicitly: **NEGATIVE POLARITY ON THE JUNCTION P-SIDE, POSITIVE POLARITY ON THE OHMIC N-SIDE**. Do not feck this up. You will fry the detector. **CHECK BEFORE YOU PUT BIAS ON**. AFRODITE sometimes bias the n-sides of detectors and thus change the settings on the MHW-4s.
- I have been biasing CAKE using NEGATIVE polarity on the JUNCTION i.e. P-SIDE.
- To change the polarity, consult the MHW-4 guide-book.
- Having put the required bias on the detector (taking regular leakage currents at different voltages and plotting the curve as you go along), you now should know what bias the detector should use.
- The next job is to put signals into the amplifiers. This is done using the ribbon cables for the p-sides. These go from the preamps to the input on the amplifiers. Make sure that the grounds are correct on both side - in most cases you will have already done so because the cables have teeth and so can only go in one way.
- For the n-sides: there are not enough amplifiers to make a good separation between different species. Each n-side has 8 channels - I usually combine these after the preamps and put them into one amplifier. This can be done using the breakout boards which can be attached to the front of the NIM racks. However, these require the ribbon cables with the swapped-over pair of channels to ensure that the ground is in the right place. We (PA+JWB) noticed during the setup of PR254 that these cables frequently caused the preamps to lock up. We therefore decided to borrow some of the breakout cables from AFRODITE. These are cables with ribbon cable connectors and then 16 BNC outputs. If you use three of these per detector, you can take the 8 relevant channels from the two plugged into the preamps and slot them into the 16 channels for the connector on the amplifier. I was terminating the outputs which were connected to nothing on the basis that it's probably for the best.
- However, I (PA) cannot give you too much guidance on this. You probably have to find your own solution based on what's available at the time you are setting things up.
- Note that a problem with the AFRODITE breakout cables has been noticed: sometimes when power is put onto the preamps, the preamps can 'lock up'. This is made evident in the green LED on the preamp going dim. To fix this unbias the detector, and then

try unplugging the breakout signal cable from the preamp and then replace it. If this doesn't work, disconnect the input cables to the preamp (easiest to do this at the vacuum chamber feedthrough) and then try again with the breakout cable. Then, after having put the breakout cable back in, put the preamp input cables back into the feedthrough.

- Having got the signals into the amplifiers, you need to put the outputs into the DAQ. The shaper outputs go to the ADCs and the ECL outputs to the TDCs. Again, check that the grounding direction is correct but the teeth on the cables should guide you. It is a good idea to try to make sure that each ADC module contains signals from the front of one detector and the back of another. This means that there is an online check as to whether there is a correlation between events in different ADC modules.
- Having done all of this, it is now time to put data into the DAQ. First of all, construct a trigger from the trigger outputs on the MSCF-16s. If you are feeling cunning, you can make a front-back coincidence trigger for the silicon detectors. I don't usually bother with CAKE as the combination of 2x8 into 1x16 channels makes things difficult. To make the trigger, get a logic FIFO and put all of the trigger inputs into it and take the output to the DAQ spoof trigger (which is in the TFA under the focal plane next to the pulser). This should then provide spurious paddle signals which should cause the DAQ to trigger. With the ^{228}Th source at the target position, this should give a trigger rate of 30-50 Hz assuming that the thresholds on the modules are clear of the noise.
- To set thresholds and pole-zeros, consult the MSCF-16 manual. There is an auto-PZ on the MSCF-16s. I suggest using it when you've got a source in the chamber.
- Finally, you need to set the amplifier gains. Depending on what you want to look at, these will be different. I would however note that the silicons are 400-um thick which limits you to 7-MeV protons before they punch through. Therefore, if you are looking at proton decays, then set the modules so that the top peak from the ^{228}Th target (which is the ^{212}Po to ^{208}Pb decay with $E_a = 8.954$ MeV) sits at the top of the ADC range (something like 3800 is a good position).

G.3.1 Using CAKE in experiments

I'm not going to discuss how the offline analyser for CAKE is set up here as it's been done elsewhere. I'm going to discuss how CAKE is used in experiments.

Firstly, you need to set up the K600 (see earlier in this manual). Once you are happy, you should put CAKE into the target chamber as described above. You need to make sure that the target ladder is in a low position (1 or 2 usually works) so that you have some space to get CAKE past the ladder. Once CAKE is installed, you can put the ladder back into the chamber. Do this slowly! If you lose your grip of the ladder and it falls upstream, you could destroy a detector or five.

Once you have the target ladder in place and before you pump down you should check the ladder movement. The two potential problems are is the space between detectors 1 and 5 isn't lined up with the target ladder base, and if the cable from detector 3 is in the way. The easiest way to do this is to get someone to move the ladder up position-by-position and check that it looks OK. Note that there is an emergency stop button on the ladder control which should be used if there's a problem. You can get some idea of how the ladder related to the detector 3 cable from Figures G.11 and G.14.

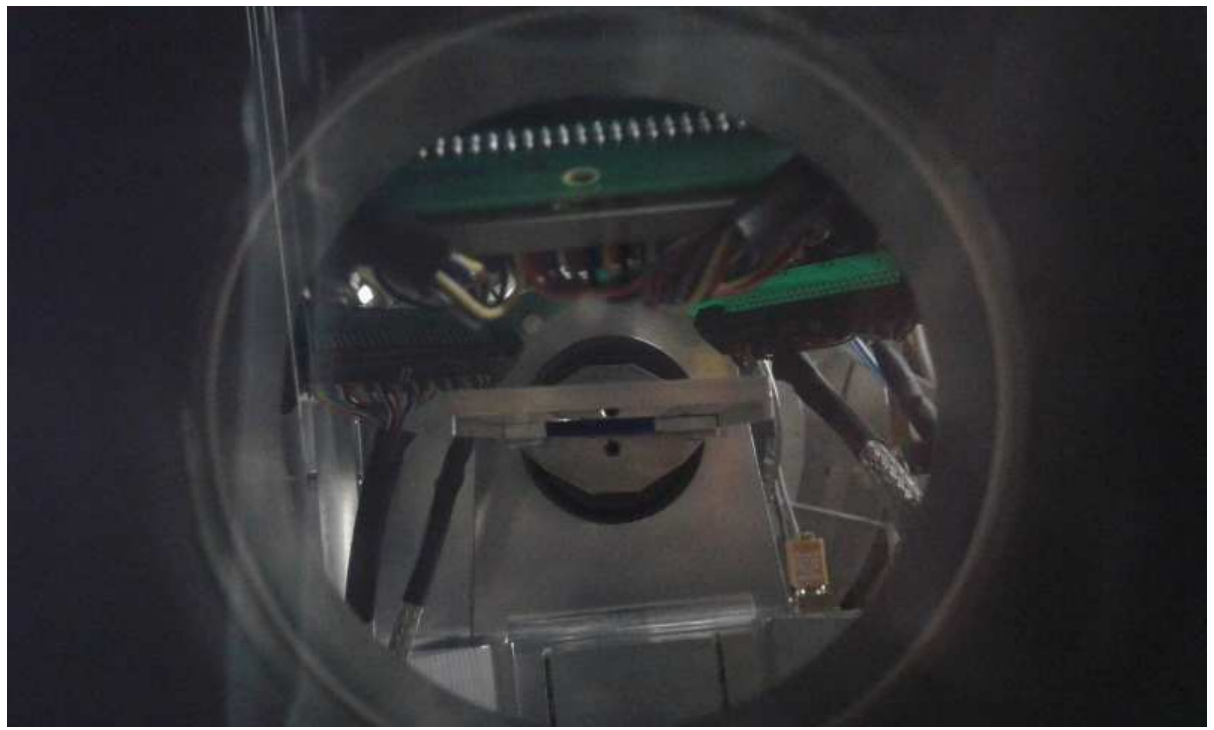


Figure G.14: A top-down photo of how the K600 target ladder and the cable for detector 3 should look like, looking through the port on the top of the new K600 scattering chamber.

Once this is checked, close up and pump down (slowly). Once you are on the turbo pump and it's up to speed, you can put bias on the detectors and open the valves upstream and downstream.

Now the next job is to check that the beam is still well-tuned. Put the empty frame in and check for the focal plane halo rate as usual. When you do this, you should also look at the leakage currents on the silicon bias supplies and at the rates in the silicon detectors. With an empty frame in you should not see either of these values increase at all. However, you may see some increase if there's halo especially if it's hitting the target frame.

List of Tables

1.1	Technical specifications for the medium dispersion mode of K600 Magnetic Spectrometer. Note that the maximum diameter collimator refers to the maximum diameter that was tested. According to the Schwandt lectures [Sch86] the maximum acceptance is $\pm 44\text{mr}$	9
1.2	Design parameters of the three dispersion modes of the K600 spectrometer from [Sch86]. Note that some of these values are different from those in table 1.1. (From Ricky's notes these values originate from 1983 IUCF proposal for fp detectors and electronics) These matrix elements can also be calculated with the MATRIX command of TRACK.	10
1.3	TRACK calculated ion-optical properties near the central momentum of the medium and high-dispersion focal-planes of the $K = 600$ magnetic spectrometer in vertical focus mode. Note the High dispersion focal plane is used in a new mode where the ratio of magnets are different from the designed 1.33.	11
1.4	Technical specifications for the original focal plane detectors.	14
1.5	Technical specifications for the new focal plane detectors.	17
1.6	FWHM associated with distributions used to determine the VDC intrinsic cell accuracy.	19
1.7	<i>Position resolution in the first X-wireplane of 200 MeV protons and alphas as per simulation.</i>	20
1.8	Relative differential cross section measured using the variable-slot collimator.	26
2.1	Mapping of wire number to TDC channel for a old X followed by a new XU detector setup.	32
2.2	<i>Comparison between the values of the peaks (taken from NNDC) and the obtain ones from the rough calibration.</i>	72
2.3	<i>Identified peaks (left) and their corresponding rigidity (right) [?].</i>	73
2.4	<i>Identified peaks (left) and their corresponding rigidity (right).</i>	74
2.5	<i>Values of the ^{26}Al excitation energies from the literature (left) compared with those values obtained from the calibration (right) [?].</i>	76
3.1	Information about the NMR probes and teslameter.	87
4.1	A summary of available collimators. They are all made from brass. (ID=Inner Diameter)	90
4.2	A summary of available standard inserts with OD (OD=Outer Diameter) of 78mm. Except where otherwise noted, all these inserts are made of brass. Note that there are also a few non standard inserts available, e.g. with ID=41mm, OD=74mm and 7mm thickness (ID=Inner Diameter).	91

4.3	Acceptance with different circular collimator openings.	91
4.4	Energy loss values	91
6.1	Straggling calculations from LISE++V7.5.10. Is it not wrong that the straggling is more than the Eloss?!	112
7.1	Specification of good VDC gas	121
9.1	Kinematic factors for proton elastic scattering as calculated with equation 9.11. .	135
9.2	Historical good resolution conditions. For the Oct 2002 results refer to the subsection 9.7.1	136
9.3	Historical good resolution conditions. For the Oct 2002 results refer to the subsection 9.7.1	138
10.1	Sept 2007: zerodegree settings to get the beam through the K600. Fieldstrengths indicated represent the current, not the magnetic field value.	168
10.2	Comparing SPEXCIT settings and experimentally determined settings. Values indicated represent currents (amp). It is important to realize that the ratio between the magnets that is specified in SPEXCIT applies to the REAL MAGNETIC FIELD, and not to the currents. There is a subtle, but real, difference between the two.	169
10.3	The third row indicates the ratio that should be used in the TRACK calculation to be able to follow the particle track through the K600, since the fieldmaps we have are valid at the 200 MeV (p, p') settings in the medium dispersion focal plane.	169
B.1	Preamp card, signal wire, TDC unit and TDC channel numbering of VDC1. VDC1 has 198 wires, connected to TDC channels 8-205. Channels 208-223 represent the second half of TDC unit nr.7, which is unused.	178
B.2	Preamp card, signal wire, TDC unit and TDC channel numbering of VDC2. VDC2 has 198 wires, connected to TDC channels 232-429. Channels 432-447 represent the second half of TDC unit nr.14, which is unused.	179
B.3	Preamp card, signal wire, TDC unit and TDC channel numbering of the HDC. The HDC has 16 wires, connected to TDC channels 448-463. Channels 464-479 represent the second half of TDC unit nr.15, which is unused.	179

List of Figures

1.1	The K600 magnetic spectrometer in 2016.	5
1.2	A schematic overview of the K600 magnetic spectrometer.	7
1.3	A schematic overview of the magnetic elements in K600 magnetic spectrometer (from a 1986 talk by P.Schwandt [Sch86]).	7
1.4	Dipole face windings: showing how the K coil has a quadrupole component (and the H-coil a sextupole component) as well as dipole components. (from a 1986 talk by P.Schwandt [Sch86]).	8
1.5	The main components of the original VDC.	12
1.6	A design drawing of the new VDC.	12
1.7	An old paddle with the black paper stripped off	13
1.8	Garfield calculated VDC fieldlines.	15
1.9	The new trigger scintillators/paddles	16
1.10	Schematic representation of a charged particle's trajectory intersecting the VDC resulting in a six-wire event.	18
1.11	Gaussian fit to a distribution of differences in trajectory slope.	19
1.12	Simulation of 200 MeV protons incident on the first X-wireplane, illustrating the effect that different materials has on the position resolution. See text for details. .	21
1.13	Simulation of 200 MeV alphas incident on the first X-wireplane, illustrating the effect that different materials has on the position resolution. See text for details. .	22
1.14	Simulation of 200 MeV alphas incident on the first X-wireplane, illustrating the effect of the detector position has on position resolution. See text for details. .	22
1.15	The high dispersion focal plane opening of the K600 vacuum chamber. The arrow on the right indicates the effective size of the vertical opening, which is 7cm and is also the case for the medium and low dispersion planes.	24
1.16	Schematic two-dimensional representation of the trajectory associated with a particle moving from the target to the K600 spectrometer focal plane (reproduced from Ref. [Sch86]).	25
1.17	Drawing of the 51.0 mm thick variable-slot/multi-slot collimator used to study spectrometer transmission. All dimensions are in mm.	25
2.1	A typical layout of the K600 trigger electronics.	27
2.2	Extract from logbook of PR128, where the channel numbering of the preamplifier cards are indicated in.	29
2.3	Mapping of wire number to TDC channel for 2 new VDC's in an XUXU wireplane configuration.	31

2.4	Top left: two dimensional resolution plot as optimized for ${}^3\text{He}$, compared to the two dimensional resolution plot for all events, shown in the top right. From the paddle1-versus-tof PID plot in the bottom right it is clear that the ${}^3\text{He}$ particles are not as abundant as the protons, which is represented by the strongest locus. Clearly an optimized LUT offset for one type of particle is not optimized for another type of particle. This is from experiment PR153, $E_{beam} = 80 \text{ MeV}$ and $\theta_{K600} = 30^\circ$	41
2.5	Left column: X2 Res2D for LUT offset (from top to bottom): 60,40,20,0,-20. Middle column: X1 Res2D for LUT offset (from top to bottom): 40,20,0,-20,-40. Right column: U2 Res2D for LUT offset (from top to bottom): 60,40,20,0,-20.	42
2.6	Driftlength and resolution plots for a good LUT.	44
2.7	Driftlength and resolution plots for a good LUT but in need of a negative LUT offset correction.	45
2.8	Driftlength and resolution plots for a good LUT but in need of a positive LUT offset correction.	46
2.9	PID plots, showing the position of the gated regions (black solid line)	57
2.10	Focal plane position spectrum for the X1 wireplane for run 1104 of PR236, with (black line) and without (red line) PID cuts.	58
2.11	Plot of thetaSCAT <i>versus</i> the focal plane position spectrum for run 1104 of PR236. Some modifications to the conversion parameters are still required to ensure that the band of events form a rectangle in the $\pm 2^\circ$ angle range.	59
2.12	Relative time-of-flight to the CAKE vs silicon energy loci for (a) the case where no correction is made for shifts in the trigger time relative to the RF pulse and (b) with the correction in the shift of the trigger time included. The upper locus, terminating at around 7000 keV represents the observed protons and the lower locus is represents α particles.	65
2.13	Simplified diagram to show the relative timing information for the RF reference from the cyclotron, the K600 trigger time and the time of the event recorded in the silicon detectors. Note that the K600 trigger time is drawn with a jitter (dotted lines) to account for the different flightpaths through the spectrometer. The spectrometer time-of-flight as previously defined is labelled ' T_{K600} '. The silicon time, as recorded by the data acquisition, is ' T_{si} '. The true silicon time-of-flight is labelled 'True T_{si} '.	66
2.14	<i>Paddle-one versus time-of-flight for the ${}^{26}\text{Mg}({}^3\text{He},t){}^{26}\text{Al}$ reaction, black-line box represents the gate used for the selection of the particles of interest (tritons).</i>	67
2.15	<i>Paddle-one versus time-of-flight for the ${}^9\text{Be}({}^3\text{He},t){}^9\text{B}$ reaction, black-line box represents the gate used for the selection of the particles of interest (tritons).</i>	68
2.16	<i>Focal plane position (X1pos) without any cut.</i>	68
2.17	<i>TOF v.s. focal lane position (X1pos).</i>	69
2.18	<i>Zoom-in of Fig. 2.17, TOF v.s. Focal Plane position (X1pos).</i>	69
2.19	<i>Plot and fitting of the set of points selected in Fig. 2.17.</i>	69
2.20	<i>Corrected TOF v.s. Focal Plane position X1pos.</i>	70
2.21	<i>Zoom of corrected TOF v.s. Focal Plane position.</i>	71
2.22	<i>Comparison between the focal plane position (X1pos) with the corrected one using the TOF.</i>	71
2.23	<i>Excitation energies of the populated states in ${}^{26}\text{Al}$ obtained by a rough calibration.</i>	71
2.24	<i>Rigidity values v.s. excitation energy of the identified peaks[?].</i>	73

2.25	<i>Rigidity values for the tritons.</i>	74
2.26	<i>Momentum of the tritons.</i>	74
2.27	<i>Tritons kinetic energy calculated through the rigidity.</i>	74
2.28	<i>Excitation energy spectrum of ^{26}Al corrected using the magnetic rigidity of the tritons detected at the Focal Plane.</i>	76
2.29	<i>Excitation energy spectrum of ^9B corrected using the magnetic rigidity of the tritons detected at the Focal Plane for ^{26}Al.</i>	77
2.30	<i>Time-gate applied to the plot in Fig. 2.29 in order to reduce bad coincidences.</i>	77
2.31	<i>Low excitation energy region in ^9B (all runs).</i>	77
2.32	<i>Coincidences between excitation energy v.s. those events detected in the silicon detector array. Solid-line box shows the proton decay locus, which has been selected as a "cut" for further analysis (<i>draw the box!!</i>).</i>	78
2.33	<i>Comparison of the total excitation energy spectrum in ^9B (blue-colour-line) with that selected region (proton-decay channel) selected in Fig. 2.32 (red-color-line).</i>	78
2.34	<i>Excitation energy spectrum with the subtraction of the proton-decay locus of Fig. 2.33.</i>	79
3.1	The relation between the current setting and the magnetic field of the 2 K600 dipoles for the medium dispersion magnet setting scenario of D1/D2=1.	81
3.2	The hysteresis loop [web10].	82
3.3	The size of the overshoot current was decided by making various measurements of the dipole field after different time constants for different overshoot currents. The final selected overshoot current was selected to be at the waist of the different curves in B versus I [Gar10].	83
3.4	The fieldset procedure for D1, indicating the rate of change for the currents, the duration of the waiting points and the equation to determine the overshoot current [Gar10].	84
3.5	The fieldset procedure for D2, indicating the rate of change for the currents, the duration of the waiting points and the equation to determine the overshoot current [Gar10].	85
3.6	(OLD DAQ) From left to right: K-coil 0V, H-coil -30V → K-coil 30V, H-coil -30V → K-coil 15V, H-coil -30V → K-coil 15V, H-coil -40V. Top figure: x_{fp} vs θ_{fp} . Bottom figure: x_{fp} vs TOF.	88
4.1	Clockwise from top left: 11mm thick 55mm diameter (tapered), 7mm thick slot 6x55mm, 11mm thick 55mm diameter (tapered), 7mm thick 63mm diameter.	92
4.2	Clockwise from top left: 11mm thick slot 14x36mm, 7mm thick 41mm diameter, 7mm thick slot 14x55mm, 7mm thick slot 10x70mm with 1mm wide slits in 2mm thick Ta??.	92
4.3	The slight tapering of the $\phi=49\text{mm}$ 11mm thick insert can be seen in this picture.	93
4.4	A 63mm diameter 39mm thick collimator (type A1): the insert has a diameter of 49mm and is 11mm thick.	93
4.5	A 63mm diameter 39mm thick collimator (type A1 or A2): the insert is not in position in this picture.	94
4.6	A 63mm diameter 51mm thick collimator (type B1): the insert has a diameter of 55mm and is 7mm thick.	94
4.7	A 49mm diameter 51mm thick collimator with no inserts possible (type C).	95

4.8	A small 25mm diameter 51mm thick thick collimator (type C): the insert has a diameter of 14mm and is either 7 or 11 mm thick.	95
4.9	A 63mm diameter 51mm thick collimator: the insert is a slot of 55×14 mm and is 7 mm thick.	96
4.10	The multihole collimator	96
4.11	The blank collimator	97
4.12	A picture of the blank collimator in the carousel: it should not be removed from its present position (in-beam is position nr 5) as it forms part of the interlock system for ZeroDegrees	97
4.13	98
4.14	A schematic of the pepper-pot collimator. It was modified in April 2005 to be only 15 mm thick for the central region of 63.5 mm diameter (the back of the collimator is therefore 735.5-(51-15) mm from the target, if the pepperpot side is towards the beam; otherwise it is the standard 735.5 mm). Also, an insert was made end 2006 to put in one of the holes to make it smaller, thereby giving a reference point to correlate the picture in the focal plane with the real scattering angles. If the pepperpot is placed such that the holes are on the K600 side, the first hole from the middle on the x-axis/y-axis is at 0.78° (13.6mrad), the second is at 1.60° (27.9mrad), and the third is at 2.14° (37.4mrad). The holes span approximately 0.39° (6.80 mrad), except for the smaller hole which spans approx 0.19° (3.40 mrad).	98
4.15	The 51mm thick multislot is only 7mm thick for the inner d=63mm. See Fig. 1.17 for dimensions.	98
4.16	The active collimator has a slotted opening ??mm \times ??mm.	99
5.1	The internal beamstop for angles $5^\circ < \theta_{K600} < 21^\circ$ as viewed from the target ladder for the original small sliding seal opening. Note that there are two permanent magnets in the top and bottom of the beamstop.	101
5.2	The internal beamstop for angles $5^\circ < \theta_{K600} < 21^\circ$ as viewed from the target ladder for the new 64mm \times 64mm sliding seal opening.	101
5.3	An overview of the small angle internal beamstop for $2^\circ < \theta_{K600} < 5^\circ$	102
5.4	The small angle internal beamstop as seen by the beam.	102
5.5	The 0° beamline and beamstop (2005 version). On the right hand side a section of the high dispersion exit window can be seen. While this picture is good to illustrate the 0° beamstop, note that the beampipe configuration was since changed to have the bellows on the beamedump side, and not just after vacuum valve. Refer to Fig. 10.17.	103
5.6	The (p, t) beamstop used in PR137. Note that it consists of three separate brass blocks, each with its own cable to go to the current integrator box inside the K600 vault.	103
5.7	The dimensions of the (p, t) beamstop used in PR137.	104
5.8	The (p, t) beamstop used in PR170. Note that it consists of two separate brass blocks, each with dimensions 70 mm (deep) \times 55.5 mm (wide) \times 55 mm (high). These dimensions includes the lip, which is 5 mm wide and 10 mm deep.	104

5.9	The distribution box on the K600 is indicated in the top left. The bottom right illustrate the electronics in the movement control electronics tower as well as the remote control unit, while the top right show 'dummy break' without which the system will not function.	106
5.10	An old scattering chamber, from an undated picture. One assumption is that this picture dates from the middle 1990's.	107
5.11	An old scattering chamber, from the (p,2p) research of Cowley and Neveling. Circa 1999.	108
5.12	The sliding seal scattering chamber (originally from NIKHEF) with the small angle mode from 2015.	108
5.13	The new scattering chamber, designed by Paul Papka, during its commissioning run in 2014.	109
5.14	The original design for the exit sliding seal.	110
5.15	The so-called 'Nolan chamber' and the $64 \times 64 \text{ mm}^2$ opening in the sliding seal .	110
5.16	The $64 \times 64 \text{ mm}^2$ opening in the sliding seal connected to a new connection between the scattering chamber and the K600. The waist just before the vacuum valve was opened up.	111
5.17	An overview of the new begger entrance to the scattering chamber, with a $64 \times 64 \text{ mm}^2$ opening in the sliding seal.	111
6.1	An empty target ladder.	112
6.2	A semi-filled 0° target ladder, with the material on the low momentum side cut off. Notice that one of the target frames are modified to also have less material on the low momentum side. is	113
6.3	Two target ladders filled with varios targets.	113
6.4	Notes on the target ladder height and angle.	114
6.5	The BLM	115
6.6	The so-called Hatanaka mesh/viewer. It was designed so that viewed from 45° (as it is used in the beamline) the small blocks are 1mm by 1mm. Each bigger block represents 5mm in x and y. The mesh is approximately 3.1m from the target.	116
6.7	The so-called Hatanaka mesh/viewer. It was designed so that viewed from 45° (as it is used in the beamline) the small blocks are 1mm by 1mm. Each bigger block represents 5mm in x and y. The small blocks are 1mm by 1mm. Each bigger block represents 5mm. Note that due to a water leak in the beamline the mesh was replaced and this mesh is smaller, though subdivisions are still same size.	116
6.8	A picture of the focal plane blocker. The extra 10mm of brass that was added in 2004(2005?) can clearly be seen	117
6.9	The focal plane blocker: then (50mm) and now (60mm).	117
6.10	The slits at 9X looks like this.	118
7.1	The gas handling station	121
7.2	The oxygen and water filters.	122
9.1	A typical target beamspot for an achromatic beam, as seen in the October 2004 development run. The lines on the ZnS screen are at 5mm from the target center.	133

9.2	The target beamspot for an achromatic beam, as seen in the July 2009 (p,t) run PR137. The lines on the ZnS screen are at 5mm from the target center. This beamspot is not small enough, and definitely bigger than in Fig. 9.1.	133
9.3	A typical target beamspot for a dispersion matched beam, as seen in the October 2004 development run.	134
9.4	The S-line quadropole (still showing its original label Q16J, but since then relabeled Q0S) in front of the 2 triplets, to be used for angular dispersion matching.	134
9.5	October 2002, 66 MeV beam. Normal resolution conditions, before attempting dispersion matching with the new faintbeam method.	139
9.6	October 2002, 66 MeV beam. Resolution after doing dispersion matching with the faintbeam method. Refer to the Protokolbuch 934 ~p175,	140
9.7	Refer to the Protokolbuch, entry at 6 June 2003 for the data 200 MeV scattering data as well as the 8 August 2003 faintbeam data.	141
10.1	PR137: After dispersion matching optimization with faintbeam we had the beamspot on target indicated on the left of this figure. As PR137 was a zero degree experiment it was important to have a flat beamspot on target. After recursively tuning Q5S and optimizing the resolution with faintbeam we eventually ended with the beamspot on the right.	147
10.2	PR138: Due to wrong alignment procedures where we steered too much in the P-line we found that the settings of Q21P affected steering. The left figure shows the beamspot on target with Q21P=29.1A, and the right figure shows the beamspot with Q21A=22.8A.	149
10.3	The red arrows indicate where the beam attenuation meshes are located.	155
10.4	The mesh on the left hand side only allows through 1/100'th of the beam, and the two meshes on the right hand side (factors 10 and 1000) collectively allows through 1/10000'th of the beam.	156
10.5	$Q_4=18.43$ with Q_5 and Q_6 search: faint beam DM, Overfocus +15%, 49mm collimator, Run 127 of the October 2004 development period. Final resolution was 24 keV	157
10.6	Some plots of the faint beam tuning process for dispersion matched beam, over-focus mode +15%, with no collimator (PR137 logbook p143-155).	157
10.7	Faint beam for achromatic beamline settings. From left to right, K coil =20, 40, 55 (PR138 test weekend runs 4032, 4028, 4030 respectively). Note that the only effect is the shift in position. The general shape of the x-theta locus stays the same (take into account the different total counts in each run). In the position spectrum the sigma of a gaussian fitted to the faint beam peak was 2 mm for all three runs.	157
10.8	Pepperpot collimator during weekend 1 of PR137: from top left to right, first row then second row: underfocus -6.5%, overfocus +7.5%, +8.6%,+11.9%,+15%, PR137 logbook p30-32	159
10.9	Pepperpot collimator calibration runs from experiments PR244 (top left) and PR242 (bottom left). PR244 utilized underfocus mode, and PR242 overfocus mode. A typical beamspot image for experiment PR244 (top right) and PR242 (bottom left) is also shown.	159
10.10	Pepperpot collimator for different overfocus modes during experiment PR183. Note that the nominal setting of 4% overfocus mode is the real focus mode.	160

10.11	Pepperpot collimator for different underfocus modes during experiment PR183. Note that the nominal setting of 4% overfocus mode is the real focus mode.	161
10.12	Position sensitivity of the pepperpot collimator plots for 4% underfocus mode (which is in reality a 8% underfocus mode) during experiment PR183.	162
10.13	With a lateral dispersion matched beam there exists an ambiguity in the horizontal scattering angle. This very rough figure illustrates that 0 degree scattering has a certain focal plane angular range, which is not that different from the focal plane angle range experienced by small non-zero angle scattering, represented by the red lines.	163
10.14	Pepperpot collimator during weekend 1 of PR137 +15% overfocus mode, PR137 logbook p32	163
10.15	Pepperpot collimator for run 21336 of PR170 (PR170 logbook p8): 200 MeV proton beam, dispersion matched beam, K600 quad in -7% underfocus mode, $\theta_{K600}=10^\circ$.	164
10.16	The detector setup in the high dispersion focal plane, with the 0-degree beamline (2005 version). Notice the beamviewer just before the beandump entrance. In this scenario the old VDCs were still used in the focal plane. Since then the bellows was moved towards the beam viewer side and the detector support rod on the low momentum side was shifted. See Fig.10.17.	165
10.17	The new detector setup in the high dispersion focal plane, with the 0° beamline. Notice the beamviewer just before the beandump entrance. The support rod on the low momentum side was moved to accomodate the new shorter detector. Also, the bellows was moved further downstream compared to Fig. 10.16. The angle between the 0° beamline and the detectors is 29.15°	166
10.18	The proton beam as seen on the viewer (left of the two shown) just in front of the zero degree beandump, during experiment PR101 in 2005. The blue line represents the full size of the viewer ($50\text{mm} \times 70\text{mm}$).	166
10.19	The control box for the collimator carousel, with the new indicator lights that indicate whether the key at the back of the control box (see inset) is set to zero or not. (apologies for quality of picture)	167
10.20	The display of K600 magnet settings. The interlock settings for the K600 magnet settings are displayed at the bottom of the screen, as well as the status of the zero-degrees interlock.	167
B.1	An overview of typical internal autotrim results for half of the channels for VDC1 and VDC2.	175
B.2	A close-up view of typical internal autotrim results.	175
B.3	External autotrim results with suspect datapoints higher than 512ns	177
B.4	External autotrim results common to most recent experiments: a couple of TDC channels in the 2nd wire chamber are completely dead (see data at 512ns), and a couple of other TDC channels require software correction to shift them in line with the rest of the channels (see data below 256ns).	178
B.5	An overview of the K600 timing electronics in the vault.	181
B.6	This RES2D spectrum indicates that a lut shift of roughly -3 is required.	185
B.7	This RES2D spectrum that results from a properly shifted LUT.	185

G.1	The parts required for mounting CAKE - the plastic frame, 2 black spacers, the holder for the detector point and the back bracket.	199
G.2	The assembled version of the parts required for mounting CAKE	200
G.3	Another view of the assembled CAKE mount.	200
G.4	A picture showing where the spacers go.	201
G.5	The corner bracket and the rail: how they fit together.	201
G.6	The corner bracket and rail with the uh... next bracket.	202
G.7	The rib with the two rails and the mounting plate for the MMM detectors. Note that the circular inset is separate from the metal bracket that comes around and and must be secured with two locking nuts before the detectors are mounted. . .	202
G.8	How the MMM detectors go onto the frame. One detector position has no frame but has the small metal connecting piece shown while another detector position has the MMM frame shown without the associated detector. The detector numbers have been added to this figure.	203
G.9	MMM detector cable. The upper cable with more wires at the grey connector is the junction (p-side) cable. It carries 16 signals. The lower cable is the ohmic (n-side) cable. It carries 8 signals.	204
G.10	CAKE cabling inside the chamber. Note the folding back of the cable from detector 3. Make sure that this doesn't flop onto the detector below when you're connecting it or when you are putting the side on the chamber.	206
G.11	A closer-up picture of how the cable for detector 3 is secured on the beam-left side. It's bent back around upstream from the detector and is then secured to the rib before going to the LEMO feedthrough. You have to ensure that that cable isn't going to flop onto detectors 2 or 3 when you're connecting it up or when the side of the chamber is put on.	207
G.12	CAKE Junction LEMO	207
G.13	CAKE Ohmic LEMO	208
G.14	A top-down photo of how the K600 target ladder and the cable for detector 3 should look like, looking through the port on the top of the new K600 scattering chamber.	211

Bibliography

- [AnRep91] NAC Annual Report (1991).
- [Ber77] W. Bertozzi, M. V. Hynes, C. P. Sargent, C. Creswell, P. C. Dunn, A. Hirsch, M. Leitch, B. Norum, F. N. Rad, and T. Sasanuma, Nucl. Instrum. Methods **141** (1977) 457.
- [Berg05] G.P.A. Berg, private communication (2005).
- [Blo71] H.G. Blosser *et al.*, Nucl. Instrum. Methods 91 (1971) 61.
- [But90] J.M. Butler *et al.*, Nucl. Instrum. Methods **A290** (1990) 122.
- [Leo87] Leo
- [Coh59] B.L. Cohen, Rev.Sci.Instr.30(1959) 415.
- [Eng81] H.A. Enge, Nucl. Instrum. Methods 187 (1981) 1.
- [Fis01] K.G.. Fissum *et al.*, Nucl. Instrum. Methods **A474** (2001) 108.
- [Fuj00] Y. Fujita *et al.*, J. Mass Spectrom. Soc. Jpn., Vol. 48, No.5 (2000) 306
- [Fuj01] H. Fujita *et al.*, Nucl. Instrum. Methods **A469** (2001) 55.
- [Fuj02] H. Fujita *et al.*, Nucl. Instrum. Methods **A484** (2002) 17.
- [Jam75] F. James and M. Roos, Comput. Phys. Commun. **10** (1975) 343.
- [Jam89] F. James and M. Roos, document no. **D506**, (CERN, Geneva, 1989).
- [NAC92] J.C.Cornell, J.G.de Villiers and D.T.Fourie, NAC Report, NAC/92-04, 1992.
- [Nev08] R. Neveling, Report on RCNP beamtime and beam tuning methods, not published, 2008.
- [New96] R.T. Newman, Ph.D. thesis, University of Cape Town, (1996), unpublished.
- [Sch86] P. Schwandt, Notes on the Indiana University Cyclotron Facility K600 spectrometer (1986) unpublished.
- [Tam09] A. Tamii *et al.*, Nucl. Instrum. Methods **A605** (2009) 326.
- [Tra02] Program *TRACK*, V8.6, Magnet Section, Paul Scherrer Institute (PSI), Switzerland, 2002.

- [Wak02] T. Wakasa *et al.*, Nucl. Instrum. Methods **A**482 (2002) 79.
- [Gar10] G. de Villiers, private communication (2010).
- [web10] <http://hyperphysics.phy-astr.gsu.edu/hbase/solids/hyst.html>
- [Mid] The MIDAS (Maximum Integration Data Acquisition System) Data Acquisition System, Paul Scherrer Institute, <https://midas.psi.ch>.